UNIVERSITAT DE BARCELONA

Single-cell transcriptomics of zebrafish heart regeneration with subcellular spatial resolution

Ioannis Lazis

UNIVERSITAT DE BARCELONA

FACULTAT DE MEDICINA I CIÈNCIES DE LA SALUT

PROGRAMA DE DOCTORAT EN BIOMEDICINA

2024

TESIS DOCTORAL

Single-cell transcriptomics of zebrafish heart regeneration with subcellular spatial resolution

Memòria presentada per

Ioannis Lazis

Per optar al títol de

Doctor

Per la Universitat de Barcelona

Tesi doctoral realitzada sota la direcció del Dr. Ángel Raya Chamorro i Dra. Mireya Plass Portulas al Institut d'Investigació de Bellvitge (IDIBELL)

Signat,

El Director:	La Directora:	La tutora:	El Doctorando:
Dr. Ángel Raya Chamorro	Dra. Mireya Plass Portulas	Dra. Antonella Consiglio	Ioannis Lazis

Table of Contents

ABSTRACT

Adult zebrafish (*Danio rerio*), in contrast to mammals, can efficiently regenerate large portions of the heart after experimental damage or amputation. This process has been extensively studied we are beginning to understand the key events necessary for this regenerative response to happen. However, the cellular interplay and molecular mechanisms that govern the proliferation and migration of cardiomyocytes, as well as the termination of the regenerative process, have been only fragmentary explored. Understanding these mechanisms and exploiting them in the human context could open new therapeutic approaches to promote myocardial regeneration and prevent the development of heart failure. With this aim, we sought to determine the transcriptomic profile of healthy and regenerating zebrafish hearts at single-cell resolution, using novel transcriptomic approaches, and to analyze the importance of candidate genes in the regeneration process.

For this purpose, in the first part of the current thesis, we developed a tissue dissociation protocol using a cold active protease, from *B. licheniformis,* to minimize collagenase-associated artifacts introduced in single-cell RNA sequencing (scRNA-seq) analyses. We also made use of a droplet-based microfluidics encapsulation device that is particularly suitable for capturing both large (cardiomyocytes) and small (fibroblasts, endothelial, myeloid) size cells. Using these protocols, we have investigated changes in cell types and cardiomyocyte cell states in uninjured (Sham) zebrafish hearts, and after 7- and 30-days post amputation (DPA) . Due to the high sensitivity of scRNA-seq, we could find changes in gene expression that were not detected in previous bulk RNA-seq analyses. Our results identified novel markers to describe cardiomyocyte cell-states that are present in both healthy and regenerating myocardium. We then studied the transcriptomic changes of these cell-states, and we identified candidate genes with possible implication in heart regeneration.

In the second part of the current thesis, we sought to examine the importance of candidate genes in zebrafish heart regeneration. Our previous results showed that *anxa2a, mustn1b, fhl1a* and *casq2* are dynamically expressed in cardiomyocytes and upregulated at 7 DPA. We followed a CRISPR/Cas9-based approach for loss-of-function experiments of these genes. Knock-out zebrafish did not exhibit any developmental defects or abnormal adult

phenotypes but failed to regenerate their myocardium after apex resection. For further characterization of the role(s) that these genes play during zebrafish heart regeneration, we developed two novel experimental platforms: 1) a cardiomyocyte-specific Ca^{2+} indicator reporter transgenic zebrafish line for monitoring calcium handling during zebrafish heart regeneration, and 2) an *in vitro* platform for measuring cell-autonomous behaviors in response to matrices of controlled stiffness.

In the third part, we have examined the transcriptomic changes in *periostin b* (*postnb*) knock-out animals that exhibit increased cardiomyocyte proliferation but fail to regenerate the ventricle upon injury. We found similar cellular composition between $postnb^{-/-}$ and wild type ventricles. However, $postnb^{-/-}$ mutant hearts showed changes in the proportions of cardiomyocytes, macrophages, fibroblasts, and epicardial cells at 7 DPA. To include spatial information about the expression of genes and infer gene regulatory networks, we performed spatial transcriptomics experiments. Our results demonstrate the suitability and efficiency of the technique for finding gene specific domains in the regenerating zebrafish heart.

List of figures

List of tables

List of abbreviations

^{14}C	carbon-14
4sU	4-thiouridine
ANX	Annexin
AP	Action potential
bCMS	biosynthetic Cardiomyocytes
BDM	2,3-Butanedione monoxime
BMP	Bone morphogenetic protein
bp	base pairs
BSA	Bovine serum albumin
CaM	Calmodulin
Cas9	CRISPR associated protein-9
CCA	Canoncial correlation analysis
cCMs	cortical Cardiomyocytes
cDNA	complementary DNA
cECs	coronary endothelial cells
CMs	Cardiomyocytes
CPCs	Cardiovascular progenitor cells
cpEGFP	Circularly permutated enhanced GFP
Cre	Cyclic recombinase
CRISPR	Clustered Regularly Interspaced Short Palindromic Repeats
crRNA	CRISPR RNA
CSCs	cardiac stem cells
Ct	Cycle threshold value
CTD	carboxyl-terminal domain
DAPI	4',6-diamidino-2-phenylindole
dCMS	dedifferentited Cardiomyocytes
DE	Differential expression
dH_20	distilled water
DNA	Deoxyribonucleic acid
DNB	DNA nanoball

dpa	Days post amputation
dpf	days post fertilization
dpi	days post injury
DSB	Double strand breaks
DTA	diphteria toxin chain A
ECM	Extracellular matrix
ECs	Endothelial cells
EdU	5-ethynyl-2'-deoxyuridine
eECs	endocardial endothelial cells
ENU	N-ethyl-N-nitrosourea
FACS	Flow-activated cell sorting
FBS	Fetal bovine serum
Fgf	Fibroblast growth factor
FHL	four and a hlaf LIM domain
GFP	Green fluorescent protein
GO	Gene Ontology
GSVA	gene set variation analysis
HA	Hyaluronic acid
hCMs	hypertrophic Cardiomyocytes
HDR	Homology Directed Repair
hiCMs	hibertnating Cardiomyocytes
hpa	hours post amputation
hpi	hours post injury
HSCs	Hematopoioetic stem cells
HVGs	High variable genes
IER	Immediate Early Response
Igf	Insulin-like growth factor
IHC	Immunohistochemistry
ISH	in situ hybridization
KI	knock-in
KO	knock-out

LCM	Laser capture microdissection
lECs	lymphatic endothelial cells
LEN	lepb-linked regeneration enhancer
LOF	loss of function
mCMs	mature Cardiomyocytes
MET	Mesenchymal to epithelial transition
MI	Myocardial infarction
miRNAs	micro-RNAs
MO	morpholino
mRNA	messenger RNA
mtRNA	mitochondrial RNA
Mtz	Metronidazole
NES	Nuclear export sequence
NGF	Nerve growth factor
NGS	Next-generation sequencing
NHEJ	Non-Homologous End Joining
NTR	Nitroreductase
OPP	O-Propargyl Puromycin
ORF	Open Reading Frame
PAA	Polyacrylamide
PAM	Protospacer associated motif
PBS	Phosphate buffered saline
PCA	Principal Component Analysis
PCR	Polymerase chain reaction
Pdgf	Platelet-derived growth factor
PFA	Paraformaldehyde
RA	Retinoic acid
RIN	RNA integrity number
RNA	Ribonucleic acid
RNAi	RNA intereference
RNP	Ribonucleoprotein

RT	Room Temperature
RT-qPCR	Reverse Transcription quantitative Polymerase Chain Reaction
SB	Stopping Buffer
SCC	spatially constrained-clustering
scRNA-seq	single-cell RNA sequencing
SDS	Sodium-dodecyl disulfate
SEM	Standard error of mean
sgRNA	single-chimeric guide RNA
Shh	Sonic hedgehog
SpCas9	Streptococcues pyogenes Cas9
stereo-seq	Spatial ehnanced resolution omics-sequencing
Sulfo-SANPAH	sulfosuccinimidyl 6-(4’-azido-2’-nitrophenylamino)hexanoate
t-SNE	t-distributed stochastic neighbour embedding
TALEN	Transcription Activator-like Effector Nucleases
TF	transcription factor
Tgfb	Transforming growth factor
tomo-seq	Spatial resolved RNA sequencing
tracrRNA	Trans-activating CRISPR RNA
TREEs	Tissue Regeneration Enhancer Elements
UMAP	Uniform Manifold Approximation and Projection
UMI	Unique Molecular Identifier
WT	Wild type
ZFN	Zinc finger nucleases

List of abbreviations for genes and proteins

acta2	Actin alpha 2
ank1a	Ankyrin 1a
anxa2a	Annexin A2a
atf3	Activating transcription factor 3
btg2	B-cell translocation gene 2
casq2	Calsequestrin 2
cav1	Caveolin 1
cdh6	Cadherin 6
cldn11a	Claudin 11a
cldn5b	Claudin 5b
cmlc2a	Cardiac myosin light chain a (official nomenclature *myl7*)
col12a1a	Collagen type XII alpha 1a
col1a2	Collagen type I, alpha 2
col5a1	Collagen type V, alpha 1
csrp3	Cystein and glycine-rich protein 3
Cx40	Connexin 40
f8	Coagulation factor VIII
fhl1a	Four and a half LIM domain 1 a
fhl1b	Four and a half LIM domain 1 b
Fhl2	Four and a half LIM domain 2
fn1b	Fibronectin 1b
fosab	v-fos FBJ murine osteosarcoma viral oncogene homolog Ab
gspt1	G1 to S phase transition 1
hapln1a	Hyaluronan and proteoglycan link protein 1a
hapln1b	Hyaluronan and proteoglycan link protein 1b
hbaa1	Hemoglobin alpha adult 1
hbba2	Hemoglobin beta adult 2
heg	Heart of glass
Hey2	Hes-related family bHLH transcription factor with YRPW motif 2
hmgn2	High mobility group nucleosomal binding domain 2

hopx	HOP homeobox
hoxd3a	Homeobox D3a
ier2a	Immediate early response 2a
ier2b	Immediate early response 2b
Isl1	ISL LIM homeobox 1a
ITLN1	Intelectin 1
krt15	Keratin 15
lepb	Leptin b
LGR5	Leucine-rich repeat containing G protein-coupled receptor 5
mdka	Midkine a
mef2ca	Myocyte enhancer factor 2ca
mmp14a	Matrix metallopeptidase 14a
mmp14b	Matrix metallopeptidase 14b
mmp2	Matrix metallopeptidase 2
mpeg1	Macrophage expressed 1
mpx	Myeloid-specific peroxidase
Mustn1	Musculoskeletal embryonic nuclear protein
mustn1a	Musculoskeletal embryonic nuclear protein 1a
mustn1b	Musculoskeletal embryonic nuclear protein 1b
Myh6	Myosin heavy chain 6
myoD	Myogenic differentiation
ndrg4	NDRG family member 4
Nkx2.5	NK2 homeobox 5
nme2b.2	NME/NM23 nucleoside diphosphate kinase 2b, tandem duplicate 2
nppa	Natriuretic peptide A
nppb	Natriuretic peptide B
nppc	Natriuretic peptide C
NRG1	Neuregulin 1
pax7	Paired box 7
Plvap	Plasmalemma vesicle-associated protein
postnb	Periostin b

raldh2	Aldehyde dehydrogenase 2
rca2.2	Regulator of complement activation group 2, tandem duplicate 2
RNASE1	Ribonuclease 1
Rnf213	Ring finger protein 213
runx1	RUNX family transcription factor 1
ryr2b	Ryanodine receptor 2b
sema3aa	Semaphorin 3Aa
serpinh1b	Serpin peptidase inhibitor 1b
socs3a	Suppressor of cytokine signaling 3a
spock3	SPARC, cwcv and kazal like domains proteoglycan 3
synpo2lb	Synaptopodin 2-like b
tbx12	T-box transcription factor 12
tbx18	T-box transcription factor 18
Tcap	Titin-cap
tcf21	Transcription factor 21
timp4.3	TIMP metallopeptidase inhibitor 4, tandem duplicate 3
tmsb1	Thymosin beta 1
tnnc1a	Troponin C type 1a
tnnc1b	Troponin C type 1b
ttn.2	titin, tandem duplicate 2
vegfaa	Vascular endothelial growth factor Aa
wt1b	WT1 transcription factor b

1. INTRODUCTION

1.1. Regeneration overview

Regeneration is a complex biological process by which some living organisms are capable of regrowing or replacing damaged or lost tissues and organs (Bely & Nyberg, 2010; Stocum, 2018). Regeneration has long been a topic of interest in the field of biology, and early studies can be traced back to the 18th century when scientists first observed the ability of certain organisms, such as planarians and salamanders, to regrow lost body parts (Okada, 1996). This remarkable phenomenon is observed in various kingdoms and species, ranging from simple organisms like bacteria and fungi to complex multicellular organisms such as plants and animals (Bely & Nyberg, 2010; Elchaninov et al., 2021; Maden, 2018). From an evolutionary point of view, regeneration has evolved independently multiple times across different phyla (Bely & Nyberg, 2010), and is widespread in the animal kingdom, indicating its adaptive significance in enhancing the survival and reproductive success of organisms.

Over the years, our understanding of regeneration has increased dramatically thanks to active research by a multitude of groups. However, the basic mechanisms underlying this fascinating phenomenon, including the recognition of the damaged structure followed by its reconstruction, are still not fully understood due to the complexity of the regeneration programs. Further understanding of how these mechanisms are initiated, regulated, and ultimately concluded, will be of great importance for advancing our fundamental knowledge of biology, and likely to be of impact for the development of regenerative medicine.

Regeneration occurs at different levels of biological organization from cellular level to the whole body (Figure I 1). At the cellular level, such as during regrowth of severed axons, this process involves organelle remodeling and elevated protein synthesis (Becker & Becker, 2001). Regeneration of tissues and/or organs requires both stimulatory factors and a permissive environment that will enable cells capable of proliferation and differentiation to reconstitute the damaged part (Carlson, 2007). In the cases of limb regeneration in amphibians and fin regeneration in zebrafish, cues that define the final form of the structures are necessary (Kragl et al., 2009; Uemoto et al., 2020). Finally, extreme examples of regenerative ability such as hydra or planarias have proven that even a small part of tissue is

capable of regenerating all the cell types, tissue patterns, and body shape of the entire organism (Kürn et al., 2011).

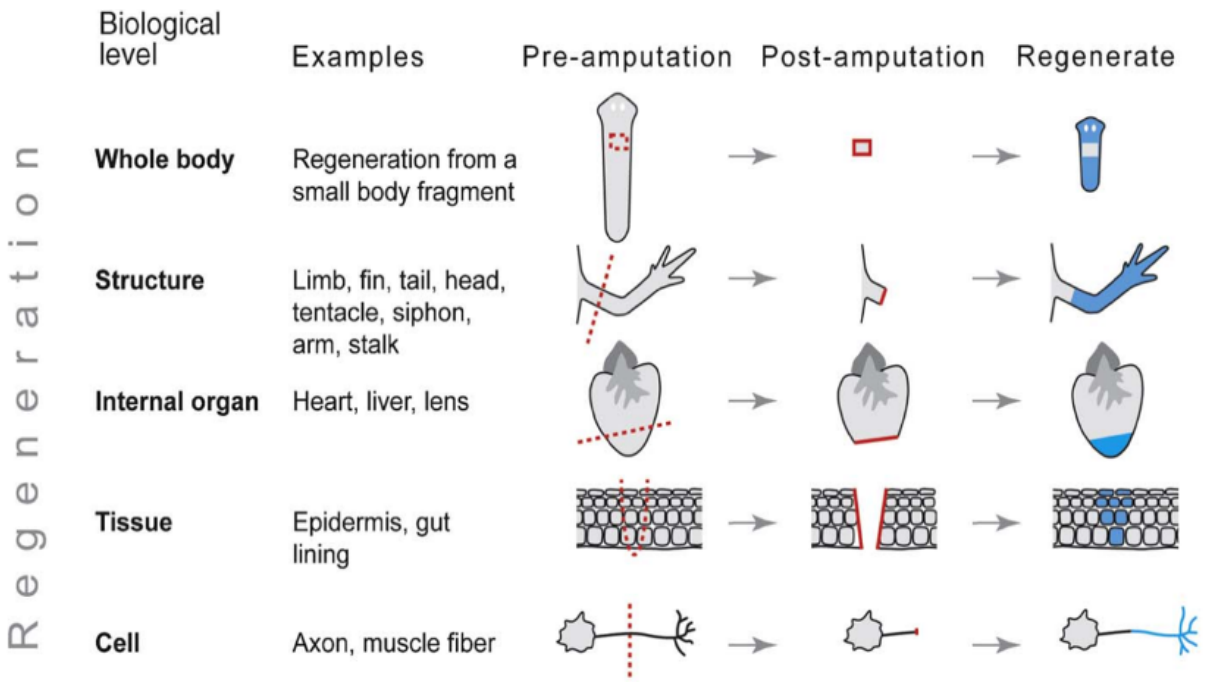

Figure I 1. Regeneration at different levels of biological organization. A specific species may exhibit regeneration at all, none, or only a portion of these levels. While functional connections between regenerative processes at different levels are likely, it is still uncertain which aspects of regeneration are homologous across these levels. Dashed red lines indicate amputation planes; solid red lines indicated wound surfaces; and blue fill indicates regenerated body parts. Adapted from Belly and Nyberg, 2010.

Irrespective of the level of organization, the new cells needed for regeneration can result from asymmetric division of resident *stem cells*, *dedifferentiation* or *transdifferentiation* (Tanaka & Reddien, 2011). In the first case, a single cell can give rise to two daughter cells, one with the properties to maintain the stem cell pool and another differentiated one that will contribute to the tissue repair (Dinulovic et al., 2017). Dedifferentiation involves the loss of the current cell identity into a proliferative state (Jopling et al., 2010; Kragl et al., 2009). In contrast, cell transdifferentiation such as mesenchymal to epithelial transition (MET) occurs when a differentiated cell changes identity directly into that of another differentiated cell type (Pei et al., 2019). These mechanisms can either act autonomously or simultaneously depending on the niche of the tissue and the activated regeneration responses.

1.1.1. Types of regeneration

Distinct biological processes are activated depending on the species and the type of tissue that is damaged or lost, (Carlson, 2007; Elchaninov et al., 2021). Many types of regeneration have been described so far, but the poor understanding of these mechanisms sometimes makes it difficult to assign them to a known category. The main categories are described below and summarized in Table I 1.

Table I 1 Types of regeneration and repair mechanisms upon tissue damage or loss.

Regeneration				Morphallaxis*	Hypertrophy**	
Physiological	Reparative				Compensatory	Regeneartive
	Epimorphic	Tissue	Cellular			
Blood replacement	*Limb*	*Muscle*	*Neuronal processes*	*Planaria*	*Kidney*	*Liver*
Epithelial regeneration	*Tail*	*Bone*	*Protozoa*	*Some annelids*	*Lungs*	*Pancreas*
Antler regeneration	*Head*	*Skin*	*Acetabularia*			
		Heart				

* Repatterning of the existing tissue with little new growth

** In the case of hypertrophy, *compensatory*, refers to increasing a paired organ size after its pair has been damaged or lost and *regenerative*, restoring the mass (either increase in cell number or cell size) of damaged internal organ.

Physiological regeneration refers to the natural process by which living organisms are capable of replacing extruded or worn-out body parts (Carlson, 2007). This type of regeneration occurs in tissues and organs that experience high cellular turnover or mechanical abrasion, such as blood or antlers, respectively. Another example of physiological regeneration in non-mammalian species would be the shedding of reptilian skin, the replacement of feathers in birds, or the exoskeletons in crustacean. As can be appreciated from these examples, physiological regeneration is highly attuned to the body's needs and is either synchronized with annual climate changes or the age of the organism. Physiological regeneration is not controlled by a global mechanism and for this reason might not be considered as a true regenerative process rather than as a term of convenience that includes processes whose functions are to maintain the normal equilibrium (homeostasis) of the body

tissues and/or organs. In contrast, reparative regeneration, a term that describes most post-traumatic regeneration events, can be classified in two regeneration mechanisms: epimorphic regeneration and tissue regeneration. In the first case, the formation of a blastema, an undifferentiated cell mass capable of growth, will give rise to the new structure as is the case for axolotl limb regeneration and zebrafish caudal fin (Kragl et al., 2009; Uemoto et al., 2020). During tissue regeneration, the repair of damaged tissue after injury is achieved without forming a blastema. In this category, the contribution of other cells and the local microenvironment, such as immune cell recruitment and remodeling of the extracellular matrix (ECM) is of great importance. For example, changes in the plasticity of the stem cell niche can lead to pathological conditions (Dinulovic et al., 2017; Hirakawa et al., 2023). Cardiac regeneration belongs to tissue regeneration. Previous findings have shown that modifications of the ECM stiffness or other components of the microenvironment, such as innervation or vascularization, can impede the regenerative capacity of the heart (Mahmoud et al., 2015; Notari et al., 2018; Ryan et al., 2020). The current thesis is focused on this mechanism of regeneration.

1.1.2. Regeneration in vertebrates and mammals

Invertebrates such as starfish, planarians, and certain types of worms can regenerate whole organisms from small fragments or even single cells (Kürn et al., 2011). In vertebrates, however, the regenerative capacity is more limited and varies among different species (Yun, 2015). Urodele amphibians and some species of teleost fish show the highest degrees of regeneration among vertebrates with the ability to regrow limbs, tail, retina, jaws, and even parts of internal organs such as the heart, intestine epithelium, and spinal cord (Carlson, 2007; Maden, 2018). The mechanisms involved in regeneration may differ depending on the different structure or organ that is injured and/or across species. However, most vertebrates, including humans, have limited ability to regenerate lost or damaged body parts (Figure I 2), even though they retain the capacity to undergo physiological regeneration, such as blood renewal, intestinal epithelium renewal and skin wound repair.

Nonetheless, some examples of epimorphic regeneration have been observed in mammals. The spiny mouse (*Acomys* species*)* possesses the remarkable ability to undergo

scarless regeneration of skin wounds including hair follicle cells, as well as ear punches (Okamura et al., 2021). Regeneration after the removal of a mass of ear tissue was first characterized in rabbit ears and then observed in different mouse strains (Beijnum et al., 2023; Goss & Grimes, 1972). Another example of true multi-tissue regeneration in mammals refers to digit tip regeneration studied in mice. The fingertip is the only part of the human limb that maintains a regenerative capacity. Amputation upon distal, but not proximal, of the mouse digit tip trigger the activation of endogenous regeneration mechanisms (Dolan et al., 2022; L. Yu et al., 2019). The amputation plane, and thus the existence or absence of the nail bed, will determine whether the tissue will regenerate or results in fibrosis.

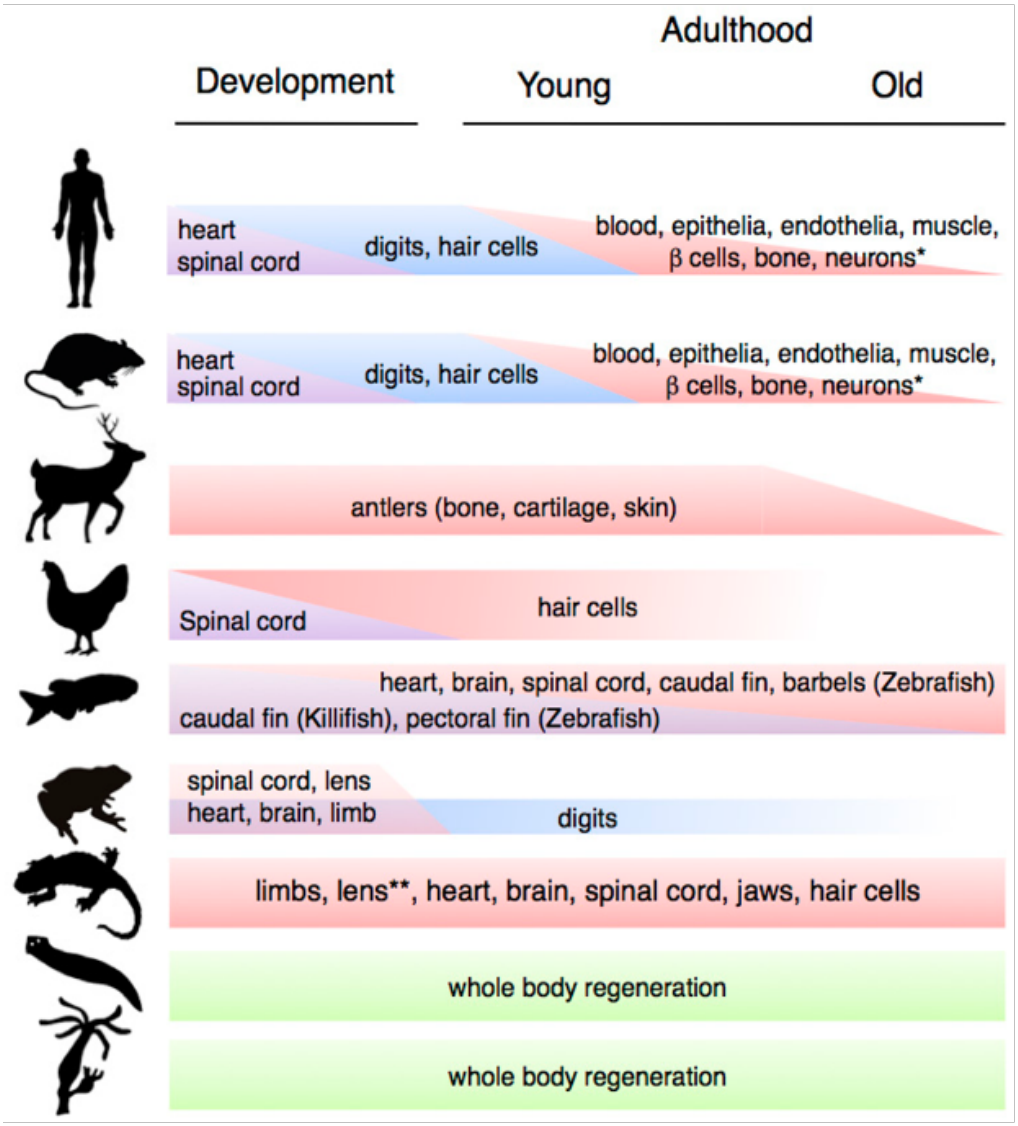

Figure I 2. Variation in regenerative capacity through phylogeny, ontogeny and aging. *Note that the ability to regenerate the indicated systems is present in most other animal groups; **Lens regeneration is observed throughout lifespan in newts, but it can only occur during a limited developmental window in axolotls. Adapted from Yun M., 2015.

The presence of vertebrates with regenerative capacities throughout their lifespan suggest the existence of species-specific regeneration genes. Yet, only a few have been described so far, such as *Prod1* in limb regeneration of salamander (K. Nomura et al., 2017; Yang & Kang, 2019). The absence of species-specific regeneration genes, in combination with limited regenerative capacities of some species in early developmental stages, might imply that the drivers of regeneration are evolutionary conserved while the mechanisms of activation differ across species. For example, *Kang et al.* demonstrated the existence of Tissue Regeneration Enhancer Elements (TREEs), *cis*-regulatory elements controlling gene expression, which are activated at the regenerating heart and fin of zebrafish (Kang et al., 2016). Years later, TREEs of zebrafish origin were used in an enhancer-based gene-therapy strategy in mice resulting in boosted regeneration and improved function of the injured heart (Yan et al., 2023). This study shows the broad-species effects of these elements and opened the path for future therapeutic strategies in human tissue repair by exploiting endogenous pathways.

1.2. Heart regeneration

Despite the advances in preventive cardiology, cardiovascular diseases remain the leading cause of morbidity and mortality worldwide, accounting for over 420 million cases and close to 18 million deaths every year (Bozkurt et al., 2023; Ziaeian & Fonarow, 2016). This is the consequence of the inability of the adult mammalian heart to regenerate after an ischemic injury, where a significant portion of the myocardium is lost and replaced by fibrotic scar tissue (Laflamme & Murry, 2011). This leads to a progressive deterioration of the heart contractile capacity, ultimately resulting in heart failure. Currently, the only curative option for patients with end-stage heart failure is heart transplantation, which is limited by organ donor availability (Shah et al., 2019). In addition, according to the *American Heart Association*, existing pharmacological treatments target the mechanical characteristics of the cardiovascular system, rather than reversing the damage caused by the cardiovascular disease (American Heart Association, 2024). Given the lack of feasible therapeutic approaches to reverse the loss of functional myocardium, the development of efficient and safe regenerative procedures is an urgent need in the field of modern cardiovascular research. Therefore, the study of organisms with the innate ability for heart regeneration and the

understanding of the mechanisms orchestrating the regenerative response stands out as of great importance for the successful development of clinical therapies for *bona fide* regeneration of the human cardiac tissue.

1.2.1. Heart regeneration across species

Heart regeneration is a phenomenon that varies across species (P. D. Nguyen et al., 2021; Vivien et al., 2016). In warm-blooded species, cardiac regeneration appears to be limited to a specific period during fetal and early neonatal life (Figure I 3). During this period, immature mammalian hearts exhibit a robust capacity of cardiac regeneration, which gradually decreases as the heart matures during adulthood. Interestingly, animal species with close evolutionary kinship may have very different heart regeneration capabilities (Vivien et al., 2016). For example, while zebrafish and goldfish have strong regenerative abilities, the medaka heart can be scarred after injury without undergoing regeneration (Lai et al., 2017). Young adult *Xenopus tropicalis*, a species closely related to *Xenopus laevis*, has the ability to regenerate heart tissue after ventricular resection, while mature adults of *X. laevis* are not capable of cardiac regeneration (He et al., 2022; Marshall et al., 2017).

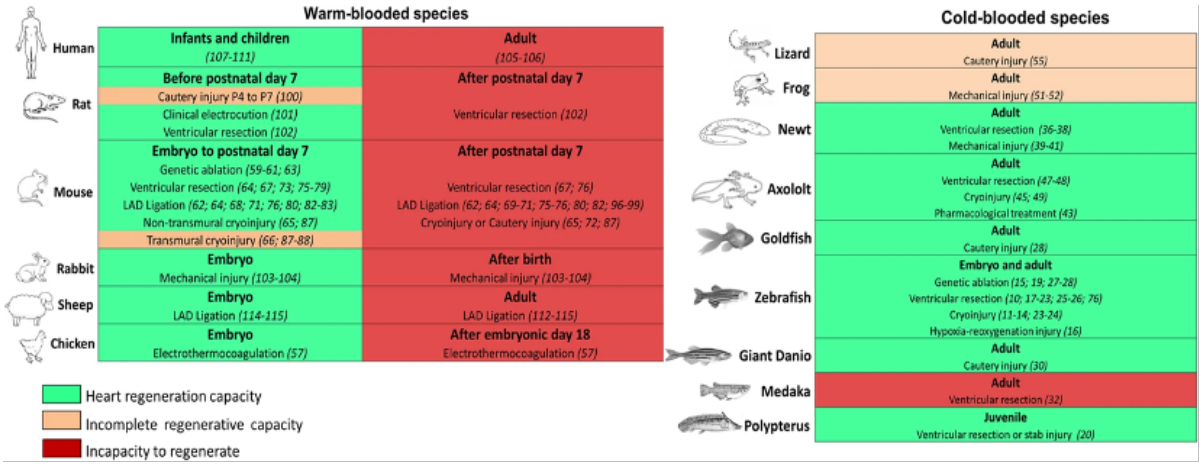

Figure I 3. Heart regenerative capacity in warm- or cold-blooded animals. Each species is represented with a color-coded system denoting its cardiac regenerative capability: green for the ability to regenerate, orange for incomplete regenerative capacity, and red for the inability to regenerate. The approach employed to induce cardiac damage and the relevant references are specified for each case. In warm-blooded species, cardiac regeneration seems confined to a specific early developmental phase encompassing embryonic and early-neonatal life. Among cold-blooded animals, six out of nine species exhibit heart regeneration capacity during adulthood, while three out of nine display either incomplete regenerative capacity or a complete inability to undergo heart regeneration. Adapted from Vivien et al., 2016.

A fascinating example of the complexity of heart regeneration is mirrored in the case of *Astyanax mexicanus* (Stockdale et al., 2018). This surface teleost, like zebrafish, can regenerate the lost tissue upon apex resection. In contrast, its cave-dwelling counterparts cannot regenerate and upon resection a permanent scar is formed. The second generation of a cross between surface and cavefish results in offspring bearing a combination of features from the two fish such as size, pigmentation, existence of eyes. When this generation was studied regarding its regenerative capacity, a spectrum of clear scar to complete regeneration was observed.

While the Mexican cavefish is an exception, the species-specific nature of heart regeneration highlights the variation in regenerative capabilities among different developmental stages and closely related species (P. D. Nguyen et al., 2021; Sahara et al., 2015; Vivien et al., 2016). Understanding the cellular and molecular drivers of regeneration among species that exhibit varying levels of heart regeneration could potentially lead to the development of genetic or pharmacological interventions to enhance cardiac regeneration in humans.

1.2.2. Limitations of heart regeneration in humans and clinical significance

The adult mammalian heart is incapable of regeneration upon injury, which gives rise to fibrosis and scarring occurring at the damaged area. When compared with regeneration-competent species, the initial phases following cardiac injury appear to be the same although they have a different outcome (Figure I 4 A). The most evident factors that limit the regenerative capacity of the heart include the low turnover rate of the cardiomyocytes and the inability to replace the non-contractile scar tissue with functional myocardium after injury (Laflamme & Murry, 2011).

In order to investigate if new cardiomyocytes are generated in the human heart after birth, researchers used carbon-14 (^{14}C) dating to ascertain whether cardiac muscle cells undergo self-renewal. Taking advantage of the elevated worldwide levels of atmospheric ^{14}C resulting from nuclear bomb tests during the Cold War, these researchers were able to date the birth of cardiomyocytes in individuals of different ages (Bergmann et al., 2009). Their work

suggests that cardiomyocyte turnover rates are very low in humans and that there is an age-dependent decline from 1% at the age of 20 to 0.4% at the age of 75, resulting in less than 50% of cardiomyocyte renewal during life.

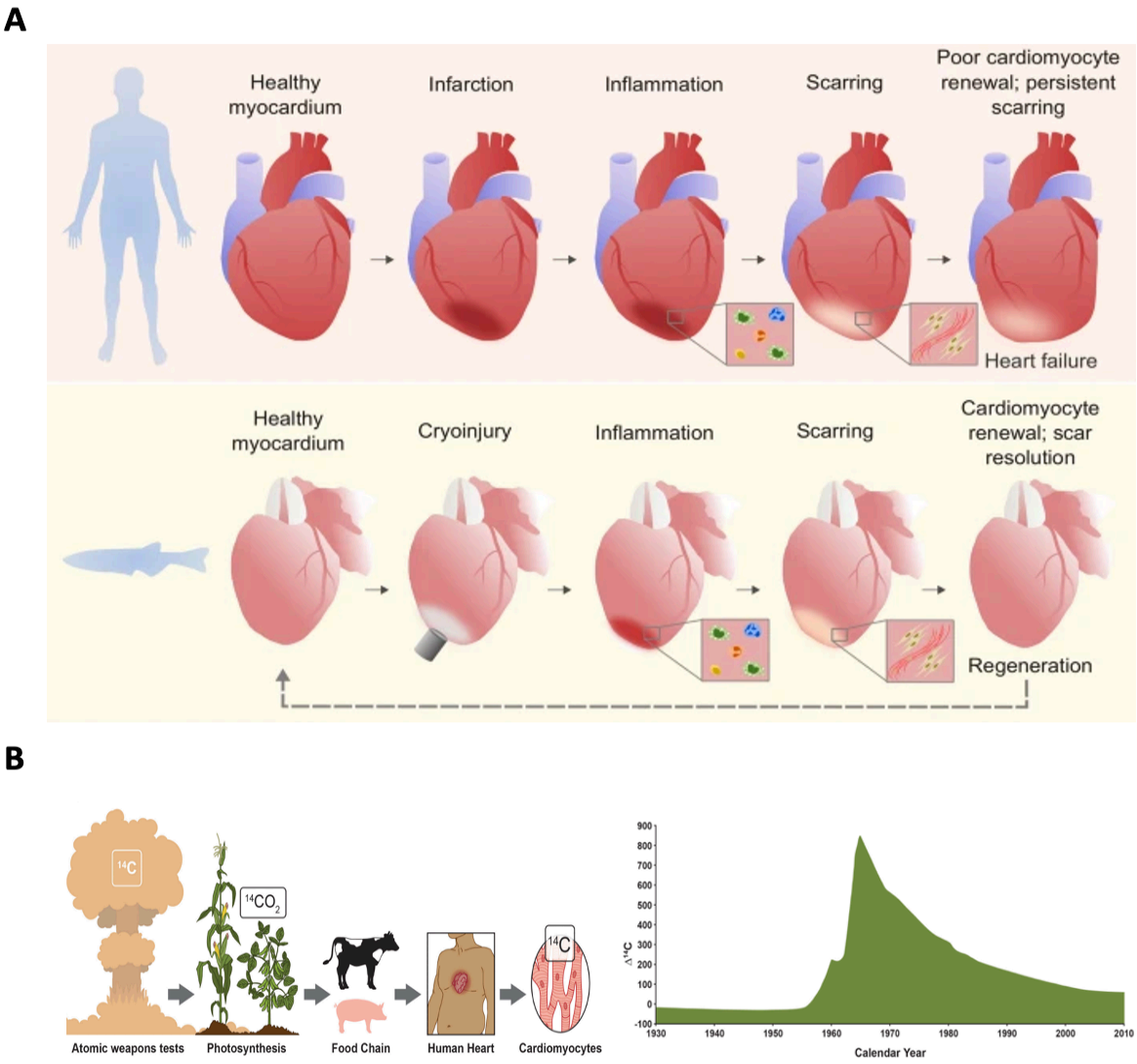

Figure I 4. Incompetence of human cardiac regeneration. (A) The phases of repair/regeneration in human and zebrafish hearts post-injury are depicted, highlighting the initial similarity in inflammatory and scarring responses. However, the final stages diverge, with humans showing persistent scar tissue and limited renewal of CMs. In contrast, after cryoinjury zebrafish hearts undergo a regenerative phase marked by scar resolution and CM proliferation, resulting in the restoration of a healthy myocardium. **(B)** Cardiomyocyte renewal rate calculations through radiocarbon dating upon a pulse that entered the food chain. Adapted from Ryan et al., 2020 and Garry et al., 2023.

Given these findings, the search for mechanisms to enhance heart regeneration has intensified, particularly focusing on the potential role of cardiac stem cells (CSCs). For many years, the existence of CSCs residing in the adult heart has been under debate with many researchers searching for such a population of cells that could repair the mammalian heart

upon injury (Edelberg et al., 2003; R. T. Lee, 2018; Mancuso et al., 2020; Tzahor & Poss, 2017). In 2018, Clevers and colleagues combined lineage tracing with novel technologies to profile proliferative cells in damaged murine hearts (Kretzschmar et al., 2018). They found cycling cardiomyocytes (CMs) in early postnatal growth phase but no evidence of adult CSC population that could give rise to more CMs in response to injury. A possible explanation for the insufficiency of cardiomyocytes to re-enter the cell cycle and proliferate once they are fully mature could be attributed to their DNA content (Gan et al., 2020; González-Rosa et al., 2018). Moreover, another limitation of heart regeneration in humans compared to regenerative competent models is the persistent scarring after fibrosis. The fibrotic tissue maintains the wall integrity of the heart but its function declines, leading to heart failure (Bertero & Murry, 2018). Furthermore, in therapeutic approaches of cardiac patches, the non-conductive scar tissue limits the electromechanical coupling of the graft and thus its efficiency (C. Yu et al., 2023). These limitations highlight the need for continued research into enhancing the regenerative capacities of the heart, whether through developing advanced biomaterials that can better integrate with cardiac tissue or stimulating endogenous regenerative pathways.

1.3. Zebrafish heart regeneration

Unlike mammals, the small tropical teleost zebrafish, *Danio rerio*, possesses the innate ability to regenerate the heart as adults (González-Rosa et al., 2018). In the laboratory, heart regeneration is induced in zebrafish after experimental injuries such as amputation of up to 20% of the ventricular apex, cryoinjury, or genetic ablation (Chablais et al., 2011; Curado et al., 2007; Poss et al., 2002; A. Raya et al., 2003). While some pathways involved in regeneration have been shown to depend on the specific injury model used, there are shared cellular and molecular mechanisms underlying heart regeneration (Botos et al., 2023).

Zebrafish heart regeneration occurs through dedifferentiation and proliferation of pre-existing cardiomyocytes adjacent to the amputation plane, which then migrate to contribute to the newly formed myocardium (Jopling et al., 2010). Moreover, the regenerative process involves the activation and migration of the epicardium, as well as the contribution of many other cell types to complete it.

1.3.1. Zebrafish as an animal model for cardiovascular research

Zebrafish has become a widely used animal model in scientific research. It is native to freshwater environments such as rivers and streams, found in South Asia (Holtzman et al., 2016). Zebrafish was first used as an animal model in the late 1920s, but its popularity as animal model started raising after the pioneering work of Streisinger and Kimmel who used it as a genetic and developmental model respectively (Kimmel, 1993; Kimmel et al., 1989; Streisinger et al., 1981). The advantages of zebrafish as an experimental model include their transparent embryos, ease of genetic manipulation, and accessibility at all stages of development. This allows researchers to study various aspects of zebrafish biology, including anatomy, physiology, genetics, development, and behavior. In addition, the large number of eggs laid in one batch, short generation time low cost, and simple care, make them an attractive model to maintain and use in the laboratory.

Zebrafish share similar anatomical and physiological features with humans, making the translation of research findings from zebrafish to human models more reliable. The zebrafish genome shows a high degree of genetic homology with the human genome with many conserved genes and regulatory elements. Around 70-75% of human genes have at least one orthologous gene in the zebrafish genome (Howe et al., 2013). Although in many cases human genes may have more than one ortholog in zebrafish due to the teleost genome duplication (Postlethwait et al., 1998). In addition, around 85% of genes associated with human disease have a zebrafish counterpart (Dooley & Zon, 2000; Howe et al., 2013). Their innate ability to regenerate numerous organs such as the brain, retina, pancreas, and heart, in combination with the great possibilities of translation to humans, positions them among the top animal models for advancing the design of therapeutic strategies for human (Kroehne et al., 2011; Pisharath et al., 2007; Vihtelic & Hyde, 2000).

Regarding cardiovascular research, zebrafish is a highly predictive model for preclinical drug assays (Genge et al., 2016; Patton et al., 2021). This is due to the similarities found in the zebrafish and human heart in terms of development, genetics, physiology, and even disease phenotypes. The electrophysiology of the human heart has more differences with the mouse heart than with the zebrafish (Brette et al., 2008; Leong et al., 2010; Salama

& London, 2007). The average human heart beats at 60-70 beats per minute, ten time less than the mouse one. On the contrary the average zebrafish heart beats at 110-130 beats per minute, similar to a young kid or exercising adult (Leong et al., 2010). The resemblance in action potential (AP) propagation shown in Figure I 5, between human and zebrafish, is further depicted in the electrocardiogram (ECG) measurements. Additionally, their similarities in drug responses and the ability to perform high-throughput screening of drugs in zebrafish larva, result in a more robust discovery of new drugs.

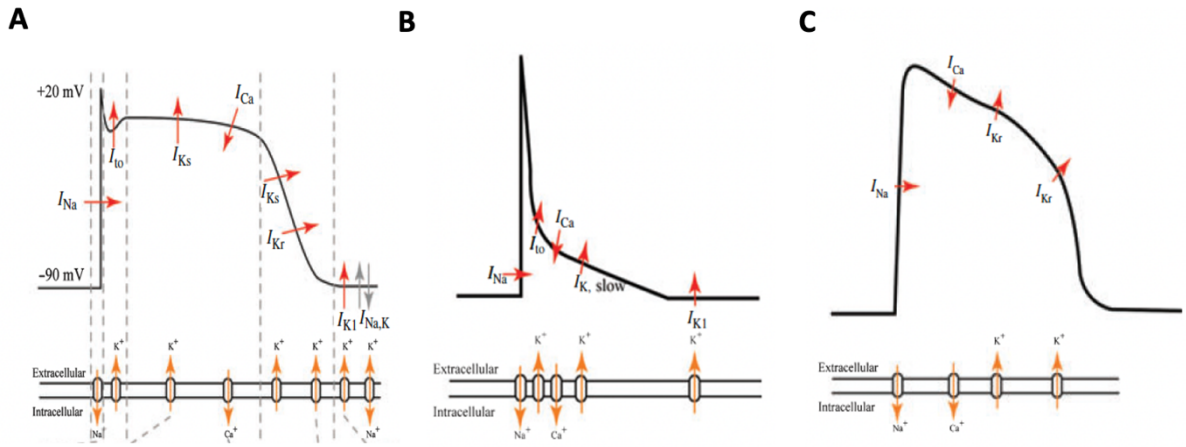

Figure I 5: Diagrammatic representation of an AP recording depicting the electrical activities from a single cardiomyocyte. The direction of the arrows indicates the direction the flow of ions into and out of the cell. **(A)** Human: AP can be divided into five main phases including phases of depolarization, early repolarization, extended repolarization with relaxation between contractions, further repolarization, and maintenance of the resting membrane potential until the next electrical stimulation. **(B)** Mouse: There is rapid depolarization at the beginning followed by rapid repolarization that slows to form a shoulder/low plateau phase before returning back to resting membrane potential. **(C)** Zebrafish: There is a rapid depolarization followed by a large plateau phase before repolarization takes place. Adapted from Salama & London, 2007, Brette et al., 2008 and Leong et al., 2010.

1.3.2. Anatomy and physiology of the zebrafish heart

The heart is the first organ to form and function during vertebrate embryo development. The development of the zebrafish heart can be divided into several stages, including the *early heart tube formation*, *looping morphogenesis*, *valve development* and *chamber maturation (*Kemmler et al., 2021). Although composed of only two chambers compared with the four-chambered human heart, the general processes and cellular lineages of cardiovascular development, heart structure and composition are well conserved between the two species (Bakkers, 2011; Genge et al., 2016; C. T. Nguyen et al., 2008).

The adult zebrafish heart is composed of **two chambers**, *one atrium* and *one ventricle*, **the sinus venosus** and **the bulbus arteriosus** (or outflow tract) (Figure I 6 A, B) and it has an average size of »1-1,5 mm^3 (N. Hu et al., 2001). The blood from all the body is collected from the sinus venosus and enters the atrium. Then is pumped to the ventricle and finally exits through the outflow tract, which transfers the blood to the gills for oxygenation. The lack of pulmonary circulation permits this single-circulation blood flow system.

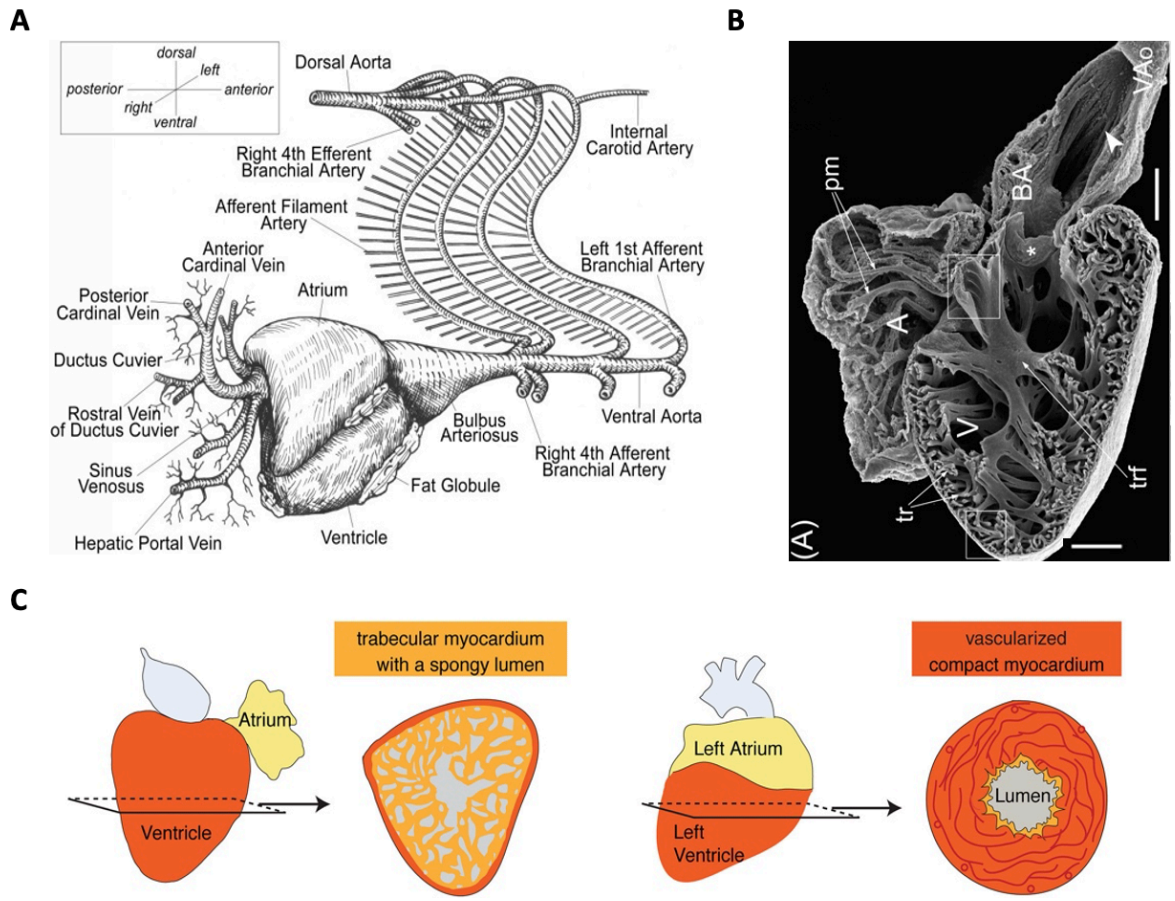

Figure I 6 Anatomy and morphology of the zebrafish heart. (A) An illustration of a posteroanterior view of an adult zebrafish heart and the major vasculature in the cardiac region. **(B)** Scanning electron microscopy of the sagittal section of the left half of a zebrafish heart depicting the atrium (A), ventricle (V), bulbus arteriosus (BA), and a portion of the smooth-walled ventral aorta (VAo). The asterisk indicates the bulboventricular valve. **(C)** The diagram compares ventricular anatomy in fish (left) and mammals (right). In poikilothermic vertebrates like fish, amphibians, and reptiles, the trabecular, sponge-like ventricle allows for direct oxygenation of cardiomyocytes, facilitating heart regeneration in species like zebrafish, newts, and axolotls. In contrast, the compaction of the myocardial wall and elaboration of the coronary vasculature in endothermic vertebrates, correlated with increased cardiac workload, are associated with a lack of regenerative capabilities. Abbreviations: tr, trabeculae; trf, trabecular fold; pm, pectinate muscle. Scale bar = 100 µm in B. Adapted from Hu et al., 2001 and Jaźwińska et al ., 2016.

The zebrafish ventricle, similar to mammals, is composed of three tissue layers. The **myocardium,** which comprises the contractile cardiomyocytes, is surrounded by a single-cell-thick layer both inside and outside named **endocardium** and **epicardium** respectively. The myocardium can structurally be divided in a peripheral wall of compact muscle and an inner trabecular muscle. The compact myocardium can be further categorized into the primordial and the cortical layers (N. Hu et al., 2001). However, some differences can be observed, such as the high proportion of trabecular myocardium and lower metabolic state in zebrafish when compared to human (Jaźwińska & Sallin, 2016). This change in cardiac anatomy in homeothermic mammals, could potentially had an impact on the regenerative capabilities of the heart, that is not correlated with this architecture (Figure 6 C).

1.3.3. Zebrafish cardiac injury and regeneration models

Due to its relatively small size, common methods used in larger animals to induce infarction of the myocardium, like coronary artery ligation (or LAD ligation) are not readily applicable to zebrafish. Instead, the first method used to induce injury in the zebrafish heart was ventricular amputation (Poss et al., 2002), although the great interest in heart regeneration research has since led to the development of other injury models to induce tissue death in the zebrafish heart.

The **ventricular apex resection** is a surgical procedure that is performed to remove approximately 20-25% of the ventricle with fine scissors, leading to significant bleeding (Figure I 7 A) (Poss et al., 2002; A. Raya et al., 2003). The reduced blood pressure and volume of the zebrafish heart allows for an immediate clotting that is sufficient to seal the ventricle and prevent exsanguination. Within the first 2-3 days post-amputation (dpa), there is a temporary deposition of collagen, which is eventually replaced by contractile cardiomyocytes. The correct cardiac regeneration involves other key processes such as the activation of epicardium and endocardium, cardiomyocyte proliferation, revascularization, and innervation of the newly formed myocardium (González-Rosa et al., 2017; Lien et al., 2012). It takes 30-60 days for the regeneration process to be complete after apex resection, as evaluated by the complete growth of the lost tissue that is indistinguishable from a non-injured myocardium (Poss et al., 2002; A. Raya et al., 2003).

In the **cryoinjury** model, a thin metal filament is precooled in liquid nitrogen and then applied briefly to the ventricular surface to freeze a portion of it (Figure I 7 B) (Chablais et al., 2011; González-Rosa et al., 2011). The fast freezing and thawing results in tissue necrosis. Compared to apex resection, cryoinjury induces a more severe apoptotic response in the area surrounding the injury site. After the injury, the immune system is activated leading to an infiltration of immune cells in the area that trigger remodeling of the extracellular matrix (ECM) and deposition of fibrotic tissue. Finally, the fibrotic scar is cleared and then repopulated by cardiomyocytes (González-Rosa et al., 2017; Jaźwińska & Sallin, 2016). The regeneration of the myocardium after cryoinjury is significantly slower than that induced by apex resection, and the injury severity affects the recovery window (Bise et al., 2020). The process can take up to 3-4 months for fully regeneration or even more (6 months) when thicker filaments are used to induce a greater injury and thus greater scar tissue formation. The cryoinjury model has shown that fibrosis is not an inhibitory process for heart regeneration (Lien et al., 2012; Ryan et al., 2020). After regeneration, the functionality of the heart is fully restored, although signs of ventricular remodeling may appear such as enlargement of the ventricle, thickening of the wall of the damaged area, and acquisition of more rounded ventricular shape.

A third strategy to induce heart regeneration in the zebrafish is to cause cardiomyocyte death by **genetic ablation**. This system relies on the inducible expression of toxins such as the diphtheria toxin chain A (DTA) or of enzymes that catalyze the production of cytotoxic metabolites (Figure I 7 D) (Curado et al., 2007; J. Wang et al., 2011). Metronidazole (Mtz) is a non-toxic agent that can be metabolized by the bacterial nitroreductase (NTR), generating a toxic metabolite that induces cell death. The NTR method is a conditional system that allows temporal control of the ablation as Mtz can be removed from water at will, resulting in cardiomyocyte recovery (Figure I 7 C) (Curado et al., 2007). It has also been used for the genetic ablation of other cardiac cell types like epicardial cells, fibroblasts, or immune cells (Cao et al., 2017; Hui et al., 2017; Sánchez-Iranzo, Galardi-Castilla, Sanz-Morejón, et al., 2018).

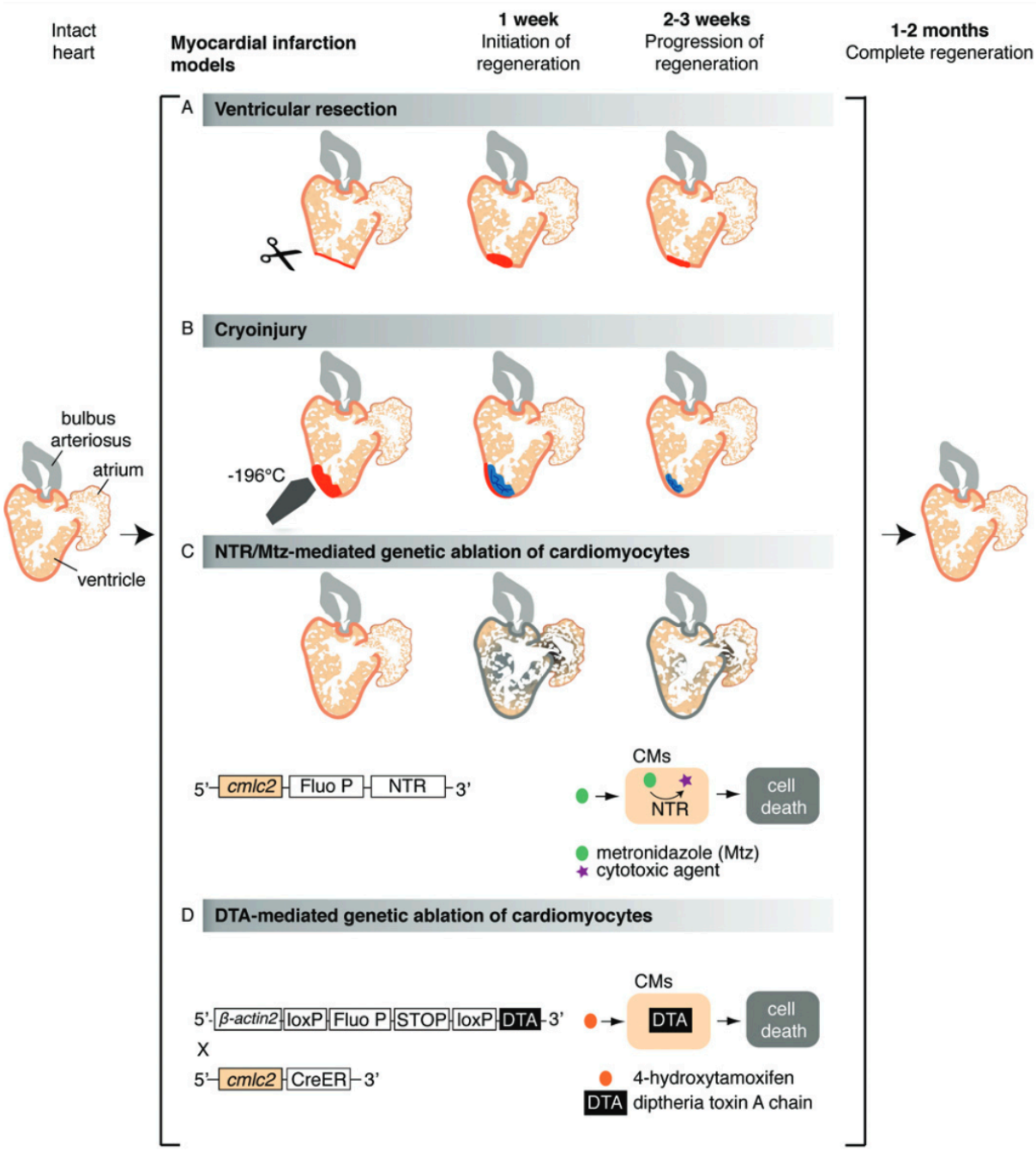

Figure I 7 Cardiac injury models in zebrafish. (A) Apex amputation removes approximately 20% of the ventricle, leading to the formation of a fibrin clot. **(B)** Cryoinjury induces local tissue necrosis (around 20% of the ventricle) and triggers apoptosis. **(C)** The NTR/Mtz genetic ablation system allows the inducible depletion of specific cardiac cell types, first applied to zebrafish in 2007. This method involves the expression of a bacterial nitroreductase fused to a fluorescent protein (Fluo P) under the control of a tissue-specific promoter, such as cardiac myosin light chain 2 (cmlc2), specific for CMs. This enzyme converts the prodrug metronidazole into a cytotoxic agent, inducing cell death in the NTR-expressing cells. **(D)** The Cre/loxP transgenic system, developed in 2011, involves the inducible expression of DTA in CMs. This system uses a double transgenic approach, including Tg(βactin2:loxP-Fluo P-STOP-loxP-DTA), containing an inducible cytotoxic DTA gene, and Tg(cmlc2:CreER) 98, allowing the expression of the 4-hydroxytamoxifen (4-HT)-inducible Cre recombinase in cardiomyocytes. Treatment of intercrossed fish cmlc2:CreER;βactin2:loxP-Fluo P-STOP-loxP-DTA results in significant myocardial cell depletion, up to 60% of the ventricle. Adapted from Jaźwińska et al ., 2016.

An approach to better model the human myocardial infarction has led to the establishment of the **hypoxia/reoxygenation** model. The animals are exposed for a short time to hypoxia conditions before returning them to normoxic water (Parente et al., 2013). This results in the reduction of the functionality of the cardiac tissue. Although the injury induces cardiomyocyte apoptosis and proliferation, no evident alterations are visible histologically. The main limitation of this model is the lack of specificity of the injured tissue, as other organs are affected as well due to the exposure to hypoxia.

Apart from these models, various approaches have been followed to create less severe injuries such as piercing or scratching of adult hearts (Itou et al., 2014). In the first one, a similar but milder response to apex resection is observed with shorter duration, while the second can be used for epicardium regeneration studies.

1.3.4. Cellular and molecular dynamics of zebrafish heart regeneration

Zebrafish heart regeneration is a dynamic process that involves the contribution of many different cardiac cell types and the interactions between cardiomyocytes and non-cardiomyocytes (Gemberling et al., 2013; González-Rosa et al., 2017). Transcriptomic data meta-analysis identifies gene expression changes in the regenerating zebrafish heart that are shared across different injury models, as well as those that are specific to each model (Botos et al., 2023). However, the main molecular and cellular mechanisms involved in zebrafish heart regeneration appear to be common for all injury models. The main events that occur chronologically, in a simplified manner, during heart regeneration are shown in Figure I 8. The main key regulators of cardiac regeneration are described below:

Upon cardiac injury, the first line of action includes the triggering of the **immune response** and the activation of the endocardium. As early as 3 hours post-amputation (hpa), we observe the recruitment of phagocytes and neutrophils by cytokines and other molecules (González-Rosa et al., 2017; Ross Stewart et al., 2022). Anti-inflammatory drug administration or ablation of these immune cells impairs regeneration by hindering revascularization and cardiomyocyte proliferation, resulting in accumulation of fibrotic scar (Huang et al., 2013). The timing of immune cell recruitment at the injury also appears of great importance. By

delaying macrophage recruitment in regenerating hearts, Lai et al observed impairments in the revascularization, cardiomyocyte proliferation, neutrophil clearance, and scar resolution (Lai et al., 2017).

A few hours after injury, the **endocardial cells** partially detach from the adjacent myocardium and acquire a rounder shape. These changes in morphology coincide with the reactivation of embryonic genes such as *raldh2,* encoding for retinoic acid (RA) synthesizing enzyme, and the transmembrane receptor *heart of glass (heg)* (Kikuchi et al., 2011). Although these changes are initially organ-wide, they become rapidly localized to the wound area. Following activation, the endocardium undergoes rapid proliferation and migrates internally to contribute regenerating the injured area.

As early as 1-3 DPA, the **epicardium** is activated and re-expresses embryonic markers such as *raldh2*, *wt1b*, and T-box transcription factors such as *tbx12* and *tbx18* (Kikuchi et al., 2011). Epicardial activation initially occurs throughout the entire organ, but gradually becomes limited to the injury site. A study by Wang et al. demonstrated that enclosure of the wound by the epicardium is crucial, given that genetic ablation of epicardial cells (tcf21-positive cells) dramatically diminished cardiomyocyte proliferation and hampered the overall regeneration process (J. Wang et al., 2011). This directional migration of epicardial cells to the injury area is controlled by the hedgehog signaling pathway (J. Wang et al., 2015). Studies by Uroz et al., underscored the significance of mechanical interactions between the extracellular matrix and zebrafish epicardial cells, revealing that traction forces at the cytokinetic ring regulate mitosis and polyploidy during epicardial proliferation (Uroz et al., 2019).

The establishment of **new vasculature**, both coronary and lymphatic, is another crucial event during heart regeneration. In the cryoinjury model, the revascularization starts at 15 hpi with vascular sprouting observed in the wound area (Ross Stewart et al., 2022; Ryan et al., 2020). Further experiments with overexpression of dominant negative form of *vegfaa* for inhibition of revascularization or cxcr4a$^{-/-}$ animals with an already impaired vascular network, showed impaired heart regeneration (Harrison et al., 2015; Marín-Juez et al., 2016). Also, failure in lymphatic regeneration leads to considerable scarring and lower resolution of immune cells .

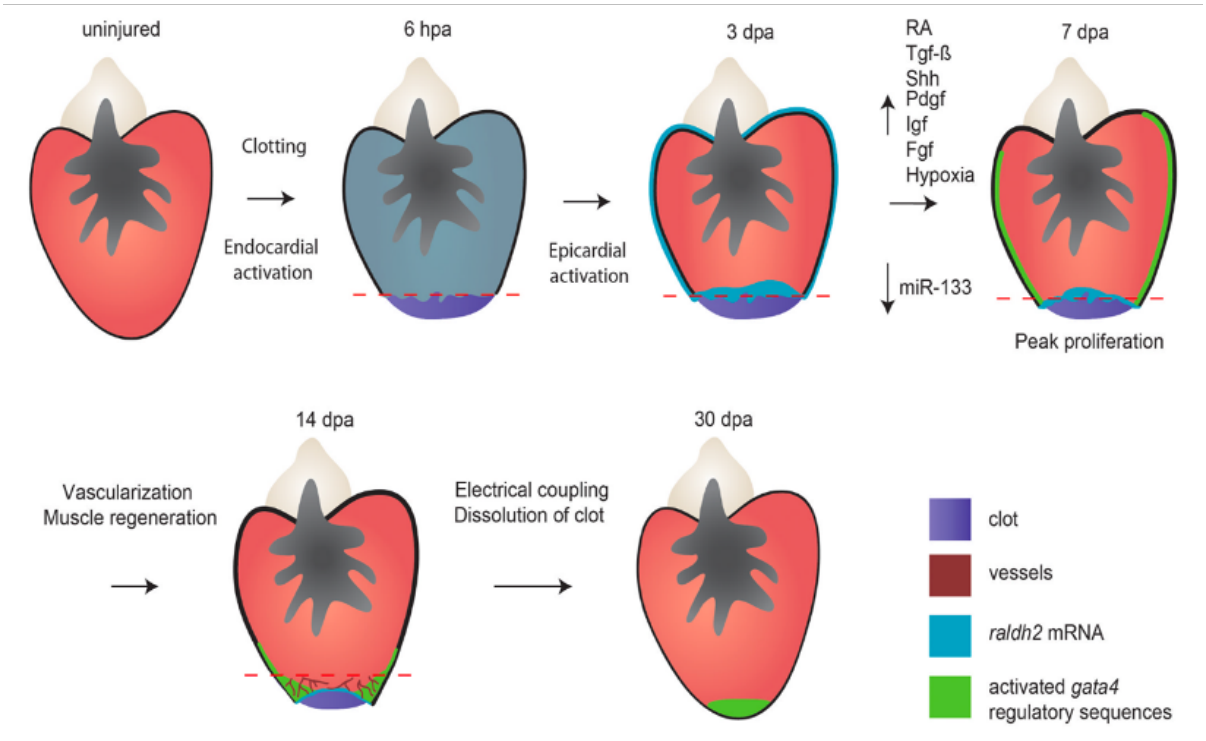

Figure I 8 Zebrafish heart regeneration after partial resection of the ventricle. Following injury, the RA-synthesizing enzyme, aldh2, is induced throughout the endocardium within a few hours of amputation, later extending to the epicardium before localizing to the wound. By 7 DPA, *gata4* regulatory sequences become active across the cortical muscle layer of the ventricle, stimulating cardiomyocyte proliferation influenced by hypoxia and signaling pathways as detailed in the main text. Epicardial cells integrate into the wound during this period. By 14 DPA, vascularization of the regenerating muscle initiates with assistance from Fgf and Pdgf signaling. By 30 DPA, a new cardiac muscle wall is typically formed, primarily by the progeny of early cardiomyocytes activating gata4 sequences. At this stage, the myocardium is vascularized and electrically coupled with the existing muscle. Adapted from Gemberling et al., 2013.

Upon injury, the **nerves** present in the ventricular surface start regrowing to the regenerated area (Ryan et al., 2020). Mahmoud et al described that inhibition of innervation upon injury impairs the cardiac regeneration, and that can be partially rescued by the administration of neuregulin 1 (NRG1) and nerve growth factor (NGF) recombinant proteins (Mahmoud et al., 2015). That was firstly shown by overexpression of a neural chemorepellent, *sema3aa,* exclusively in cardiomyocytes and further validated with pharmacological inhibition of cholinergic, but adrenergic, signaling. However, the initiation process of innervation of the regenerated area still remains unclear and further research must be done regarding the role of nerves during zebrafish heart regeneration.

The **extracellular matrix** is composed of a variety of proteoglycans, glycoproteins and collagens and forms a complex network to provide both structural and mechanical support to tissues (Garcia-Puig et al., 2019). In addition, its composition and mechanical properties provides cues for proliferation, differentiation, cell death and migration. The ECM remodeling upon heart regeneration, in neonatal mice and zebrafish, includes changes both in the composition and mechanical properties of the tissue, providing a permissive environment for regeneration to occur (Garcia-Puig et al., 2019; Notari et al., 2018). In a study by Chen et al., cardiomyocyte proliferation and enhanced cardiac function was achieved in infarcted mice by injection of purified regenerating zebrafish ECM (W. C. W. Chen et al., 2016). One of the key differences between mammalian and zebrafish hearts when an injury is induced, is how fibrosis will lead to permanent scar in one but resolution to the other (Ryan et al., 2020). In zebrafish, matrix metalloproteinases, such as *mmp2, mmp14a* and *mmp14b,* are mainly controlling the collagenolytic activity at the wound site in the middle stages of regeneration.

Understanding the **myocardial contribution,** or the key regulators of heart regeneration which are cardiomyocyte proliferation, migration, and repopulation of the area with functional cardiomyocytes, result many studies to be focused on the generated signals during regeneration that prompt cardiomyocyte to re-enter the cell cycle (Gemberling et al., 2013; Ross Stewart et al., 2022; Ryan et al., 2020). The activated epicardium, endocardium, circulating cells along with the new vasculature and permissive environment formed by the ECM remodeling are providing numerous cues and signals to the cardiomyocytes. These may include BMP, Nrg1, Shh, Igf, Tgfβ, RA, Notch and NF-κB signaling (Choi et al., 2013; Gemberling et al., 2015; Kikuchi et al., 2011; A. Raya et al., 2003; Wu et al., 2016). These signals are eventually received by the cardiomyocytes that are close to the injury site. Lineage tracing experiments have demonstrated that the new cardiomyocytes originate from pre-existing cardiomyocyte that re-enter the cell cycle upon partial dedifferentiation (Jopling et al., 2010; Kikuchi et al., 2010). These dedifferentiated cardiomyocytes are facing transcriptional and structural changes including disassembly of the sarcomere and expression of the embryonic markers. Other studies have shown that epigenetic mechanisms, post-transcriptional regulation by micro-RNAs (miRNAs) and TREEs play an important role in the regulation of cardiomyocyte proliferation and their contribution should not be left unnoticed (Kang et al., 2016; Kraus, 2022; Ribeiro et al., 2022; Yan et al., 2023).

So far, our knowledge has increased a lot regarding the regeneration of epicardium, vasculature and other components of the cardiac tissue and their contribution to regeneration but yet it remains unclear how cardiomyocyte proliferation is governed, and further study must be done to decipher the mechanism that orchestrates the whole process.

1.4. Molecular tools for genetic manipulation of zebrafish

Zebrafish embryos offer the advantage of non-invasive, high-resolution imaging, which allows researchers to visualize and study developmental processes in real time. This has generated the need for the development of a variety of tools for the genetic manipulation of zebrafish (Koster & Sassen, 2015; Rafferty & Quinn, 2018). One of the first strategies followed to introduce mutations in zebrafish embryos was the random **chemical mutagenesis** with N-ethyl-N-nitrosourea (**ENU**), an alkylating agent that modifies single DNA bases resulting in randomly distributed point mutations (Solnica-Krezel et al., 1994). These mutations can further inherit to the next generation (Figure I 9 A). This type of mutagenesis is highly efficient; however, intensive screening is needed to identify the point mutation. Another approach to interfere with a gene's function is the injection of **morpholinos**, antisense oligonucleotides, into early embryos (Figure I 9 B). These stable oligonucleotides, due to the replacement of the deoxyribose ring with a morpholine ring, are designed to block translation of splicing of targeted genes (Koster & Sassen, 2015; Rafferty & Quinn, 2018; Summerton & Weller, 1997). Although morpholinos have been commonly used among the years, many concerns have raised regarding the specificity of the technique. Due to their off-target effects, sometimes the resulting phenotypes are hard to interpret, and other studies has shown that upregulation of apoptotic activity upon morpholino injection, is masking the actual phenotype. For functional gene analysis by expression of gain- and loss-of function of a desired gene, **RNA interference (RNAi)** approaches or **injection of synthetic capped mRNA** encoding the protein of interest can be injected into early embryo stages (Figure I 9 C and D) (Koster & Sassen, 2015; Rosen et al., 2009). This method is often used to rescue loss-of-function phenotype in the early developmental stages. An alternative to these methods that do not modify the sequence of the DNA is the random **integration of exogenous DNA** (Figure I 9 E) (Koster & Sassen, 2015). This strategy relies on transposon- or viral-based methods to introduce a desired DNA fragment into the zebrafish genome.

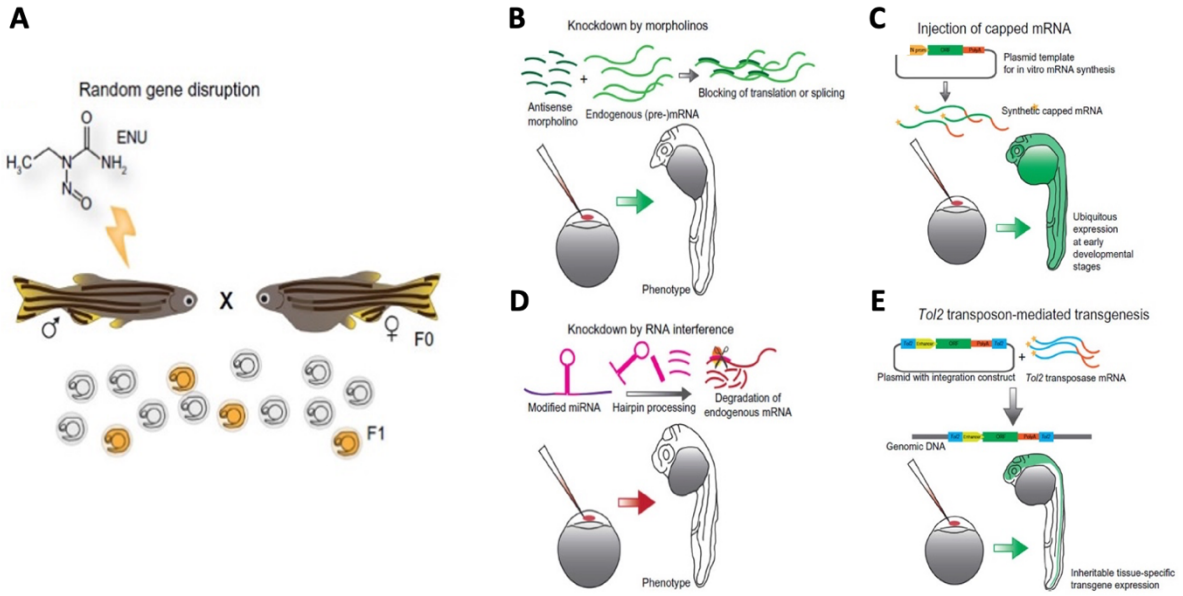

Figure I 9 Knock -out or -down of gene function & expression of transgenes in zebrafish. (A) ENU induces point mutations in the genome, which can be passed on to the next generation (orange-colored embryos). **(B)** Transient knockdown is possible through the injection of an antisense morpholino into the early embryo, blocking the translation or splicing of the mRNA encoding the protein of interest. **(C)** Injection of synthetic capped mRNA into one-cell embryos results in global expression throughout the early embryo. **(D)** A novel knockdown technique in zebrafish involves using modified miRNAs that match the mRNA encoding the protein of interest, leading to degradation by the endogenous RNA interference machinery. **(E)** Stable transgenesis is achievable through transposon-mediated integration into the genome, allowing for inheritable and even tissue-specific expression of the transgene. Abbreviations: mRNA, messenger RNA; miRNA, microRNA, ORF, open reading fram. Adapted from Sassen et al., 2014.

Finally, the sequencing and almost full annotation of the zebrafish genome has allowed researchers for the development of more precise, targeted mutagenesis approaches (Howe et al., 2013; Rafferty & Quinn, 2018, 2018). **Genome editing** can produce heritable changes in the genome for the generation of stable mutant zebrafish lines and utilizes specifically designed endonucleases for sequence-specific manipulation (Figure 1 10 A and B). This includes Zinc Finger Nucleases (**ZFNs**), Transcription Activator-like Effector Nucleases (**TALENs**) and Clustered Regularly Interspaced Short Palindromic Repeats (**CRISPR**) (Koster & Sassen, 2015; Ott de Bruin et al., 2015; Rafferty & Quinn, 2018; Uribe-Salazar et al., 2022). All three techniques work in similar mechanism, where double strand breaks (DSB) are introduced in the DNA, which are fixed by endogenous DNA repair pathways. These DSBs, are more frequently repaired by the error-prone Non-Homologous End Joining (NHEJ) rather than the Homology Directed Repair (HDR) pathway (Figure I 12 B) (Chatterjee & Walker, 2017).

Thus, random insertion or deletion (indel) of nucleotide bases are introduced in the genome, that can lead to a variety of mutations. Disruption of the open reading frame (ORF) can subsequently alter the protein structure and lead to a loss-of-function phenotype. On the contrary, **Prime editing** and **Base editors** allow for precise alteration of a specific DNA sequence or individual nucleotide respectively, without the need of causing DSB or donor DNA template (Petri et al., 2022; Rosello et al., 2022). For this reason, are emerging as a cutting-edge technology with potential therapeutic applications.

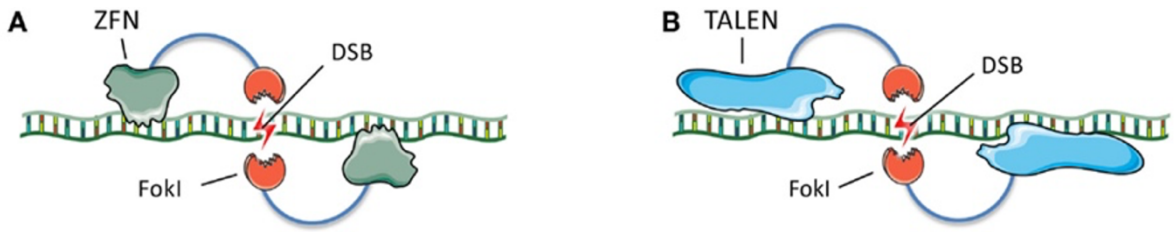

Figure I 10 Schematic representation of ZFNs and TALENs. (A) Two ZFN dimers bind DNA and position their FokI nuclease domains such that they dimerize and generate a DSB between the binding sites. **(B)** TALENs, similar to ZFNs, bind DNA and generate a DSB upon dimerization of their FokI domains. Adapted from Bruin et al., 2015.

The availability of molecular tools for the genetic manipulation of zebrafish has greatly facilitated studies in many areas and contributed advancing research in fields such as genetics, developmental biology, and neuroscience.

1.4.1. Tol2 transposon system

Transgenesis is an essential tool for any genetic model and the method used can vary between the different model systems. The integration of a transgene into the genome of an organism enables the labeling and live imaging of cells, lineage tracing experiments and can also be combined with spatio-temporally expression of other genes of interest for the investigation of molecular pathways (Clark et al., 2011; Koster & Sassen, 2015). In zebrafish transgenesis, different transposon-based tools have been utilized over the years such as *Sleeping Beauty, Tol1* and *Tol2.* However, the Tol2 system is the most commonly used due to its high integration efficiency and well characterized function, resulting in germline transmission and inheritance of the transgenic trait.

The Tol2 system consists of the transposase mRNA and a Tol2 transposon-donor plasmid which contains the transgene of interest (Kikuta & Kawakami, 2009). The synthetic capped mRNA and the plasmid are introduced into one-cell stage embryos with microinjection (Figure I 11 A). The *Tol2* transposon element was first reported in Medaka fish and since its initial characterization of transposon activity in zebrafish a lot of progress has been made. Minimal *Tol2 cis* sequences (around 200 base pairs (bp)) are necessary and can be cloned to the flanking sites of any desired transgene (Clark et al., 2011; Kikuta & Kawakami, 2009). This led to the generation of the Tol2 kit, a three-fragment gateway multisite

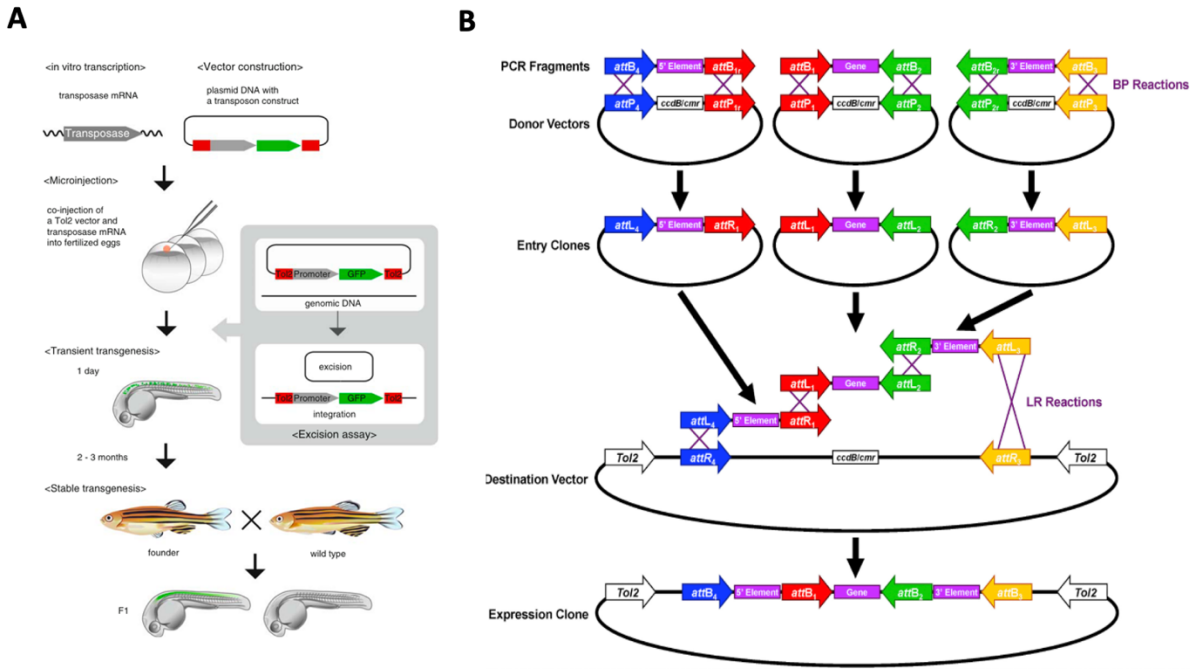

Figure I 11 A scheme for transient and stable transgenesis in zebrafish with the Tol2 kit. (A) In zebrafish, co-injecting in vitro-synthesized transposase mRNA and a Tol2 construct-containing plasmid into fertilized eggs leads to the integration of Tol2 into somatic cells, causing mosaic GFP expression. Stable transgenesis results in efficient integration into germ cells, with over 50% of injected fish transmitting Tol2 insertions to a portion of their F1 generation. F1 embryos carrying Tol2 insertions display non-mosaic expression of the reporter gene. **(B)** Multisite Gateway cloning facilitates the assembly of multiple fragments into a single destination vector. Differing from standard Gateway cloning, this method leverages the site-specificity of four distinct att sites to recombine multiple fragments into a unified construct in a single step. Adapted from Kikuta et al., 2009, and Raffeti et al., 2018

recombination cloning strategy that can easily generate a Tol2-based onstruct in a fast modular assembly of [promoter]-[transgene of interest]-[3' tag] in a *Tol2* transposon

backbone (Figure I 11 B) (Kwan et al., 2007). The Tol2 kit is famous among the zebrafish community and constantly updated with new entry/destination plasmid clones.

However, the integration takes place stochastically leading to problems such as position effects and silencing of transgene. For these reasons, and also depending on the application, a more targeted approach maybe be required to be followed, for the creation of knock-in (KI) zebrafish lines (Kimura et al., 2014; Ranawakage et al., 2021).

1.4.2. CRISPR/Cas9 system

The CRISPR and CRISPR associated protein-9 (Cas9) have revolutionized the field of genetic engineering due to the simplicity of the system, high precision, reduced cost, and numerous applications (Doudna & Charpentier, 2014). The CRISPR/Cas9 system is part of the bacterial adaptive immune response, found in most bacteria and archaea, recognizing, and cleaving foreign genetic elements. The presence of a protospacer associated motif (PAM) is required for the endonuclease activity of the protein. In the case of the most commonly used CRISPR associated protein, the Cas9, derived from the human pathogen *Streptococcus pyogenes* (SpCas9) a native 5'-NGG-3' is required (Figure I 12 A) (Doudna & Charpentier, 2014; Koster & Sassen, 2015; Uribe-Salazar et al., 2022). Other Cas enzymes found in nature or engineered variants may require different, or none, PAM sites. The system also needs an engineered single-chimeric guide RNA (sgRNA) that bears homology to a genetic locus and provides target specificity.

The Cas9 can be delivered in different forms such as plasmid, mRNA, or protein. In the last case, an extra step of assembling the Cas9 with the sgRNA is required for the generation of the ribonucleoprotein (RNP) complex (Doudna & Charpentier, 2014). Studies has shown that for zebrafish genome editing, microinjection of RNPs is protecting sgRNA degradation and efficiently increase the rate of indels when compared with other forms of delivery (Hoshijima et al., 2019; Kroll et al., 2021).

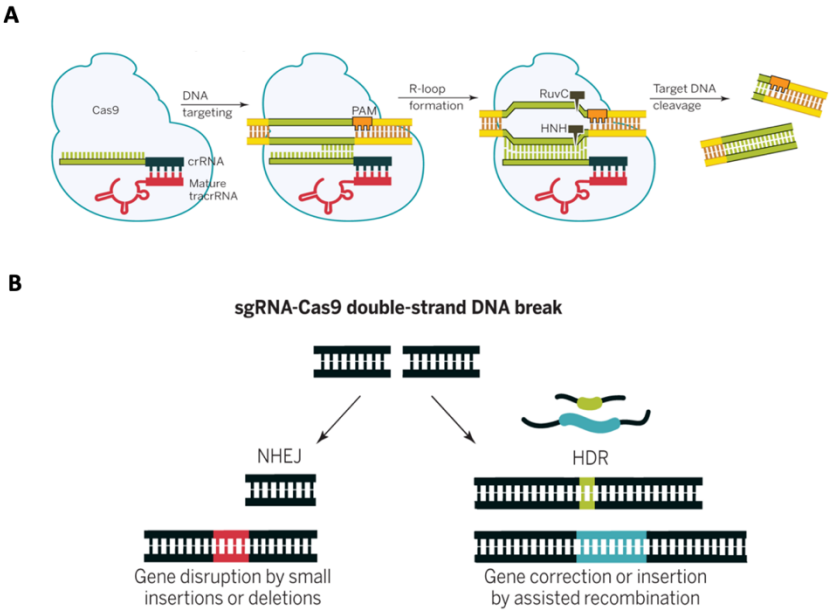

Figure I 12 Genome engineering mediated by CRISPR/Cas9 system. (A) Site-specific DNA recognition is mediated by the chimeric tracrRNA:crRNA, which harbours complementarity to the protospacer. The presence of 5'-NGG-3', PAM site, is required for Cas9 endonuclease activity. DSBs is produced by the HNH and RuvC nuclease domains. **(B)** DSBs can be repaired by NHEJ or HDR repair mechanisms. Adapted from Doudna and Charpentier, 2014.

A variety of efficient Cas9 variants and derivatives has resulted in a broad range of application of the system including the modulation of the transcriptome or epigenome editing (Goell & Hilton, 2021; C. Xu et al., 2021). Generation of genetic scars in zebrafish, has been successfully used for lineage tracing experiments and identification of rare cell type origins (B. Hu et al., 2022; Spanjaard et al., 2018).

1.5. Single-cell transcriptomics technologies & Next Generation Sequencing

Next-generation sequencing (NGS) is a technology that can massively sequence in parallel hundreds and thousands of genes or whole genomes in short period of times. It has a variety of applications and already been used both in research and diagnostics (Anaparthy et al., 2019; Jovic et al., 2022). NGS-based technologies for transcriptomics or epigenomics has reshaped the field of genetics and are currently providing insightful knowledge in subjects like cancer, neurobiology, and embryology. Technological advancements and the decreasing cost of NGS have revolutionized the field of single-cell transcriptomics to profile cells at the individual level (B. Hwang et al., 2018). This technology, also known as **single-cell RNA**

sequencing (scRNA-seq), has the potential to gain insight in the ''uniqueness'' of individual cells leading to the identification of rare cell populations, track cell trajectories and study the expression of genes that were masked in bulk populations (Anaparthy et al., 2019; Baysoy et al., 2023; Jovic et al., 2022). For this reason, single-cell technologies have emerged as a powerful tool to dissect the heterogeneity of cells in cases like cancer tumors, development, immunology, and regenerative biology (Anaparthy et al., 2019; Ashton et al., 2021; B. Hwang et al., 2018).

Over the years, different techniques have been developed for single-cell isolation (Figure I 13). The isolation of individuals cells may include manual micromanipulation, flow-activated cell sorting (FACS), laser capture microdissection (LCM) or magnets conjugated with antibodies (Guo et al., 2017; Julius et al., 1972; Nichterwitz et al., 2016; Riethdorf et al., 2018). The rapid expansion of microfluidic technology has given rise to the development of **Droplet-based microfluidic** systems that permits the encapsulation of cells in oil droplets. Monodispersing of aqueous droplets in a continuous oil phase allows the encapsulation of a single cell with a single microparticle, known as uniquely barcoded bead (Islam et al., 2014; Utada et al., 2005). The microenvironment, or compartmentalization, created by the oil droplet is used for the first steps of the library preparation. After cell lysis, the mRNA molecules are captured by the barcoded beads and then reverse transcribed into first-strand complementary DNA (cDNA).

Among the different sequencing platforms available, some examples include Drop-seq, STRT-seq, InDrop, Smart-seq2, SNARE-seq and TEA-seq (Baysoy et al., 2023). Chromium from 10x Genomics, is a commercial droplet-based platform, that offers high-throughput profiling of cells with high capture efficiency (Ashton et al., 2021). These methods may vary in the cell isolation, cell lysis, library preparation and Unique Molecular Identifier (UMI) tagging (3' end or 5' end). Nonetheless, their main difference is their transcript coverage with some of them providing full-length sequencing and some other only partial from either 3' or 5' of the transcript.

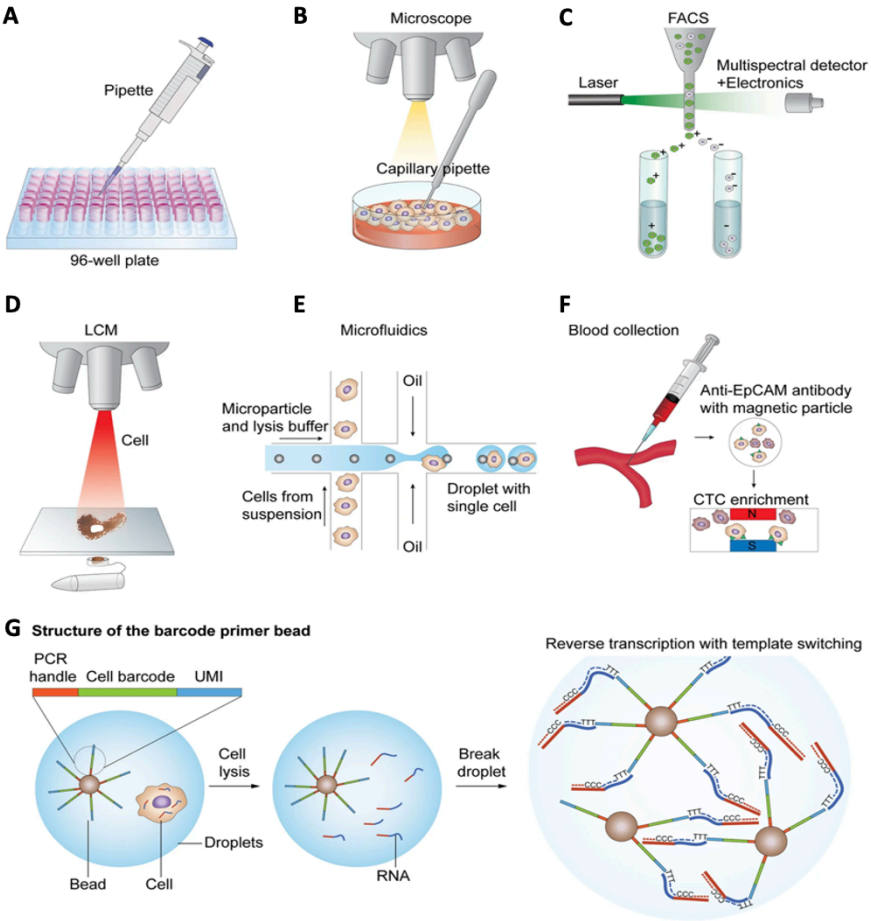

Figure I 13 Methods for single-cell isolation. (A) The limiting dilution method isolates individual cells, leveraging the statistical distribution of diluted cells. **(B)** Micromanipulation involves collecting single cells using microscope-guided capillary pipettes. **(C)** FACS isolates highly purified single cells by tagging cells with fluorescent marker proteins. **(D)** Laser capture microdissection (LCM) utilizes a laser system aided by a computer system to isolate cells from solid samples. **(E)** Microfluidic technology for single-cell isolation requires nanoliter-sized volumes. An example of in-house microdroplet-based microfluidics (e.g., Drop-Seq). **(F)** The CellSearch system enumerates CTCs from patient blood samples by using a magnet conjugated with CTC binding antibodies. **(G)** A schematic example of droplet-based library generation. Libraries for scRNA-seq are typically generated via cell lysis, reverse transcription into first-strand cDNA using uniquely barcoded beads, second-strand synthesis, and cDNA amplification Adapted from Byungjin et al., 2018.

Depending on the single-cell technology used, the bioinformatic pipeline necessary for the analysis of the data may differ. However, there are basic steps that are common among the different analysis tools such as Seurat (Hao et al., 2021) or Scanpy (Wolf et al., 2018) and may include (Figure I 14): *Normalization* of the counts to make expression rates comparable between cells. *Filtering of low-quality cells* by excluding cells with high amount in total reads, high mitochondrial RNA (mtRNA) content or low number of genes. *Feature*

selection by identifying high-variable genes that contain biological information and will further facilitate the *Dimensionality Reduction* of the data through linear *(Principal Component Analysis (PCA))* or non-linear *(t-distributed stochastic neighbour embedding (t-SNE)* or *Uniform Manifold Approximation and Projection (UMAP))* transformation algorithms. And finally, *clustering* of the cells based on similarities in their transcriptomic profile (Jovic et al., 2022; Paik et al., 2020).

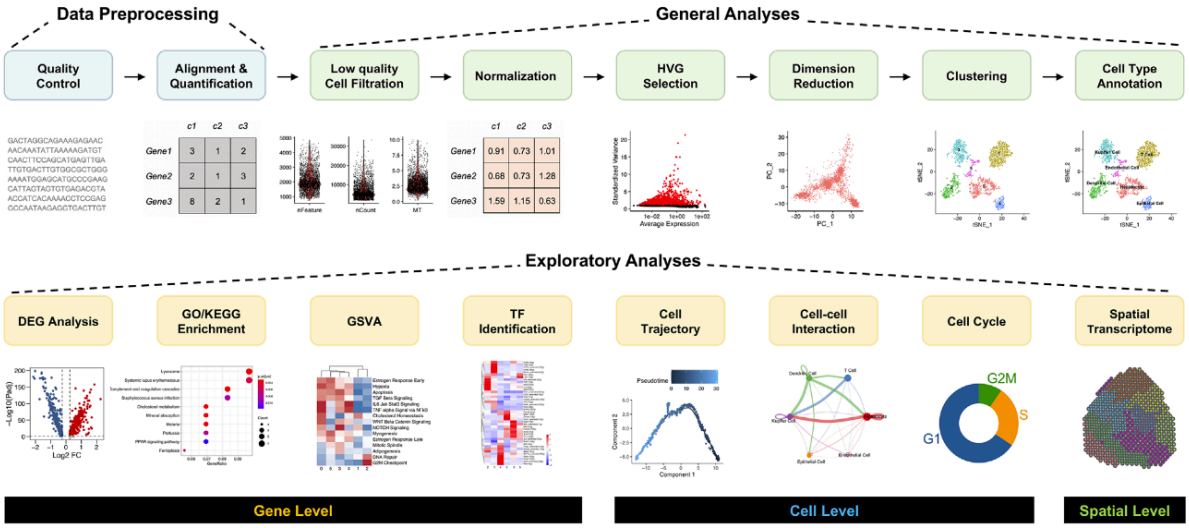

Figure I 14 Workflow for typical single-cell RNA sequencing data analysis. The conventional framework for analyzing scRNA-seq data comprises three main stages: data preprocessing (blue panel), general analyses (green panel), and exploratory analyses (yellow panel). Abbreviations: HVG, highly variable gene; DEG, differentially expressed gene; GSVA, gene set variation analysis; TF, transcription factor. Adapted from Jovic et al., 2022.

Despite the continuous success of scRNA-seq, in most cases the cells must be isolated intact and viable from tissues, which results in cell death, stress responses and the loss of the spatial information (Adil et al., 2021; Baysoy et al., 2023; Williams et al., 2022). The location of cell within a tissue and its arrangement concerning its neighboring cells and structures can provide information regarding its identity, cell state, and interaction with other cells. For these reasons the field of **spatial transcriptomics** is gaining more and more interest over the years and named 'Method of the Year 2020' by *Nature Methods* ('Method of the Year 2020', 2021). **Spatial enhanced resolution omics-sequencing (Stereo-seq)** is an emerging new technology that enables simultaneous profiling of hundreds to thousands of genes at subcellular resolution. Stereo-seq combines DNA nanoball (DNB)-patterned arrays and *in situ* RNA capture from fixed tissue (Figure I 15) (A. Chen et al., 2022). The high-resolution of

Stereo-seq allows efficient image-based cell segmentation, larger capture area and higher number of captured transcripts than other reported methods such as DBiT-seq (Y. Liu et al., 2020) and Visium (10x Genomics) (Ke et al., 2013).

Both spatial and single-cell technologies are evolving rapidly and the simultaneous integration of single-modality methods is constantly giving rise to new single-cell multi-omics technologies (Jovic et al., 2022; J. Lee et al., 2020; Williams et al., 2022). Single-cell multi-omics approaches present a promising tool for therapeutic strategies and precision medicine.

1.5.1. Single cell & spatial transcriptomics for heart development and disease

The analysis of differentiation cell trajectories, identification of novel cell populations and the comparison of healthy and disease phenotypes in single-cell resolution have transformed cardiovascular research over the past years (Fudge, 2023; Paik et al., 2020; Tucker et al., 2020). To further understand the differentiation of the first and second field progenitors, scRNA-seq from Nkx2-5^{+} and Isl1^{+} cells has shown a crosstalk between cardiovascular progenitor cells (CPCs) and terminally differentiated cells along with the variation in timing of differentiation between the two progenitors (Jia et al., 2018). Analysis of CPCs transition states reveal that continuous Nk2-5 expression directs CPCs to an irreversible cardiomyocyte fate while Isl1$^{+/+}$ CPCs pass through a transitional state before giving rise to different developmental fates. Transcriptomic profiles of early development revealed differences between human and mice timeline of differentiation and maturation of the cardiac cell types and identified species-specific markers (Cui et al., 2019). For example, *RNASE1* (endothelial cells) and *ITLN1* (epicardial cells) were specifically expressed in human and in lower levels in the mouse heart, whereas *Icam2* (endothelial cells) and *Rnf213* (epicardial cells) distinctly expressed in mouse. Moreover, scRNA-seq revealed endothelial cell clusters that are enriched in murine hearts after myocardial infarction (MI) compared with healthy hearts that upregulate Plasmalemma vesicle-associated protein (Plvap) (Z. Li et al., 2019). Interestingly, endothelial cells adjacent to the infarcted area in the ischemic human heart show an increase in the Plvap expression.

1.5.2. Zebrafish heart regeneration: Lessons from scRNA-seq studies

As described above, single-cell technologies offer a great tool for dissecting cell heterogeneity, elucidating dynamic cell transitions, and inferring gene-expression patterns. In the field of tissue regeneration, this technology has contributed already to many studies, deepening our understandings of the cellular reprogramming during axolotl limb regeneration, uncovering transcription factors that control retinal regeneration or creating a whole-animal atlas of the transcriptome of the regenerating planaria (Gerber et al., 2018; Hoang et al., 2020; Plass et al., 2018). This section will explore and examine the contribution of specific cell types in zebrafish heart regeneration, drawing insights from studies that utilize scRNA-seq and spatial transcriptomics (Table I 2)

1.5.2.1. Cardiomyocytes contribution

The first study on scRNA-seq of the zebrafish regenerating heart was published in 2019. Honkoop et al. used FACS and SORT-seq (Muraro et al., 2016), to investigate the transcriptomic profile of nppa:citrine^{+} cells of cryoinjured hearts. The single-cell analysis showed that cardiomyocytes close to the border zone of the injury bear a unique transcriptomic signature, expressing embryonic markers and glycolytic genes. In addition, it also showed that the metabolic reprogramming that is important for cardiomyocyte proliferation is induced by the Nrg1/Erb2 signaling (Honkoop et al., 2019). In a previous publication, the same group used spatially resolved RNA sequencing (tomo-seq) of the regenerating heart to show that bone morphogenetic protein (BMP) signaling is required for cardiomyocyte dedifferentiation and proliferation, and that its inhibition results in impaired cardiac regeneration (Wu et al., 2016).

1.5.2.2. Fibroblasts contribution

In a more complex study, Hu et al. dissected the heterogeneity of activated cell states of fibroblasts with parallel lineage tracing based on the CRIPSR/Cas9 technology (Hu et al., 2022). By performing scRNA-seq of uninjured, 3 days post injury (dpi), 7- and 30-dpi of cryoinjured hearts they found that canonical Wnt signaling is the key regulator for the

Table I 2 Comparison of literature on zebrafish heart regeneration using scRNA-seq technology.

Efficiency	Single-cell technology		Experimental setup					Cell types			Study	
# of cells	Single-cell isolation	Platform	Injury model	Dissociation enzyme	Transgenic animals	Adult or Larvae	Timepoints	# of clusters	CMs	Non-myocytes	Main finding	Reference
NA	FACS	Chromium (10x Genomics)	Apex resection	Liberase TM	lyz:EGFP	Adult	1 DPI	4	No	Neutrophils	Neutrophils activate epicardial cells through FGF signaling	Peterson et al 2024
81.810	FACS	Chromium (10x Genomics)	Cryoinjury	Liberase DH	mpx:EGFP/ mpeg1:mCherry	Adult	Sham, untreated, 1 DPI, 3 DPI, 7 DPI	18	No	Immune cells, Macrophages	hbaa^{+} Mac and timp4.3^{+} Mac essential for regeneration	Wei et al 2023
NA	FACS	Chromium (10x Genomics)	Cryoinjury	Liberase TM	*adra1-3i-T2A-CFP–/* adra1-3i-T2A-CFP+	Adult	7 DPI	23	Yes	Yes, all non-myocytes	adra1a-activated macrophages determine activation of collagen-12-expressing fibroblasts for ECM remodeling	Apaydin et al 2023
15.141	FACS	Chromium (10x Genomics)	Apex Resection	Liberase DH	tcf21:nucEGFP	Adult	Sham, 3 DPA, 7 DPA	11	Yes	Epicardial, Endothelial, Mural, Immune cells	Progenitor population of the adult epicardium	Xia et al 2022
7.477	FACS	Chromium (10x Genomics)	Apex Resection	(Metadata analysis)	*runx1P2:Citrine/ kdrl:mCherry*	Adult	Uninjured, 3 DPI	23	Yes	Yes, all non-myocytes	*lepb* marks an injury-activated subset of ECs	Shin et al 2022
202.255	Dissociation	Chromium (10x Genomics)	Cryoinjury	Liberase Mix	Genetic scars	Adult	Sham, 3 DPI, 7 DPI , 30 DPI	19	Yes	Yes, all non-myocytes	Col12^{+} Fibroblasts with proregenerative response/ Wnt signaling as regulator of epicardial fibroblast response	Hu et al 2022
18.739	FACS	Chromium (10x Genomics)	Apex Resection	TrypLE, Collagenases (II and IV)	WT-AB	Adult	Uninjured, Sham, 3 DPA, 7 DPA, 14 DPA	15	Yes	Yes, all non-myocytes	tal1, an endocardial developmental gene is involved in cardiac regeneration	Rolland et al 2022
7.869	FACS	Chromium (10x Genomics)	Genetic Ablation	Liberase, thermolysin	tcf21:nucEGFP/ tcf21:nucEGFP;Z-CAT	Adult	Sham, 7 DPI	7	No	Epicardial cells	Hapln1b required for CM proliferation and successful heart regeneration	Sun et al 2022
61.977	Dissociation	Chromium (10x Genomics)	Apex Resection	Collagenases (II and IV)	WT-AB	Adult	Uninjured, 2 DPA, 7 DPA, 14 DPA	6	No	Yes, all non-myocytes	markers for four subset of endothelial cell populations are described	Ma et al 2021
15.415	FACS	Chromium (10x Genomics)	Cryoinjury	Liberase DH	*runx1$^{w84x/w84x}$ Tg(BAC-runx1P2:Citrine;kdrl:Hsa.HRAS-mCherry)*	Adult	Uninjured, 3 DPI	27	Yes	Yes, all-non myocytes	Runx1 promotes scar deposition and inhibits cardiomyocyte proliferation	Koth et al 2020
352	FACS	SORT-seq	Cryoinjury	Liberase IV and Elastase	nppa:citrine/ myl7:GFP	Adult/ larvae	7 DPI	12	Yes	Fibroblasts, Endothelial and Immune cells	Nrg1/Erb2 signaling essential for cardiomyocyte proliferation	Honkoop et al 2019

activation of *nppc* fibroblasts derived from the endocardium while the *col11a1a* and *col12a1a* fibroblasts share their lineage origin with the epicardium.

1.5.2.3. Immune cells contribution

The role the immune response was investigated by Wei et al. By doing scRNA-seq of *mpx:EGPF*$^{+}$ and mpeg1:*mCherry*$^{+}$ sorted cells from a macrophage-delayed recruitment model upon cryoinjury and an uninjured model they identify two cardiac resident subpopulations (*hbaa*$^{+}$ Mac and *timp4.3*$^{+}$ Mac) of macrophage necessary for heart regeneration. Different subpopulations of macrophages with unique spatiotemporal distributions and role in the regeneration process have been validated by other studies as well (K.-H. Wei et al., 2023). Recently, it has been described by Apaydin et al. that alpha-1 adrenergic signaling activates a subset of macrophages leading to activation of the ECM remodeling transcriptional program by stimulation of *col12a1a* fibroblasts (Apaydin et al., 2023). Finally, *mmp14* macrophages are required for cardiac regeneration.

1.5.2.4. Epicardial cells contribution

The identification of epicardial cell states during heart regeneration is described by Sun and colleagues (Sun et al., 2022). By investigating the transcriptomic profile of tcf21^{+} epicardial cells at uninured and 7 DPA upon cardiomyocyte genetic ablation they show epicardial cells expressing genes encoding the hyaluronic-acid (HA) organizing factors *hapln1a* and *hapln1b* are needed for normal HA deposition and organization during cardiac regeneration. *Hapln1b* is required for injury-induced cardiomyocyte proliferation and successful heart regeneration.

1.5.2.5. Endothelial cells contribution

The endothelial regenerative response and the behavior of other interstitial cells was described by Rolland et al. scRNA-seq analysis of uninjured, 3 DPA, 7 DPA and 14 DPA using the apex resection injury model revealed that *tal1*, an endocardial developmental gene is involved in cardiac regeneration (Rolland et al., 2022). Overexpression of a dominant negative Tal1 isoform specifically in endothelial cells (ECs) inhibited the regenerative process, resulting

in scarring. In the study by Ma et al., newly identified markers for four subset of endothelial cell populations are described. The maker genes *spock3* and *f8* for endocardial ECs (eECs), *cldn11a* and *cdh6* for lymphatic ECs (lECs), *rca2.2* and *cldn5b* for coronary ECs (cECs), *hopx* and *tmsb1* for mural cells (Ma et al., 2021). A more recent study by Shin et al utilizes the injury-specific factor *leptin b (lepb)* and its TREE to identify emerging non-myocyte cell-types (Shin et al., 2024). They demonstrated that *lepb* marks an injury-activated subset of ECs and that loss of *lepb*-linked regeneration enhancer (LEN) activity results in elimination of expression of *lepb*, without affecting the expression of other nearby genes.

Most studies so far are centered in non-myocyte populations during zebrafish heart regeneration and cardiomyocyte cell numbers are few or not present at all at the scRNA-seq datasets (Ma et al., 2021; Rolland et al., 2022; Sun et al., 2022; K.-H. Wei et al., 2023). The study by Hu et al., has managed to include in their analysis a big number of cardiomyocytes that they do not analyze in detail (Hu et al., 2022). If the key driver of cardiac regeneration is the regeneration of myocardium is remains unclear how no research has been focused on cardiomyocyte clusters. A possible explanation to this riddle might be the unique challenges during the bioinformatic analysis of myocyte populations compared to other cell types, as well as during the preparation of the sample for scRNA-seq experiments (B. Hu et al., 2022; Paik et al., 2020). Some further examples are described below.

1.5.3. Bottlenecks and limitations of single-cell experiments

Despite the plethora of applications and potential benefits, single-cell technologies and scRNA-seq experiments come with several limitations and difficulties (Paik et al., 2020; M. Wang et al., 2021). The multiple steps required, from cell isolation and library preparation to sequencing, are prone to technical variability that can lead to potential biases and errors. Batch effects, or the variability introduced during different experimental runs or protocols might impact the data and hinder meaningful comparisons between experiments (Andreatta et al., 2024). One variable that should be taken into consideration when setting-up scRNA-seq experiments is the cell capture efficiency of the different single-cell technologies. Some cells might not be captured efficiently, leading to a bias toward specific cell types or missing rare cell populations (Yamada & Nomura, 2020). Currently, droplet-based scRNA-seq

platforms cannot be used for adult cardiomyocytes, which typically measure between 120-200μm in their long axis (Paik et al., 2020). This limitation arises because microdroplets have a diameter of 30 μm, which make unfeasible to encapsulate cells of such size. Plate-based or microwell-based methods have been used for scRNA-seq experiments of bigger cell types (Ashton et al., 2021; Baysoy et al., 2023). Another alternative to the problem might be the use of technologies like inDrop (Klein et al., 2015), where hydrogel microspheres are used to introduce the oligonucleotides, or microfluid-based methods that can generate droplets of bigger diameter.

Furthermore, sample preparation and handling should be done properly to minimize the introduction of biases. Tissue dissociation into a single-cell suspension could be a challenging task. Maximizing single-cell yield while maintaining a highly viable cell population might require optimization of the duration of dissociation and choice of proteolytic enzyme (Paik et al., 2020; M. Wang et al., 2021; Yamada & Nomura, 2020). Cardiac tissue is really compact and rich in ECM thus needing both enzymatic and mechanical dissociation. As a consequence, cells might experience stress during isolation and processing altering their gene expression profiles and affecting data accuracy (Denisenko et al., 2020; Machado et al., 2021). Studies have demonstrated that using a psychrophilic protease that is active at low temperatures (4-6^{o}C), can mitigate artifacts introduced in the scRNA-seq data due to enzymatic incubations at 37^{o}C (Adam et al., 2017; O'Flanagan et al., 2019). Junker and colleagues, used the uridine analog 4-thiouridine (4sU) to label newly synthesized transcripts to measure such stress-response artifacts due to the dissociation and used computational methods to remove them from the subsequent analysis (Neuschulz et al., 2023). In a recently published study by Konturek-Ciesla et al., the authors compare the effect of cell isolation procedure at different temperatures, with or without the presence of the transcriptional inhibitor triptolide (TP), on the induction of Immediate Early Response (IER) genes in mouse hematopoietic stem cells (HSC). Their findings suggest alterations in gene expression previously described in HSC aging studies, which are associated with the induction of IER signatures rather than solely being attributed to the aging process (Konturek-Ciesla et al., 2024). This work enhances our understanding of the proper design and interpretation of scRNA-seq studies.

Addressing these limitations requires advancements in experimental techniques, computational methodologies, and standardization across protocols to ensure robustness, reproducibility, and comprehensive insights from scRNA-seq experiments.

1.6. Annexins: A superfamily of Ca^{2+}-dependent phospholipid binding proteins

Annexins (ANX) are a large family of calcium-dependent membrane-binding proteins. Over 100 proteins have been found across various species mostly among eukaryotes (Mirsaeidi et al., 2016). In humans, twelve annexin proteins have been identified (Figure I 16 A). Comparative analysis between zebrafish and mammalian annexin genes reveals three ANX genes homologous to human, two to human ANX2, and two to human ANX11, suggesting that zebrafish annexin genes might have emerged from duplications after the divergence of the two genomes (de Souza Ferreira et al., 2023; Mirsaeidi et al., 2016).

The protein structure of all annexins share a conserved C-terminal domain of at least four similar repeats, approximately 70 amino acids in length (Figure I 16 B and C). These subunits usually contain characteristic ‘’type 2’’ calcium binding sites. The N-terminal domain is characteristic for the individual annexins with a variable length and hydrophobic groups, thus determining its interactions with other intracellular proteins (Figure I 16 D).

Annexins are commonly found in the cytoplasm in both soluble and stable forms but can also interact with the elements of the cytoskeleton or facilitate interactions between the cell and the ECM (de Souza Ferreira et al.,2023.; Gerke & Moss, 2002; Mirsaeidi et al., 2016). However, annexins such as ANXA2 and ANXA11 have been detected in the nucleus during cell cycle (de Souza Ferreira et al., 2023.; Gerke & Moss, 2002). In other occasions, annexins might be expressed on the cell surface even in the absence of a secretory signal peptide. Annexins form protein complexes with other proteins such as the S100 proteins.

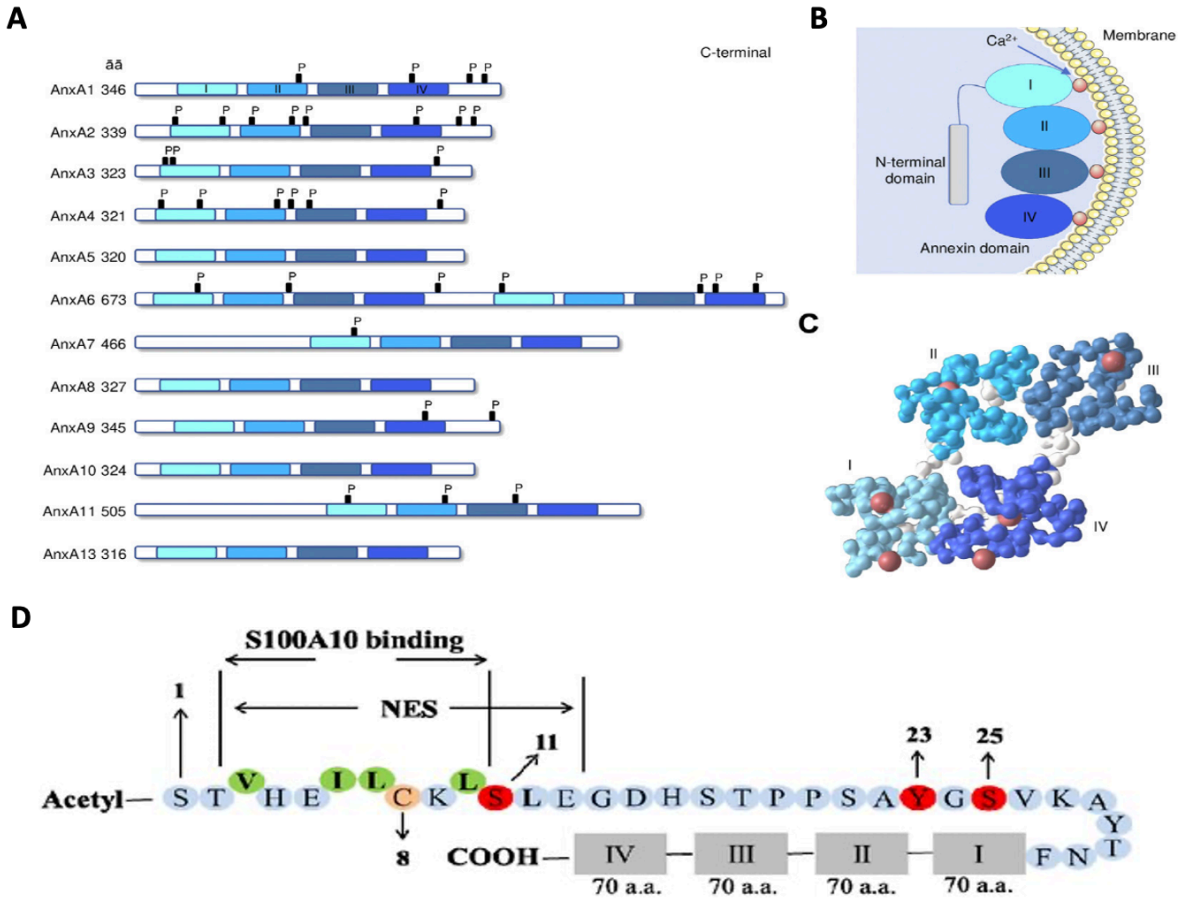

Figure I 15 Domain structure of annexins. (A) Domain structures for the twelve human annexin proteins and their phosphorylation sites **(B)** Schematic drawing of annexin peripherally attached to a membrane surface through bound Ca^{2+} ions. **(C)** 3D structure of AnxA1 with different color indicating the different repeated domains (blue), spacer regions (white) and Ca^{2+} ions (red) **(D)** Annexin A2 is composed to two domains—the amino-terminal domain and carboxyl-terminal domain. The amino-terminal is the site for post-translational modifications such as acetylation (Ser-1) and phosphorylation (Ser-11, Tyr-23, Ser-25). Additionally, it also encompasses the redox reactive cysteine residue (Cys-8) and the nuclear export sequence (NES) (Val-3-Leu-12). The S100A10 binding site is an amphipathic α -helix, with the hydrophobic residues, Val-3, Ile-6, Leu-7 and Leu-10 making contacts with S100A10. The carboxyl-terminal core domain includes four predominantly alpha-helical domains each containing 70 amino acids. This carboxyl-terminal core domain contains binding sites for heparin and RNA, calcium and phospholipid and as well as for F-actin. Adapted from Bharadwaj et al., 2013 and Barbero et al., 2022.

1.6.1. Annexins and their role in regeneration

The family of annexins exhibits a variety of functions such as in intracellular membrane organization, exocytotic processes and endocytic pathways, phagocytosis, and stabilization of membrane domains. In addition, they play an important role in the regulation of ion channel activity. Recent studies are indicating the implication of annexins in regeneration (Grewal et

al., 2016; Häger & Nylandsted, 2019; Leikina et al., 2015; Quoseena et al., 2020). For instance, AnxA6 deficient mice fail to regenerate the liver and die after partial hepatectomy, while muscle regeneration is slowed down in AnxA1$^{-/-}$ mice. In addition, a CRISPR-based knockdown of Anxa2a and Anxa2b in the zebrafish caudal fin demonstrated their role in fin regeneration.

1.6.2. Annexins and Ca^{2+} handling in the heart

Due to the significance of Ca^{2+} homeostasis in the heart and the abundance of AnxA2, A5 and A6 in cardiomyocytes it is important to understand the roles of cardiac annexins (Camors et al., 2005; de Souza Ferreira et al., 2023). For instance, overexpression of AnxA6 results in reduced cardiomyocyte contractility and results in hypertrophy and heart failure in mice. Further studies in AnxA2 knock-out mice have linked AnxA2 with the regulation of fibrin homeostasis and neo angiogenesis (Grewal et al., 2016). AnxA5 and AnxA6 are the most expressed annexins in the human and rat myocardium are known for the formation of active Ca^{2+} channel. Transgenic mice overexpressing AnxA6 manifested alteration in the Ca^{2+} homeostasis and contractility (Babiychuk & Draeger, 2000; Camors et al., 2005; de Souza Ferreira et al., 2023). All these studies, suggest a possible implication between annexins and altered $Ca2^{+}$ homeostasis in the heart. However, there's been limited attention toward annexins and their correlation with calcium handling in the heart and further investigation is needed.

2. OBJECTIVES

The general objective of the present thesis is to investigate the regenerating capacity of the zebrafish heart with the usefulness of novel transcriptomic approaches.

To address this general goal, we defined two specific objectives:

Objective 1: Determine which is the transcriptomic profile of the cells during zebrafish heart regeneration.

Objective 2: Based on the obtained results from specific objective 1, determine the importance of candidate genes that play a role during zebrafish heart regeneration.

To pursue the mentioned objectives, the specific tasks for each objective were planned:

For objective 1:

Task 1.1: Develop a cold active protease dissociation protocol suitable for downstream single-cell transcriptomic analysis
Task 1.2: Perform a transcriptomic analysis of the of the zebrafish heart and its changes during regeneration in a single-cell resolution
Task 1.3: Perform spatial transcriptomic profiling of wild-type and *postnb*$^{-/-}$ zebrafish heart during regeneration

For objective 2:

Task 2.1: Characterize the expression of candidate genes during cardiac regeneration
Task 2.2: Generate F_0 biallelic knock-out animal lines using the CRISPR-Cas9 technology
Task 2.3: Determine whether the candidate genes are essential for zebrafish heart regeneration

3. MATERIALS & METHODS

3.1. Zebrafish breeding and husbandry

All the experiments performed in this work have been conducted under the approbation of the Ethics Committee on Experimental Animals of the Institut d'Investigació Biomèdica de Bellvitge (IDIBELL).

Adult zebrafish between 3 and 18 months old were used to conduct all the experiments. According to standard protocols for zebrafish husbandry (Westerfield, 2000), the animals were maintained in a density of 3 fish/liter. The tanks were part of a closed system with controlled temperature of 28.5ºC. The zebrafish have been fed one time per day with fish food, one time per day with *Artemia salina* and a third time with a combination of fish food and *Artemia salina.*

In this work, the following strains have been used:

- Wild type AB (ZIRC_ZL1)
- tTg ((mlc2a:H2A-mChery)(periostin:citrine)(fli1a:GFP)). Previously created in our laboratory.
- Tg (mlc2a:GCaMP6f). Created in this thesis.
- *postnB*$^{-/-}$. Previously created in our laboratory.
- *anxa2a*$^{-/-}$. Created in this thesis.
- *mustn1b*$^{-/-}$. Created in this thesis.
- *fhl1a*$^{-/-}$. Created in this thesis.
- *casq2*$^{-/-}$. Created in this thesis.

3.2. Apex resection injury

To study cardiac regeneration in zebrafish, we used the ventricular amputation protocol described by Raya et al., 2003. Following the protocol, zebrafish were anaesthetized in 0.02% Tricaine solution (Sigma, Cat. No. A5040), and the level of sedation was determined by pinching the caudal fin. Once there was no response to stimulus, the fish was arranged in a prewet sponge with the ventral part of the animal facing upwards. A binocular magnifier

was used to locate the heart area of the fish, and the scales of the area were removed with the help of microdissection tweezers (Dumount #5 – fine forceps, Cat. No. 11254-20). A small aperture was ripped through the body wall and the pericardial sac, without damaging the heart. The incision was kept opened with curved microdissection tweezers (Dumount #5/45 forceps, Cat. No. 11251-35) in way that the area of the ventricular apex was visible. The amputation of around 20% of the ventricular volume was achieved by using iridectomy scissors (Moria Pascheff-Wolff Spring Scissors, Cat. No. 15371-92). To stop the bleeding, the wound was gently pressed with a tip of absorbent paper. The animals were returned in a tank with fresh aquarium water, and they were recovered from the anesthetic by pipetting water to the gills until a reestablishment of the mobility of the operculum was observed, and the animal began to swim normally. Once the animals were fully recovered, they were introduced to the aquarium system. As a control of the procedure, a sham intervention was performed. In this case, the process followed was the same but causing any ventricular injury.

3.3. Genomic DNA extraction from adult fish (Fin Clips) or embryos

Genomic DNA extraction for genotyping was achieved by adding 100µl 50 NaOH (Sigma, Cat. No. S8045) to one embryo of piece of tissue (caudal fin in the case of fin clips) to a 200 µl tube or to a well of a 96 well plate. Samples were incubated at -20^{o}C for at least 15 min and then at 95^{o}C for 5 min. For the neutralization of the NaOH, 10µl of 1 M Tris-HCl pH=7.5 (Sigma, Cat. No. T3253) was added. The resulting solution was used immediately or stored at -20^{o}C. For the Fin clip procedure, the fish were anesthetized as described before, and the caudal fin was cut with a blade or scalpel.

3.4. Cardiac tissue collection

Regenerating hearts at different time points (1, 3, 7, 14, and 30 DPA) were collected for further analysis. The animals were euthanized in an overdose of Tricaine and 20µl of heparin solution (Sigma, Cat. No. H3149-50KU) in a concentration of 1.000 U/ml were intraperitoneally injected with a 27G needle, to prevent blood coagulation. Once extracted, the hearts were cleansed in a solution of PBS 1x (Capricorn Scientific, Cat. No. PBS-1A) supplemented with heparin (100 U/ml) to minimize further blood clotting.

3.5. Sample processing for histological staining

Once extracted, the hearts were fixed over-night with 4% paraformaldehyde (PFA) (Sigma, Cat. No. P6148-500G) at 4°C with agitation. The next day, the hearts were washed 3 times with PBS 1x and balanced with 30% sucrose (Sigma, Cat. No. S1888) over-night at 4°C. Finally, the hearts were orientated in a tissue mold full of OCT (Tissue Tek, Cat. No. 4565) and frozen at -80°C until further processing. For immunohistochemistry and other staining, the hearts were cut at 10µm and for *in situ hybridization** at 16µm, with a Leica CM3050S cryostat. The sections were positioned in series over 5-10 Superfrost Plus slides (VWR, Cat. No. J1800ABDH), so that a whole-hearted representation could be found on each slide. The sections were air-dried at RT over-nigh and stored at -20°C until further use. For ISH experiments, the PFA used was prepared with nuclease-free H_20, and the cryostat and slides were previously cleaned with RNase Zap (Thermo Fisher Scientific, Cat. No. AM9780).

3.6. Dissociation of zebrafish heart in single cells

To dissociate the hearts in single cells, two different protocols were used. For scRNA-seq experiments, we adapted a protocol using a cold active protease from *B. licheniformis* and the whole process was carried out at low temperatures (4-6°C) (Adam et al., 2017). For cell culture experiments and for studying the effect of cold active protease on the expression of IER genes, a collagenase-based dissociation protocol was used as described at section 3.6.2 and adapted from (Sander et al., 2013) and (Patra et al., 2017).

3.6.1. Cold active protease-based enzymatic digestion

The harvesting of the tissue was performed as described in section 3.4. The blood clot, the atrium and the outflow tract were removed with the help of a blade or scalpel, and the part of interest of the ventricle was cut in smaller pieces to facilitate the digestion. The pieces of the tissue were put into a 1.5 ml tube containing ice cold Perfusion Buffer and maintained on ice. Once the desired number of ventricles were processed, the sample was spun down and the perfusion buffer was aspirated. We added 750µl of Enzyme Digestion mix and pipette gently 3-5 times, with a P1000, to mix well. The samples were incubated on ice for 2min, and then triturated again for 5 times. The trituration process was repeated every 2-3 minutes for

a maximum of 25 min. Once a single cell state was observed under the microscope, we briefly spun the tube to pellet the cell clumps and the rest of undigested tissue. Around 80% of the supernatant was removed and added in ice cold PBS 1x + 1% BSA (Sigma, Cat. No. A9647-100G). We added 750µl of enzyme mix in the rest of undigested tissue and repeated the incubation-trituration steps. We centrifuged the cells at 300g, at 4°C for 5min and resuspended in PBS 1x + 0.01% BSA. We filtered the cell suspension with a 70µm filter and maintained them on ice until the encapsulation or further use.

Perfusion Buffer: 5mM Glucose (Sigma, Cat. No. G7021) in PBS1x w/o $Ca2^+$ and $Mg2^+$

Digestion mix: 10mg/ml protease from *Bacillus licheniformis* (Sigma, P5380-100MG), 2.5 mM EDTA (Sigma, Cat. No. 03690) in Perfusion Buffer.

3.6.2. Collagenase-based enzymatic digestion

The ventricles were harvested and put in perfusion buffer as described in section 3.6.1. The perfusion buffer was aspirated and 750 µl of Collagenase mix was added and the tissue was pipetted gently x5 times. The tube was incubated in a thermomixer at 32°C for 1-1.5h. Every 15-20min the tissue was triturated gently x5 times with a P1000. We monitored the single-cell state and health of the cells under the microscope. When the digestion was considered finished, we added the same volume of Stopping Buffer $(SB)_1$ and centrifuge the cells at 300g at 4°C for 5min. We aspirated the supernatant, without disturbing the cell pellet or the cell smear that might appear on the wall of the tube.

For cell culture experiments:

Cell pellet was resuspended in SB_2 and incubated on ice for 5min. From this moment on, every 5 min the appropriate concentration of $CaCl_2$ was added in the mix, and the tube was flicked gently with the fingers and put back on ice. Once reaching SB_7, the cells were pelleted at 300g, 4°C for 5min. The cells were resuspended in cell culture medium, filtered with a 100µm filter (BD Biosciences ,Cat. No. 340610) and seeded on a MatTek plate in a density of 100.000 cells.

A more detailed list of the solutions and reagents is shown below:

Collagenase mix: Collagenases type II and IV (5mg/ml each) in perfusion buffer

Perfusion Buffer (PB): PBS 1x (w/o Ca^{2+} or Mg^{2+}), 10 mM Hepes(Cat. No.), 30 mM Taurine (Sigma, Cat. No. T8691), 5.5 mM Glucose (Sigma, Cat. No. G7528) and 10 mM BDM (Sigma, Cat. No. B0753)

$CaCl_2$ stock solutions (1 mM, 10 mM, 100 mM): Caclium Chloride anhydrous, BioReagent suitable for insect cell culture, suitable for plant cell culture =>96% (Sigma, Cat. No. C5670-100g), with M_r=110.98g/mol, prepared in Milli-Q H_2O

Plating medium: 8,73ml of MEM, 0.5ml of GlutaMax, 0.5ml of FBS (5%), 0.25 ml of P/S (100U/ml) and 20ul of Normocin (1:500)

Cell culture medium: 50% plating medium + 50% EGM-2 ,supplemented with all reagents (Lonza, Cat. No. CC-3162)

The Stopping buffers are described above have the following concentrations and are prepared as:

- SB_1 (12.5 µM $CaCl_2$): 887.5µl of PB, 100µl of FBS, 12.5ul of $CaCl_2$ (1mM)
- SB_2 (12.5 µM $CaCl_2$): 937.5µl of PB, 50µl of FBS, 12.5ul of $CaCl_2$ (1mM)
- SB_3 (62 µM $CaCl_2$): 2.49µl of $CaCl_2$ (10mM) in 0.5ml of SB_2
- SB_4 (112 µM $CaCl_2$): 2.5µl of $CaCl_2$ (10mM) in 0.5ml of SB_3
- SB_5 (212 µM $CaCl_2$): 0.5µl of $CaCl_2$ (100mM) in 0.5ml of SB_4
- SB_6 (500 µM $CaCl_2$): 1.47µl of $CaCl_2$ (100mM) in 0.5ml of SB_5
- SB_7 (1000 µM $CaCl_2$): 2.57µl of $CaCl_2$ (100mM) in 0.5ml of SB_6

3.7. Immunohistochemistry (IHC)

Before performing the immunofluorescence detection of proteins in tissues, the sections were thawed and air-dried the night before. Antigen retrieval treatment was performed with a sodium citrate buffer of pH 8.5 or 9 target retrieval solution for 40 min, at 80°C in a decloaking chamber (Biocare Medical). Sections were washed 3 x 5min with TBS 1x and the non-specific junctions were blocked with blocking solution. Subsequently, the sections were incubated over-night at 4°C with the primary antibodies dissolved in TBS++ solution. The, the sections were washed 3 x 5min in TBS++ and then incubated with the

desired secondary antibodies, also dissolved in TBS++ solution, for 2h at 37°C. After the incubation of the secondary antibody, sections were washed 3 x 5min with TBS and self-fluorescence of the tissue was decreased by treating the samples with Sudan Black for 4min at RT; samples were again washed 3 x 5min with TBS 1x and counter stained with 1:10.000 DAPI for 10min at RT. The samples were mounted with mounting medium and stored at 4°C before imaging.

A more detailed list of the solutions and reagents is shown below:

Sodium citrate buffer: 10mM sodium trihydrate (Sigma, Cat. No. C8532) dissolved in MiliQ-H_2O. The pH was adjusted at 8.5.

Target retrieval solution pH 9: Dilute 1:10 the 10x pH9 Target retrieval solution (Dako, Cat. No. S2367) in MiliQ-H_20

TBS 10x: 1M Tris-HCl (Sigma, Cat. No. T3253), 160 mM Trizma Base (Sigma, Cat. No. T6791) and 1.5M NaCl (Sigma, Cat. No. S7653) d in MiliQ-H_2O. Adjust pH at 7.5.

Blocking solution: 1x TBS with 0.5% of Triton X-100 (Sigma, Cat. No. X100) and 3% Donkey Serum (Chemicon, Cat. No. S30-100ml).

TBS ++ solution: 1x TBS with 0.1% Triton X-100 (Sigma, Cat. No. X100) and 3% Donkey Serum (Chemicon, Cat. No. S30-100ml).

Sudan Black: 1% Sudan Black (Panreac, Cat. No. 252069) in 70% Ethanol.

DAPI: DAPI compound (4',6-diamino-2-phenylindole) (Invitrogen, Cat. No. D21490) rehydrated with 2ml of filtered dH_2O to achieve a final concentration of 5mg/ml. As a working solution, use a 1:10.000 dilution in TBS1x.

Mounting medium: 56mM Glycine (Sigma, Cat. No. G7126), 5mM (Sigma, Cat. No. S8045), 87mM NaCl (Sigma, Cat. No. S7653), 4.6mM Sodium azide (Sigma, Cat. No. S2002), 0.23M Propyl gallate (Sigma, Cat. No. P3130) and 70% Glycerol (Sigma, Cat. No. G9012) in dH_20. Dissolve the reagents by heating, with maximum temperature 40°C.

Table MM 1 List of antibodies, dilutions & applications.

1^{ry} Antibody	Species	Isotype	Clonality	Dilution		Application	Reference
Myosin heavy chain (**MF20**)	Mouse	IgG	Polyclonal	1:100		IHC	DHSB, Cat. No. MF-20 conc
Annexin 2 A (**ANXA2**)	Rabbit			1:100 / 4:1000		IHC / WB	Proteintech, Cat. No. 11256-1-AP
Muscoloskeletal embryonic nuclear protein 1 (**MUSTN1**)				1:25			Merck, Cat. No. ABD115-25UG
Four and a half LIM protein 1 (**FHL1**)				1:50			Proteintech, Cat. No. 10991-1-AP
Calsequestrin 2 (**CASQ2**)				1:50			Proteintech, Cat. No. 18422-1-AP
a-Tubulin (**TUBA4A**)	Mouse	IgG_1	Monoclonal	1:1000		WB	Sigma, Cat. No. T6074
β-Catenin (**CTNNB1**)				1.5:1000			BD Biosciences, Cat. No. 610154
2^{ry} Antibody	**Species**	**Isotype**	**Clonality**	**Conjugated**	**Dilution**	**Application**	**Reference**
Anti-Mouse IgG	Donkey	IgG	Polyclonal	AlexaFluor 488	1:200	IHC	Jackson, Cat. No. 715-545-151
Anti-Rabbit IgG				Cy3	1:200		Jackson, Cat. No.711-165-152
Anti-Mouse IgG				Cy3	1:200		Jackson, Cat. No. 715-165-151
Anti-Rabbit IgG				AlexaFluor 488	1:200		Jackson, Cat. No. 711-545-152
Anti-DIG	Sheep			Alkaline Phosphatase	1:5000	ISH	Roche, Cat. No. 11093274910
Anti-Rabbit	$F(ab)'_2$			Horseradish Peroxidase	1:5000	WB	GE Healthcare, Cat. No. NA934
Anti-Mouse				Horseradish Peroxidase	1:5000		GE Healthcare, Cat. No. NA931

3.7.1. OPP incorporation and signal development

For the studies of the newly synthesized peptides with O-Propargyl Puromycin (OPP), the animals were injected intraperitoneal with 10µl OPP (2mg/kg), diluted 1:50 in DMSO from stock concentration 20mM, with the help of Hamilton syringe (Hamilton, Cat No. 20736). The injection was performed one time at 7 DPA animals, and 2 hours prior of the extraction of heart extraction. OPP signal development was performed using the Click-It OPP Alexa Fluor 647 Imaging kit (Thermo Scientific, Cat No. 10458).

3.8. RNA extraction

For the RNA extraction we used the Maxwell® (Promega) system. Depending on the nature of the experiments we used a pool of 3-5 or 5-10 ventricles, and we processed the samples with Maxwell® RSC simply RNA Tissue kit (Promega Biotech, Cat. No. AS1340) or Maxwell® RSC Cultured Cell kit (Promega Biotech, Cat. No. AS1390). The extraction was achieved by following manufacturer's instructions and the RNA was either immediately processed or stored at -80^{o}C until further use.

3.9. cDNA synthesis

cDNA was synthesized ideally from 1µg RNA with Transcriptor First Strand cDNA Synthesis Kit (Roche, Cat. No. 04379012001) using random hexamers and following manufacturer's instructions.

3.10. Probe synthesis for *in situ* hybridization (ISH)

Primers were designed to amplify a » 500bp region specific of the gene of interest and the PCR product was cloned into the pCR4-TOPO TA vector (Life Technologies, Cat. No. 450030). As a template for the PCR, the cDNA used, came from either Sham or 7 DPA samples. For the transformation of bacteria, DH5a strain (Thermo Fisher Scientific, Cat. No. 11583117) was used and the selected colonies were sequenced to check the directionality of the inserted fragment. Then, the vectors were digested either with NotI (New England Biolabs, Cat. No. R3189L), PstI (New England Biolabs, Cat. No. Ro1040) or SpeI (New England Biolabs, Cat. No. R3133L). The probes were synthesized with the DIG RNA-labelling Mix (Roche, Cat. No. 11277073910) and the T7 or T3 Rna polymerases (Roche Diagonostics, Cat. No. 10881775001 and 11031171001 respectively). The resulted synthesized RNA was purified using the RNA Clean and Concentrator-5 kit (Zymo research, Cat. No. R1015). The probes were stored at -80oC until use for *in situ* hybridization experiments. All the primers used, and their corresponding fragment size are listed in Appendix I.

3.11. *in situ* hybridization in cryosections

For the ISH experiments, all solutions were nuclease free and equipment along with surface area were cleaned RNAse Zap prior to use. As mentioned in section 3.5, the samples were cut at 16µm. Hybridization was performed over-night at 68^{o}C, with probes diluted 1:200 in Hybridization buffer. Slides were washed 4 x 30min in wash solution and then washed 3 x 30min in MABT solution. Blocking was performed for 2-4h in blocking solution and then the solution was changed for new blocking solution containing anti-DIG antibody (Roche, Cat. No. 11093274910) in a 1:5.000 dilution. The antibody was incubated at 4^{o}C, over-night. The next day, slides were firstly washed 5 x 30min with MABT and then 2 x 10min with AP staining buffer. Signal was developed in Poly(vinyl)alcohol solution containing NBT (Roche Diagnostics, Cat. No. 11383213001) and BCIP (Roche Diagnostics, Cat. No. 11383221001) over-night at 37^{o}C in a hybridization oven. When signal appeared, slides were washed twice with PBT and dehydrated with ethanol series (75%, 95% and 100%) before moving to Xylene (Panreac, Cat. No. 251769.2711). Finally, the slides were mounted in DPX (Thermo Scientific, Cat. No. 8312-4).

A more detailed list of the solutions and reagents is shown below:

10X Salts Solution: 2M NaCl (Sigma, Cat. No. S7653), 100mM Tris HCl (Sigma, Cat. No. T3253), 10mM Tris Base (Sigma, Cat. No. T6791), 50 mM NaH_2PO_4 (Sigma, Cat. No. S8282), 50mM Na_2HPO_4 (Sigma, Cat. No. S7907) and 50mM EDTA (Sigma, Cat. No. 03690) in nuclease free H_2O (Sigma, Cat. No. W4502) and adjust pH at 7.4.

Hybridization buffer: 1x Salts Solution, 50% deionized formamide (EMD Millipore, Cat. No. S4117), 10% Dextran Sulfate (Sigma, Cat. No. D8906), 1mg/ml yeast RNA (Sigma, Cat. No. R6570) and 1x Denhardt's solution (Sigma, Cat. No. D2532).

Wash Solution: 1x SCC (Sigma, Cat. No. S6639), 50% Formamide (Sigma, Cat. No. F7503) and 0.1% Tween-20 (Sigma, Cat. No. P1379).

5X Maleic Acid Solution: 0.5M Maleic Acid (Sigma, Cat. No. 8.00380), 0.75M NaCl (Sigma, S7653). Dissolve in MiliQ-H_2O and adjust pH at 7.5.

MABT Solution: 0.1% Tween-20 (Sigma, Cat. No. P1379) and 1x Maleic Acid solution. Dilute in MiliQ-H_2O.

Blocking reagent stock Solution: 10% Boehringer Blocking Reagent (Roche, Cat. No. 11096176001) in 1x Maleic Acid Solution. Heat to dissolve, autoclave, and store in aliquots at -20^{o}C.

Blocking solution: 20% Sheep Serum (Sigma, Cat. No. S3772) and 2% Blocking reagent (Stock solution at 10%) in MABT.

AP (alkaline phosphatase) staining buffer: 100mM NaCl (Sigma, Cat. No. S7653), 50mM $MgCl_2$ (Sigma, Cat. No. M2393), 100mM Tris-HCl pH 9 (Sigma, Cat. No. T3253) and 0.1% Tween-20 (Sigma, Cat. No. P1379). Prepare a stock solution for each component in MiliQ-H_2O.

Poly(vinyl) alcohol Solution: Dissolve 4g of PVA (Sigma, Cat. No. 341584) in 40 ml of AP staining buffer.

PBT: 0.1% Tween-20 (Sigma, Cat. No. P1279) in PBS 1x.

3.12. qRT-PCR, primer design and data processing

Primers for qPCR were designed with the help of the Primer3plus Tool (Untergasser et al., 2007). The characteristics of the chosen primers were the following: (1) 50% GC content, (2) similar Tm between forward and reverse primer, (3) a size of around 20nt for each primer and (4) an amplicon between 70-150 bp.

The qRT-PCRs were done with SybrGreen (LifeTechnologies, Cat. No. 4364344) and specific primers (listed in Appendix I) in a 7900HT Fast Real-Time PCR system (Applied Biosystems). For each reaction, we used 5ng of cDNA and 100nM primers in a final volume of 10µl. For each sample we performed triplicates

The triplicate Ct values for each sample were averaged and normalized subtracting the Ct average of the housekeeping gene (*β-actin*) of the given sample. Then, ΔCt was calculated as $2^{-\text{normalized Ct}}$. The results were multiplied by 100 before plotted.

3.13. Single-cell encapsulation

For the single-cell encapsulation we used the NADIA instrument from Dolomite Bio (Cat. No.: 3200590) and followed the protocol provided by the manufacturer. Briefly, a total of 75.000 cells in a volume of 250ul (300.000 cells/ml) of PBS+0.01% BSA and 150.000 Macosko oligodT beads (ChemGenes Corporation, Cat. No.: Macosko-2011.10(V+)) in 250ul of lysis buffer. Cells and beads co-flowed in the microfluidic chip of the device with a capture efficiency of 2.5-5%.

After the droplet emulsion breakage, we performed a reverse transcription reaction by using the Maxima H RT Master Mix (Thermo, Cat. No. ER0751) for the RNAs that were captured by the oligodT tails of the beads. Then, we removed the excess of the oligos that did not capture any mRNA molecules by incubating the beads with Exonuclease I (New England Biolabs, Cat. No.: 174M0293L) for 45min at 37^{o}C in rotation.

Before moving to the library preparation, the beads were counted, washed, centrifuged, and resuspended in nuclease-free water at a concentration of 400 beads/µl.

3.14. Next Generation Sequencing (NGS)

The preparation of the libraries was performed in two steps. In the first step, the cDNA was amplified. In the second step, the amplified PCR was tagmented and the adapters needed

for the Illumina sequencer were added through PCR reaction. In both cases, the reactions were performed by following manufacturer's instructions. For the purification of both PCR products, we used AMPure XP beads (Agencourt, Cat. No.: A63881) in a ratio of 0.6:1 (beads to sample ratio), following again manufacturer's instructions.

3.14.1. Library preparation

Briefly, for each reaction of cDNA amplification, a final concentration of 4000 beads was used. For a final volume of 50ul, we used 1x Kapa Hifi Hotstart Ready Mix (Roche Diagnostics, Cat. No. KK2601) and SMART PCR Primer (1µM). The thermocycler settings are shown in Table MM1.

Table MM 2 Thermocycler settings for cDNA amplification – PCR Library.

Cycle numbers	Temperature	Time
1 cycle	95°C	3 min
4 cycles	98 °C	20 s
	65 °C	45 s
	72 °C	3 min
12 cycles	98 °C	20 s
	67 °C	20 s
	72 °C	3 min
1 cycle	72 °C	3 min
Hold	4 °C	∞

For the tagmentation of the cDNA generated library we used the Nextera XT DNA Library Prep kit (Illumina, Cat. No.:FC-131-1096). Briefly, 600pg of DNA were used for each reaction. The reaction mix was composed of Nextera PCR Master Mix, New-P5-SMART PCR hybrid oligo and Nextera N7XX indexing oligo. In Appendix I Table A VI are shown the index oligo sequences used for each sequenced library. The thermocycler settings used for the Nextera reaction can be seen in Table MM2.

Table MM 3 Thermocycler settings for cDNA Tagmentation – Nextera Library.

Cycle numbers	Temperature	Time
1 cycle	95 °C	30 s
12 cycles	95 °C	10 s
	55 °C	30 s
	72 °C	30 s
1 cycle	72 °C	5 min
Hold	4 °C	∞

3.14.2. Library quantification and quality control

For the quantification of the libraries two different approaches were followed. For the quantification of the first library, we used a fluorometric method and more specifically the Qubit dsDNA HS Assay kit (Thermo, Cat. No. Q32851) by following manufacturer's instruction. For each sample, we used 2ul of stock library.

For the quantification of the second library as well as for the pool library that would be used for sequencing, we performed a qPCR by using the NEBNext Library Quant Kit (New England Biolabs, Cat. No. 174E630L) and following manufacturer's instruction.

The fragment size of the libraries check-up was performed by using a 4200 TapeStation System (Agilent, Cat. No.: G2991BA). QC TapeStation Traces of PCR library and Nextera library as shown in Fig A 17A and Fig A17B respectively.

3.14.3. Library sequencing

For the sequencing of the libraries, we used an Illumina NextSeq 550 sequencer and for the preparation of the samples we followed the instructions of the NextSeq 550 High Output v2 (75 cycles) kit (Illumina, Cat. No. 20024906) in pair-end mode. For sequencing parameters used was the following: 20bp for Read 1 using the Read1CustSeqB primer, 64bp for Read 2 and 8bp for i7 index.

Briefly, the reagents and cartridge were thawed the same morning of the sequencing. The dilution of the buffers needed, Tris-HCl pH 7.0 (200mM) and NaOH (0.2N), for the denature of the library were prepared fresh. A denatured 20pM library solution was diluted to 1.8pM with prechilled HT1 buffer before loaded to the cartridge. The sequencing was performed using the Custom Read Primer shown at Table A III.

3.15. Snap-freeze protocol

For precooling, 2-methylbutane (Isopentane) (Sigma, Cat. No. M32631) was poured in a plastic recipient and then partially immersed in dry ice. When the bottom of the recipient appeared to have a white color, we started with the extraction of the hearts. Zebrafish were injected with heparin as previously described in section 3.4. The hearts were left in a petri dish with PBS1x + heparin (100U/ml) for 2-3min, until spontaneous beating would facilitate the pumping out of the remaining blood. Then, the tissue was embedded in OCT and the cryomold was introduced on the top of the isopentane for the snap-freeze of the tissue to occur. The cryomold was hold with tweezers so that would not completely be embedded in the isopentane. The samples were stored at -80^{o}C until shipping.

3.16. NGS data processing

The data processing of the scRNA-seq experiments were performed in our laboratory while the part of stere-seq were processed by our collaborators in Guangzhou, China. The two methodologies are briefly explained in the next sections.

3.16.1. Mapping and filtering of single-cell data

The scRNA-seq libraries were processed using Drop-seq_tools 2.4 (Mitchell *et. al.,* 2020) pipeline for the generation of Digital Gene Expression (DGE) matrices and the alignment with the annotated zebrafish genome (GRCz11, using version 100 of Ensembl) was done using STAR 100 (Dobin *et al.,* 2013) (v2.7.8a). We used exonic, intronic and intragenic reads. For the estimation of the number of obtained cells, a knee-plot was used. DGE matrices were analyzed using the library Seurat v4.1.1 (Hao *et al.,* 2021) in R (v4.2.0) and quality control filters were applied. DoubletFinder (v2.0.3) was used to remove doublets (McGinnis *et al.,*

2019). Then, cells with high percentage of mitochondrial DNA (max=5% for Sham_1 and 30 DPA_1 and max=10% for Sham_2, 7 DPA_1, 7 DPA_2 and 30 DPA_2), high number of reads (max=10.000 UMIs) and low number of genes (min=200) were considered low-quality cells and discarded from the analysis.

3.16.2. Data integration and clustering

The individual Seurat objects were integrated with SCTransform using Canonical Correlation Analysis (CCA), and genes that were expressed in less than 3 cells were discarded from the analysis. For feature selection we used 2000 High Variable Genes (HVGs) in both analyses. For dimensionality reduction we used Principal Component Analysis (PCA), retaining 16 and 20 principal components for all cells and CMs analysis respectively. The Uniform Manifold Approximation and Projection (UMAP) visualization was performed based on the initial PCA and k-nearest-neighbour graph (k=30). Louvain clustering with multilevel refinement was used to determine the number of cellular clusters with resolution 0.4 and 0.1 for all cells and CM cell-states respectively. Top markers were calculated using Seurat's FindAllMarkers function (p_val_adj<0.01) and we used the Top 12 markers of each cluster for generating the heatmap.

3.16.3. Differential expression, Cell cycle and Gene Ontology analysis

Differential expression (DE) analysis was performed with default parameters (logfc.thr=0.25, p_val_ajd.thrs=0.01) and using Seurat's Wilcoxon test, Likelihood-ratio, Student's t-test, Logistic Regression, MAST (v1.22.0) (Finak *et al.,* 2015) and DEseq2 (v1.36.0) (Love *et al*., 2014). Cell cycle analysis was achieved with Seurat's Cell cycle scoring function using the list of genes as described by Sur *et. al.,* 2023. Gene Ontology (GO) analysis was performed in Python using GSEAapy (Fang *et al.,* 2022) and library (v0.10.8), to the annotate the functional identity of the CM clusters. The gene sets used were KEGG_2019, GO_Biological Process_2018, GO_Molecular Function_2018 and GO_Cellualr Component_2018.

3.16.4. Mapping and filtering of stereo-seq data

Fastq files generated from MGI DNBSEQ-Tx sequencer contain CID (Coordinate Identifier) and MID (Molecular Identifier) information in read 1 and cDNA sequences in read 2. CID sequences are mapped to designed chip coordinates with 1 base mismatch tolerance. Reads with low-quality MID or containing N bases are filtered out. CID and MID are appended to read headers. Retained reads are aligned to reference genome using STAR (Dobin et al., 2013), with only reads having MAPQ > 10 counted and annotated to genes. UMIs with the same CID and gene locus are collapsed with 1 mismatch allowance. The pipeline, integrated into SAW (https://github.com/BGIResearch/SAW), produces a CID-containing expression profile matrix.

3.17. Masson's Trichrome Staining

The sections were incubated overnight at room temperature in Bouin solution (Panreac, Cat. No. 254102.1611,). Then, the sections underwent a series of steps: rinsing with running distilled water for 10min, a 3min staining with Weigert Hematoxylin, sequential rinsing with running tap water for 5min and running distilled water for 3min. Next, the sections were immersed in a Xylidine Ponceau - Acid Fuchsin solution for 2.5min, followed by a 5min incubation with a phosphotungstic acid/phosphomolybdic acid solution. Afterward, the sections were rinsed for 5min in running distilled water and stained for 3min with an aniline blue solution. Finally, they were incubated for 2min in 1% acetic acid and rinsed for 3min with running distilled water. Before mounting with DPX (8312-4, Thermo Scientific), the sections underwent dehydration with 96% ethanol, 100% ethanol, and Xylene (251769.2711, Panreac). All dyes were pre-filtered before use.

<u>A more detailed list of the solutions and reagents is shown below:</u>

Weigert's Hematoxylin: mix at equal volumes solution A (Panreac, Cat. No. 253453.1210) and solution B (Panreac, Cat. No. 253454.1210) of weigert Hematoxylin.

Xilidine Ponceau - Acid Fuchine solution: to prepare 300ml dissolve 2.7g of Biebrich scarlet (Panreac, Cat. No. 253986.1605), 0.3g Acid fuchsine (Panreac, Cat. No. 251331.1605), 3ml Acetic acid glacial (Merck, Cat. No. 1.00063.1000) in 300ml of dH2O.

Phosphotungic acid / phosphomolibdic acid solution: to prepare 400ml dissolve 10g of phosphotungic acid (Sigma, Cat. No. 79690) and 10g of phosphomolibdic acid (Sigma, Cat. No. 79560) in 400ml of dH2O.

Aniline blue solution: to prepare 300ml dissolve 7.2g of aniline blue (Panreac, Cat. No. 253708.1606) and 6ml Acetic acid glacial (Merck, Cat. No. 1.00063.1000) in 300ml of dH2O.

1% acetic acid solution: to prepare 500ml mix 5ml of Acetic acid glacial (Merck, Cat. No. 1.00063.1000) with 495ml of dH2O.

Ethanol: all ethanol solutions are prepared as a dilution with dH2O of absolute ethanol (Panreac, Cat. No. 251086.1214).

3.18. Generation of a Ca^{2+} indicator cardiomyocyte-specific reporter zebrafish transgenic line with Tol2 system

The mlc2a:GCaMP6f reporter zebrafish line was generated following the basic principles published by *Kikuta & Kawakami, 2009)*. Briefly the workflow is shown in Figure MM 1 and described in detail in the next sections.

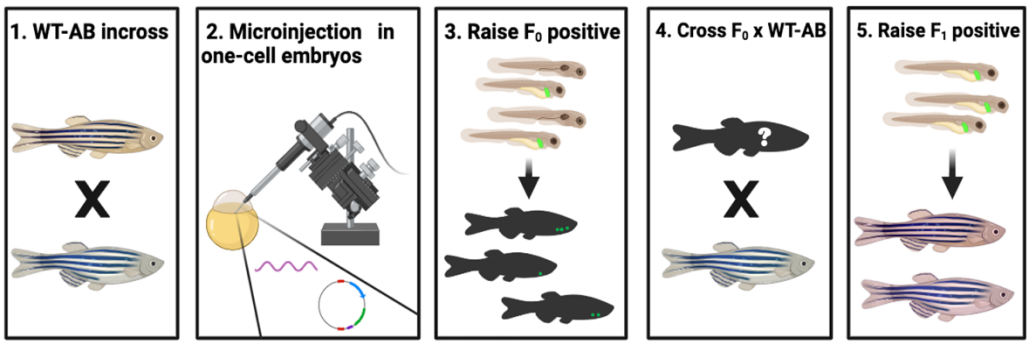

Figure MM 1 Workflow for the generation of a stable transgenic reporter line in zebrafish using the Tol2 system.

3.18.1. Generation of the construct

The transgenic fish were generated taking advantage of the Tol2 transposon system and the Tol2kit. The first part of the construct contained the cardiomyocyte specific promoter *mlc2a*. The second part of the construct contained the gene *GCaMP6f*, cloned from a purchased plasmid (Addgene, Cat. No. # 100835) into a middle entry clone with a multicloning

site from the Tol2kit. The third part of the construct contained the polyA signal. Based on the multisite Gateway cloning, the three entry vectors were recombined, with a single LR clonase reaction inside the pDestTol2pA2 (394) destination vector. The detailed cloning protocol is explained below. All primer used are available in Appendix I Table IV and the plasmid maps are available in Appendix II.

3.18.2. µNeedles and injection plates for zebrafish embryo injection

Glass capillaries (Kwik-Fil, Cat. No.: 1B100-4) were pulled with a micropipette puller (Model P-97, Sutter Instrument). With a ramp test of 865 ± 15, the puller program chosen was: Heat 788; Velocity 45; Time 210; and Pull 65.

For the preparation of injection plates, 1.5% agarose (Sigma, Cat. No: A9939) dissolved in Embryo medium 1x. The agarose solution was poured into a Petri Dish and a microinjection mold was placed to generate six lanes. Each ramp had one 90^{o} and one 45^{o} beveled side.

Embryo medium stock solution (60x): For 1L of 60x medium add 17.2g NaCl (Sigma, Cat. No. S7653), 4.9g $MgSO4 \cdot 7H_2O$ (Sigma, Cat. No. M1880), 2.9g $CaCl2 \cdot 2H2O$ (Sigma, Cat. No. C3306) and 0.76g KCl (Sigma, Cat. No. P5405) in 1L of $dH2O$. Adjust pH to 7.2 with NaOH (Sigma, Cat. No. 221465). When needed, dilute the stock solution at 1x working solution.

3.18.3. Embryonic injection of Tol2-construct and transposase mRNA

The previous day of the injection, *in-cross* of WT-AB fish were set. For the microinjection, a FemtoJet (Eppendorf) was used. More precisely, the embryos were injected in the yolk at one-cell stage with 5nl of injection mix. The injection mix was composed of 1ul transposase mRNA (50 ng/µl), 1ul of pDest-mlc2a:GCaMP6f plasmid (section 3.18.1.), 1µl of Phenol Red (Sigma, Cat. No.: P0290) and 7ul of nuclease-free water (Sigma, Cat. No.: 3098). At 72hpf embryos were screened, and those expressing green fluorescent protein (GFP) fluorescence were selected and grown into adulthood.

3.18.4. Founder (F_0), F_1 and F_2 screening

The screened fish (F_0) that reached adulthood (3-4 months of age), were outcrossed with WT-AB and those which generated offspring positive for GFP signal were selected as Founders. The positive larvae were grown to adulthood (F_1). Two founders were chosen out of ten, over their intensity and homogeneity of signal. Each founder was used to generate an individual line. When F_1 reached adulthood was again crossed with WT-AB to generate the F_2.

3.19. CRISPR-Cas9 biallelic KO zebrafish lines

For the generation of an *anxa2a, mustn1b, fhl1a, casq2* KO zebrafish line we used the basic principles published by *Kroll et al., 2021*.

3.19.1. gRNA design

The gRNA targeted sequences were designed with the Chop-Chop online tool (https://chopchop.cbu.uib.no/). A total of 3 gRNAs per locus were designed against anxa2a, fhl1a, casq2 and 2 against mustn1b. crRNAs were ordered from IDT (Alt-R CRISPR-Cas9 custom crRNAs). The sequences of the crRNAs used are available in Appendix I Table V.

3.19.2. Cas9/gRNA preparation and injection

The crRNAs and Alt-R® CRISPR-Cas9 tracrRNA, ATTO™ 550 (IDT, Cat. No. 1075927) were resuspended in Nuclease-Free Duplex buffer (IDT, Cat. No.: 11-01-03-01) to a final concentration of 200μM and stored at -80^{o}C before use.

The crRNA was annealed with the tracrRNA to form the gRNA by mixing each crRNA for each gene separately with an equal molar of tracrRNA and diluting to 57 μM in Duplex Buffer. Each reaction was incubated at 95^{o}C for 5min and then cooled on ice. For the gRNA/Cas9 assembly, equal volumes of gRNA and Cas9 solutions were mixed, incubated at 37^{o}C for 5min and then cooled on ice, generating a 28.5 μM RNP solution. The Cas9 protein was bought from IDT (Alt-R Cas9 Nuclease V3, 62 μM) and diluted to 57 μM in Cas9 buffer.

The three RNP solutions in the case of *anxa2a* and two RNP solutions for *mustn1b* were pooled in equal amounts before injections, leaving the total RNP concentration at 28.5 µM. For the injections the same procedure was followed as described in section 3.18.2., and approximately 1-5nL of the pool was injected into the yolk at the single-cell stage before cell inflation.

3.19.3. gRNA efficiency and F_0 screening

To check the efficiency of the gRNAs and assure the functionality of the Cas9, around 80-90% of the injected embryos were used for screening. A pool of embryos was used for gDNA extraction. The acquired gDNA was used as a template for PCR amplification and sent for Sanger sequencing. All the targeted exons were amplified and sequenced, and the acquired sequences were introduced to ICE analysis tool by Synthego (https://ice.synthego.com/#/), to analyze the data. The primers used for the screening of each exon are available at Appendix I Table VII. The rest of the embryos were raised to adulthood and at the age of 1 month, were fin-clipped and genotyped for *anxa2a, mustn1b, fhl1a* and *casq2* for insertions and deletions.

3.20. Polyacrylamide gradient gel preparation

Before starting to prepare the polyacrylamide (PAA) solution, we first treated the MatTek plates (MatTek Life Sciences, Cat. No. P35G-0-14-C) with Bind solution and the coverslips with Repel Saline (GE Healthcare, Cat. No.: 17+1332-01). For the polymerization of the gradient gel, we used a photo initiator called Irgacure-2959 (Sigma, Cat. No.: 410896-10G) and a UV lamp, UVP XX-15L series Black Ray 230V (Cat. No.: R/N 95-0042-13).

First, we removed the Bind saline solution and dry out the glass part of the MatTek. We added 25ul of PAA solution in the center of the well and placed a dried coverslip. Once the solution was equally distributed and no air bubbles were present, we located in a 3D printed case designed to be used on top of a syringe pump on one side. A 3D printed mask was designed to fit on the moving part of the syringe part in a way that would reveal the MatTek plate to the UV light along time. The UV lamp was located on top of the pump in 10cm

(Supplementary, Figure A 34). The settings used for the pump are the following. For a 4,7 mm diameter syringe, we used a velocity of 31.2 μm/min. The polymerization lasted 420 sec and then, PBS10x (Biowest, Cat. No. X0515-500) was added on top of the coverslip. The gels were stored in PBS 10x at 4°C until stiffness measurements and cell culture experiments.

Bind Solution: For 2ml of Bind solution, 1,6 ml of Absolute Ethanol, 0,32 ml of MiliQ H_20, 0,2ml of Acetic Acid (Merck, Cat. No. 1.00063.1000) and 0,1ml of Bind Saline (Sigma, Cat. No. M6514-25ML)

Polyacrylamide solution (PAA): For 2ml of PAA solution, 0,750ml of Acrylamide 40% (Biorad, Cat. No.), 1ml of Bis-acrylamide 2% (Biorad, Cat. No.), 0,05ml of MiliQ H2O and 0,2 ml of PBS 10x (Biowest, Cat. No. X0515-500)

3.21. Nanoindentation for mechanical properties characterization

For measuring the stiffness of the PAA gels, we used the nanoindentation instrument *Chiaro* from Optics 11. The displacement mode was employed for the measurement, and the Young's Modulus (E) of the PAA gels was calculated using the Hertz model. Before every use, the system was calibrated in 1x PBS using a glass surface. All the measurements were carried out manufacturer's instructions with a 9.5μm radius and 0.32 N/m stiffness probe. The basic principle of how the instrument operates is shown below (Figure MM 3).

3.22. Functionalization and coating of PAA gels

Prior to cell culture experiments, PAA gels were functionalized with Sulfo-SANPAH (sulfosuccinimidyl 6-(4'-azido-2'-nitrophenylamino)hexanoate) (Sigma, Cat. No. 22589) before their use. Briefly, 20 μl of Sulfo-SANPAH diluted in 480 μl MiliQ-H_2O, were added on the of the gel and let under UV for 5min. Then, the gel was washed 3 times with PBS1x, and coated with MatriGel® (1:100) and incubated overnight at 4°C.

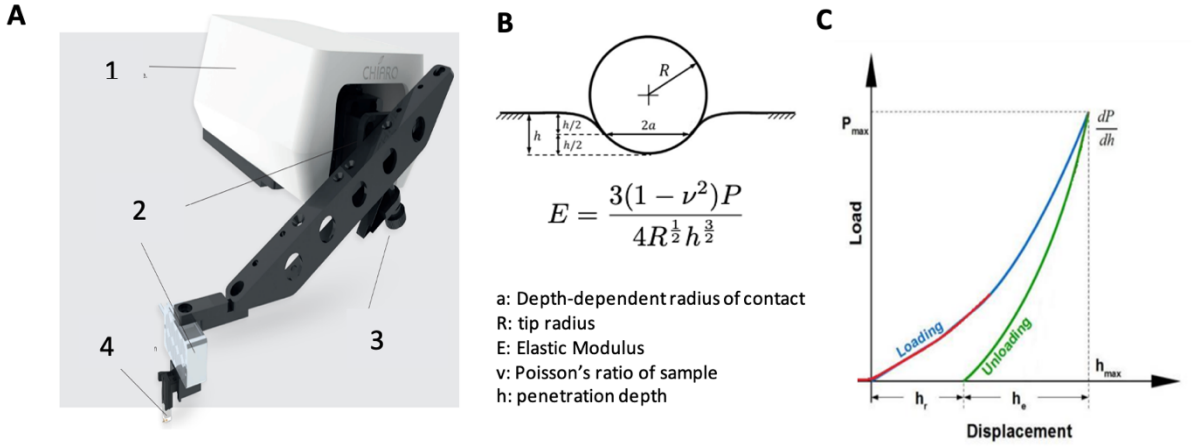

Figure MM 2 The Chiaro nanoindentation instrument. (A) The Chiaro nanoindenter device. 1: Chiaro, 2: Closed loop XYZ stages, 3: Manual sliding stage, 4: probe **(B)** Representation of a spherical indentation and mathematical equation calculating Eff based on Hertzian contact. Hertz model assumes material to be purely linear elastic instead of elastic-plastic **(C**) The loading curve is used to derive the effective Young's modulus.

3.23. Statistical analysis

Statistical analysis for most computational analyses was performed in R using the implemented packages. To calculate the changes in the proportion of cell types we used scCODA tool (Büttner *et al.,* 2021) in Python.

GraphPad Prism 10 software (Version 10.1.1 (270)) was used to carry out all the statistics that were not part of the bioinformatic analysis. All results are expressed as mean ± standard error of mean (SEM). The number of samples (n) used in each independent experiment is shown in the legends and each specific statistical test is specified in each figure legend.

4. RESULTS

Chapter I

Study of the transcriptomic changes in zebrafish heart regeneration in single-cell resolution

4.1.1. Development and characterization of a cold active protease dissociation protocol

To minimize dissociation-induced artifacts and mitigate collagenase-associated stress responses, we developed a protocol suitable for downstream single-cell transcriptomics analysis of cardiac tissues. The dissociation method uses a serine protease purified from *Bacillus licheniformis;* a soil psychrophilic bacteria isolated from glaciers. The high enzymatic activity of the protease in low temperatures, makes it possible for most of the process to been carried out at 4^{o}C (Figure R 1A). In the digestion mix, we added EDTA, a chylic compound, to facilitate the dissociation and assure that the excess of Ca^{2+} , released from dead cells, would not provoke any apoptotic response or transcriptomic changes in the cardiomyocytes, due to the calcium paradox (Frank et al 1982). This phenomenon is observed during isolation of primary cardiomyocytes, where the reintroduction of calcium to calcium-depleted cardiomyocytes leads to cellular death. The combination of enzymatic and mechanical dissociation produced a high-quality single-cell suspension where the heterogeneity in cell populations can be maintained intact after the dissociation (Figure R 1B). For the identification of the of three main populations of zebrafish ventricle we used reporter lines labeling cardiomyocytes, endothelial cells, and fibroblasts. Then, we wanted to ensure that the morphology of the CMs would not have an impact at the process of encapsulation. We performed single-cell encapsulation using NADIA, a droplet-based microfluidic platform, but omitting *Sarkosyl* in the lysis buffer, to image the cells inside the oil droplets (Figure R 1C). We demonstrated that we can successfully encapsulate both CMs and other cell types, in the oil droplets in a single-cell state and also that we were able to encapsulate cells as big as 50μm.

Moreover, to determine the quality of the RNA after the tissue dissociation and before encapsulation of the cells, we extracted the RNA of a single-cell suspension derived from 10 non-amputated zebrafish ventricles, by using the Maxwell system. Then, we used the Agilent Tape Station to measure the RNA quality of the sample. The electrophoresis showed a high-quality RNA, with an RNA Integrity Number (RIN) of 8.7 (Figure R 1D). Finally, we checked the viability of the cells after the dissociation with flow cytometry and Trypan Blue assay (Figure R 1E). Both methods, showed high percentage of viability (> 90%), ensuring top quality cells for single-cell transcriptomics experiments.

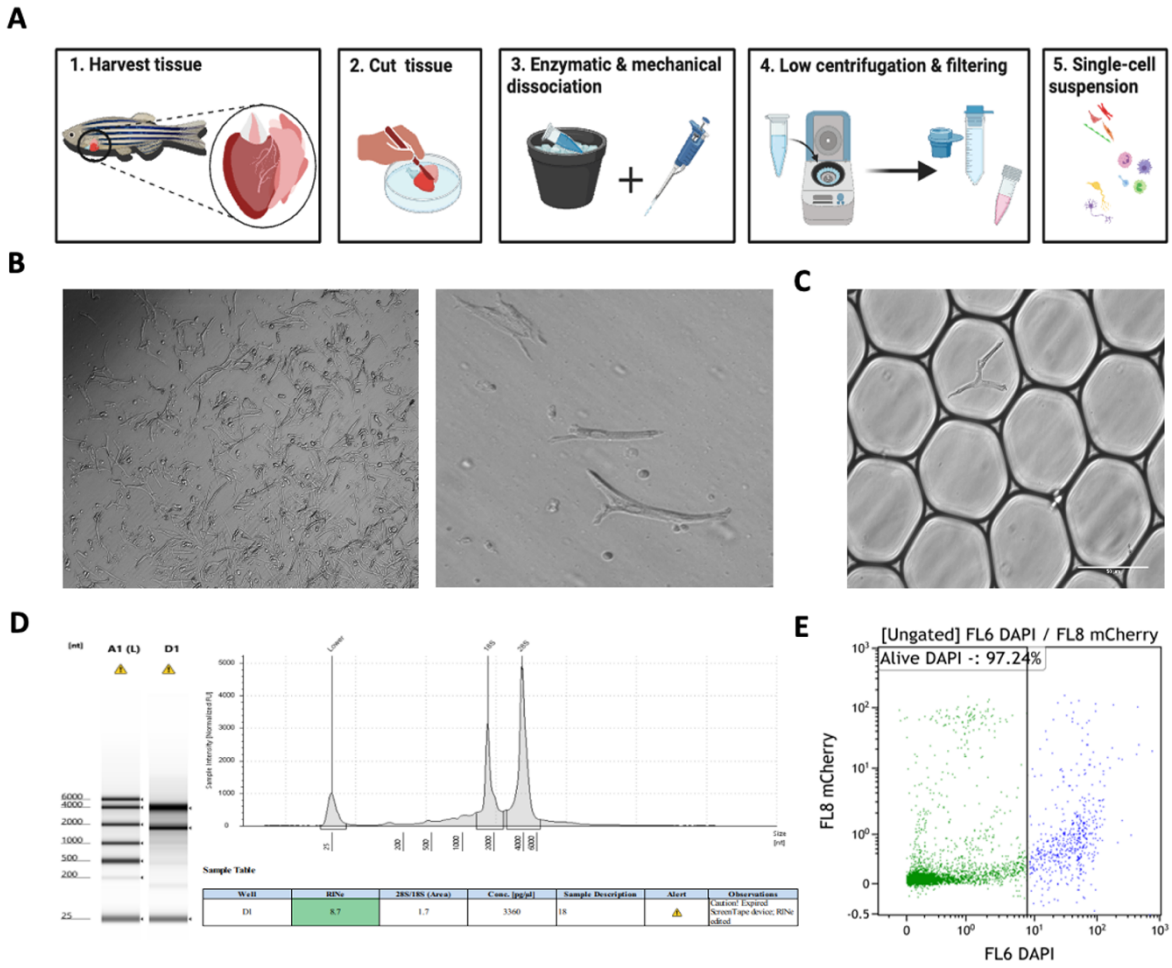

Figure R 1 Characterization of a cold active protease dissociation protocol. **(A)** Cartoon representation of the cold-active protease dissociation protocol. (B) Single-cell suspension after tissue dissociation showing the heterogeneity in cell morphology. **(C)** Encapsulated cells in oil droplets using the NADIA platform; cardiomyocyte (black arrow); other cell type (white arrow). **(D)** RNA QC after dissociation using the Agilent Tapestation. **(E)** FACS analysis of isolated cells gated for DAPI.

The result of the dissociation protocol was, therefore, a single-cell suspension enriched in high viable cells, good RNA quality, and composed of all main cardiac cell types. Thus, validating that our zebrafish heart dissociation protocol is suitable for single-cell transcriptomic experiments.

4.1.2. Changes in the profile of IER Genes

The IER genes are prime candidates for expression changes upon tissue dissociation (Adam et al., 2017; Konturek-Ciesla et al., 2024; O'Flanagan et al., 2019). To uncover the effect of our dissociation protocol on the expression of these genes, we performed Reverse Transcription quantitative Polymerase Chain Reaction (RT-qPCR) from RNA samples extracted

directly from the zebrafish ventricle and from single-cell suspension upon dissociation at low (4°C) and high temperature (37°C) for 15 minutes. We chose the orthologs of temperature-depended dissociation signature IER genes that were previously described in literature. The list include six genes upregulated at high temperature dissociation (*atf3, fosab, socs3a, ier2a, ier2b, hoxd3a*), two at low temperatures (*ank1a* and *gspt1*) and one in both conditions (*serpinh1b*) (Adam et al., 2017; Neuschulz et al., 2023). We confirmed that we have an increase in the levels of expression in five out of six genes after dissociating cardiac tissue at

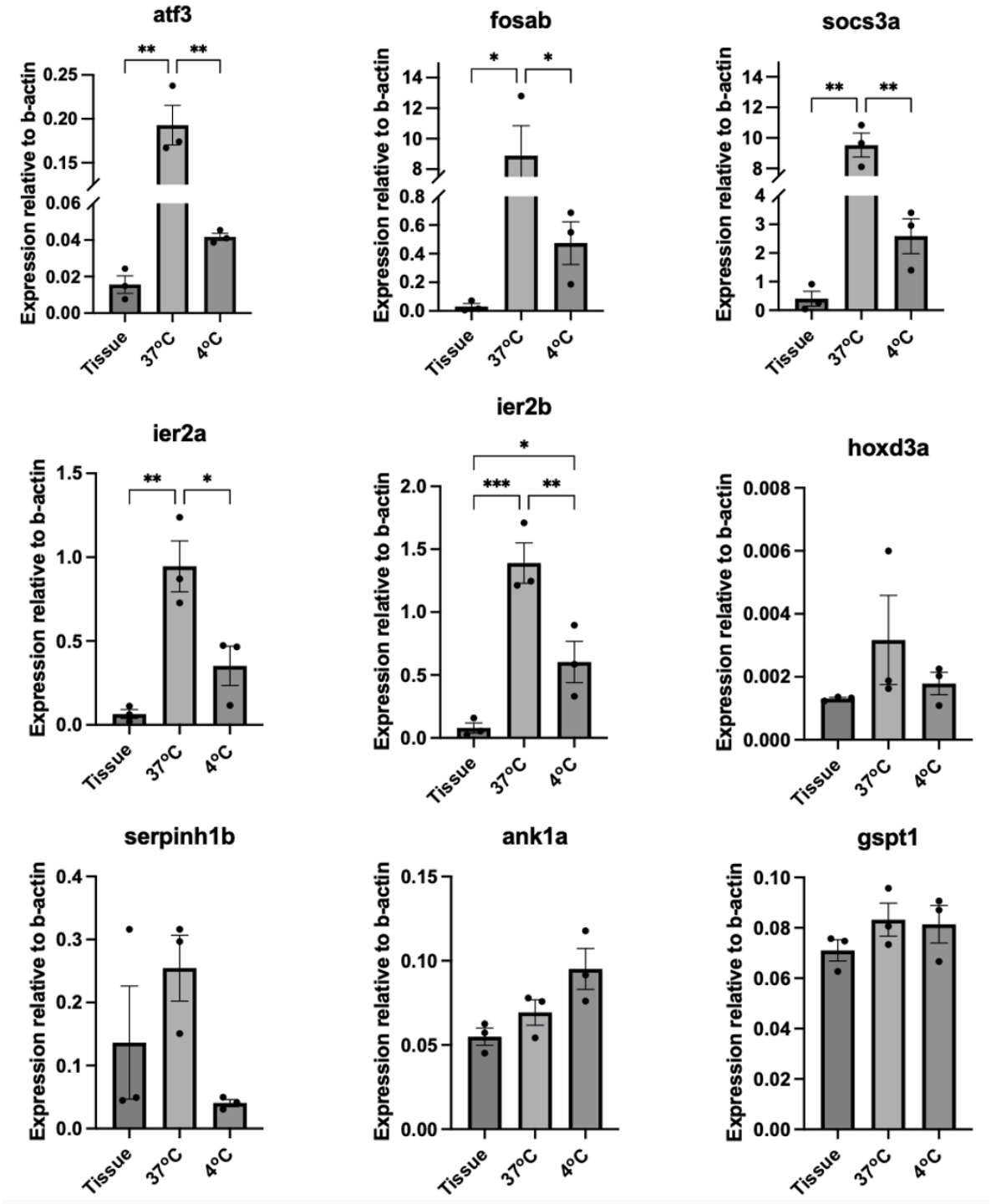

Figure R 2 Changes in the profile of IER genes upon different dissociation methods. RT-qPCR of IER genes after tissue dissociation with collagenase-based protocol (37°C), cold active protease (4°C) or directly extracted from fresh tissue. With N=3 the number of independent experiments and n=3 the number of hearts pooled per condition in each experiment. Statistical significance was assessed with Two-way ANOVA using Tukey's multiple comparison test analysis. ***, p<0.001; **, p<0.01; *,p<0.05

high temperatures, with *fosab* and *socs3a* reaching 9-fold increase above baseline tissue levels. Interestingly, we observed an increase in the expression of *ier2b*, one of two paralogs of IER2 found in zebrafish, after dissociation in both low and high temperatures. Although we observe a downregulation of *serpinh1b* at 4°C, no significant difference in the expression levels were found when comparing the three conditions. Finally, we could not observe a significant increase in the expression of *ank1a* and *gspt1* at low dissociation temperature compared to basal tissue level (Figure R 2).

These results reveal that cardiac tissue dissociation shows a similar stress response signature as found in other tissues, induced by high temperature of dissociation. Also suggest, that the cold active protease protocol could minimize artificial changes in gene expression.

4.1.3. Transcriptomic profile in adult zebrafish hearts during regeneration

To profile the transcriptomic changes of cardiac cell types in healthy and regenerating zebrafish ventricles, we used our dissociation protocol and performed scRNA-seq of » 16,000 cells. To focus the study on the regenerative myocardium, we used the bottom half ventricles of uninjured (Sham), regenerating hearts at 7 DPA and upon homeostatic recovery at 30 DPA (Figure R 3A). For each timepoint, we used a total of n= 15-20 ventricles, we encapsulated the cells using NADIA platform, and sequenced the generated libraries with a NextSeq 500/550 system from Illumina. We aimed for at least 25.000 reads/cell, and we used a pipeline suitable for droplet-based encapsulation for data demultiplexing and transcriptome mapping. Then, we used the R package Seurat for quality control filtering, clustering, and visualization. More specifically, cells with low number of genes (nFeature_RNA), high number of reads (nCount_RNA) and high % of mtDNA (percent.mt) were discarded from the analysis (Supplementary, Figure A 18). Also, batch correction was achieved by integration of the

datasets with CCA to avoid any bias generated by the variability of each independent experiment (Supplementary, Figure A 19).

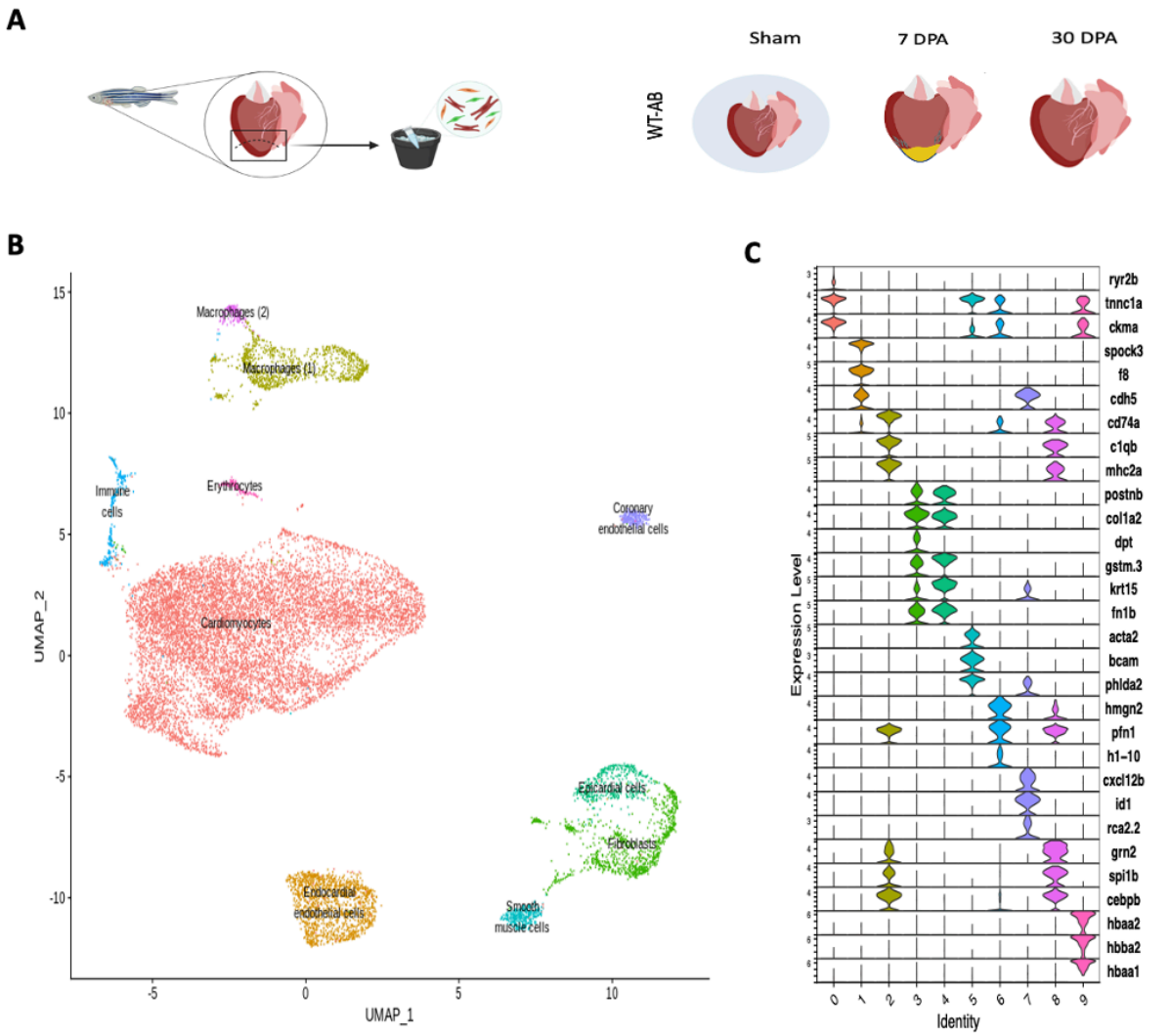

Figure R 3 The cellular composition of the zebrafish heart. (A) Cartoon representation of the experimental design. **(B)** UMAP plot of integrated datasets showing clusters and cluster cell-type annotations **. (C)** Violin plots depicting the average expression of Top 3 selected markers for each cell-type population.

After unsupervised clustering of the scRNA-seq data and for a resolution of r=0.4 (Supplementary, Figure A 20), we could find 10 clusters comprising all major cell types of the cardiac tissue (Figure R 3B). Based on known marker gene expression (Figure R 3C) we were able to identify these clusters. For convenience in the first part of our analysis, we unified the different cardiomyocyte clusters into a single cluster under the pan-cardiomyocyte marker (*clmc2*) (Supplementary, Figure A 21). The major populations included cardiomyocytes (*tnnc1a*), endocardial endothelial cells (*spock3*), macrophages (*cd74a*), fibroblasts (*col1a2*)

and epicardial cells (*krt15*). Smaller populations included immune cells (*hmgn2*), smooth muscle cells (*acta2*) and erythrocytes (*hbba2*).

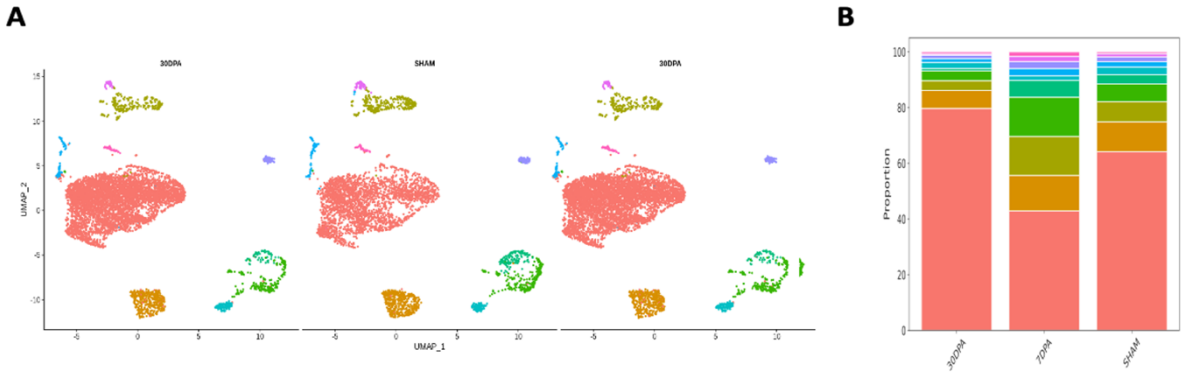

Figure R 4 Cell population dynamics during zebrafish heart regeneration. (A) Joint analysis of data from non-amputated hearts and hearts at 7- and 30-DPA **(B)** Bar plots showing the contribution of different cell types at each time point.

We can observe that all cell types can be found in the three timepoints (Figure R 4A). Although we could observe an increasing of fibroblasts and immune cells at 7 DPA, when we further used the scCODA toolbox in R investigate the cellular diversity dynamics along the regeneration process, we could not find any statistically significant changes (Figure R 4B).

4.1.4. Novel cardiomyocyte cell-states characterization during heart regeneration

Detailed scRNA-seq studies on non-myocytes have shed light on their contribution during heart regeneration. However, little is known about the role of the cardiomyocytes and their crosstalk with other cell types. To address these questions, we first analyzed the cardiomyocyte cluster separately, using the same approach as before.

By repeating unsupervised clustering and for a resolution of r=0.1 (Supplementary, Figure A 22 and A 23), with biological sense, we were able to identify six clusters, each one corresponding to a different cardiomyocyte cell state present in the zebrafish regenerating heart (Figure R 4 A). The markers characterized each cluster are depicted in the Bubble plot (Figure R 4 B). We performed Gene Ontology (GO) analysis to check the pathways and biological processes that are enriched in each cluster for further characterization of their identities (Supplementary, Figure A 24). Also, we performed cell cycle analysis of the clusters

and plotted ribosomal genes to assure that none of them were formed due to bias generated from these processes (Supplementary, Figure A 25).

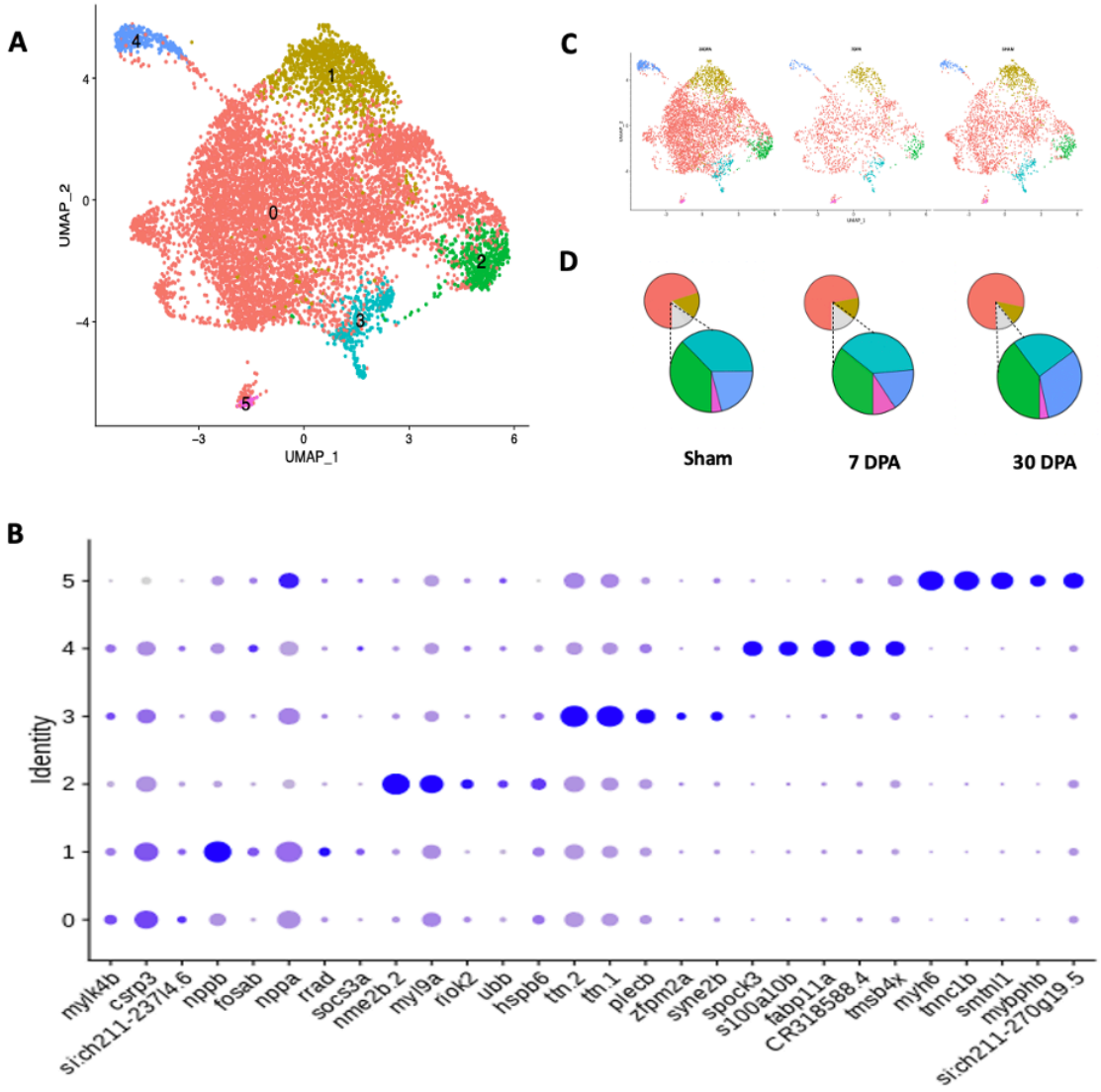

Figure R 5 In depth analysis of the cardiomyocytes populations. (A) UMAP plot of integrated with CCA datasets showing clusters of different cardiomyocyte cell states **(B)** Bubble plot of Top 5 markers for each cluster **(C)** UMAP plot for the three timepoints studied **(D)** scCODA analysis of the cellular dynamics during regeneration

Taking all these together, we suggest that Cluster 0, the biggest size cluster, composed of cardiomyocytes with role to maintain the basic function of the heart in healthy and regenerating hearts. Cardiomyocytes express markers of cluster 1 in homeostatic condition across the whole myocardium but upon injury, cardiomyocytes closer to the border zone of the wound increase the expression of these markers. Cluster 2, a middle size cluster, express many markers related to protein translation and regulation of ribosomal activity (Figure R 7

A). Cluster 3 is consisted of cardiomyocytes that they are actively undergoing cytoskeleton changes and have activated the Apelin signaling pathway. Cluster 4 express many markers also found in endothelial cell types or fibroblasts. To assure that during the bioinformatic analysis only cardiomyocytes were re-analyzed we plotted the cells of cluster 4 in the UMAP with all the cardiac cell types and confirmed that these cells belong to the cardiomyocyte cluster (Supplementary, Figure A 25). The smallest cluster is characterized by markers usually expressed in atrial cardiomyocytes. The upregulation of these markers in ventricular cardiomyocytes, could be an indication that cluster 5 consists of cardiomyocytes that developed hypertrophy to sustain the extra workload.

Then we wanted to know how the population dynamics of these cell populations change during the regeneration process. Similarly, as in the first scCODA analysis, we were not able to detect any differences in the composition of the regeneration heart regarding the identities of these cardiomyocytes (Figure R 5 D). In order to exclude any artifact introduced during the independent experiments, we checked how the markers of each cluster change during regeneration (Supplementary, Figure A 26). We observed that, indeed, at 7 DPA the expression of many of these markers were increased corresponding with the cell identity assigned to each cluster. Dedifferentiating CMs and CMs with a possible hypertrophic phenotype upregulate titin and atrial markers respectively, in accordance with their function. On the contrary, cardiomyocytes of cluster 2, seem to downregulate many of their markers, reinforcing the idea that these cardiomyocytes are no longer in *hibernating* state.

To validate the clusters and examine expression pattern of marker genes we performed *in situ* hybridization with DIG-labeled RNA probes in SHAM and 7 DPA heart sections. The selected markers, cell identity and ISH for each cluster are shown in Figure R 6. We observed that *csrp3* shows a uniform distribution across the myocardium. The patterns of cluster 1 and 3 show similarities as the expression of both *nppb* and *ttn.2* is located close to the injury site. Cluster 4 is small group of cardiomyocytes with specific markers. However, the expression of those markers by other cell types, result in an expression pattern along the whole myocardium, indicating that a double-ISH would been needed for further characterization of the localization of this cluster. The expression pattern of *tnnc1b,* markers of Cluster 5, is mainly detected in thicker parts of myocardium, with minor staining in the

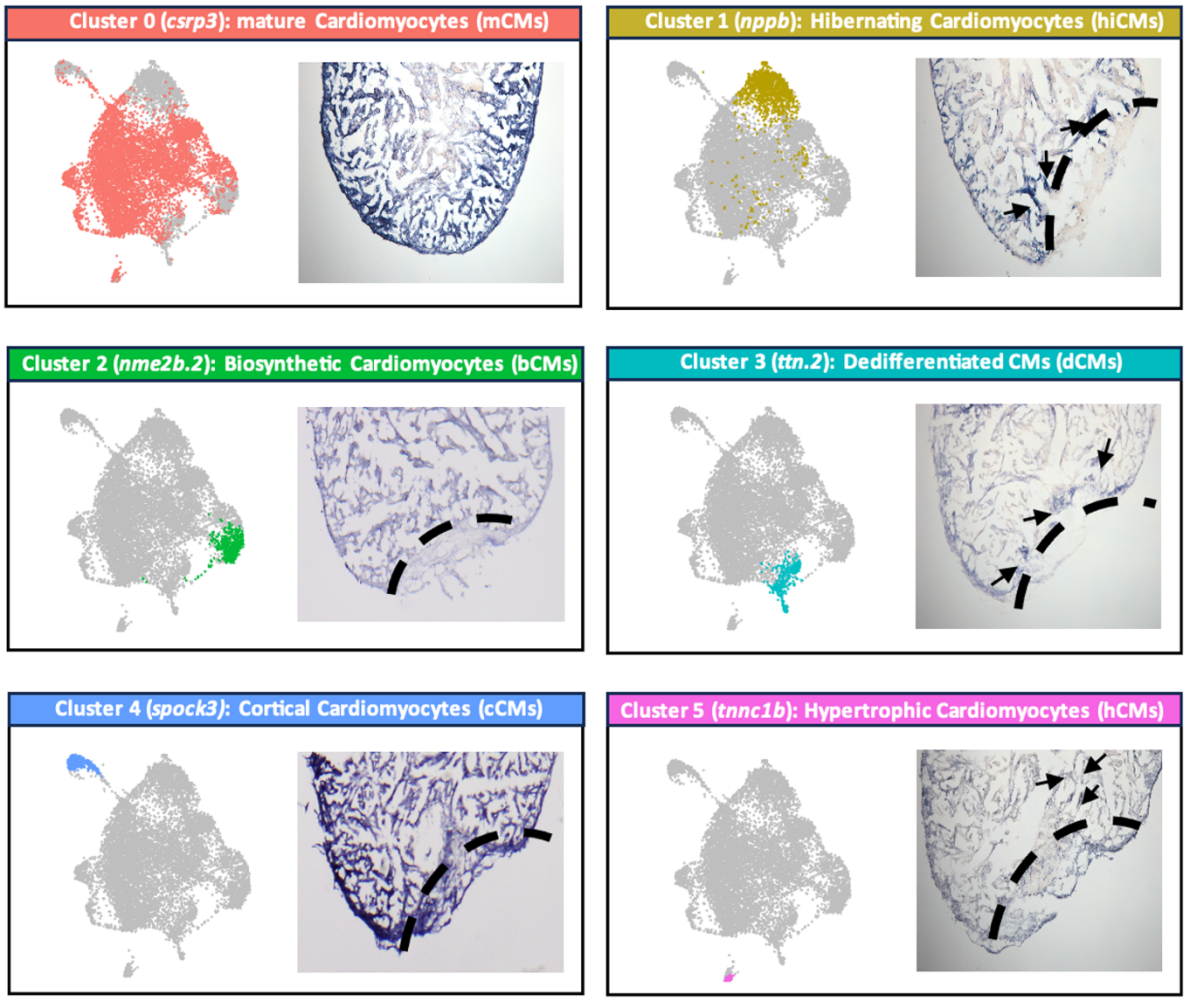

Figure R 6 Validation of cardiomyocyte cell states clusters with *in situ* hybridization. (A) Mature CMs expressing *csrp3* **(B)** Hibernating CMs expressing *nppb* **(C)** Biosynthetic CMs with high ribosomal activity expressing *nme2b.2* **(D)** Dedifferentiated CMs expressing *ttn.2* **(E)** Cortical CMs expressing *spock3* and **(F)** CMs with a Hypertrophic phenotype expressing *tnnc1b.*

epicardium/cortical cells, enhancing the idea of hypertrophic cardiomyocyte composing this cluster. Finally, in addition to ISH of *nme2b.2*, that showed a uniform distributed expression across the whole ventricle, we wanted to validate cluster 2 with an assay suitable to label cells undergoing proteinosynthesis. We used O-Propargyl Puromycin (OPP), an analog of puromycin that incorporates to newly synthesized peptides and thus labels cells with higher ribosomal activity (Figure R 7B). We observed a homogenous pattern across the myocardium in both Sham and 7 DPA but a higher signal adjacent to the wound are at 7 DPA.

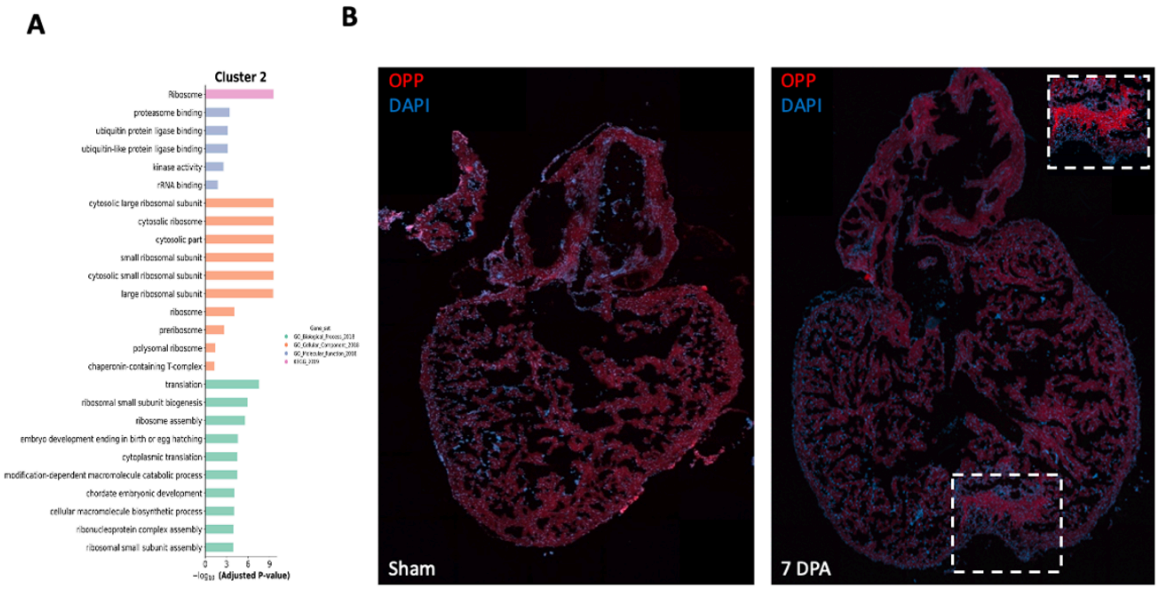

Figure R 7 Validation of Biosynthetic CMs cluster. (A) GO analysis **(B)** OPP detection at Sham and 7 DPA hearts

These results revealed the existence of novel cardiomyocyte cell states at all timepoints of regeneration with distinct function. Further investigation is needed for understanding the contribution of each cluster in the regeneration process.

4.1.5. Dynamic transcriptomic changes during heart regeneration

To determine the transcriptomic changes between the different cardiomyocyte cell-states during zebrafish heart regeneration we performed DE analysis using Seurat's default Wilcoxon test and other alternative ones, including Likelihood-ratio, Student's t-test, Logistic Regression, MAST and DESeq2. More specifically, we performed pair-wise comparison for the three timepoints and found the intersections of common genes detected with every test (Supplementary, Figure A 27). We observed that DESeq2 leads in an overestimation of DE genes, compared with other tests that present only a small deviation in the total number of detected genes among them. Logistic Regression and MAST are the only tests that intersect with at least one more test. Then, we checked the number distribution of the DE genes among the clusters. Five out of six tests show similar numbers of detected genes per cluster. The decrease in number of DE genes detected for each cluster correlates with the reduction of its size and not the number of intersections between the tests (Supplementary, Table A 7). The

majority of DE genes are observed in cluster 0, followed by cluster 1 and 2. On the contrary, cluster 3 and 4 only contain one or two genes for most of the tests. For cluster 5, the smallest cluster of the dataset consisted of 57 cells, detection of DE genes was not achieved with any test but with DESeq2. For the rest of the analysis, we chose to continue with MAST as the most stringent of all tests. We detected 100 genes when compared for Sham - 7 DPA, 166 genes for Sham - 30 DPA, and 290 genes for 7 DPA - 30 DPA, that are differentially expressed.

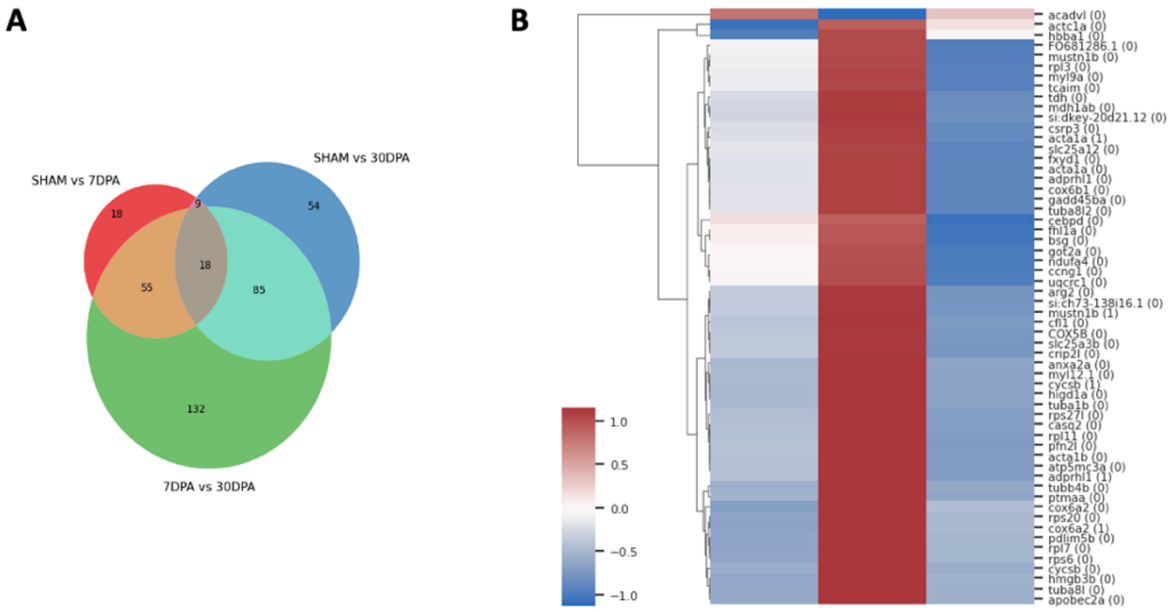

Figure R 8 Differential gene expression analysis during heart regeneration. (A) Venn diagram depicting the intersection and number of DEGs which expression changes at 7 DPA and then recovers to basal levels at 30 DPA **(B)** Heatmap of DGE that are up- or down- regulated at 7 DPA, their average expression and the cluster they are represented

To understand the molecular signatures that govern cardiomyocyte proliferation, migration, and further maturation to fully differentiated cardiomyocytes, we focused our analysis on the genes that are up- or down- regulated at 7 DPA and their expression returns to baseline levels upon homeostatic recovery at 30 DPA. The intersection with this expression pattern, includes a total number of 55 genes, for all clusters (Figure R 8A). Gene ontology (GO) analysis showed that most of the genes are enriched in processes such as metabolism, protein translation, apoptosis, and cytoskeleton organization (Supplementary, Figure A 29). Heatmap representation of the average expression of these genes showed that the vast majority are upregulated at 7 DPA and only 1 gene (*acadvl)* present at cluster 0, showed a decrease in the expression level at the same timepoint (Figure R 8B). In cluster 1, we detected 12 upregulated

genes and in cluster 2 only one (*anxa2a*). A more detailed list of the DE genes is shown in Supplementary Table A 8. We observed that *anxa2a* was upregulated in three out of six clusters, and *mustn1b* in two at 7 DPA, which is highly suggestive of implication in the regeneration process. We also considered *fhl1a* and *casq2*, based on their function, as other genes that are likely to play important roles in regeneration, and thus amenable to further investigation.

Chapter II

Study of novel markers with possible implication in zebrafish heart regeneration

4.2.1. Characterization of *anxa2a* in zebrafish cardiac regeneration

One of the most dynamically expressed gene in our cardiomyocyte analysis was *anxa2a* encoding for Annexin A2A. First, we sought the expression of *anxa2a* in other cell types during heart regeneration (Figure R 9A). We observed that other cell types also express *anxa2a* in both healthy and regenerating conditions. For the expression pattern of *anxa2a* we performed ISH experiments. We observed that the gene is first detected at the adjacent to the injury site in cardiomyocytes and epicardial cells, with minor staining in the remote myocardium, epicardium and bulbus arteriosus (Figure R 9B). Finally, we checked the spatiotemporal localization of the protein by IHC against Annexin A2 (Anxa2) and MF20, a cardiomyocyte specific marker (Figure R 9C). IHC detection of Anxa2 showed expression mainly in the epicardium across all timepoints. However, at 7 DPA a higher signal is detected adjacent to injury site and the cortical CM layer, which is maintained until 30 DPA.

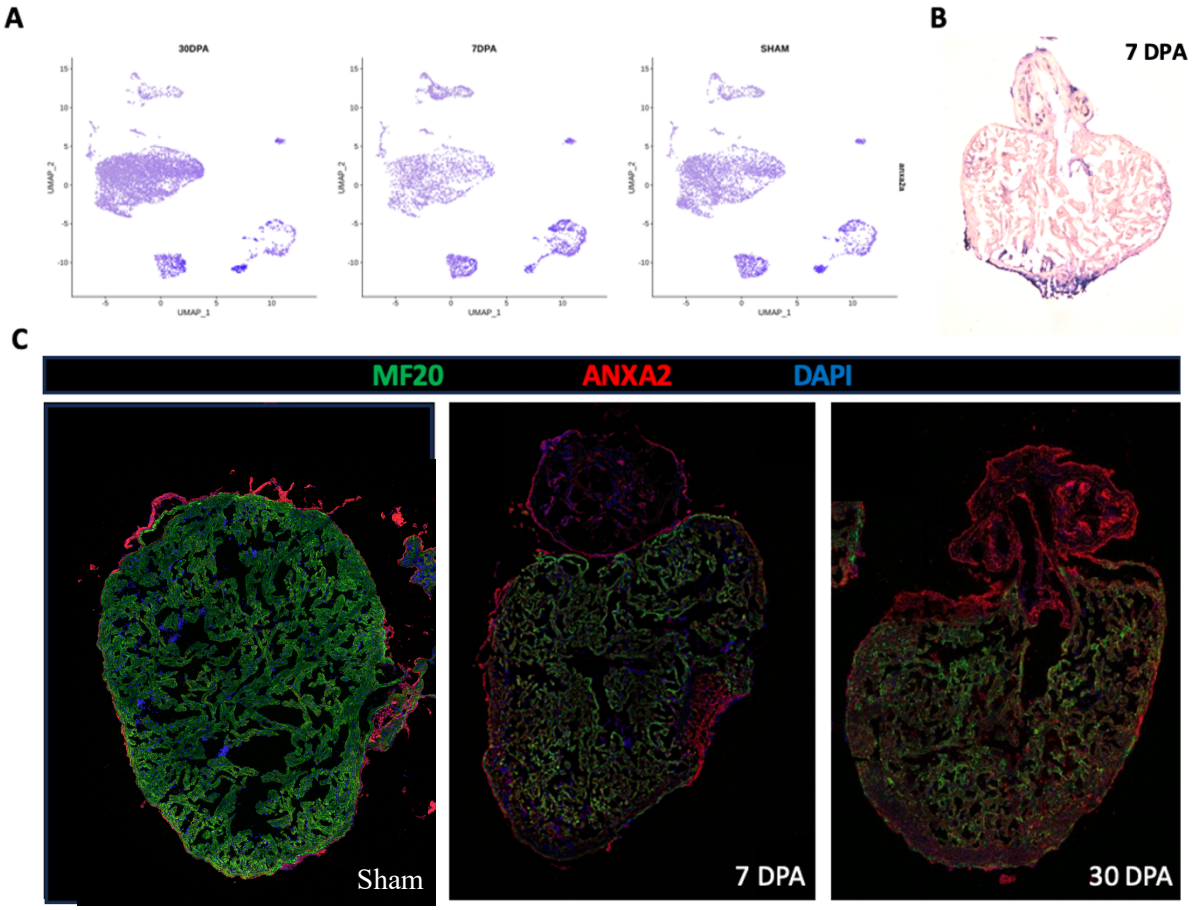

Figure R 9 Spatiotemporal detection of anxa2a in mRNA and protein level. (A) UMAP representation of the expression of *anxa2a* in all cells at three analyzed timepoints. **(B)** ISH of *anxa2a* at 7DPA cryosection. **(C)** Immunohistochemistry of MF20 (cardiomyocytes), ANXA2 (annexin A2) and DAPI (nuclei) during regeneration.

4.2.2. Generation of knock-out lines using CRISPR-Cas9 technology to study cardiac regeneration

For functional characterization of the candidate genes and their role during heart regeneration, we decided to generate a KO line for each gene with the CRISPR/Cas9 technology. For rapid characterization of the KO phenotype since the first generation of fish (F_0: fish injected with gRNA and Cas9) we followed the *F_0 biallelic knock-out strategy* described by (Kroll et al., 2021), by targeting multiple exons of the same gene simultaneously.

The locus of *anxa2a,* coding for Annexin 2A, is located at the forward strand of chromosome 25 and has two splice variants transcripts. We designed three gRNAs against exon 2,3 and 4 of *anxa2a* (Figure R 10A). The cutting efficiency of the gRNAs was assessed in a pool of n=15 injected embryos (Supplementary, Figure A 30).

The locus of *mustn1b,* coding for Musculoskeletal embryonic nuclear protein 1B, is located at the reverse strand of chromosome 11 and has one transcript. We designed two gRNAs against exon 2 and 3 of *mustn1b* (Figure R 11A). The cutting efficiency of the gRNAs was assessed in a pool of n=20 injected embryos (Supplementary figure, Figure A 31).

The locus of *fhl1a,* coding for four and a half LIM domains 1A, is located at the forward strand of chromosome 14 and has two protein coding splice variant transcripts. We designed three gRNAs against exon 2,3 and 5 of *fhl1a* (Figure R 12A). The cutting efficiency of the gRNAs was assessed in a pool of n=20 injected embryos (Supplementary, Figure A 32).

The locus of *casq2,* coding for Calsequestrin 2, is located at the reverse strand of chromosome 9 and has one transcript. We designed three gRNAs against exon 1,2 and 4 of *casq2* (Figure R 13A). The cutting efficiency of the gRNAs was assessed in a pool of n=10 injected embryos (Supplementary, Figure A 33).

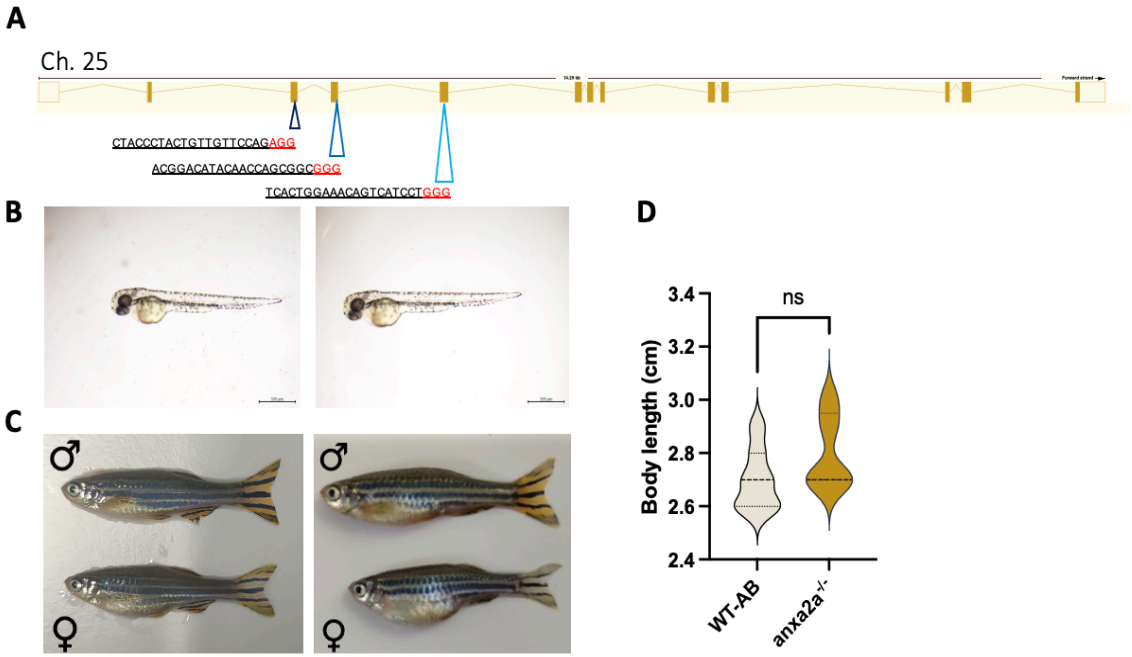

Figure R 10 anxa2a$^{-/-}$ F0 biallelic KO line with CRISPR/Cas9. (A) Design of the gRNAs against anxa2a targeting the exon 2,3 and 4 **(B)** Images of 3 dpf WT and anxa2a$^{-/-}$ larvae **(C)** Image of adult male and female WT and anxa2a$^{-/-}$ zebrafish **(D)** Boxplot of the body length from head to tail-base of WT and anxa2a$^{-/-}$ zebrafish.

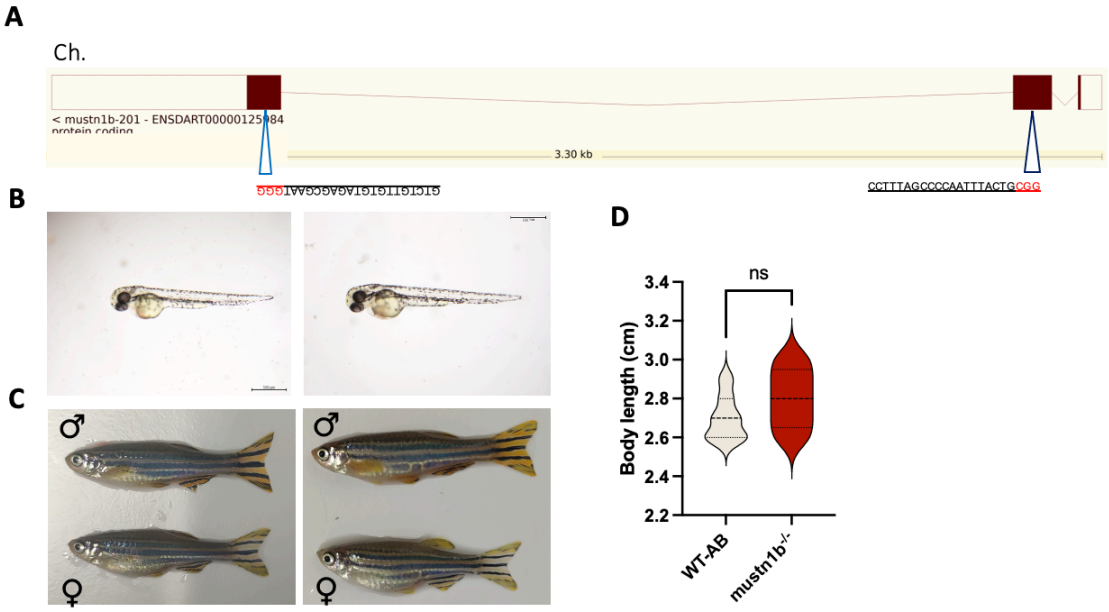

Figure R 11 mustn1b$^{-/-}$ F0 biallelic KO line with CRISPR/Cas9. (A) Design of the gRNAs against mustn1b targeting the exon 2 and 3 **(B)** Images of 3 dpf WT and mustn1b$^{-/-}$ larvae **(C)** Image of adult male and female WT and mustn1b$^{-/-}$ zebrafish **(D)** Boxplot of the body length from head to tail-base of WT and mustn1b$^{-/-}$ zebrafish.

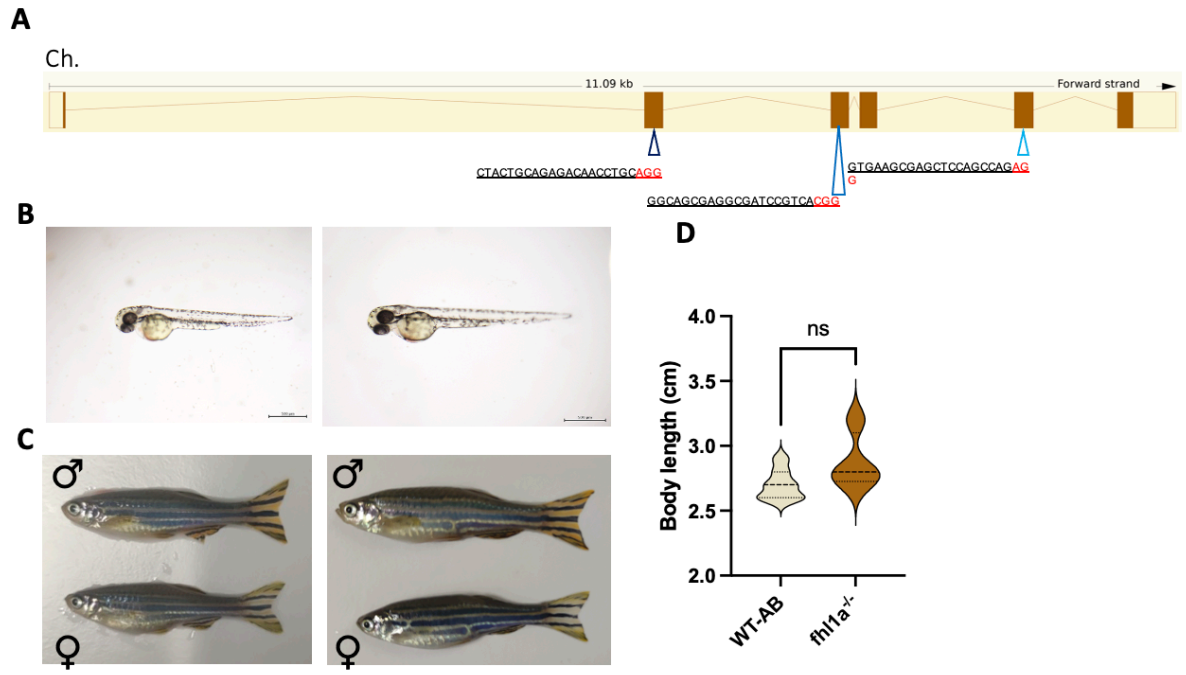

Figure R 13 fhl1a$^{-/-}$ F0 biallelic KO line with CRISPR/Cas9. (A) Design of the gRNAs against fhl1a targeting the exon 2,3 and 4 **(B)** Images of 3 dpf WT and fhl1a$^{-/-}$ larvae **(C)** Image of adult male and female WT and fhl1a$^{-/-}$ zebrafish **(D)** Boxplot of the body length from head to tail-base of WT and fhl1a$^{-/-}$ zebrafish.

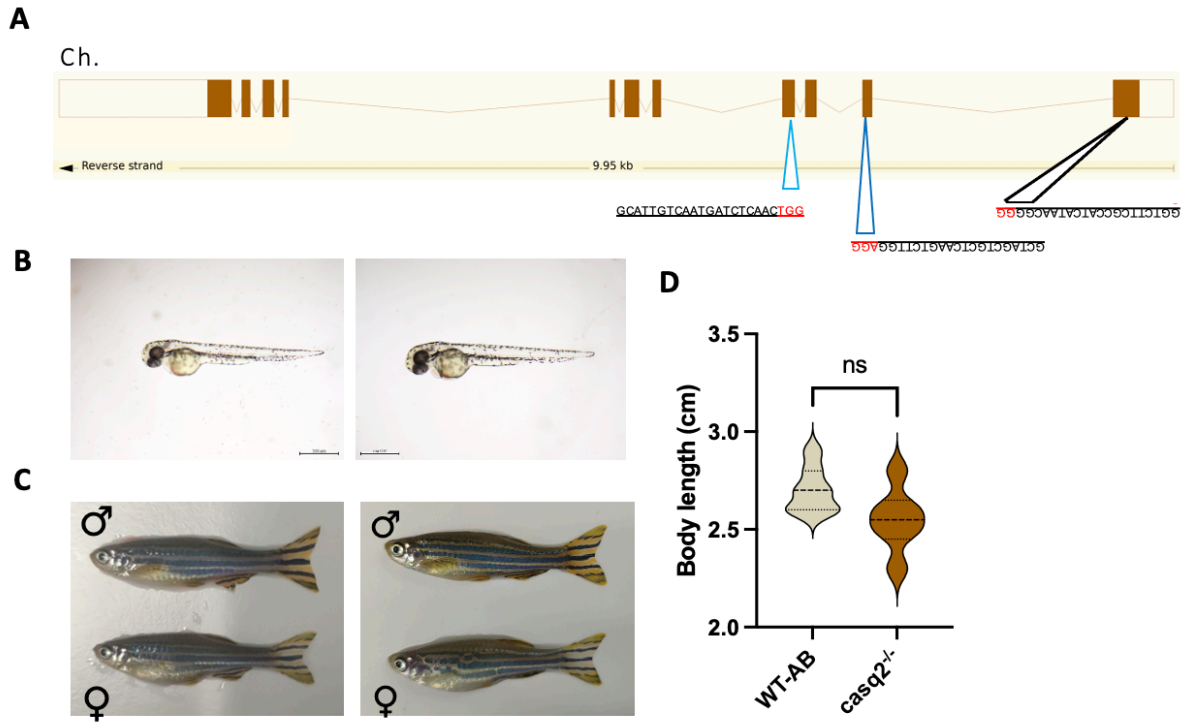

Figure R 12 casq2$^{-/-}$ F0 biallelic KO line with CRISPR/Cas9. (A) Design of the gRNAs against casq2 targeting the exon 1,2 and 4 **(B)** Images of 3 dpf WT and casq2$^{-/-}$ larvae **(C)** Image of adult male and female WT and casq2$^{-/-}$ zebrafish **(D)** Boxplot of the body length from head to tail-base of WT and casq2$^{-/-}$ zebrafish**.**

If indels were generated successfully, the rest of injected embryos were raised to adulthood for the generation of a stable KO line and heart regeneration experiments. In all four cases, injected embryos did not display any developmental defect (Figure R 10B, 11B, 12B and 13B) and the adult fish do not display any detectable phenotype (Figure R 10C,11C, 12C and 13C). Zebrafish had a normal growth and neither their body length nor fertility were affected (Figure R 10D, 11D, 12D and 13D).

4.2.3. Competence of Anxa2a, Mustn1b, Fhl1a and Casq2 mutants for heart regeneration

To assess heart regeneration competence of the four KOs, we performed apex resection injuries to 4 months KO and WT animals. After 30 DPA we observed that the KOs were not able to regenerate the myocardium compared to most of the WT animals (Figure R

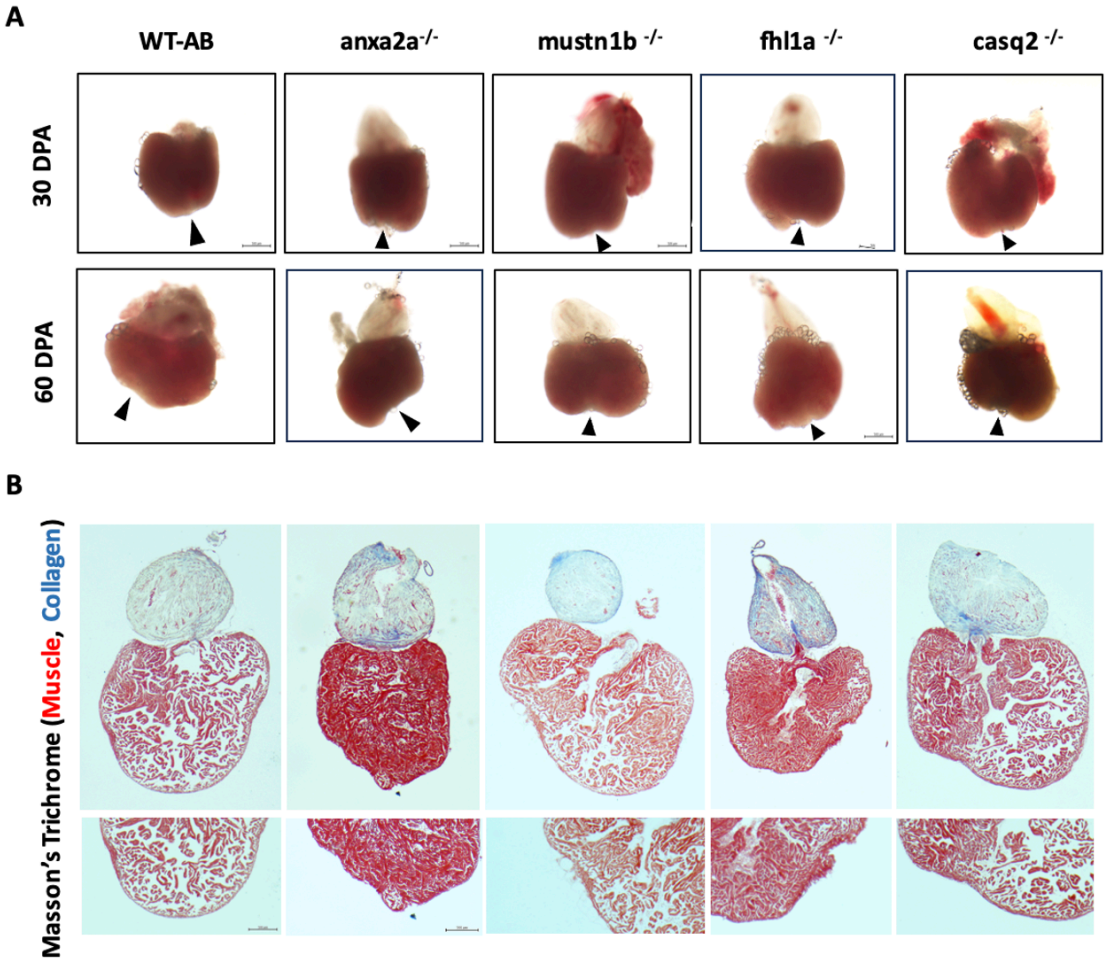

Figure R 14 Cardiac regeneration in the generated KO animals. (A) Representative regenerating hearts of WT and KO zebrafish at 30- and 60-DPA **(B)** Masson's Trichrome straining of regenerating heats at 60- DPA. Black arrows indicate injury site.

14 A). To assure that the regeneration process is impaired and not just delayed, we studied hearts at 60 DPA and stained them for Masson's trichrome (Figure R 14 A and Figure R 14 B).

We observed that in the case of anxa2a$^{-/-}$ all of the animals displayed failed regeneration. In the case of mustn1b$^{-/-}$, fhl1a$^{-/-}$ and casq2$^{-/-}$ the wounds were not as wide and big, but still not regenerated. Based on that, we assume that *anxa2a, mustn1b, fhl1a* and *casq2* are necessary for correct regeneration of the zebrafish myocardium. Further experiments are needed to increase the number of studied hearts to assure the implication of the genes in the regeneration process.

4.2.4. Generation of a cardiomyocyte specific Ca^{2+} indicator reporter zebrafish line to study calcium handling during zebrafish heart regeneration

Both Anxa2A and Casq2 display Ca^{2+} binding activity. In the field of heart regeneration, little attention has been paid to the contribution of Ca^{2+} handling in the process. Recently, the role of intracellular calcium dynamics in the regulation between proliferation and maturation of the cardiomyocytes was demonstrated by (P. D. Nguyen et al., 2023). To study the mechanisms by which the previously generated KOs animals fail to regenerate their hearts and the possible implication of Ca^{2+}, we generated a cardiomyocyte-specific Ca^{2+} indicator zebrafish reporter line using Tol2 transgenesis.

We used GCaMP6f, fast version of a circularly permutated GFP protein that is fused to a calmodulin and M13 peptide (Figure R 15 A). When intracellular Ca^{2+} rises, CaM binds to M13, and the conformational change of the protein causes increased brightness of GFP signal. To make the expression of GCaMP6f specific to the cardiomyocytes, we used the *cmlc2a* promoter. The 5' entry clone bearing the promoter, necessary for the Tol2 transgenesis, was previously generated in our lab (Appendix II Figure A). The 3' entry clone with SV40 late polyA signal is part of the Tol2 kit (Appendix II Figure A). To create the middle entry clone with the GCaMP6f gene, we purchased pAAV.CAG.Flex.GCaMP6f.WPRE.SV40 plasmid from Addgene and clone it in pME-MCS (Appendix II Figure A and). This middle entry clone vector has a multi-cloning site from pBluescript so we followed a restriction enzyme cloning approach with

XbaI and HindIII single-cutters.After double digestion of pAAV.CAG.Flex.GCaMP6f.WPRE.SV40 we observe the insert at 1785 base pairs (bp) and after double digestion of pME-MCS we observe the backbone at 2733 bp (Figure R 15B). Further ligation reaction of the two resulted in the GCaMP6f middle entry clone (Supplementary Figure). For the construction of the final clone needed for the transgenesis, and with a single LR reaction we used the three entry clones and the destination vector with the Tol2 minimum sequences in a ratio of 10:10:10:20 femtomoles. The generated plasmid (pmlc2a:GCaMP6f) was sequenced for all of its components and correct orientation of the elements (Figure R 15C).

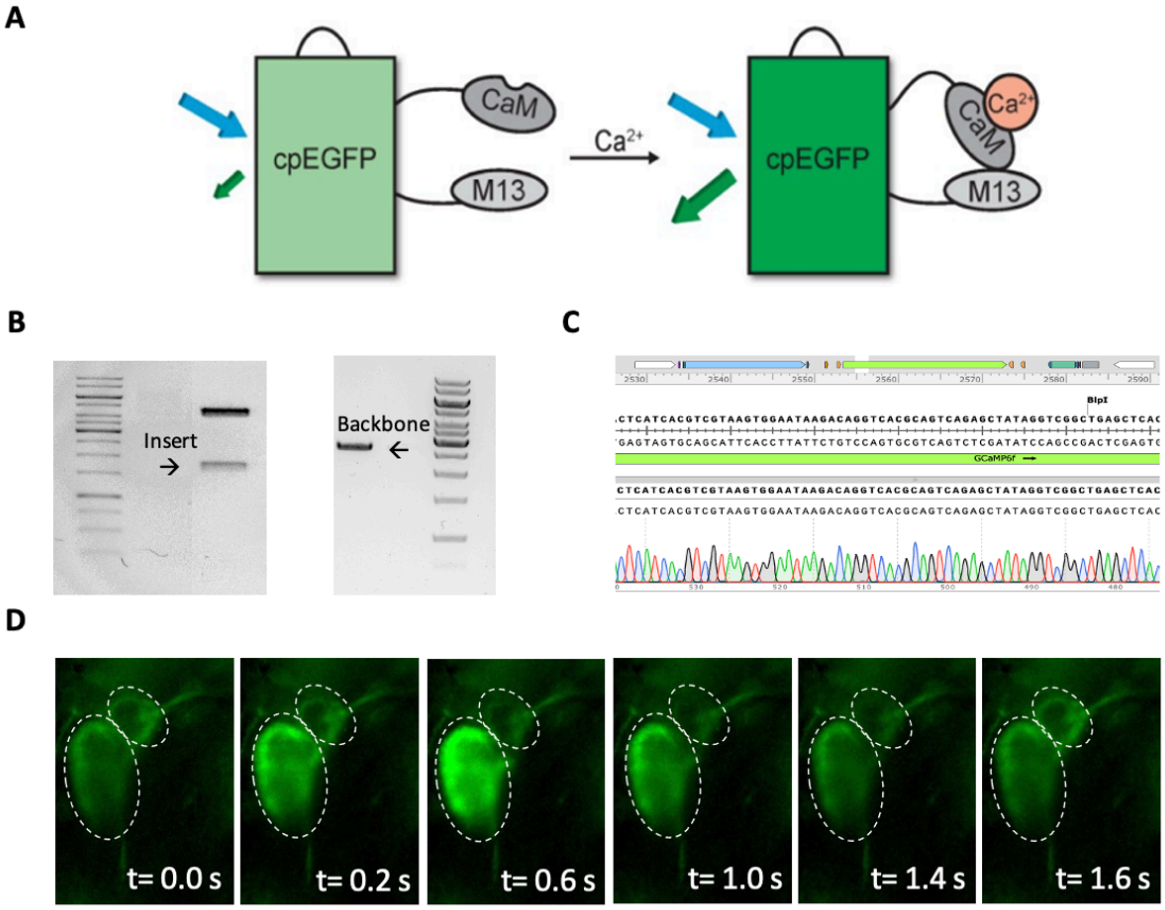

Figure R 15 Generation of stable reporter zebrafish line expressing GCaMP6f in cardiomyocytes. (A) GCaMP consist of a circularly permutated enhanced green fluorescence protein (cpEGFP) fused to calmodulin (CaM) and the M13 Peptide. **(B)** Generation of middle entry clone for Tol2 transgenesis with restriction enzyme cloning**.** Arrows indicating the insert and the backbone **(C)** Sequencing of the final vector used for the generation of the reporter line **(D)** Ca^{2+} propagation in a single heartbeat of 3 dpf larvae.

The plasmid (50 ng/µl) was injected in one-cell stage embryos along with transposase mRNA (50 ng/µl) and phenol red. After screening of the injected embryos, positive for GFP

signal larvae were raised to adulthood (F_0 generation). Adult F0 animals were crossed with WT-AB and the selection of Founders were done by screening of the offspring. Founder #1 and Founder #7 were chosen for the generation of a stable transgenic line. Live-imaging of 3 dpf larvae at 5 frames sec^{-1} show the *in vivo* cytosolic Ca^{2+} dynamics of the embryonic zebrafish heart (Figure R 15D). We observed a faster Ca^{2+} release in the atrium and the Ca^{2+} propagation in the ventricle.

Our reporter line can serve as platform for future Ca^{2+} handling studies in larvae, adult heart (*explant* cultures) or in cell-autonomous behaviors (*in vitro).* When crossed with the KO lines, GCaMP6f intensity over time can be used for the examination of diastolic Ca^{2+} levels, speed of intracellular Ca^{2+} release or maximal Ca^{2+} amplitudes.

4.2.5. *In vitro* characterization of cell-autonomous behaviors on matrices with a gradient stiffness

During zebrafish heart regeneration the ECM undergoes dynamic changes leading to changes in the mechanical properties of the microenvironment. Changes in the stiffness of ECM, affects many cellular functions such as cell proliferation, migration, (de)differentiation. The second platform consists of an *in vitro* cell culture system for zebrafish cardiac cell types that can be combined with matrices of pre-determined stiffness values, to study the mechanisms of cell-autonomous behaviors that might affect cardiac regeneration impairment in the KO models.

First, we set up the conditions for the cell culture of the main cardiac cell types including cardiomyocytes, endothelial cells, and fibroblasts. A variety of coatings were tested including poly-L-lysine, gelatin 0.01%, fibronectin and Matrigel®, and we found that Matrigel® in a dilution of 1:100 is optimal for the attachment of all cell types. For the cell culture medium, a combination of 50% MEM and 50% EGM-2 is needed to assure the survival of both cardiomyocytes and endothelial cells. Also, for a 34mm MatTek dish with 14 mm glass diameter bottom, the optimal density is 100.000 cells. For tracking the cells, we used

transgenic reporter lines for nuclear mCherry labeling cardiomyocytes (mlc2a:H2A-mCherry) and cytoplasmatic eGFP labeling endothelial cells (fli1a:GFP) (Figure R 16 A).

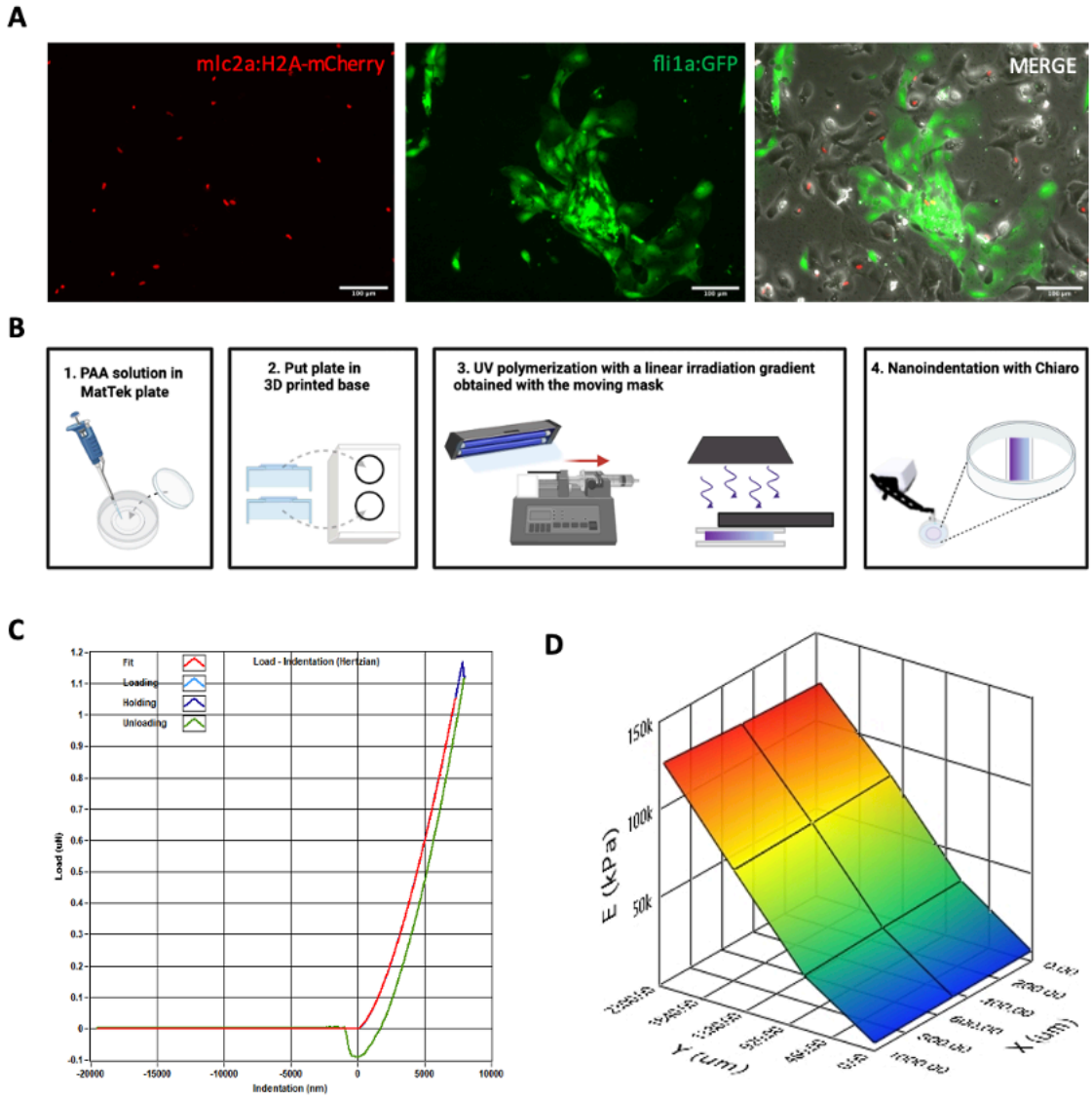

Figure R 16 Cell culture optimization and fabrication of PAA with a gradient of stiffness. (A) Zebrafish cardiac cell types cultured on a PAA gel; cardiomyocytes (nuclear red), endothelial cells (green) or other cell types (bright field) **(B)** Workflow for the fabrication and characterization of PAA gels for their mechanical properties **(C)** Typical nanoindentation curve and (**D)** matrix scan of a gradient gel measured with Chiaro.

Polyacrylamide (PAA) gels of varying stiffness or a gradient of stiffness can be fabricated and characterized for their mechanical properties. As shown briefly in the workflow (Figure R 16 B), a photopolymerization approach of the PAA gels was followed. Different ratios of acrylamide/bis-acrylamide were mixed for the gel formation and we used Irgacure-2959 as a photoinitiator. With a controlled speed movement of a mask, the PAA

solution was exposed to the UV light in linear gradient irradiation manner. The time of exposure to the UV light correlates with polymerization process, that would further lead to different mechanical properties along the PAA. We used Chiaro (Optics 11), a nanoindentation device, for measuring the gels with a gradient of stiffness (Figure R 16vC). The measured area can be visualized as a matrix scan, where the E_{ff} modulus of the measurements is shown in correlation with the coordinates on the gel (Figure R 16 D). The fabricated gels can be of different ranges, from 1-20 kPa or in a steeper format of 1-150kPa.

Our *in vitro* platform can provide information of the mechanobiological cues and behaviors of individual cells during heart regeneration that would not be possible to study *in vivo* either due to inability of visualization or application of parameters in a controlled manner such as substrates with defined mechanical properties.

Chapter III

Study of the transcriptomic changes in postnb$^{-/-}$ regenerating hearts in single-cell and subcellular spatial resolution

4.3.1. Single-cell transcriptomic profile of postnb$^{-/-}$ zebrafish hearts during regeneration

To gain further understanding of the mechanisms involved in heart regeneration, we incorporated in our studies a *postnb* mutant zebrafish line, previously generated in our lab, that fails to regenerate the heart. Similar to the WT, we used the bottom-half ventricles of Sham, 7- DPA and 30- DPA regenerating hearts (Figure R 17 A). We encapsulated the cells using the NADIA platform and sequenced the generated libraries with a NextSeq 500/550 system from Illumina. After quality control filtering, we have captured the transcriptomic profile of around 6.300 cells that can be further grouped in 10 clusters, with 3 of them belonging to cardiomyocyte populations (Figure R 17 B). This time, there was no need for integration of the scRNA-seq data, as with simple combination of the Seurat objects we did not observe any batch effect between the replicates (Supplementary, Figure A 35).

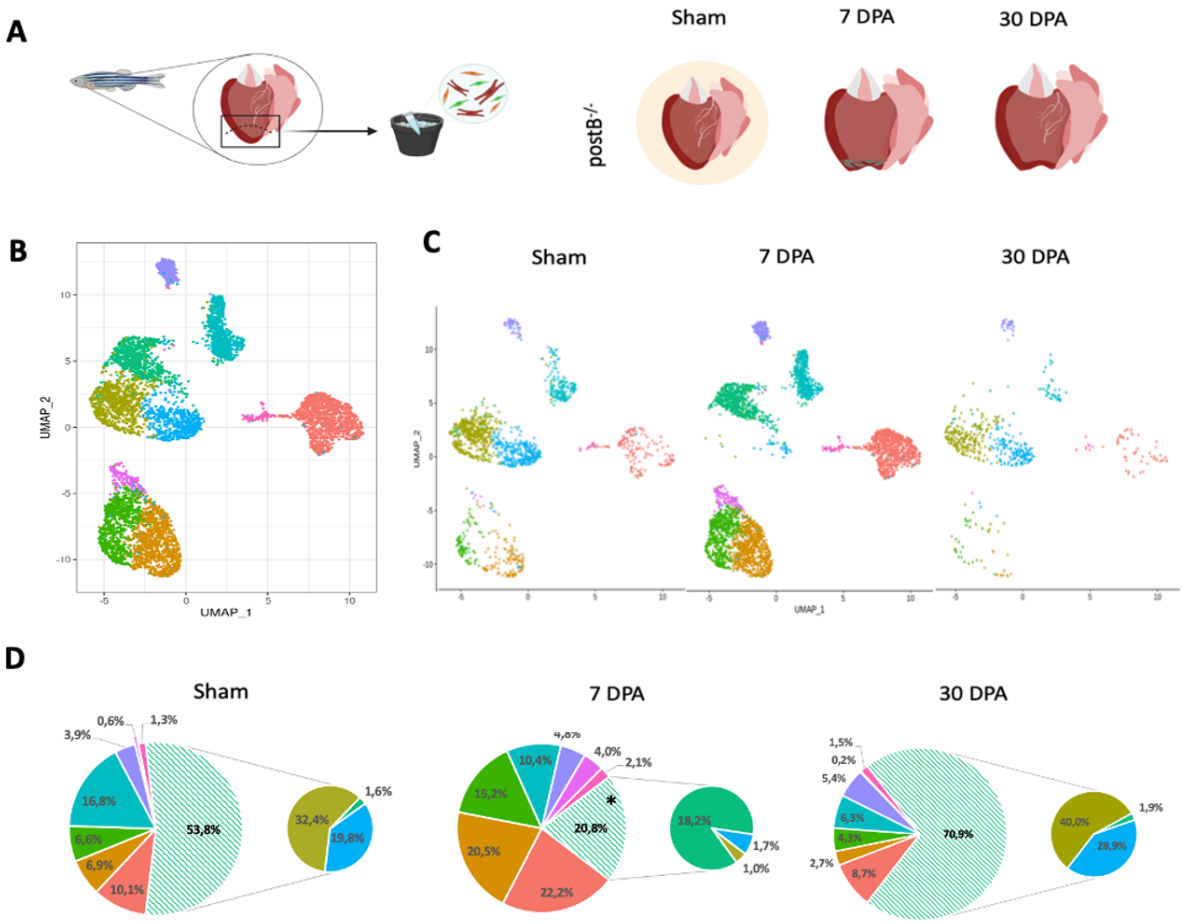

Figure R 17 Transcriptomic profile of cardiac single-cells of postnB KO during heart regeneration. **(A)** Cartoon representation of the experimental design **(B)** UMAP plot of integrated datasets **(C)** UMAP representation of clusters at Sham, 7- and 30- DPA **(D)** Pie charts showing the contribution of each cell type at the different timepoints of regeneration and asterisk denote statistically significant change in proportions when compared with uninjured control.

Interestingly, we could identify similar CM cluster at Sham and 30 DPA, but CMs with a distinct transcriptomic signature at 7 DPA (Figure R 18C). The first two clusters appear as mature (Cluster 2) or metabolically more active CMs (Cluster 6). However, some of the top markers of the third cluster (Cluster 4) such as *nppa, nppb, csrp3, tnn.1,* and *tnn.2,* were previously used to describe three distinct cardiomyocyte cell-states. Surprisingly *mustn1b, fhl1a* and *casq2* appear as markers of the same cluster. When we searched for the expression of *anxa2a* between the three CM clusters*,* we realized that is exclusively expressed only by the cluster of CM that appear at 7 DPA (Supplementary, Figure A 36). Finally, we looked for changes in the cellular composition of *postnb*$^{-/-}$ hearts during regeneration using scCODA tool. We observed statistically significant changes only in the CM populations and more specifically a decrease of cluster 2 and 6, and an increase in the size of cluster 4. This data from scRNA-seq of *postnb*$^{-/-}$ zebrafish hearts showed that the cellular composition is similar to that of WT animals, with the main cellular type populations being present in both. However, a distinct population of CM appears at 7 DPA in the *postnb*$^{-/-}$ regenerating heart.

4.3.2. Comparison of the cellular landscape between wild-type and postnb$^{-/-}$ regenerating hearts

Then, we wanted to compare the transcriptomic profile of WT and KO cells during regeneration. To achieve that, we first integrated the scRNA-seq data with CCA and for a resolution of r=0.6, we obtained a total of 13 clusters (Figure R 18 A). Among them, 4 clusters corresponding to CM populations, as in our previous analysis before joining the clusters under pan-cardiomyocyte marker (*cmlc2a*) (Supplementary Figure A 21).

Then, we aimed to see any general changes in the cellular composition of the WT and postnb$^{-/-}$ heart. After performing scCODA analysis, we observed statistical change in proportion of cells of 7 DPA *postnb*$^{-/-}$ hearts when compared to the corresponding uninjured control (Figure R 18 B). We noticed a decrease in cardiomyocytes (Cluster 0 and 1) and an increase in macrophages (Cluster 4), fibroblasts (Cluster 5) and epicardial cells (Cluster 6).

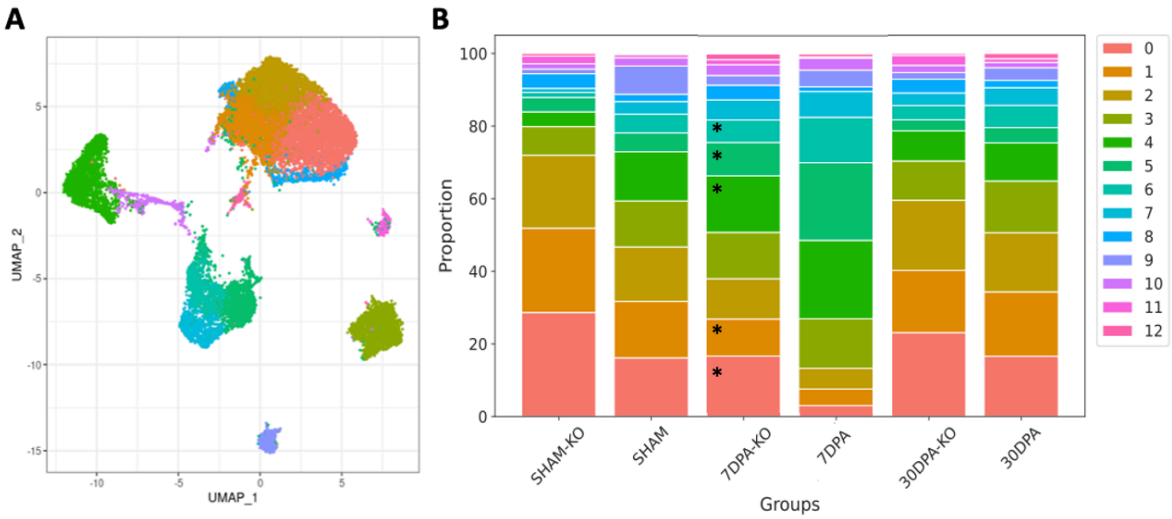

Figure R 18 Integration with scRNA-seq data of wild type and PostnB KO regenerating hearts. (A) Cellular landscape of wild type and *postnb*$^{-/-}$ regenerating hearts **(B)** scCODA analysis of cellular dynamics. Asterisks denote cell types with a statistically significant change compared with Sham.

4.3.3. Comparative analysis of the cardiomyocyte cell-states dynamics between wild-type and postnb$^{-/-}$ regenerating hearts

To understand the differences in CM cell-states that are present between the two models, we made an in-depth analysis of the CM populations. After applying the same bioinformatic pipeline and quality control filters as before, we have ended up with 10,874 cardiomyocytes, with 1,481 of them being *postnb*$^{-/-}$. With a resolution of r=0.7 we identified 7 clusters of cardiomyocytes, each one corresponding to a different cell-state during regeneration (Figure R 19A). Although we observed the existence of an extra cluster compared to WT, none of them was specific to KO.

We observed that main clusters as in our previous analysis, section 4.1.4, including mCMs (Cluster 0), bCMs (Cluster 2), dCMs (Cluster 4), hCMs (Cluster 5) and cCMs (Cluster 6) are also present in the KO. The cluster hypertrophic CMs was not detected in this analysis. However, the existence of two new clusters is present. In Cluster 1 we can find CMs enriched in genes related to metabolism whilst in Cluster 3 we detect markers of both *mature* and *hibernating* CMs such as *csrp3, nppa, nppb* or even *mustn1b* and *fhl1a.* Then, we used scCODA toolbox to study how these populations change between WT and KO during heart

regeneration, but we could not observe any statistically significant differences in the proportions of these cell types (Figure R 19B).

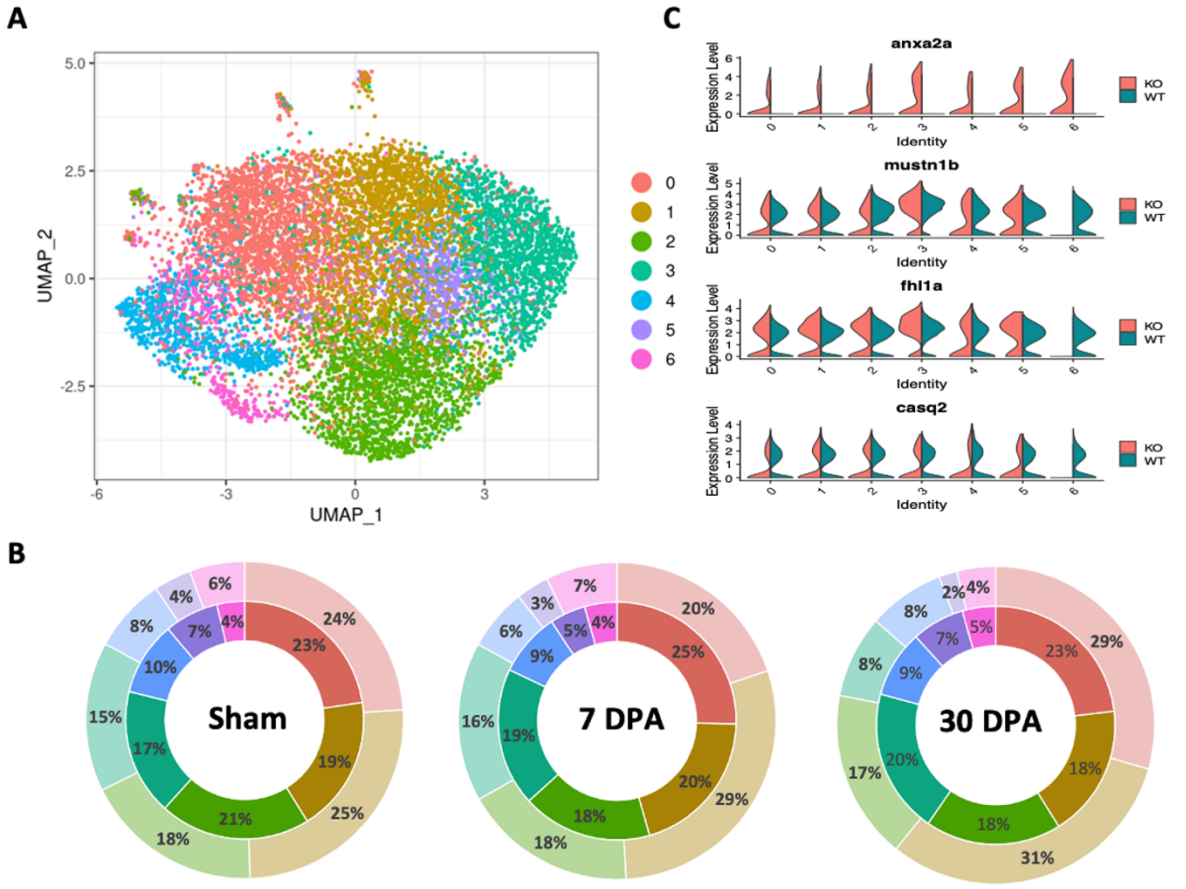

Figure R 19 Comparison of cardiomyocyte cell-states between wild type and postnB KO during heart regeneration. (A) UMAP representation of WT and KO integrated datasets **(B)** Cluster dynamics of CM cell states during regeneration. Inner circle (WT) and outer circle (KO) **(C)** Violin plots showing the expression of selected markers in WT and KO in CM clusters

Finding two out of four selected candidate genes from section 4.1.5 as markers of cluster 3 led us to seek for the expression of these genes between WT and KO (Figure R 19 C). We observed that CMs of postnb KO, have a higher expression of *anxa2a* at 7 DPA compared to WT. All together, these results suggest that the main CM cell-states observed in WT regenerating hearts are also present in postnb KO. The appearance of a new cluster expressing multiple markers of previously characterized clusters might indicate the existence of a hybrid cell-state. Further experiments for the validation of this cluster and its biological significance have to be performed.

4.3.4. Spatial transcriptomic analysis of wild type and postnb$^{-/-}$ zebrafish hearts during regeneration

To validate the results of section 4.3.3. and further look for gene specific domains in the regenerating heart, we extended our study to spatial transcriptomics using the Stereo-seq technology (A. Chen et al., 2022). To obtain a more complete picture of the regeneration process we included two extra timepoints, 3 DPA and 14 DPA, for both WT and postnb$^{-/-}$

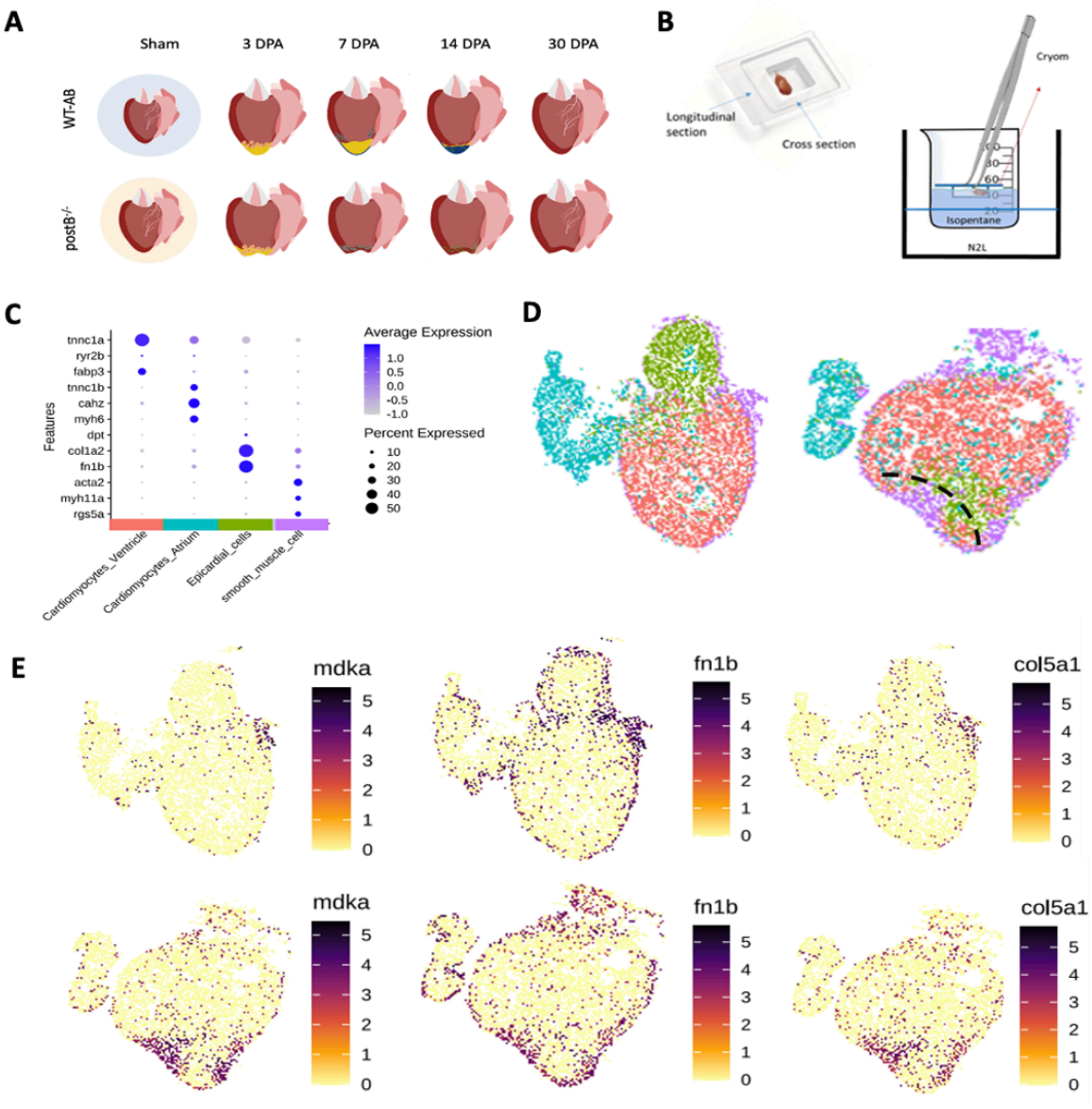

Figure R 20 Stereo-seq analysis of the regenerating hearts. (A) Cartoon representation of the experimental design **(B)** Orientation of the hearts in OCT and snap freeze in pre-chilled isopentane **(C)** Bubble plot of Top 3 markers for the segmented cell clusters **(D)** Unsupervised SCC of WT uninjured and 7 DPA zebrafish heart sections **(E)** Spatial visualization of the expression of the indicated genes related to regeneration

hearts (Figure R 20 A). Once the hearts were extracted, they were embedded in OCT and preserved using the snap freezing method before shipping to our collaborators in Guangzhou, China (Figure R 20 B).

Spatially constrained-clustering (SCC) of stereo-seq data of uninjured and 7 DPA WT hearts showed the existence of four main segmented cell clusters of the zebrafish heart including two types of cardiomyocytes, *atrial CM* and *ventricular CM*, *smooth muscle cells* and *fibroblast/epicardial cells* (Figure R 20 C). The spatial distribution of these clusters follows the anatomical architecture of the zebrafish heart (Figure R 20 D). In addition, the localization of these cell types, changes at 7 DPA where we observe an increase of fibroblast/epicardial cells and smooth muscle cells close to the injury site as described in literature.

The area close to the injury site is characterized by proliferative cells (*mdka*) and deposition of ECM proteins (*fn1b, col5a1*) by fibroblasts and epicardial cells. We used these markers, with known spatial distribution, to check if we could detect changes in gene expression in our samples (Figure R 20E). Our data suggests that we can successfully see changes in the expression of these genes and also their localization across a section of the regenerating heart. Thus, a deeper analysis of the Stereo-seq data could help infer gene regulatory networks that are active during zebrafish regeneration, identify the spatial distribution of cell type clusters and make comparative analysis between WT and postnb$^{-/-}$ hearts.

5. DISCUSSION

Harnessing CM endogenous renewal mechanism to promote heart regeneration has been proposed as an attractive therapeutic strategy for cardiovascular diseases (Garbern & Lee, 2022; Kraus, 2022). Over the years many advances have been made to better understand the mechanisms that govern zebrafish heart regeneration and regulation of CM proliferation (González-Rosa et al., 2017). In the present work, we dissected the cardiomyocyte cell-states during zebrafish heart regeneration, and unmasked genes that are necessary for complete regeneration. We have developed a dissociation protocol, for zebrafish cardiac tissue that results in a single-cell suspension of all the major cell types of the heart, ensuring high cell viability and RNA quality, and minimizes any dissociation-induced artifacts to the scRNA-seq data. Moreover, we established two platforms for functional assays and further studies on the mechanisms that impede completion of heart regeneration in our generated knock-out models. Finally, we studied the transcriptomic profile and cellular composition of *postnb*$^{-/-}$ regenerating hearts and highlighted the importance of spatial information and the numerous possibilities that arise through the combination of single-cell and spatial transcriptomic technologies.

The recent advances in single-cell technologies have facilitated the dissection of the cellular heterogeneity of the cardiac tissue (Paik et al., 2020). Recent scRNA-seq studies have shed light in the cellular composition of the developing and adult mammalian heart, as well as the regenerating zebrafish heart (Cui et al., 2019; Koenig et al., 2022; Ma et al., 2021; Rolland et al., 2022). However, to our knowledge, most studies are either focused on the characterization of the non-myocyte populations or fail to obtain a representative number of cardiomyocytes in their dataset. Rolland and colleagues analyzed the healthy and regenerating zebrafish heart, upon apex resection, at 3 DPA, 7 DPA and 14 DPA. They have identified 9 clusters, mostly composed of blood cells (*Neutrophils, Myeloid, Lymphoid, Erythrocytes* and *Thrombocytes*), 2 big cluster of *endothelium* and *epicardium* cells, 1 cluster of cardiac neural crest-derived cells, and a small population of cardiomyocytes (Rolland et al., 2022). In the present study, and in accordance with (Ma et al., 2021), we have been able to dissect the endothelial cells in two subtypes with unique transcriptomic signature: *endocardial endothelial cells* (*spock3*) and *coronary endothelial cells* (*cxcl12b*). Also, we distinguished between *epicardial cells* (*krt15*), and *fibroblasts* (*col1a2*) and we additionally described the presence of a small population of *smooth muscle cells* (*acta2*). Due to the

variability between the independent experiments, we were not able to observe any statistically significant differences in cell populations during heart regeneration. Another explanation would be the computational workflow used for the analysis. Recent studies suggest new algorithms with increased power and more precision for differential abundance testing and detection of cell subpopulations on scRNA-seq data (Maity & Teschendorff, 2023; Zhao et al., 2021). However, Hu et al, (B. Hu et al., 2022) and similarly to our results, also observed fluctuations in cell type proportions, in their scRNA-seq data, that attribute to the to the variability of the cardiac injury, regeneration time and/or depletion of bigger cells during tissue dissociation (B. Hu et al., 2022). Thus, the droplet-based encapsulation method and the cold-active protease dissociation protocol we used in our study, permitted us to obtain a high number of cardiomyocytes in our analysis, define with precision the major cellular types of the zebrafish heart and continue with further downstream transcriptomic analysis.

The heterogeneity of the zebrafish heart at single-cell resolution has been mainly exploited to study the contribution of non-myocytes and the interactions with CMs, thus CM heterogeneity has not been fully investigated in depth (Cao et al., 2016; B. Hu et al., 2022; Ma et al., 2021; K.-H. Wei et al., 2023). In the past, lineage-tracing experiments have been used to study the source of the newly formed myocardium, but their full transcriptomic profile has been poorly characterized (Gupta & Poss, 2012; Kikuchi et al., 2010; Sánchez-Iranzo, Galardi-Castilla, Minguillón, et al., 2018; Tekeli et al., 2017). Single-cell and spatial transcriptomic approaches have sought to profile different zones of the regenerating myocardium and revealed distinct gene expression profiles, with wound border zone re-expressing embryonic cardiac markers and undergoing metabolic reprogramming (Honkoop et al., 2019; Wu et al., 2016). In another study, Hu and colleagues, have successfully captured the transcriptomic profile of around 200.000 cells, including great number of CMs of uninjured and regenerating hearts upon cryoinjury. They identified four distinct subtypes composing of *ventricular CMs*, *atrial CMs*, *proliferating CMs* and *dedifferentiating CMs*. Nonetheless, their work is mainly focused on the origin and states of activated fibroblasts and the do not extend on further characterization of the cardiomyocyte clusters (B. Hu et al., 2022). There was no other study to our knowledge that describes the different cardiomyocyte cell-states, at single-cell resolution during zebrafish heart regeneration. In our study, we detected six cardiomyocyte

clusters present in both healthy and regenerating conditions. Due to the efficiency of our dissociation protocol, we obtain different types of cardiomyocytes and distinguish them based on unique transcriptomic signatures that previously could had been masked due to the introduction of artifacts in the scRNA-seq data. The six clusters could be roughly divided into two main groups as adult cardiomyocytes and renewal cardiomyocytes. In the first case, we have cells that compose or maintain the primer functions of the heart and like CMs with high metabolic rate, proteinosynthesis and/or mechanical workload. In the second case, we have cells that could contribute to the renewal of CMs due to natural turnover or upon injury and thus, including *hibernating* CMs with higher expression of embryonic markers yet on negative regulation of processes like cell cycle or translation initiation, and dedifferentiating CMs. In our analysis, we could not detect any changes in the cell state proportions during heart regeneration. One possible explanation could be the batch effect correction methods that were applied, prior to downstream analysis, that could result to loss of biological variability. In a recent study, Andreatta and colleagues propose a semi-supervised integration of scRNA-seq data where prior cell type information is provided for batch effect correction and thus preserving biological variability (Andreatta et al., 2024). On the other hand, our scRNA-seq data is capturing only a moment of the regeneration process with possible changes in the CM cell-state populations taking place prior or after the analyzed timepoint. Finally, CM cell-states might not necessarily change in absolute numbers during the regeneration process but rather their localization on the regenerating myocardium. Thus, further investigation is required to examine the cell-states dynamics and unravel the relationships and possible trajectories between them, during cardiac regeneration.

The biggest CM cluster in our analysis is composed of mature CMs, with only few markers to characterize them. *Csrp3* encoding for a cysteine and glycine rich protein of LIM domain proteins, is involved in regulatory processes including development and differentiation or structural maintenance of myocyte cells (Chang et al., 2019; Geier et al., 2008). A recent study has also shown that Csrp3 mutants fail to regenerate their heart due to impaired CM dedifferentiation and sarcomere reassembly (Liang et al., 2024). In our results, GO analysis of the same cluster showed that the cells belonging to this cluster are mostly linked to processes seen in the most abundant cell-state CM of the heart like calcium signaling pathway, heart process and heart contraction. ISH validation showed that these CMs, can be

found all over myocardium both in healthy and regenerating conditions. Thus, we suggest that the cells of this cluster belong to a mature state of CMs rather than dedifferentiated or committed to other functions.

In contrast with Hu et colleagues, where they identified dedifferentiated CMs expressing genes such as *nppa, tnn.1, tnn.2* and *synpo2lb,* we were able to dissect the same population in two distinct clusters (B. Hu et al., 2022). The cluster of *hibernating* CMs is characterized by cardiac developmental regulators genes such as *nppa* and *btg2,* and enriched in processes like cardiac muscle cell proliferation, insulin receptor signaling pathway and negative regulation of mitotic cell cycle (Honkoop et al., 2019; Kemmler et al., 2021; Man et al., 2018; Xiang et al., 2016). On the other hand, the cluster of *dedifferentiated* CMs is characterized by the expression of a plethora of embryonic and dedifferentiation markers including *tnn.1, tnn.2, myh7l, ryr2b, synpo2lb, ndrg4* and is enriched in processes related to cytoskeleton organization, muscle contraction, myosin filament assembly and cardiac muscle tissue development (Jopling et al., 2010; Kikuchi et al., 2010; P. D. Nguyen et al., 2023; Wu et al., 2016). We observed that the two clusters have similar ISH patterns suggesting a possible tight relationship between them. Further experiments are needed to investigate the interplay between the two CM cell-states.

Our results showed that biosynthetic CMs can be detected in both healthy and regenerating conditions across the myocardium. However, OPP signal, at 7 DPA, has shown localization adjacent to the border zone of the injury. The markers from the scRNA-seq analysis of this cluster cannot be specific for cardiomyocytes as shown in the ISH validation, due to the fact that other cell types are also in a constant proteinosynthesis process. However, GO analysis of the genes detected in the cluster highlights its identity. Morral and colleagues demonstrated that increased translation defines stemness in both LGR5 dependent and independent colorectal cancer tumors. The subset of these cells is located in defined niches inside the tumor while the differentiated cells undergo a permanent loss of protein synthesis (Morral et al., 2020). The existence of such subset of CMs in the regenerating heart arises new questions about their importance during the process and its link between hibernating and dedifferentiated CMs.

Although there are plenty of markers for distinguishing between trabecular and cortical CMs in mouse like Tbx5, Cx40 and/or Hey2*,* in zebrafish the markers were limited to the expression of *nppa* in trabecular CMs (Jensen et al., 2012; Koibuchi & Chin, 2007). Sánchez-Iranzo and colleagues demonstrated with lineage-tracing experiments that *tbx5a* expression is also restricted to trabecular CMs, which can transdifferentiate in cortical CMs during heart regeneration (Sánchez-Iranzo, Galardi-Castilla, Minguillón, et al., 2018). The genes expressed in the cluster of cortical CMs in our scRNA-seq data, are enriched in processes such as regulation of *actin cytoskeleton, cardiac muscle tissue regeneration* and *focal adhesion*. Moreover, the markers expressed in this cluster corroborate with their transcriptomic study, where *tbx5a*$^{-}$ CMs showed upregulation of *tmsb4x, cav1* or *anxa2a.*

Increased pressure or volume overload can induce cardiac hypertrophy as an adaptive mechanism to prevent heart failure (Komuro & Yazaki, 1993). Single-cell analysis of murine CMs by Nomura and colleagues showed that CM remodeling during cardiac hypertrophy, is controlled by the expression of modules of genes. These can include either structural or functional genes associated to metabolism, heart contraction, cell junction and others. Many of the genes found in hypertrophic or failing cardiomyocytes included genes such as *Myh6, Tcap* and *Fhl2* (S. Nomura et al., 2018). Previous studies in newts and rats showed that atrial CMs exhibit a proliferative response upon ventricular injury (McDonnell & Oberpriller, 1983, 1984; Oberpriller et al., 1987). In zebrafish, transdifferentiation of atrial to ventricular CMs has been shown to contribute during heart regeneration in larvae stages (Zhang et al., 2013). However, a similar *in vivo* reprogramming contribution was declined in adult animals (Zhang et al., 2013). Whether dedifferentiated ventricular CMs activate an embryonic atrial program prior to proliferation and/or redifferentiation or upon a hypertrophic state, needs to further be investigated.

Then, we sought the changes in the transcriptomic profile of the different cardiomyocyte cell-states during heart regeneration. The signal of low or transiently expressed genes can be masked across a population of cells or if the average gene expression is below the detection threshold of the assay as it happens in bulk RNA-seq (X. Li & Wang, 2021). Our single-cell approach and dissociation protocol enabled us to unmask novel genes that were not detected in previous transcriptomic studies. To validate the importance and

role of some candidate genes during the regeneration process we decided to generate knock-out models. The generation of homozygous KO zebrafish is obtained after two generation of adult animals (K. Liu et al., 2019). In addition, there were no previous reports that deficiency to any of our candidate genes could lead to development defects. Thus, we followed a CRISPR/Cas9 gene editing strategy as described by Kroll and colleagues, to obtain F_0 biallelic KO animals (Kroll et al., 2021). Our results collaborated the efficiency of the strategy with more than 90% obtained edited embryos in F_0 and thus permitting us to cut down the experimental time in half and validate if deficiency of any of the genes could be lethal.

One of the genes that was most dynamically expressed in our single-cell analysis was *anxa2a,* encoding for plasminogen receptor annexin A2. Annexins are Ca^{2+} and phospholipid binding proteins with principal function to bind and possibly hold together biological structures, particularly membranes and dysregulation in their expression in human can be linked to diseases, broadly known as *annexinopathies* (Babiychuk & Draeger, 2000; Gerke & Moss, 2002). The role of annexins cardiovascular disease and calcium handling in the heart has been studied in both human and mice (Camors et al., 2005; Grewal et al., 2016). Overexpression of AnxA6 results in reduced cardiomyocyte contractility, alterations in Ca^{2+} homeostasis and heart failure in mice (de Souza Ferreira et al.,2023). Recent studies are indicating the implication of annexins in regeneration (Häger & Nylandsted, 2019; Leikina et al., 2015). For instance, AnxA6 deficient mice fail to regenerate the liver and fie after partial hepatectomy, whereas muscle regeneration is slowed down in AnxaA1$^{-/-}$ mice. Further studies in AnxaA2 knock-out mice have linked Anxa2A with the regulation of fibrin homeostasis and neo angiogenesis (Grewal et al., 2016; Ling et al., 2004). However, the role of annexin 2A in zebrafish and their possible contribution in the regeneration process have been poorly studied. A CRISPR-based knockdown approach of Anxa2a and Anxa2b in the zebrafish caudal fin demonstrated that regeneration was delayed (Quoseena et al., 2020). Interestingly, in the context of zebrafish heart regeneration, Koth and colleagues, have shown that *runx1*$^{-/-}$ zebrafish hearts with increased regenerative capacity and decreased fibrosis, are upregulating *anxa2a* at 3 DPA, more than wild-type injured hearts, in both myocardium and endocardium (Koth et al., 2020).

Musculoskeletal embryonic nuclear protein 1 (MUSTN1) exhibits a highly preserved pattern of expression specific to muscle and skeletal tissues across various vertebrate species (Camarata et al., 2016). *Mustn1* is upregulated during bone repair and skeletal muscle regeneration in rat and mouse respectively (Hadjiargyrou et al., 2002; Krause et al., 2013). Further knock-down approaches *in vitro* have linked its function to proliferation and differentiation of mouse and chicken skeletal muscle cells (Z. Hu et al., 2021; C. Liu et al., 2010). The zebrafish orthologs of the gene, *mustn1a* and *mustn1b*, are expressed during early zebrafish developmental stages with a similar spatial distribution pattern including Kupffer's vesicle, paraxial mesoderm, and otic vesicle. The expression of *mustn1b* is restricted to heart and musculoskeletal system (Camarata et al., 2016). Injection of a morpholino against *mustn1a* leads to manifestation of impaired motile cilia phenotypes including abnormalities such as curved body axis, defects in otoliths, and disrupted left/right asymmetry. Spatially resolved RNA sequencing of cryoinjured zebrafish hearts identifies *mustn1b* as a marker of CMs close to the border zone adjacent to the site of the injury (Wu et al., 2016). However, there is no study to our knowledge investigating the role of *mustn1b* in zebrafish development or heart regeneration. Our results showed how the deficiency of *mustn1b* does not result in any detectable defect during early developmental stages or in adulthood but can lead to impaired zebrafish heart regeneration upon apex resection. A recent study by Ducommun and colleagues demonstrated that *Mustn1* expression is upregulated during skeletal muscle remodeling in mouse and in addition to its previously reported intracellular localization, is also secreted from smooth muscle cells regulating the ECM composition of the tissue (Ducommun et al., 2024). The mechanism of action of Mustn1b during zebrafish heart regeneration remains to be investigated, opening the path to potential new therapeutic strategies.

Synchronized CM contraction is orchestrated by the correct exchange of calcium ions between the Sarcoplasmic Reticulum (SR) and the cytoplasm (Valle et al., 2014). Ca^{2+} handling is related to the cell maturity, but little is known about the mechanisms that control this event during dedifferentiation and redifferentiation of the CMs in zebrafish heart regeneration (Beisaw & Wu, 2024). Nguyen and colleagues in a recent study, demonstrated the importance of LRCC10, a component of the cardiac dyad; that controls the levels of intracellular levels of Ca^{2+}, and how acts as a negative regulator of proliferation in zebrafish and mammalian CM

and thus controlling the initiation of their maturation (P. D. Nguyen et al., 2023). Our scRNA-seq analysis revealed *casq2,* encoding for Calsequestrin 2 (Casq2), as another marker with possible implication in the regeneration process. Casq2 is primarily found in the SR and plays a crucial role in the regulating Ca^{2+} storage and release within it (Viatchenko-Karpinski et al., 2004). In our results, deficiency of Casq2 in zebrafish impaired the regeneration of the myocardium. Overall, we suggest that better understanding the intricate interplay between calcium handling and heart regeneration in zebrafish might offer valuable insights into potential strategies for promoting cardiac repair and regeneration in humans.

Members of the four and a half LIM domain (FHL) family are involved in diverse cellular processes, such as organization of the cytoskeleton, cell signaling, gene regulation, cell migration and they play a role in the development and homeostasis of many tissues (Shathasivam et al., 2010; X. Wei & Zhang, 2020). The FHL family in human consists of five members (FHL1-5) with distinct pattern of expression, and mutations in their sequences have been associated with cardiac disorders (Lyon et al., 2015; Qi et al., 2024). Studies has shown that the expression of FHL1 is upregulated in both mouse models with pressure overload-induced hypertrophy and in human hearts of patients with hypertrophic cardiomyopathy, thus suggesting that FHL1 may be involved in mechanotransduction in cardiac hypertrophy and failure (Gaussin et al., 2003; D. M. Hwang et al., 2000). Another study has demonstrated that FHL1-3 are implicated in suppression of tumor growth by negative regulation of VEGF expression (Hubbi et al., 2012; Lin et al., 2012). In zebrafish Fhl1 has two orthologs, *fhl1a* and *fhl1b,* that are highly expressed throughout cardiac and skeletal muscle development. In the heart, *fhl1a* is mainly expressed in the ventricle and atrium, whereas *fhl1b* in the outflow tract (Keßler et al., 2018). MO-oligonucleotide mediated knockdown of *fhl1a* resulted in zebrafish embryos with skeletal muscle myopathy, reduced cardiac contractility and arrythmias (Keßler et al., 2018). The severity of the impaired skeletal muscle function was also shown in the increased number of morphants that lost their ability to hatch autonomously. Chen et al., showed a decrease in the number of satellite cells and changes in the expression of key gene regulators of skeletal muscle development including *myoD, pax7* and *mef2ca* (F. Chen et al., 2018). Our findings contrast with these previous results reported in the literature. A possible explanation could be the proven off-target activity of morpholinos (Bedell et al., 2011). Over the years, the CRISPR/Cas9 technology has been proven as more precise strategy for LOF

experiments with high specificity to the desired gene. Our results showed that the *fhl1a*$^{-/-}$ animals demonstrate normal development and growth but impaired cardiac regeneration. Although, skeletal muscle development was not studied in detail, no apparent abnormality was observed. Finally, a study by Xu et al., demonstrated that liver or pancreas fate specification of the endodermal progenitors and the regeneration of insulin-secreted β-cells are regulated by Fhl1b (J. Xu et al., 2016). They high homology between *fhl1a* and *fhl1b*, might suggest a conserved role of *Fhl1* in regeneration with tissue specificity for the two orthologs.

Despite our ongoing understanding of the induction of CM proliferation, the mechanisms that control it and/or lead to redifferentiation and maturation of CMs are poorly studied. For CMs to restore their full function, they have to reassembly their sarcomere structures, undergo metabolic reprogramming and control the Ca^{2+} handling and excitation-contraction coupling cycles (Beisaw & Wu, 2024). In our findings, both Anxa2A and Casq2 exhibit Ca^{2+} binding activity, with the latter one directly involved in calcium regulation. As mentioned before, investigating the interplay between calcium and the regeneration process will help understand the mechanisms the CM re-differentiate and maturate. Another important aspect that plays a role these two processes, both in development and regeneration, is the composition of the ECM and the mechanical cues it provides (Beisaw & Wu, 2024; Ryan et al., 2020). Previous studies have shown that changes in the mechanical properties of the ECM, lowering of its stiffness, take place during zebrafish regenerating myocardium and act as a permissive environment for CM proliferation in neonatal mice (Garcia-Puig et al., 2019; Notari et al., 2018). Recently, the ability of ECM remodeling to promote CM migration to the injured area has been recently assessed by Constanty and colleagues (Constanty et al., 2024). Our *in vitro* platform can be used for the investigation of cell-autonomous behaviors on response to matrices with varying stiffness including cell proliferation, migration, differentiation and/or apoptosis. In addition, enables the application of imaging techniques and assays that are not possible to perform in living animals such as time-lapse experiments of individual cells or administration and removal of chemical reagents in a controlled manner . The combination of our *in vitro* culture platform with our Ca^{2+} indicator reporter, when out-crossed with any of the generated knock-out models, could shed light on investigating the changes of Ca^{2+} handling in response to stiffness and/or further understand the mechanisms that cardiac regeneration is impaired.

To further deepen our knowledge in the zebrafish heart regeneration process, we included in our study a non-regenerating model that was previously generated in our lab and extended the transcriptomic studies including spatial information with the Stereo-seq technology. Our scRNA-seq data from healthy and regenerating postnb$^{-/-}$ ventricles not only demonstrated the existence of the same cell type population in the heart but we also observed changes in the cell type populations similar to wilt-type hearts according to literature (B. Hu et al., 2022). The changes mainly include an increase in macrophages/immune cells as well as fibroblasts and epicardial cells. In addition, a decrease in some clusters of CMs were observed. When analyzing in-depth the CM populations we were able to identify the same cell-states as in wild type hearts as well as two new more states that were not previously seen. One of them included metabolically more active CMs and the other CMs expressing a compilation of markers of different cell states. Capybara is a bioinformatic tool used to identify cell types and capture hybrid cell states. Kong and colleagues that developed this tool, could capture the cell fate transition dynamics during hematopoiesis or direct cardiac reprogramming (Kong et al., 2022). Thus, using this tool could further help dissecting the fate transitions and hybrid states, if any, during zebrafish heart regeneration. Another interesting aspect of *postnb*$^{-/-}$ is the increased expression of *anxa2a.* In a previous study by Koth et al., they observed increased expression of *anxa2a* in *runx1*$^{-/-}$ CMs when compared to WT (Koth et al., 2020) Both *postnb*$^{-/-}$ and *runx1*$^{-/-}$ exhibit increased myocardial proliferation*,* but with opposing outcomes upon cardiac injury. In addition, Shalhout and colleagues, used a small molecule, PY-60, targeting annexin A2 that activated YAP transcription activity and promoted proliferation of keratinocytes *in vitro* (Shalhout et al., 2021). All together, these might suggest a correlation between annexin A2 and CM proliferation that could be controlled in a drug dependent manner and thus promoting cardiac regeneration. However, more experiments are needed to understand why they *anxa2a*$^{-/-}$ fail to regenerate and if they exhibit reduced CM proliferation. in compromising. Finally, further analysis of the spatial transcriptomic data and integration with the scRNA-seq could provide mechanistic insight into the zebrafish cardiac regeneration.

6. CONCLUSIONS

Conclusions

- The cold active protease dissociation protocol implemented in this thesis is suitable for downstream single-cell transcriptomic analysis of cardiac tissue, ensuring high RNA quality and cell viability while maintaining low expression of IEGs and thus permitting better detection of transcriptomic changes during zebrafish heart regeneration.

- The major cardiac cell types of the zebrafish heart were detected at the timepoints studied, SHAM, 7 DPA and 30 DPA, using the NADIA platform, but no apparent change in cell populations was observed during regeneration.

- Novel cardiomyocyte cell states were characterized in the regenerating zebrafish heart in addition to the most abundant mCMs (*csrp3*), including hiCMs (*nppb*), bCMs (*nme2b.2*), dCMs (*ttn.2*), cCMs (*spock3*), and hCMs (*tnnc1b*).

- During heart regeneration there are changes in the transcriptomic profile of CMs. At 7 DPA there is an increase in the expression of *anxa2a, mustn1b, fhl1a* and *casq2* that return to basal levels at 30 DPA.

- CRISPR/Cas9 generated F_0 biallelic knock-out zebrafish showed that *anxa2a*$^{-/-}$, *mustn1b*$^{-/-}$, *fhl1a*$^{-/-}$ and *casq2*$^{-/-}$ animals fail to regenerate their heart at 60 DPA.

- The preliminary results of spatial transcriptomics analysis combined with scRNA-seq technology emerges as a powerful tool for finding gene specific domains in the regenerating heart.

REFERENCES

Adam, M., Potter, A. S., & Potter, S. S. (2017). Psychrophilic proteases dramatically reduce single-cell RNA-seq artifacts: A molecular atlas of kidney development. *Development (Cambridge, England)*, *144*(19), 3625–3632.

Adil, A., Kumar, V., Jan, A. T., & Asger, M. (2021). Single-Cell Transcriptomics: Current Methods and Challenges in Data Acquisition and Analysis. *Frontiers in Neuroscience*, *15*.

American Heart Association. (2024, February 25). *Heart Attack Treatment. https://www.heart.org/en/health-topics/heart-attack/treatment-of-a-heart-attack*

Anaparthy, N., Ho, Y.-J., Martelotto, L., Hammell, M., & Hicks, J. (2019). Single-Cell Applications of Next-Generation Sequencing. *Cold Spring Harbor Perspectives in Medicine*, *9*(10), a026898.

Andreatta, M., Hérault, L., Gueguen, P., Gfeller, D., Berenstein, A. J., & Carmona, S. J. (2024). Semi-supervised integration of single-cell transcriptomics data. *Nature Communications*, *15*(1), 872.

Apaydin, O., Altaikyzy, A., Filosa, A., & Sawamiphak, S. (2023). Alpha-1 adrenergic signaling drives cardiac regeneration via extracellular matrix remodeling transcriptional program in zebrafish macrophages. *Developmental Cell*, *58*(22), 2460-2476.e7.

Ashton, J. M., Rehrauer, H., Myers, J., Myers, J., Zanche, M., Balys, M., Foox, J., Mason, C. E., Steen, R., Kuentzel, M., Aquino, C., Garcia-Reyero, N., & Chittur, S. V. (2021). Comparative Analysis of Single-Cell RNA Sequencing Platforms and Methods. *Journal of Biomolecular Techniques : JBT*, *32*(4), 3fc1f5fe.3eccea01.

Babiychuk, E. B., & Draeger, A. (2000). Annexins in Cell Membrane Dynamics: Ca2ƨ-regulated Association of Lipid Microdomains. *The Journal of Cell Biology*, *150*.

Bakkers, J. (2011). Zebrafish as a model to study cardiac development and human cardiac disease. *Cardiovascular Research*, *91*(2), 279–288.

Baysoy, A., Bai, Z., Satija, R., & Fan, R. (2023). The technological landscape and applications of single-cell multi-omics. *Nature Reviews Molecular Cell Biology*, *24*(10), Article 10.

Becker, T., & Becker, C. G. (2001). Regenerating descending axons preferentially reroute to the gray matter in the presence of a general macrophage/microglial reaction caudal to a spinal transection in adult zebrafish. *The Journal of Comparative Neurology*, *433*(1), 131–147.

Bedell, V. M., Westcot, S. E., & Ekker, S. C. (2011). Lessons from morpholino-based screening in zebrafish. *Briefings in Functional Genomics*, *10*(4), 181–188.

Beijnum, H. van, Koopmans, T., Tomasso, A., Disela, V., Lindert, S. te, Bakkers, J., Alemany, A., Berezikov, E., & Bartscherer, K. (2023). Spatial transcriptomics reveals asymmetric cellular responses to injury in the regenerating spiny mouse (Acomys) ear. *Genome Research*.

Beisaw, A., & Wu, C.-C. (2024). Cardiomyocyte maturation and its reversal during cardiac regeneration. *Developmental Dynamics: An Official Publication of the American Association of Anatomists*, *253*(1), 8–27.

Bely, A. E., & Nyberg, K. G. (2010). Evolution of animal regeneration: Re-emergence of a field. *Trends in Ecology & Evolution*, *25*(3), 161–170.

Bergmann, O., Bhardwaj, R. D., Bernard, S., Zdunek, S., Barnabé-Heider, F., Walsh, S., Zupicich, J., Alkass, K., Buchholz, B. A., Druid, H., Jovinge, S., & Frisén, J. (2009). Evidence for Cardiomyocyte Renewal in Humans. *Science*, *324*(5923), 98–102.

Bertero, A., & Murry, C. E. (2018). Hallmarks of cardiac regeneration. *Nature Reviews. Cardiology*, *15*(10), 579–580.

Bise, T., Sallin, P., Pfefferli, C., & Jaźwińska, A. (2020). Multiple cryoinjuries modulate the efficiency of zebrafish heart regeneration. *Scientific Reports*, *10*(1), 11551.

Botos, M. A., Arora, P., Chouvardas, P., & Mercader, N. (2023). Transcriptomic data meta-analysis reveals common and injury model specific gene expression changes in the regenerating zebrafish heart. *Scientific Reports*, *13*(1), 5418.

Bozkurt, B., Ahmad, T., Alexander, K. M., Baker, W. L., Bosak, K., Breathett, K., Fonarow, G. C., Heidenreich, P., Ho, J. E., Hsich, E., Ibrahim, N. E., Jones, L. M., Khan, S. S., Khazanie, P., Koelling, T., Krumholz, H. M., Khush, K. K., Lee, C., Morris, A. A., … Ziaeian, B. (2023). Heart Failure Epidemiology and Outcomes Statistics: A Report of the Heart Failure Society of America. *Journal of Cardiac Failure*, *29*(10), 1412–1451.

Brette, F., Luxan, G., Cros, C., Dixey, H., Wilson, C., & Shiels, H. A. (2008). Characterization of isolated ventricular myocytes from adult zebrafish (Danio rerio). *Biochemical and Biophysical Research Communications*, *374*(1), 143–146.

Camarata, T., Vasilyev, A., & Hadjiargyrou, M. (2016). Cloning of zebrafish *Mustn1* orthologs and their expression during early development. *Gene*, *593*(1), 235–241.

Camors, E., Monceau, V., & Charlemagne, D. (2005). Annexins and Ca2+ handling in the heart. *Cardiovascular Research*, *65*(4), 793–802.

Cao, J., Navis, A., Cox, B. D., Dickson, A. L., Gemberling, M., Karra, R., Bagnat, M., & Poss, K. D. (2016). Single epicardial cell transcriptome sequencing identifies Caveolin 1 as an essential factor in zebrafish heart regeneration. *Development (Cambridge, England)*, *143*(2), 232–243.

Cao, J., Wang, J., Jackman, C. P., Cox, A. H., Trembley, M. A., Balowski, J. J., Cox, B. D., De Simone, A., Dickson, A. L., Di Talia, S., Small, E. M., Kiehart, D. P., Bursac, N., & Poss, K. D. (2017). Tension Creates an Endoreplication Wavefront that Leads Regeneration of Epicardial Tissue. *Developmental Cell*, *42*(6), 600-615.e4.

Carlson, B. M. (2007). Chapter 1—An Introduction to Regeneration. In B. M. Carlson (Ed.), *Principles of Regenerative Biology* (pp. 1–29). Academic Press.

Chablais, F., Veit, J., Rainer, G., & Jaźwińska, A. (2011). The zebrafish heart regenerates after cryoinjury-induced myocardial infarction. *BMC Developmental Biology*, *11*, 21.

Chang, Y., Geng, F., Hu, Y., Ding, Y., & Zhang, R. (2019). Zebrafish cysteine and glycine-rich protein 3 is essential for mechanical stability in skeletal muscles. *Biochemical and Biophysical Research Communications*, *511*(3), 604–611.

Chatterjee, N., & Walker, G. C. (2017). Mechanisms of DNA damage, repair and mutagenesis. *Environmental and Molecular Mutagenesis*, *58*(5), 235–263.

Chen, A., Liao, S., Cheng, M., Ma, K., Wu, L., Lai, Y., Qiu, X., Yang, J., Xu, J., Hao, S., Wang, X., Lu, H., Chen, X., Liu, X., Huang, X., Li, Z., Hong, Y., Jiang, Y., Peng, J., … Wang, J. (2022). Spatiotemporal transcriptomic atlas of mouse organogenesis using DNA nanoball-patterned arrays. *Cell*, *185*(10), 1777-1792.e21.

Chen, F., Yuan, W., Mo, X., Zhuang, J., Wang, Y., Chen, J., Jiang, Z., Zhu, X., Zeng, Q., Wan, Y., Li, F., Shi, Y., Cao, L., Fan, X., Luo, S., Ye, X., Chen, Y., Dai, G., Gao, J., … Wu, X. (2018). Role of Zebrafish fhl1A in Satellite Cell and Skeletal Muscle Development. *Current Molecular Medicine*, *17*(9), 627–636.

Chen, W. C. W., Wang, Z., Missinato, M. A., Park, D. W., Long, D. W., Liu, H.-J., Zeng, X., Yates, N. A., Kim, K., & Wang, Y. (2016). Decellularized zebrafish cardiac extracellular matrix induces mammalian heart regeneration. *Science Advances*, *2*(11), e1600844.

Choi, W.-Y., Gemberling, M., Wang, J., Holdway, J. E., Shen, M.-C., Karlstrom, R. O., & Poss, K. D. (2013). In vivo monitoring of cardiomyocyte proliferation to identify chemical modifiers of heart regeneration. *Development*, *140*(3), 660–666.

Clark, K. J., Urban, M. D., Skuster, K. J., & Ekker, S. C. (2011). Transgenic Zebrafish Using Transposable Elements. *Methods in Cell Biology*, *104*, 137–149.

Constanty, F., Wu, B., Wei, K.-H., Lin, I.-T., Dallmann, J., Guenther, S., Lautenschlaeger, T., Priya, R., Lai, S.-L., Stainier, D. Y. R., & Beisaw, A. (2024). *Border-zone cardiomyocytes and macrophages contribute to remodeling of the extracellular matrix to promote cardiomyocyte invasion during zebrafish cardiac regeneration*.

Cui, Y., Zheng, Y., Liu, X., Yan, L., Fan, X., Yong, J., Hu, Y., Dong, J., Li, Q., Wu, X., Gao, S., Li, J., Wen, L., Qiao, J., & Tang, F. (2019). Single-Cell Transcriptome Analysis Maps the Developmental Track of the Human Heart. *Cell Reports*, *26*(7), 1934-1950.e5.

Curado, S., Anderson, R. M., Jungblut, B., Mumm, J., Schroeter, E., & Stainier, D. Y. R. (2007). Conditional targeted cell ablation in zebrafish: A new tool for regeneration studies. *Developmental Dynamics*, *236*(4), 1025–1035.

de Souza Ferreira, L. P., da Silva, R. A., Gil, C. D., & Geisow, M. J. (2023). Annexin A1, A2, A5, and A6 involvement in human pathologies. *Proteins: Structure, Function, and Bioinformatics*, *91(9),* 1191-1204.

Denisenko, E., Guo, B. B., Jones, M., Hou, R., de Kock, L., Lassmann, T., Poppe, D., Clément, O., Simmons, R. K., Lister, R., & Forrest, A. R. R. (2020). Systematic assessment of tissue dissociation and storage biases in single-cell and single-nucleus RNA-seq workflows. *Genome Biology*, *21*(1), 130.

Dinulovic, I., Furrer, R., & Handschin, C. (2017). Plasticity of the Muscle Stem Cell Microenvironment. *Advances in Experimental Medicine and Biology*, *1041*, 141–169.

Dobin, A., Davis, C. A., Schlesinger, F., Drenkow, J., Zaleski, C., Jha, S., Batut, P., Chaisson, M., & Gingeras, T. R. (2013). STAR: Ultrafast universal RNA-seq aligner. *Bioinformatics (Oxford, England)*, *29*(1), 15–21.

Dolan, C. P., Yang, T.-J., Zimmel, K., Imholt, F., Qureshi, O., Falck, A., Gregory, J., Mayes, M., Ritchie, K., Koester, H., Daniel, B., Yan, M., Yu, L., Suva, L. J., Gaddy, D., Dawson, L. A., Muneoka, K., & Brunauer, R. (2022). Epimorphic regeneration of the mouse digit tip is finite. *Stem Cell Research & Therapy*, *13*(1), 62.

Dooley, K., & Zon, L. I. (2000). Zebrafish: A model system for the study of human disease. *Current Opinion in Genetics & Development*, *10*(3), 252–256.

Doudna, J. A., & Charpentier, E. (2014). Genome editing. The new frontier of genome engineering with CRISPR-Cas9. *Science (New York, N.Y.)*, *346*(6213), 1258096.

Ducommun, S., Jannig, P. R., Cervenka, I., Murgia, M., Mittenbühler, M. J., Chernogubova, E., Dias, J. M., Jude, B., Correia, J. C., Van Vranken, J. G., Ocana-Santero, G., Porsmyr-Palmertz, M., McCann Haworth, S., Martínez-Redondo, V., Liu, Z., Carlström, M., Mann, M., Lanner, J. T., Teixeira, A. I., … Ruas, J. L. (2024). Mustn1 is a smooth muscle cell-secreted microprotein that modulates skeletal muscle extracellular matrix composition. *Molecular Metabolism*, *82*, 101912.

Edelberg, J. M., Xaymardan, M., Rafii, S., & Hong, M. K. (2003). Adult Cardiac Stem Cells—Where Do We Go from Here? *Science of Aging Knowledge Environment*, *2003*(26), pe17–pe17.

Elchaninov, A., Sukhikh, G., & Fatkhudinov, T. (2021). Evolution of Regeneration in Animals: A Tangled Story. *Frontiers in Ecology and Evolution*, *9*, 621686.

Fudge, J. B. (2023). Spatial transcriptomics of the human heart. *Nature Biotechnology*, *41*(8), Article 8.

Gan, P., Patterson, M., & Sucov, H. M. (2020). Cardiomyocyte Polyploidy and Implications for Heart Regeneration. *Annual Review of Physiology*, *82*(1), 45–61.

Garbern, J. C., & Lee, R. T. (2022). Heart regeneration: 20 years of progress and renewed optimism. *Developmental Cell*, *57*(4), 424–439.

Garcia-Puig, A., Mosquera, J. L., Jiménez-Delgado, S., García-Pastor, C., Jorba, I., Navajas, D., Canals, F., & Raya, A. (2019). Proteomics Analysis of Extracellular Matrix Remodeling During Zebrafish Heart Regeneration. *Molecular & Cellular Proteomics: MCP*, *18*(9), 1745–1755.

Gaussin, V., Tomlinson, J. E., Depre, C., Engelhardt, S., Antos, C. L., Takagi, G., Hein, L., Topper, J. N., Liggett, S. B., Olson, E. N., Lohse, M. J., Vatner, S. F., & Vatner, D. E. (2003). Common Genomic Response in Different Mouse Models of β -Adrenergic-Induced Cardiomyopathy. *Circulation*, *108*(23), 2926–2933.

Geier, C., Gehmlich, K., Ehler, E., Hassfeld, S., Perrot, A., Hayess, K., Cardim, N., Wenzel, K., Erdmann, B., Krackhardt, F., Posch, M. G., Bublak, A., Nägele, H., Scheffold, T., Dietz, R., Chien, K. R., Spuler, S., Fürst, D. O., Nürnberg, P., & Özcelik, C. (2008). Beyond the sarcomere: CSRP3 mutations cause hypertrophic cardiomyopathy. *Human Molecular Genetics*, *17*(18), 2753–2765.

Gemberling, M., Bailey, T. J., Hyde, D. R., & Poss, K. D. (2013). The zebrafish as a model for complex tissue regeneration. *Trends in Genetics*, *29*(11), 611–620.

Gemberling, M., Karra, R., Dickson, A. L., & Poss, K. D. (2015). Nrg1 is an injury-induced cardiomyocyte mitogen for the endogenous heart regeneration program in zebrafish. *eLife*, *4*, e05871.

Genge, C. E., Lin, E., Lee, L., Sheng, X., Rayani, K., Gunawan, M., Stevens, C. M., Li, A. Y., Talab, S. S., Claydon, T. W., Hove-Madsen, L., & Tibbits, G. F. (2016). The Zebrafish Heart as a Model of Mammalian Cardiac Function. *Reviews of Physiology, Biochemistry and Pharmacology*, *171*, 99–136.

Gerke, V., & Moss, S. E. (2002). Annexins: From Structure to Function. *Physiological Reviews*, *82*(2), 331–371.

Goell, J. H., & Hilton, I. B. (2021). CRISPR/Cas-Based Epigenome Editing: Advances, Applications, and Clinical Utility. *Trends in Biotechnology*, *39*(7), 678–691.

González-Rosa, J. M., Burns, C. E., & Burns, C. G. (2017). Zebrafish heart regeneration: 15 years of discoveries. *Regeneration*, *4*(3), 105–123.

González-Rosa, J. M., Martín, V., Peralta, M., Torres, M., & Mercader, N. (2011). Extensive scar formation and regression during heart regeneration after cryoinjury in zebrafish. *Development (Cambridge, England)*, *138*(9), 1663–1674.

González-Rosa, J. M., Sharpe, M., Field, D., Soonpaa, M. H., Field, L. J., Burns, C. E., & Burns, C. G. (2018). Myocardial Polyploidization Creates a Barrier to Heart Regeneration in Zebrafish. *Developmental Cell*, *44*(4), 433-446.e7.

Goss, R. J., & Grimes, L. N. (1972). Tissue Interactions in the Regeneration of Rabbit Ear Holes. *American Zoologist*, *12*(1), 151–157.

Grewal, T., Wason, S. J., Enrich, C., & Rentero, C. (2016). Annexins – insights from knockout mice. *Biological Chemistry*, *397*(10), 1031–1053.

Guo, F., Li, L., Li, J., Wu, X., Hu, B., Zhu, P., Wen, L., & Tang, F. (2017). Single-cell multi-omics sequencing of mouse early embryos and embryonic stem cells. *Cell Research*, *27*(8), 967–988.

Gupta, V., & Poss, K. D. (2012). Clonally dominant cardiomyocytes direct heart morphogenesis. *Nature*, *484*(7395), 479–484.

Hadjiargyrou, M., Lombardo, F., Zhao, S., Ahrens, W., Joo, J., Ahn, H., Jurman, M., White, D. W., & Rubin, C. T. (2002). Transcriptional profiling of bone regeneration. Insight into the molecular complexity of wound repair. *The Journal of Biological Chemistry*, *277*(33), 30177–30182.

Häger, S. C., & Nylandsted, J. (2019). Annexins: Players of single cell wound healing and regeneration. *Communicative & Integrative Biology*, *12*(1), 162–165.

Hao, Y., Hao, S., Andersen-Nissen, E., Mauck, W. M., Zheng, S., Butler, A., Lee, M. J., Wilk, A. J., Darby, C., Zager, M., Hoffman, P., Stoeckius, M., Papalexi, E., Mimitou, E. P., Jain, J., Srivastava, A., Stuart, T., Fleming, L. M., Yeung, B., … Satija, R. (2021). Integrated analysis of multimodal single-cell data. *Cell*, *184*(13), 3573-3587.e29.

Harrison, M. R. M., Bussmann, J., Huang, Y., Zhao, L., Osorio, A., Burns, C. G., Burns, C. E., Sucov, H. M., Siekmann, A. F., & Lien, C.-L. (2015). Chemokine-guided angiogenesis directs coronary vasculature formation in zebrafish. *Developmental Cell*, *33*(4), 442–454.

He, S.-Y., Zhou, Y.-M., Wen, N., Meng, K., Cai, D.-Q., & Qi, X.-F. (2022). An Apical Resection Model in the Adult Xenopus tropicalis Heart. *Journal of Visualized Experiments: JoVE*, *189*.

Hirakawa, H., Gao, L., Tavakol, D. N., Vunjak-Novakovic, G., & Ding, L. (2023). Cellular plasticity of the bone marrow niche promotes hematopoietic stem cell regeneration. *Nature Genetics*, *55* (11).

Holtzman, N. G., Iovine, M. K., Liang, J. O., & Morris, J. (2016). Learning to Fish with Genetics: A Primer on the Vertebrate Model Danio rerio. *Genetics*, *203*(3), 1069–1089.

Honkoop, H., de Bakker, D. E., Aharonov, A., Kruse, F., Shakked, A., Nguyen, P. D., de Heus, C., Garric, L., Muraro, M. J., Shoffner, A., Tessadori, F., Peterson, J. C., Noort, W., Bertozzi, A., Weidinger, G., Posthuma, G., Grün, D., van der Laarse, W. J., Klumperman, J., … Bakkers, J. (2019). Single-cell analysis uncovers that metabolic reprogramming by ErbB2 signaling is essential for cardiomyocyte proliferation in the regenerating heart. *eLife*, *8*, e50163.

Hoshijima, K., Jurynec, M. J., Shaw, D. K., Jacobi, A. M., Behlke, M. A., & Grunwald, D. J. (2019). Highly Efficient CRISPR-Cas9-Based Methods for Generating Deletion Mutations and F0 Embryos that Lack Gene Function in Zebrafish. *Developmental Cell*, *51*(5), 645-657.e4.

Howe, K., Clark, M. D., Torroja, C. F., Torrance, J., Berthelot, C., Muffato, M., Collins, J. E., Humphray, S., McLaren, K., Matthews, L., McLaren, S., Sealy, I., Caccamo, M., Churcher, C., Scott, C., Barrett, J. C., Koch, R., Rauch, G.-J., White, S., … Stemple, D. L. (2013). The zebrafish reference genome sequence and its relationship to the human genome. *Nature*, *496* (7446).

Hu, B., Lelek, S., Spanjaard, B., El-Sammak, H., Simões, M. G., Mintcheva, J., Aliee, H., Schäfer, R., Meyer, A. M., Theis, F., Stainier, D. Y. R., Panáková, D., & Junker, J. P. (2022). Origin and function of activated fibroblast states during zebrafish heart regeneration. *Nature Genetics*, *54*(8), 1227–1237.

Hu, N., Yost, H. J., & Clark, E. B. (2001). Cardiac morphology and blood pressure in the adult zebrafish. *The Anatomical Record*, *264*(1), 1–12.

Hu, Z., Xu, H., Lu, Y., He, Q., Yan, C., Zhao, X., Tian, Y., Yang, C., Zhang, Z., Qiu, M., & Wang, Y. (2021). *MUSTN1* is an indispensable factor in the proliferation, differentiation and apoptosis of skeletal muscle satellite cells in chicken. *Experimental Cell Research*, *407*(2), 112833.

Huang, W.-C., Yang, C.-C., Chen, I.-H., Liu, Y.-M. L., Chang, S.-J., & Chuang, Y.-J. (2013). Treatment of Glucocorticoids Inhibited Early Immune Responses and Impaired Cardiac Repair in Adult Zebrafish. *PLoS ONE*, *8*(6), e66613.

Hubbi, M. E., Gilkes, D. M., Baek, J. H., & Semenza, G. L. (2012). Four-and-a-Half LIM Domain Proteins Inhibit Transactivation by Hypoxia-inducible Factor 1*. *Journal of Biological Chemistry*, *287*(9), 6139–6149.

Hui, S. P., Sheng, D. Z., Sugimoto, K., Gonzalez-Rajal, A., Nakagawa, S., Hesselson, D., & Kikuchi, K. (2017). Zebrafish Regulatory T Cells Mediate Organ-Specific Regenerative Programs. *Developmental Cell*, *43*(6), 659-672.e5.

Hwang, B., Lee, J. H., & Bang, D. (2018). Single-cell RNA sequencing technologies and bioinformatics pipelines. *Experimental & Molecular Medicine*, *50* (8).

Hwang, D. M., Dempsey, A. A., Lee, C. Y., & Liew, C. C. (2000). Identification of differentially expressed genes in cardiac hypertrophy by analysis of expressed sequence tags. *Genomics*, *66*(1), 1–14.

Islam, S., Zeisel, A., Joost, S., La Manno, G., Zajac, P., Kasper, M., Lönnerberg, P., & Linnarsson, S. (2014). Quantitative single-cell RNA-seq with unique molecular identifiers. *Nature Methods*, *11*(2), 163–166.

Itou, J., Akiyama, R., Pehoski, S., Yu, X., Kawakami, H., & Kawakami, Y. (2014). Regenerative responses after mild heart injuries for cardiomyocyte proliferation in zebrafish. *Developmental Dynamics: An Official Publication of the American Association of Anatomists*, *243*(11), 1477–1486.

Jaźwińska, A., & Sallin, P. (2016). Regeneration versus scarring in vertebrate appendages and heart. *The Journal of Pathology*, *238*(2), 233–246.

Jensen, B., Boukens, B. J. D., Postma, A. V., Gunst, Q. D., van den Hoff, M. J. B., Moorman, A. F. M., Wang, T., & Christoffels, V. M. (2012). Identifying the Evolutionary Building Blocks of the Cardiac Conduction System. *PLoS ONE*, *7*(9), e44231.

Jia, G., Preussner, J., Chen, X., Guenther, S., Yuan, X., Yekelchyk, M., Kuenne, C., Looso, M., Zhou, Y., Teichmann, S., & Braun, T. (2018). Single cell RNA-seq and ATAC-seq analysis of cardiac progenitor cell transition states and lineage settlement. *Nature Communications*, *9*(1), Article 1.

Jopling, C., Sleep, E., Raya, M., Martí, M., Raya, A., & Izpisúa Belmonte, J. C. (2010). Zebrafish heart regeneration occurs by cardiomyocyte dedifferentiation and proliferation. *Nature*, *464*(7288), 606–609.

Jovic, D., Liang, X., Zeng, H., Lin, L., Xu, F., & Luo, Y. (2022). Single-cell RNA sequencing technologies and applications: A brief overview. *Clinical and Translational Medicine*, *12*(3), e694.

Julius, M. H., Masuda, T., & Herzenberg, L. A. (1972). Demonstration That Antigen-Binding Cells Are Precursors of Antibody-Producing Cells After Purification with a Fluorescence-Activated Cell Sorter. *Proceedings of the National Academy of Sciences of the United States of America*, *69*(7), 1934–1938.

Kang, J., Hu, J., Karra, R., Dickson, A. L., Tornini, V. A., Nachtrab, G., Gemberling, M., Goldman, J. A., Black, B. L., & Poss, K. D. (2016). Modulation of tissue repair by regeneration enhancer elements. *Nature*, *532* (7598).

Ke, R., Mignardi, M., Pacureanu, A., Svedlund, J., Botling, J., Wählby, C., & Nilsson, M. (2013). In situ sequencing for RNA analysis in preserved tissue and cells. *Nature Methods*, *10*(9), 857–860.

Kemmler, C. L., Riemslagh, F. W., Moran, H. R., & Mosimann, C. (2021). From Stripes to a Beating Heart: Early Cardiac Development in Zebrafish. *Journal of Cardiovascular Development and Disease*, *8*(2), 17.

Keßler, M., Kieltsch, A., Kayvanpour, E., Katus, H. A., Schoser, B., Schessl, J., Just, S., & Rottbauer, W. (2018). A zebrafish model for FHL1-opathy reveals loss-of-function effects of human FHL1 mutations. *Neuromuscular Disorders*, *28*(6), 521–531.

Kikuchi, K., Holdway, J. E., Major, R. J., Blum, N., Dahn, R. D., Begemann, G., & Poss, K. D. (2011). Retinoic acid production by endocardium and epicardium is an injury response essential for zebrafish heart regeneration. *Developmental Cell*, *20*(3), 397–404.

Kikuchi, K., Holdway, J. E., Werdich, A. A., Anderson, R. M., Fang, Y., Egnaczyk, G. F., Evans, T., Macrae, C. A., Stainier, D. Y. R., & Poss, K. D. (2010). Primary contribution to zebrafish heart regeneration by gata4(+) cardiomyocytes. *Nature*, *464*(7288), 601–605.

Kikuta, H., & Kawakami, K. (2009). Transient and Stable Transgenesis Using Tol2 Transposon Vectors. In G. J. Lieschke, A. C. Oates, & K. Kawakami (Eds.), *Zebrafish: Methods and Protocols* (pp. 69–84). Humana Press.

Kimmel, C. B. (1993). Patterning the brain of the zebrafish embryo. *Annual Review of Neuroscience*, *16*, 707–732.

Kimmel, C. B., Kane, D. A., Walker, C., Warga, R. M., & Rothman, M. B. (1989). A mutation that changes cell movement and cell fate in the zebrafish embryo. *Nature*, *337*(6205), 358–362.

Kimura, Y., Hisano, Y., Kawahara, A., & Higashijima, S. (2014). Efficient generation of knock-in transgenic zebrafish carrying reporter/driver genes by CRISPR/Cas9-mediated genome engineering. *Scientific Reports*, *4*(1).

Klein, A. M., Mazutis, L., Akartuna, I., Tallapragada, N., Veres, A., Li, V., Peshkin, L., Weitz, D. A., & Kirschner, M. W. (2015). Droplet barcoding for single-cell transcriptomics applied to embryonic stem cells. *Cell*, *161*(5), 1187–1201.

Koenig, A. L., Shchukina, I., Amrute, J., Andhey, P. S., Zaitsev, K., Lai, L., Bajpai, G., Bredemeyer, A., Smith, G., Jones, C., Terrebonne, E., Rentschler, S. L., Artyomov, M. N., & Lavine, K. J. (2022). Single-cell transcriptomics reveals cell-type-specific diversification in human heart failure. *Nature Cardiovascular Research*, *1*(3).

Koibuchi, N., & Chin, M. T. (2007). CHF1/Hey2 plays a pivotal role in left ventricular maturation through suppression of ectopic atrial gene expression. *Circulation Research*, *100*(6), 850–855.

Komuro, I., & Yazaki, Y. (1993). Control of cardiac gene expression by mechanical stress. *Annual Review of Physiology*, *55*, 55–75.

Kong, W., Fu, Y. C., Holloway, E. M., Garipler, G., Yang, X., Mazzoni, E. O., & Morris, S. A. (2022). Capybara: A computational tool to measure cell identity and fate transitions. *Cell Stem Cell*, *29*(4), 635-649.e11.

Konturek-Ciesla, A., Olofzon, R., Kharazi, S., & Bryder, D. (2024). Implications of stress-induced gene expression for hematopoietic stem cell aging studies. *Nature Aging*, 1–8.

Koster, R., & Sassen, W. A. (2015). A molecular toolbox for genetic manipulation of zebrafish. *Advances in Genomics and Genetics*, 151.

Koth, J., Wang, X., Killen, A. C., Stockdale, W. T., Potts, H. G., Jefferson, A., Bonkhofer, F., Riley, P. R., Patient, R. K., Göttgens, B., & Mommersteeg, M. T. M. (2020). Runx1 promotes scar deposition and inhibits myocardial proliferation and survival during zebrafish heart regeneration. *Development (Cambridge, England)*, *147*(8), dev186569.

Kragl, M., Knapp, D., Nacu, E., Khattak, S., Maden, M., Epperlein, H. H., & Tanaka, E. M. (2009). Cells keep a memory of their tissue origin during axolotl limb regeneration. *Nature*, *460* (7251).

Kraus, L. (2022). Targeting Epigenetic Regulation of Cardiomyocytes through Development for Therapeutic Cardiac Regeneration after Heart Failure. *International Journal of Molecular Sciences*, *23*(19), 11878.

Krause, M. P., Moradi, J., Coleman, S. K., D'Souza, D. M., Liu, C., Kronenberg, M. S., Rowe, D. W., Hawke, T. J., & Hadjiargyrou, M. (2013). A novel GFP reporter mouse reveals Mustn1 expression in adult regenerating skeletal muscle, activated satellite cells and differentiating myoblasts. *Acta Physiologica*, *208*(2), 180–190.

Kretzschmar, K., Post, Y., Bannier-Hélaouët, M., Mattiotti, A., Drost, J., Basak, O., Li, V. S. W., van den Born, M., Gunst, Q. D., Versteeg, D., Kooijman, L., van der Elst, S., van Es, J. H., van Rooij, E., van den Hoff, M. J. B., & Clevers, H. (2018). Profiling proliferative cells and their progeny in damaged murine hearts. *Proceedings of the National Academy of Sciences*, *115*(52), E12245–E12254.

Kroehne, V., Freudenreich, D., Hans, S., Kaslin, J., & Brand, M. (2011). Regeneration of the adult zebrafish brain from neurogenic radial glia-type progenitors. *Development*, *138*(22), 4831–4841.

Kroll, F., Powell, G. T., Ghosh, M., Gestri, G., Antinucci, P., Hearn, T. J., Tunbak, H., Lim, S., Dennis, H. W., Fernandez, J. M., Whitmore, D., Dreosti, E., Wilson, S. W., Hoffman, E. J., & Rihel, J. (2021). A simple and effective F0 knockout method for rapid screening of behaviour and other complex phenotypes. *eLife*, *10*, e59683.

Kürn, U., Rendulic, S., Tiozzo, S., & Lauzon, R. J. (2011). Asexual Propagation and Regeneration in Colonial Ascidians. *The Biological Bulletin*, *221*(1), 43–61.

Kwan, K. M., Fujimoto, E., Grabher, C., Mangum, B. D., Hardy, M. E., Campbell, D. S., Parant, J. M., Yost, H. J., Kanki, J. P., & Chien, C.-B. (2007). The Tol2kit: A multisite gateway-based construction kit for Tol2 transposon transgenesis constructs. *Developmental Dynamics: An Official Publication of the American Association of Anatomists*, *236*(11), 3088–3099.

Laflamme, M. A., & Murry, C. E. (2011). Heart regeneration. *Nature*, *473*(7347), 326–335.

Lai, S.-L., Marín-Juez, R., Moura, P. L., Kuenne, C., Lai, J. K. H., Tsedeke, A. T., Guenther, S., Looso, M., & Stainier, D. Y. (2017). Reciprocal analyses in zebrafish and medaka reveal that harnessing the immune response promotes cardiac regeneration. *eLife*, *6*, e25605.

Lee, J., Hyeon, D. Y., & Hwang, D. (2020). Single-cell multiomics: Technologies and data analysis methods. *Experimental & Molecular Medicine*, *52*(9), Article 9. https://doi.org/10.1038/s12276-020-0420-2

Lee, R. T. (2018). The Adult Cardiac Stem Cell Concept and the Process of Science. *Circulation*, *138*(25), 2940–2942.

Leikina, E., Defour, A., Melikov, K., Van Der Meulen, J. H., Nagaraju, K., Bhuvanendran, S., Gebert, C., Pfeifer, K., Chernomordik, L. V., & Jaiswal, J. K. (2015). Annexin A1 Deficiency does not Affect Myofiber Repair but Delays Regeneration of Injured Muscles. *Scientific Reports*, *5*(1), 18246.

Leong, I. U. S., Skinner, J. R., Shelling, A. N., & Love, D. R. (2010). Zebrafish as a model for long QT syndrome: The evidence and the means of manipulating zebrafish gene expression. *Acta Physiologica*, *199*(3), 257–276.

Li, X., & Wang, C.-Y. (2021). From bulk, single-cell to spatial RNA sequencing. *International Journal of Oral Science*, *13*(1), 1–6.

Li, Z., Solomonidis, E. G., Meloni, M., Taylor, R. S., Duffin, R., Dobie, R., Magalhaes, M. S., Henderson, B. E. P., Louwe, P. A., D'Amico, G., Hodivala-Dilke, K. M., Shah, A. M., Mills, N. L., Simons, B. D., Gray, G. A., Henderson, N. C., Baker, A. H., & Brittan, M. (2019). Single-cell transcriptome analyses reveal novel targets modulating cardiac neovascularization by resident endothelial cells following myocardial infarction. *European Heart Journal*, *40*(30), 2507–2520.

Liang, S., Zhou, Y., Chang, Y., Li, J., Zhang, M., Gao, P., Li, Q., Yu, H., Kawakami, K., Ma, J., & Zhang, R. (2024). A novel gene-trap line reveals the dynamic patterns and essential roles of cysteine and glycine-rich protein 3 in zebrafish heart development and regeneration. *Cellular and Molecular Life Sciences: CMLS*, *81*(1), 158.

Lien, C.-L., Harrison, M. R., Tuan, T.-L., & Starnes, V. A. (2012). Heart repair and regeneration: Recent insights from zebrafish studies. *Wound Repair and Regeneration: Official Publication of the Wound Healing Society [and] the European Tissue Repair Society*, *20*(5), 638–646.

Lin, J., Qin, X., Zhu, Z., Mu, J., Zhu, L., Wu, K., Jiao, H., Xu, X., & Ye, Q. (2012). FHL family members suppress vascular endothelial growth factor expression through blockade of dimerization of HIF1α and HIF1β. *IUBMB Life*, *64*(11), 921–930.

Ling, Q., Jacovina, A. T., Deora, A., Febbraio, M., Simantov, R., Silverstein, R. L., Hempstead, B., Mark, W. H., & Hajjar, K. A. (2004). Annexin II regulates fibrin homeostasis and neoangiogenesis in vivo. *The Journal of Clinical Investigation*, *113*(1), 38–48.

Liu, C., Gersch, R. P., Hawke, T. J., & Hadjiargyrou, M. (2010). Silencing of Mustn1 inhibits myogenic fusion and differentiation. *American Journal of Physiology - Cell Physiology*, *298*(5), C1100–C1108.

Liu, K., Petree, C., Requena, T., Varshney, P., & Varshney, G. K. (2019). Expanding the CRISPR Toolbox in Zebrafish for Studying Development and Disease. *Frontiers in Cell and Developmental Biology*, *7*.

Liu, Y., Yang, M., Deng, Y., Su, G., Enninful, A., Guo, C. C., Tebaldi, T., Zhang, D., Kim, D., Bai, Z., Norris, E., Pan, A., Li, J., Xiao, Y., Halene, S., & Fan, R. (2020). High-Spatial-Resolution Multi-Omics Sequencing via Deterministic Barcoding in Tissue. *Cell*, *183*(6), 1665-1681.e18.

Lyon, R. C., Zanella, F., Omens, J. H., & Sheikh, F. (2015). Mechanotransduction in Cardiac Hypertrophy and Failure. *Circulation Research*, *116*(8), 1462–1476.

Ma, H., Liu, Z., Yang, Y., Feng, D., Dong, Y., Garbutt, T. A., Hu, Z., Wang, L., Luan, C., Cooper, C. D., Li, Y., Welch, J. D., Qian, L., & Liu, J. (2021). Functional coordination of non-myocytes plays a key role in adult zebrafish heart regeneration. *EMBO Reports*, *22*(11), e52901.

Machado, L., Relaix, F., & Mourikis, P. (2021). Stress relief: Emerging methods to mitigate dissociation-induced artefacts. *Trends in Cell Biology*, *31*(11), 888–897.

Maden, M. (2018). The evolution of regeneration—Where does that leave mammals? *The International Journal of Developmental Biology*, *62*(6-7–8), 369–372.

Mahmoud, A. I., O'Meara, C. C., Gemberling, M., Zhao, L., Bryant, D. M., Zheng, R., Gannon, J. B., Cai, L., Choi, W.-Y., Egnaczyk, G. F., Burns, C. E., Burns, C. G., MacRae, C. A., Poss, K. D., & Lee, R. T. (2015). Nerves Regulate Cardiomyocyte Proliferation and Heart Regeneration. *Developmental Cell*, *34*(4), 387–399.

Maity, A. K., & Teschendorff, A. E. (2023). Cell-attribute aware community detection improves differential abundance testing from single-cell RNA-Seq data. *Nature Communications*, *14*, 3244.

Man, J., Barnett, P., & Christoffels, V. M. (2018). Structure and function of the Nppa–Nppb cluster locus during heart development and disease. *Cellular and Molecular Life Sciences*, *75*(8), 1435–

Mancuso, T., Barone, A., Salatino, A., Molinaro, C., Marino, F., Scalise, M., Torella, M., De Angelis, A., Urbanek, K., Torella, D., & Cianflone, E. (2020). Unravelling the Biology of Adult Cardiac Stem Cell-Derived Exosomes to Foster Endogenous Cardiac Regeneration and Repair. *International Journal of Molecular Sciences*, *21* (10).

Marín-Juez, R., Marass, M., Gauvrit, S., Rossi, A., Lai, S.-L., Materna, S. C., Black, B. L., & Stainier, D. Y. R. (2016). Fast revascularization of the injured area is essential to support zebrafish heart regeneration. *Proceedings of the National Academy of Sciences of the United States of America*, *113*(40), 11237–11242.

Marshall, L., Vivien, C., Girardot, F., Péricard, L., Demeneix, B. A., Coen, L., & Chai, N. (2017). Persistent fibrosis, hypertrophy and sarcomere disorganisation after endoscopy-guided heart resection in adult Xenopus. *PloS One*, *12*(3), e0173418.

McDonnell, T. J., & Oberpriller, J. O. (1983). The atrial proliferative response following partial ventricular amputation in the heart of the adult newt. A light and electron microscopic autoradiographic study. *Tissue & Cell*, *15*(3), 351–363.

McDonnell, T. J., & Oberpriller, J. O. (1984). The response of the atrium to direct mechanical wounding in the adult heart of the newt, Notophthalmus viridescens. An electron-microscopic and autoradiographic study. *Cell and Tissue Research*, *235*(3), 583–592.

Method of the Year 2020: Spatially resolved transcriptomics. (2021). *Nature Methods*, *18*(1), Article 1.

Mirsaeidi, M., Gidfar, S., Vu, A., & Schraufnagel, D. (2016). Annexins family: Insights into their functions and potential role in pathogenesis of sarcoidosis. *Journal of Translational Medicine*, *14*(1), 89.

Morral, C., Stanisavljevic, J., Hernando-Momblona, X., Mereu, E., Álvarez-Varela, A., Cortina, C., Stork, D., Slebe, F., Turon, G., Whissell, G., Sevillano, M., Merlos-Suárez, A., Casanova-Martí, À., Moutinho, C., Lowe, S. W., Dow, L. E., Villanueva, A., Sancho, E., Heyn, H., & Batlle, E. (2020). Zonation of Ribosomal DNA Transcription Defines a Stem Cell Hierarchy in Colorectal Cancer. *Cell Stem Cell*, *26*(6), 845-861.e12.

Muraro, M. J., Dharmadhikari, G., Grün, D., Groen, N., Dielen, T., Jansen, E., van Gurp, L., Engelse, M. A., Carlotti, F., de Koning, E. J. P., & van Oudenaarden, A. (2016). A Single-Cell Transcriptome Atlas of the Human Pancreas. *Cell Systems*, *3*(4), 385-394.e3.

Neuschulz, A., Bakina, O., Badillo-Lisakowski, V., Olivares-Chauvet, P., Conrad, T., Gotthardt, M., Kettenmann, H., & Junker, J. P. (2023). A single-cell RNA labeling strategy for measuring stress response upon tissue dissociation. *Molecular Systems Biology*, *19*(2), e11147.

Nguyen, C. T., Lu, Q., Wang, Y., & Chen, J.-N. (2008). Zebrafish as a model for cardiovascular development and disease. *Drug Discovery Today. Disease Models*, *5*(3), 135–140.

Nguyen, P. D., De Bakker, D. E. M., & Bakkers, J. (2021). Cardiac regenerative capacity: An evolutionary afterthought? *Cellular and Molecular Life Sciences*, *78*(12), 5107–5122.

Nguyen, P. D., Gooijers, I., Campostrini, G., Verkerk, A. O., Honkoop, H., Bouwman, M., de Bakker, D. E. M., Koopmans, T., Vink, A., Lamers, G. E. M., Shakked, A., Mars, J., Mulder, A. A., Chocron, S., Bartscherer, K., Tzahor, E., Mummery, C. L., de Boer, T. P., Bellin, M., & Bakkers, J. (2023). Interplay between calcium and sarcomeres directs cardiomyocyte maturation during regeneration. *Science (New York, N.Y.)*, *380*(6646), 758–764.

Nichterwitz, S., Chen, G., Aguila Benitez, J., Yilmaz, M., Storvall, H., Cao, M., Sandberg, R., Deng, Q., & Hedlund, E. (2016). Laser capture microscopy coupled with Smart-seq2 for precise spatial transcriptomic profiling. *Nature Communications*, *7* (1).

Nomura, K., Tanimoto, Y., Hayashi, F., Harada, E., Shan, X.-Y., Shionyu, M., Hijikata, A., Shirai, T., Morigaki, K., & Shimamoto, K. (2017). The Role of the Prod1 Membrane Anchor in Newt Limb Regeneration. *Angewandte Chemie (International Ed. in English)*, *56*(1), 270–274.

Nomura, S., Satoh, M., Fujita, T., Higo, T., Sumida, T., Ko, T., Yamaguchi, T., Tobita, T., Naito, A. T., Ito, M., Fujita, K., Harada, M., Toko, H., Kobayashi, Y., Ito, K., Takimoto, E., Akazawa, H., Morita, H., Aburatani, H., & Komuro, I. (2018). Cardiomyocyte gene programs encoding morphological and functional signatures in cardiac hypertrophy and failure. *Nature Communications*, *9*(1), 4435.

Notari, M., Ventura-Rubio, A., Bedford-Guaus, S. J., Jorba, I., Mulero, L., Navajas, D., Martí, M., & Raya, Á. (2018). The local microenvironment limits the regenerative potential of the mouse neonatal heart. *Science Advances*, *4*(5), eaao5553.

Oberpriller, J. O., Oberpriller, J. C., & Aafedt, B. C. (1987). Changes in binucleation and cellular dimensions of rat left atrial myocytes after induced left ventricular infarction. *The American Journal of Anatomy*, *179*(3), 285–290.

O'Flanagan, C. H., Campbell, K. R., Zhang, A. W., Kabeer, F., Lim, J. L. P., Biele, J., Eirew, P., Lai, D., McPherson, A., Kong, E., Bates, C., Borkowski, K., Wiens, M., Hewitson, B., Hopkins, J., Pham, J., Ceglia, N., Moore, R., Mungall, A. J., … Aparicio, S. (2019). Dissociation of solid tumor tissues with cold active protease for single-cell RNA-seq minimizes conserved collagenase-associated stress responses. *Genome Biology*, *20*(1), 210.

Okada, T. S. (1996). A brief history of regeneration research—For admiring Professor Niazi's discovery of the effect of vitamin A on regeneration. *Journal of Biosciences*, *21*(3), 261–271.

Okamura, D. M., Brewer, C. M., Wakenight, P., Bahrami, N., Bernardi, K., Tran, A., Olson, J., Shi, X., Yeh, S.-Y., Piliponsky, A., Collins, S. J., Nguyen, E. D., Timms, A. E., MacDonald, J. W., Bammler, T. K., Nelson, B. R., Millen, K. J., Beier, D. R., & Majesky, M. W. (2021). Spiny mice activate unique transcriptional programs after severe kidney injury regenerating organ function without fibrosis. *iScience*, *24*(11), 103269.

Ott de Bruin, L. M., Volpi, S., & Musunuru, K. (2015). Novel Genome-Editing Tools to Model and Correct Primary Immunodeficiencies. *Frontiers in Immunology*, *6*.

Paik, D. T., Cho, S., Tian, L., Chang, H. Y., & Wu, J. C. (2020). Single-cell RNA sequencing in cardiovascular development, disease and medicine. *Nature Reviews Cardiology*, *17*(8), Article 8.

Parente, V., Balasso, S., Pompilio, G., Verduci, L., Colombo, G. I., Milano, G., Guerrini, U., Squadroni, L., Cotelli, F., Pozzoli, O., & Capogrossi, M. C. (2013). Hypoxia/reoxygenation cardiac injury and regeneration in zebrafish adult heart. *PloS One*, *8*(1), e53748.

Patra, C., Kontarakis, Z., Kaur, H., Rayrikar, A., Mukherjee, D., & Stainier, D. Y. R. (2017). The zebrafish ventricle: A hub of cardiac endothelial cells for in vitro cell behavior studies. *Scientific Reports*, *7*(1),

Patton, E. E., Zon, L. I., & Langenau, D. M. (2021). Zebrafish disease models in drug discovery: From preclinical modelling to clinical trials. *Nature Reviews Drug Discovery*, *20*(8), Article 8.

Pei, D., Shu, X., Gassama-Diagne, A., & Thiery, J. P. (2019). Mesenchymal–epithelial transition in development and reprogramming. *Nature Cell Biology*, *21*(1).

Petri, K., Zhang, W., Ma, J., Schmidts, A., Lee, H., Horng, J. E., Kim, D. Y., Kurt, I. C., Clement, K., Hsu, J. Y., Pinello, L., Maus, M. V., Joung, J. K., & Yeh, J.-R. J. (2022). CRISPR prime editing with ribonucleoprotein complexes in zebrafish and primary human cells. *Nature Biotechnology*, *40*(2),

Pisharath, H., Rhee, J. M., Swanson, M. A., Leach, S. D., & Parsons, M. J. (2007). Targeted ablation of beta cells in the embryonic zebrafish pancreas using *E. coli* nitroreductase. *Mechanisms of Development*, *124*(3), 218–229.

Poss, K. D., Wilson, L. G., & Keating, M. T. (2002). Heart regeneration in zebrafish. *Science (New York, N.Y.)*, *298*(5601), 2188–2190.

Postlethwait, J., Amores, A., Force, A., & Yan, Y.-L. (1998). Chapter 8 The Zebrafish Genome. In H. W. Detrich, M. Westerfield, & L. I. Zon (Eds.), *Methods in Cell Biology* (Vol. 60, pp. 149–163). Academic Press.

Qi, T., Zhang, J., Zhang, K., Zhang, W., Song, Y., Lian, K., Kan, C., Han, F., Hou, N., & Sun, X. (2024). Unraveling the role of the FHL family in cardiac diseases: Mechanisms, implications, and future directions. *Biochemical and Biophysical Research Communications*, *694*, 149468.

Quoseena, M., Vuppaladadium, S., Hussain, S., Banu, S., Bharathi, S., & Idris, M. M. (2020). Functional role of annexins in zebrafish caudal fin regeneration – A gene knockdown approach in regenerating tissue. *Biochimie*, *175*, 125–131.

Rafferty, S. A., & Quinn, T. A. (2018). A beginner's guide to understanding and implementing the genetic modification of zebrafish. *Progress in Biophysics and Molecular Biology*, *138*, 3–19.

Ranawakage, D. C., Okada, K., Sugio, K., Kawaguchi, Y., Kuninobu-Bonkohara, Y., Takada, T., & Kamachi, Y. (2021). Efficient CRISPR-Cas9-Mediated Knock-In of Composite Tags in Zebrafish Using Long ssDNA as a Donor. *Frontiers in Cell and Developmental Biology*, *8*.

Raya, Á., Consiglio, A., Kawakami, Y., Rodriguez-Esteban, C., & Izpisúa-Belmonte, J. C. (2004). The Zebrafish as a Model of Heart Regeneration. *Cloning and Stem Cells*, *6*(4), 345–351.

Raya, A., Koth, C. M., Büscher, D., Kawakami, Y., Itoh, T., Raya, R. M., Sternik, G., Tsai, H.-J., Rodríguez-Esteban, C., & Izpisúa-Belmonte, J. C. (2003). Activation of Notch signaling pathway precedes heart regeneration in zebrafish. *Proceedings of the National Academy of Sciences of the United States of America*, *100 Suppl 1*(Suppl 1), 11889–11895.

Ribeiro, A. O., de Oliveira, A. C., Costa, J. M., Nachtigall, P. G., Herkenhoff, M. E., Campos, V. F., Delella, F. K., & Pinhal, D. (2022). MicroRNA roles in regeneration: Multiple lessons from zebrafish. *Developmental Dynamics*, *251*(4), 556–576.

Riethdorf, S., O'Flaherty, L., Hille, C., & Pantel, K. (2018). Clinical applications of the CellSearch platform in cancer patients. *Advanced Drug Delivery Reviews*, *125*, 102–121.

Rolland, L., Harrington, A., Faucherre, A., Abaroa, J. M., Gangatharan, G., Gamba, L., Severac, D., Pratlong, M., Moore-Morris, T., & Jopling, C. (2022). The regenerative response of cardiac interstitial cells. *Journal of Molecular Cell Biology*, mjac059.

Rosello, M., Serafini, M., Mignani, L., Finazzi, D., Giovannangeli, C., Mione, M. C., Concordet, J.-P., & Del Bene, F. (2022). Disease modeling by efficient genome editing using a near PAM-less base editor in vivo. *Nature Communications*, *13*(1),

Rosen, J. N., Sweeney, M. F., & Mably, J. D. (2009). Microinjection of zebrafish embryos to analyze gene function. *Journal of Visualized Experiments: JoVE*, *25*, 1115.

Ross Stewart, K. M., Walker, S. L., Baker, A. H., Riley, P. R., & Brittan, M. (2022). Hooked on heart regeneration: The zebrafish guide to recovery. *Cardiovascular Research*, *118*(7), 1667–1679.

Ryan, R., Moyse, B. R., & Richardson, R. J. (2020). Zebrafish cardiac regeneration—Looking beyond cardiomyocytes to a complex microenvironment. *Histochemistry and Cell Biology*, *154*(5), 533–548.

Sahara, M., Santoro, F., & Chien, K. R. (2015). Programming and reprogramming a human heart cell. *The EMBO Journal*, *34*(6), 710–738.

Salama, G., & London, B. (2007). Mouse models of long QT syndrome. *The Journal of Physiology*, *578*(Pt 1), 43–53.

Sánchez-Iranzo, H., Galardi-Castilla, M., Minguillón, C., Sanz-Morejón, A., González-Rosa, J. M., Felker, A., Ernst, A., Guzmán-Martínez, G., Mosimann, C., & Mercader, N. (2018). Tbx5a lineage tracing shows cardiomyocyte plasticity during zebrafish heart regeneration. *Nature Communications*, *9*(1), 428.

Sánchez-Iranzo, H., Galardi-Castilla, M., Sanz-Morejón, A., González-Rosa, J. M., Costa, R., Ernst, A., Sainz de Aja, J., Langa, X., & Mercader, N. (2018). Transient fibrosis resolves via fibroblast inactivation in the regenerating zebrafish heart. *Proceedings of the National Academy of Sciences of the United States of America*, *115*(16), 4188–4193.

Sander, V., Suñe, G., Jopling, C., Morera, C., & Izpisua Belmonte, J. C. (2013). Isolation and in vitro culture of primary cardiomyocytes from adult zebrafish hearts. *Nature Protocols*, *8*(4), 800–809.

Shah, K. S., Kittleson, M. M., & Kobashigawa, J. A. (2019). Updates on Heart Transplantation. *Current Heart Failure Reports*, *16*(5), 150–156.

Shalhout, S. Z., Yang, P.-Y., Grzelak, E. M., Nutsch, K., Shao, S., Zambaldo, C., Iaconelli, J., Ibrahim, L., Stanton, C., Chadwick, S. R., Chen, E., DeRan, M., Li, S., Hull, M., Wu, X., Chatterjee, A. K., Shen, W., Camargo, F. D., Schultz, P. G., & Bollong, M. J. (2021). YAP-dependent proliferation by a small molecule targeting annexin A2. *Nature Chemical Biology*, *17*(7), 767–775.

Shathasivam, T., Kislinger, T., & Gramolini, A. O. (2010). Genes, proteins and complexes: The multifaceted nature of FHL family proteins in diverse tissues. *Journal of Cellular and Molecular Medicine*, *14*(12), 2702–2720.

Shin, K., Begeman, I. J., Cao, J., & Kang, J. (2024). *Leptin b* and its regeneration enhancer illustrate the regenerative features of zebrafish hearts. *Developmental Dynamics*, *253*(1), 91–106.

Solnica-Krezel, L., Schier, A. F., & Driever, W. (1994). Efficient recovery of ENU-induced mutations from the zebrafish germline. *Genetics*, *136*(4), 1401–1420.

Spanjaard, B., Hu, B., Mitic, N., Olivares-Chauvet, P., Janjuha, S., Ninov, N., & Junker, J. P. (2018). Simultaneous lineage tracing and cell-type identification using CRISPR-Cas9-induced genetic scars. *Nature Biotechnology*, *36*(5), 469–473.

Stockdale, W. T., Lemieux, M. E., Killen, A. C., Zhao, J., Hu, Z., Riepsaame, J., Hamilton, N., Kudoh, T., Riley, P. R., van Aerle, R., Yamamoto, Y., & Mommersteeg, M. T. M. (2018). Heart Regeneration in the Mexican Cavefish. *Cell Reports*, *25*(8), 1997-2007.e7.

Stocum, D. L. (2018). *Foundations of Regenerative Biology and Medicine:* IOP Publishing.

Streisinger, G., Walker, C., Dower, N., Knauber, D., & Singer, F. (1981). Production of clones of homozygous diploid zebra fish (Brachydanio rerio). *Nature*, *291*(5813), 293–296.

Summerton, J., & Weller, D. (1997). Morpholino antisense oligomers: Design, preparation, and properties. *Antisense & Nucleic Acid Drug Development*, *7*(3), 187–195.

Sun, J., Peterson, E. A., Wang, A. Z., Ou, J., Smith, K. E., Poss, K. D., & Wang, J. (2022). *Hapln1* Defines an Epicardial Cell Subpopulation Required for Cardiomyocyte Expansion During Heart Morphogenesis and Regeneration. *Circulation*, *146*(1), 48–63.

Tanaka, E. M., & Reddien, P. W. (2011). The cellular basis for animal regeneration. *Developmental Cell*, *21*(1), 172–185.

Tekeli, I., Garcia-Puig, A., Notari, M., García-Pastor, C., Aujard, I., Jullien, L., & Raya, A. (2017). Fate predetermination of cardiac myocytes during zebrafish heart regeneration. *Open Biology*, *7*(6), 170116.

Tucker, N. R., Chaffin, M., Fleming, S. J., Hall, A. W., Parsons, V. A., Bedi, K. C., Akkad, A.-D., Herndon, C. N., Arduini, A., Papangeli, I., Roselli, C., Aguet, F., Choi, S. H., Ardlie, K. G., Babadi, M., Margulies, K. B., Stegmann, C. M., & Ellinor, P. T. (2020). Transcriptional and Cellular Diversity of the Human Heart. *Circulation*, *142*(5), 466–482.

Tzahor, E., & Poss, K. D. (2017). Cardiac regeneration strategies: Staying young at heart. *Science (New York, N.Y.)*, *356*(6342), 1035–1039.

Uemoto, T., Abe, G., & Tamura, K. (2020). Regrowth of zebrafish caudal fin regeneration is determined by the amputated length. *Scientific Reports*, *10*(1).

Untergasser, A., Nijveen, H., Rao, X., Bisseling, T., Geurts, R., & Leunissen, J. A. M. (2007). Primer3Plus, an enhanced web interface to Primer3. *Nucleic Acids Research*, *35*(Web Server issue), W71–W74.

Uribe-Salazar, J. M., Kaya, G., Sekar, A., Weyenberg, K., Ingamells, C., & Dennis, M. Y. (2022). Evaluation of CRISPR gene-editing tools in zebrafish. *BMC Genomics*, *23*(1), 12.

Uroz, M., Garcia-Puig, A., Tekeli, I., Elosegui-Artola, A., Abenza, J. F., Marín-Llauradó, A., Pujals, S., Conte, V., Albertazzi, L., Roca-Cusachs, P., Raya, Á., & Trepat, X. (2019). Traction forces at the cytokinetic ring regulate cell division and polyploidy in the migrating zebrafish epicardium. *Nature Materials*, *18*(9).

Utada, A. S., Lorenceau, E., Link, D. R., Kaplan, P. D., Stone, H. A., & Weitz, D. A. (2005). Monodisperse double emulsions generated from a microcapillary device. *Science (New York, N.Y.)*, *308*(5721), 537–541.

Valle, G., Boncompagni, S., Sacchetto, R., Protasi, F., & Volpe, P. (2014). Post-natal heart adaptation in a knock-in mouse model of calsequestrin 2-linked recessive catecholaminergic polymorphic ventricular tachycardia. *Experimental Cell Research*, *321*(2), 178–189.

Viatchenko-Karpinski, S., Terentyev, D., Györke, I., Terentyeva, R., Volpe, P., Priori, S. G., Napolitano, C., Nori, A., Williams, S. C., & Györke, S. (2004). Abnormal Calcium Signaling and Sudden Cardiac Death Associated With Mutation of Calsequestrin. *Circulation Research*, *94*(4), 471–477.

Vihtelic, T. S., & Hyde, D. R. (2000). Light-induced rod and cone cell death and regeneration in the adult albino zebrafish (Danio rerio) retina. *Journal of Neurobiology*, *44*(3), 289–307.

Vivien, C. J., Hudson, J. E., & Porrello, E. R. (2016). Evolution, comparative biology and ontogeny of vertebrate heart regeneration. *Npj Regenerative Medicine*, *1*(1).

Wang, J., Cao, J., Dickson, A. L., & Poss, K. D. (2015). Epicardial regeneration is guided by cardiac outflow tract and Hedgehog signalling. *Nature*, *522*(7555), 226–230.

Wang, J., Panáková, D., Kikuchi, K., Holdway, J. E., Gemberling, M., Burris, J. S., Singh, S. P., Dickson, A. L., Lin, Y.-F., Sabeh, M. K., Werdich, A. A., Yelon, D., Macrae, C. A., & Poss, K. D. (2011). The regenerative capacity of zebrafish reverses cardiac failure caused by genetic cardiomyocyte depletion. *Development (Cambridge, England)*, *138*(16), 3421–3430.

Wang, M., Gu, M., Liu, L., Liu, Y., & Tian, L. (2021). Single-Cell RNA Sequencing (scRNA-seq) in Cardiac Tissue: Applications and Limitations . *Vascular Health and Risk Management*, *17*, 641–657.

Wei, K.-H., Lin, I.-T., Chowdhury, K., Lim, K. L., Liu, K.-T., Ko, T.-M., Chang, Y.-M., Yang, K.-C., & Lai, S.-L. B. (2023). Comparative single-cell profiling reveals distinct cardiac resident macrophages essential for zebrafish heart regeneration. *eLife*, *12*, e84679.

Wei, X., & Zhang, H. (2020). Four and a half LIM domains protein 1 can be as a double-edged sword in cancer progression. *Cancer Biology & Medicine*, *17*(2), 270–281.

Westerfield, M. (2000). *The Zebrafish Book. A Guide for the Laboratory Use of Zebrafish (Danio rerio)* (Eugene).

Williams, C. G., Lee, H. J., Asatsuma, T., Vento-Tormo, R., & Haque, A. (2022). An introduction to spatial transcriptomics for biomedical research. *Genome Medicine*, *14*(1), 68.

Wolf, F. A., Angerer, P., & Theis, F. J. (2018). SCANPY: Large-scale single-cell gene expression data analysis. *Genome Biology*, *19*(1), 15.

Wu, C.-C., Kruse, F., Vasudevarao, M. D., Junker, J. P., Zebrowski, D. C., Fischer, K., Noël, E. S., Grün, D., Berezikov, E., Engel, F. B., van Oudenaarden, A., Weidinger, G., & Bakkers, J. (2016). Spatially Resolved Genome-wide Transcriptional Profiling Identifies BMP Signaling as Essential Regulator of Zebrafish Cardiomyocyte Regeneration. *Developmental Cell*, *36*(1), 36–49.

Xiang, F., Guo, M., & Yutzey, K. E. (2016). Overexpression of Tbx20 in Adult Cardiomyocytes Promotes Proliferation and Improves Cardiac Function After Myocardial Infarction. *Circulation*, *133*(11), 1081–1092.

Xu, C., Zhou, Y., Xiao, Q., He, B., Geng, G., Wang, Z., Cao, B., Dong, X., Bai, W., Wang, Y., Wang, X., Zhou, D., Yuan, T., Huo, X., Lai, J., & Yang, H. (2021). Programmable RNA editing with compact CRISPR–Cas13 systems from uncultivated microbes. *Nature Methods*, *18*(5).

Xu, J., Cui, J., Del Campo, A., & Shin, C. H. (2016). Four and a Half LIM Domains 1b (Fhl1b) Is Essential for Regulating the Liver versus Pancreas Fate Decision and for β-Cell Regeneration. *PLoS Genetics*, *12*(2), e1005831.

Yamada, S., & Nomura, S. (2020). Review of Single-Cell RNA Sequencing in the Heart. *International Journal of Molecular Sciences*, *21*(21).

Yan, R., Cigliola, V., Oonk, K. A., Petrover, Z., DeLuca, S., Wolfson, D. W., Vekstein, A., Mendiola, M. A., Devlin, G., Bishawi, M., Gemberling, M. P., Sinha, T., Sargent, M. A., York, A. J., Shakked, A., DeBenedittis, P., Wendell, D. C., Ou, J., Kang, J., … Poss, K. D. (2023). An enhancer-based gene-therapy strategy for spatiotemporal control of cargoes during tissue repair. *Cell Stem Cell*, *30*(1), 96-111.e6.

Yang, K., & Kang, J. (2019). Tissue Regeneration Enhancer Elements: A Way to Unlock Endogenous Healing Power. *Developmental Dynamics*, *248*(1), 34–42.

Yu, C., Shi, M., He, S., Yao, M., Sun, H., Yue, Z., Qiu, Y., Liu, B., Liang, L., Zhao, Z., Yao, F., Zhang, H., & Li, J. (2023). Chronological adhesive cardiac patch for synchronous mechanophysiological monitoring and electrocoupling therapy. *Nature Communications*, *14*(1).

Yu, L., Dawson, L. A., Yan, M., Zimmel, K., Lin, Y.-L., Dolan, C. P., Han, M., & Muneoka, K. (2019). BMP9 stimulates joint regeneration at digit amputation wounds in mice. *Nature Communications*, *10*(1).

Yun, M. H. (2015). Changes in Regenerative Capacity through Lifespan. *International Journal of Molecular Sciences*, *16*(10).

Zhang, R., Han, P., Yang, H., Ouyang, K., Lee, D., Lin, Y.-F., Ocorr, K., Kang, G., Chen, J., Stainier, D. Y. R., Yelon, D., & Chi, N. C. (2013). In Vivo Cardiac Reprogramming Contributes to Zebrafish Heart Regeneration. *Nature*, *498*(7455), 497–501.

Zhao, J., Jaffe, A., Li, H., Lindenbaum, O., Sefik, E., Jackson, R., Cheng, X., Flavell, R. A., & Kluger, Y. (2021). Detection of differentially abundant cell subpopulations in scRNA-seq data. *Proceedings of the National Academy of Sciences of the United States of America*, *118*(22), e2100293118.

Ziaeian, B., & Fonarow, G. C. (2016). Epidemiology and aetiology of heart failure. *Nature Reviews. Cardiology*, *13*(6), 368–378.

APPENDICES

Appendix I. List of oligonucleotides

Appendix I. List of oligonucleotides

All the designed and/or used oligos in this thesis are shown in the tables below:

Table I: Oligos for RT-PCR and *ISH* probes generation			
Gene	**Primer**	**Sequence (5' → 3')**	**Amplicon (bp)**
csrp3	Fw:	AAGGTTTGGACAGCACCACA	458
	Rv:	TCACACACTCTCCTCGACCA	
nppb	Fw:	TTTCTCCTCAGCGTTCAACA	519
	Rv:	TGCGCTTCAAATGGTAACAA	
nme2b.2	Fw:	CACGGCAGTGACTCTGAGAA	326
	Rv:	GGCCAGTTTCAGGTTGAGAG	
ttn.2	Fw:	CTGCCACTGACATGTGGTCT	494
	Rv:	GCAGCACACAAACCTGACAT	
spock3	Fw:	CTCCAGGAAATCCAGCAGAG	477
	Rv:	ACTGCTGAGGCCGATAGAAA	
tnnc1b	Fw:	TAAAGCAGCGGTGGAGAACT	505
	Rv:	TCAGGGAATGAAATGGCTTC	
anxa2a	Fw:	ATGCCAGAGCCCTGTATGAC	479
	Rv:	CTCCATCTGGACCTCAGAGC	
mustn1b	Fw:	GAAGCGGCCGGTTGTAAAAG	440
	Rv:	AGCGTGACACTATAGAAATTGGC	
fhl1a	Fw:	CGGCCCATGAGGATCAGTTC	475
	Rv:	ACATCACACAGGTTCGCCAT	
casq2	Fw:	TTTACATGAGGAGGGCAGCG	527
	Rv:	CAAAGCCATCAGGGTCCTCC	

Table II: Oligos for RT-qPCR			
Gene	**Primer**	**Sequence (5' → 3')**	**Amplicon (bp)**
anxa2a	Fw:	TGACATGCAGGAGAGCATTC	109
	Rv:	CAGTCTGCTGGCGAAATACA	
mustn1b	Fw:	GAAGCGGCCGGTTGTAAAAG	104
	Rv:	ACTCCGCTGAAAACAGATGG	
fhl1a	Fw:	ATAAGAGCGATGTGGCCAAG	105
	Rv:	ATTCATGCCAGGATTTGTCC	
casq2	Fw:	GACCACAGATTGGTGTGGTTA	101
	Rv:	CCAGTTTTCCAGTTCTTCGGC	
fosab	Fw:	CCATACATGCCTGCCACAT	118
	Rv:	GCACCGGTAAACTCAGAAAAA	
hoxd3a	Fw:	ACACACCAGGGCTTCTCATC	104
	Rv:	TCTCCGTTTTTATGGGTTGC	
ier2a	Fw:	CTTGTTCAGCCCGTCATTTT	78
	Rv:	GGTGGTTTTCCCAGTCACAC	
ier2b	Fw:	TGACTCGGATGAACTGGTTG	112
	Rv:	TCTGTCTCGTTCACCGTCAC	
serpinh1b	Fw:	ATTTGAACCGCACAAAAGGA	113
	Rv:	ACACCATGGCTCAACATCAA	
socs3a	Fw:	CGACAGACACTGTGGAACAAA	108
	Rv:	AAAACACAGGCGATCCTCAG	
atf3	Fw:	TGCAAAACAGGTATGCCACT	114
	Rv:	AGCATTGACATGATGGGTGA	
gspt1	Fw:	AGCTTGCCGGTACCCTTAAT	87
	Rv:	AGGACCAAGGCCTCTTGTTT	
ank1a	Fw:	GCCTGAGATATACGGGCTCA	83
	Rv:	TACGTCCAATGTAGCGCATC	

Table III: crRNAs for generation of KOs with CRISPR/Cas9				
Gene	**Exon**	**Sequence (5' → 3')**	**PAM**	**Chain**
anxa2a	2	CTACCCTACTGTTGTTCCAG	AGG	+
	3	ACGGACATACAACCAGCGGC	GGG	+
	4	TCACTGGAAACAGTCATCCT	GGG	+
mustn1b	2	CCTTTAGCCCCAATTTACTG	CGG	-
	3	GTCTGTTGTGTAGAGCGAAT	GGG	+
fhl1a	2	CTACTGCAGAGACAACCTGC	AGG	+
	3	GGCAGCGAGGCGATCCGTCA	CGG	+
	5	TCTGGCTGGAGCTCGCTTCA	CGG	-
casq2	1	GGTCTTCGCCATCATAACGG	GGG	-
	2	GCTAGCTGCTCAAGTCTTGG	AGG	+
	5	GCATTGTCAATGATCTCAAC	TGG	+

Table IV: Miscellaneous oligos		
Name	**Application**	**Sequence (5' → 3')**
M13_Fr	Universal Primers	TGTAAAACGACGGCCAGT
M13_Rv		CAGGAAACAGCTATGACC
Tol2_5'	Sequencing pmlc2a:CCaMP6f final vector	GGGCTGAAAAGCAATCCTGC
Tol2_3'		CACAGCACCTTGACCTGG
GCaMP6f_polyA_Fr		AAGCAGACATCGATGGGG
GCaMP6f_mlc2a_Rv		GACCTATAGCTCTGACTGCG
GCaMP6f_seq_Fr		GTAGGTCAGGGTGGTCACGA
Mlc2a_promoter_Fr		TCAGGCATAGCCAGTTGTAAC
Macosko (TSO)	Template switch oligo	AAGCAGTGGTATCAACGCAGAGTGAATrGrGrG
SMART PCR Primer	cDNA library amplification	AAGCGAGTGGTATCAACGCAGAGT
New-P5-SMART PCR hybrid oligo	Nextera tagmentation	AATGATACGGCGACCACCGAGATCTACACGCCTGTCC GCGGAAGCAGTGGTATCAACGCAGAGT*A*C
Read1CustomSeqB	Illumina Seq	GCCTGTCCGCGGAAGCAGTG GTATCAACGCAGAGTAC

[1] rG stands for ribonucleotide G (to improve binding of the TSO to the cDNA
[2] * denote a base modification called phosphorothioate

Table V: Oligos for genotyping & screening KOs					
Gene	**Exon**	**Primer**	**Sequence (5' → 3')**	**Size (bp)**	**Seq**
anxa2a	2	Fr	AAACAAAATTCCTATTGCAACTACATT	420	Fr
		Rv	CGGTTGGTTCTCTTCCAGAC		
	3	Fr	GAAGAGAACCAACCGCATGA	410	Fr
		Rv	AACAGACTGACCTTCTTGGCTC		
	4	Fr	AGCTTGCCAGAATTCAAAGC	368	Fr
		Rv	CCAGTATCCAGTGAATGAGTGC		
mustn1b	2	Fr	GCAAGGAGTCAACTCAGCCAA	251	Rv
		Rv	TGAAGACCAACTCACCACACTC		
	3	Fr	TCTTCGCAATGTCTTGTTTTGT	325	Fr
		Rv	TCCAGATGGAGGTTTGGGTT		
fhl1a	2	Fr	TGCCCTTGTTTTTGTGTCTG	269	Fr
		Rv	TTGCTGTGGCAGTCAGAATC		
	3	Fr	ACCCAGGAACTGAACCATAAGA	281	Fr
		Rv	ACAAACGCTTGGCTGTAATTTT		
	5	Fr	GTCGATCAGAACTAATGGGTCC	267	Rv
		Rv	GCTGCACAGATTTGTTTACCTG		
casq2	1	Fr	GAGGTGTTAAAAGGCCAGTGAC	254	Rv
		Rv	GGAGCATGGTAGAACAGACACA		
	2	Fr	CACAAAAGGAGGCCCTACAA	351	Fr
		Rv	GATGCGTGAGAAGCTCCAGT		
	4	Fr	TGGACTTCCATCTGCTGACA	328	Fr
		Rv	TCACTCCAGCTGAAGGATAAAA		
postnb	1	Fr	TGTAAAACGACGGCCAGTACTGAAATCGCTGCCTT	458	Rv
		Rv	GTGTCTT AGCTACACGTGCAAAATAAGAAT		

Table VI: Illumina i7 indexing oligos for sample multiplexing		
Index	**Sequence (5' → 3')**	**Reverse complementary**
701	CAAGCAGAAGACGGCATACGAGATTCGCCTTAGTCTCGTGGGCTCGG	TAAGGCGA
702	CAAGCAGAAGACGGCATACGAGATCTAGTACGGTCTCGTGGGCTCGG	CGTACTAG
703	CAAGCAGAAGACGGCATACGAGATTTCTGCCTGTCTCGTGGGCTCGG	AGGCAGAA
704	CAAGCAGAAGACGGCATACGAGATGCTCAGGAGTCTCGTGGGCTCGG	TCCTGAGC
705	CAAGCAGAAGACGGCATACGAGATAGGAGTCCGTCTCGTGGGCTCGG	GGACTCCT
706	CAAGCAGAAGACGGCATACGAGATCATGCCTAGTCTCGTGGGCTCGG	TAGGCATG
707	CAAGCAGAAGACGGCATACGAGATGTAGAGAGGTCTCGTGGGCTCGG	CTCTCTAC
708	CAAGCAGAAGACGGCATACGAGATCCTCTCTGGTCTCGTGGGCTCGG	CAGAGAGG
709	CAAGCAGAAGACGGCATACGAGATAGCGTAGCGTCTCGTGGGCTCGG	GCTACGCT
710	CAAGCAGAAGACGGCATACGAGATCAGCCTCGGTCTCGTGGGCTCGG	CGAGGCTG
711	CAAGCAGAAGACGGCATACGAGATTGCCTCTTGTCTCGTGGGCTCGG	AAGAGGCA
712	CAAGCAGAAGACGGCATACGAGATTCCTCTACGTCTCGTGGGCTCGG	GTAGAGGA
714	CAAGCAGAAGACGGCATACGAGATTCATGAGCGTCTCGTGGGCTCGG	GCTCATGA

Appendix II. Plasmid Maps

The maps of all generated and used plasmids for this thesis are shown below:

Figure A 1 pCR4_csrp3 for the generation of *ISH* probe

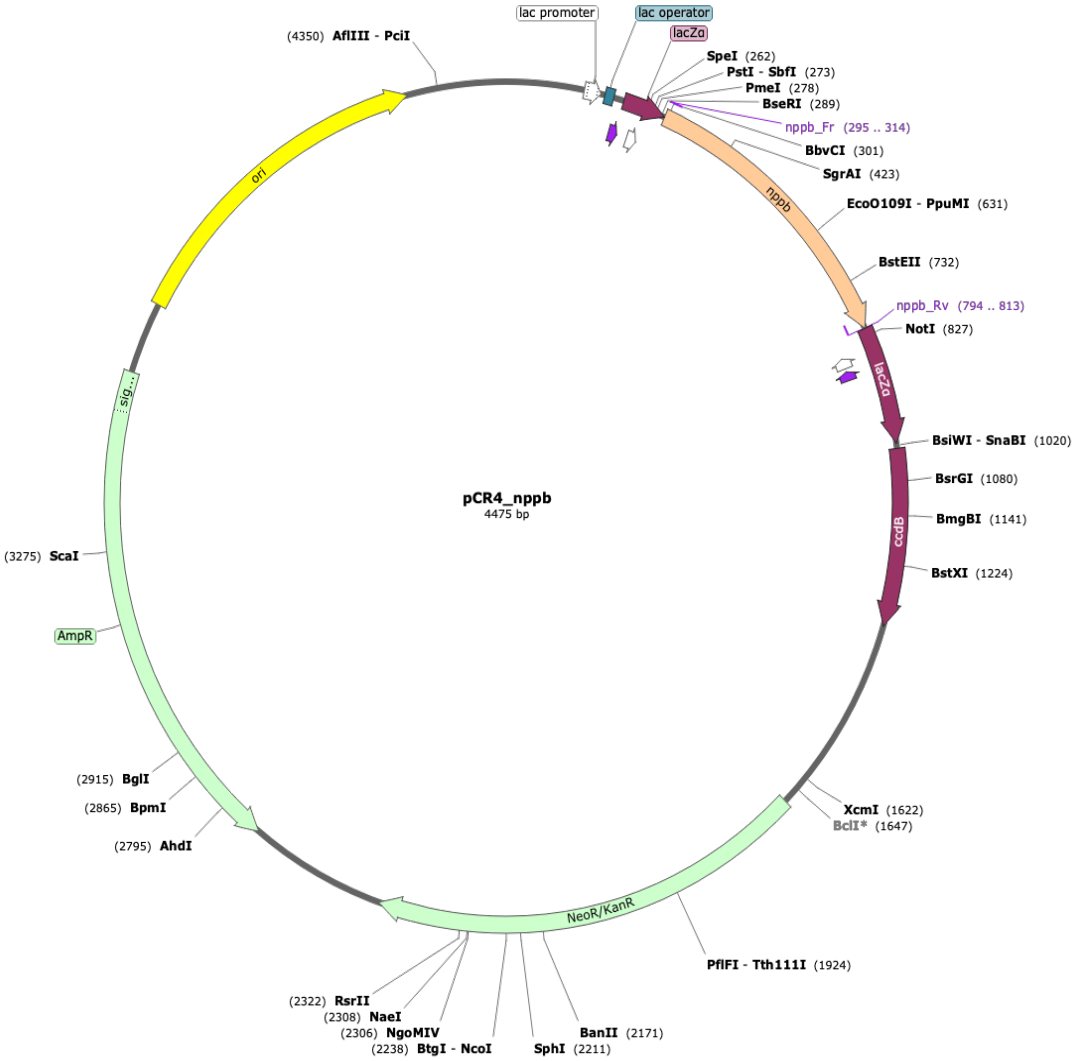

Figure A 2 pCR4_nppb for the generation of *ISH* probe

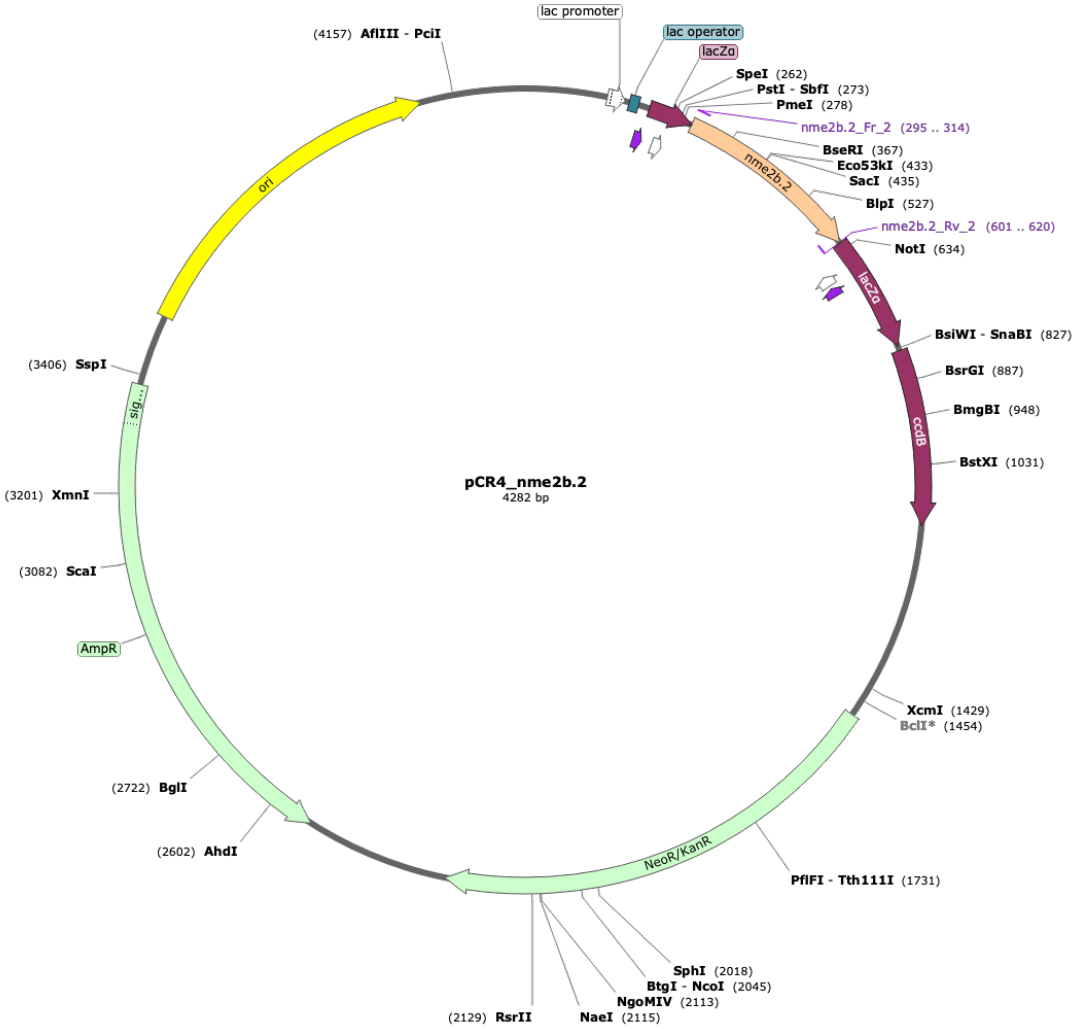

Figure A 3 pCR4_nme2b.2 for the generation of *ISH* probe

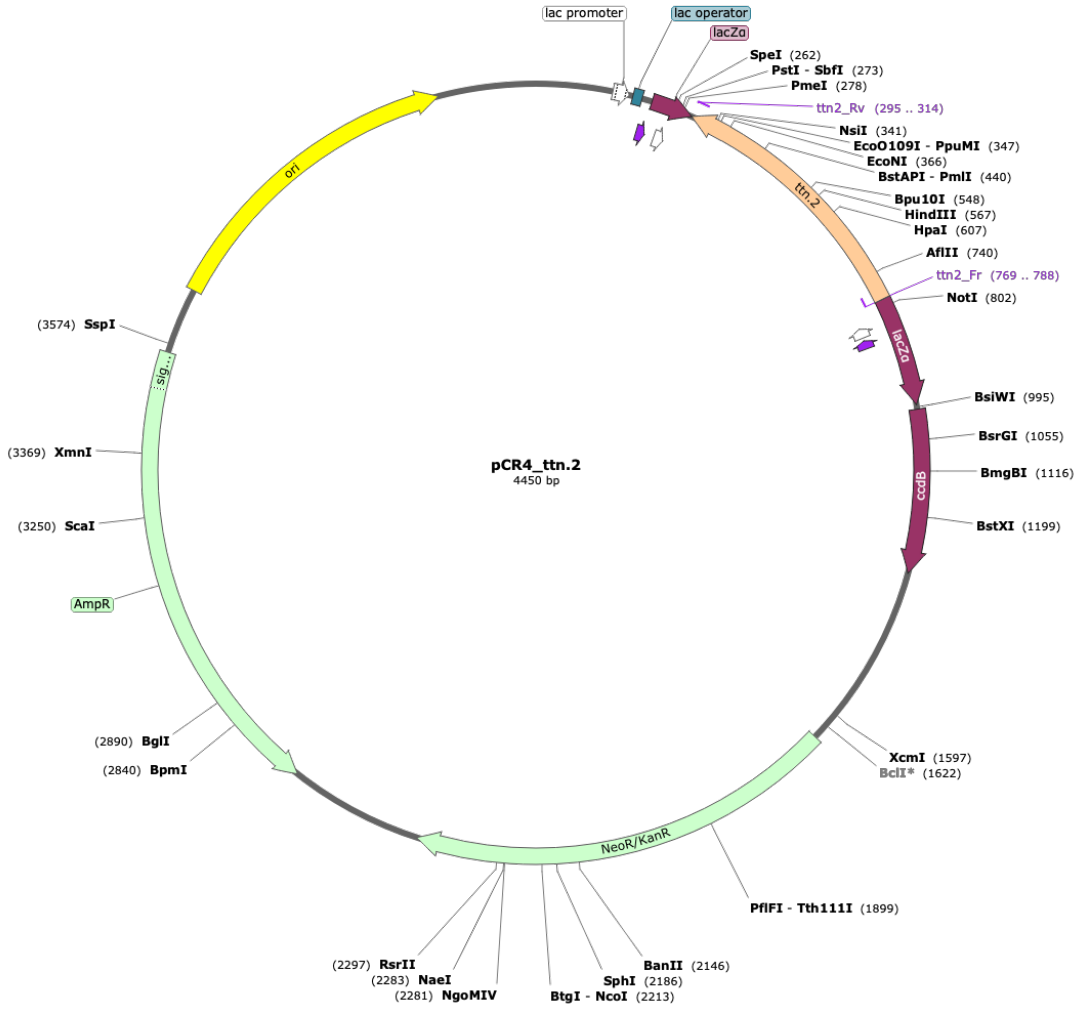

Figure A 4 pCR4_ttn.2 for the generation of ISH probe

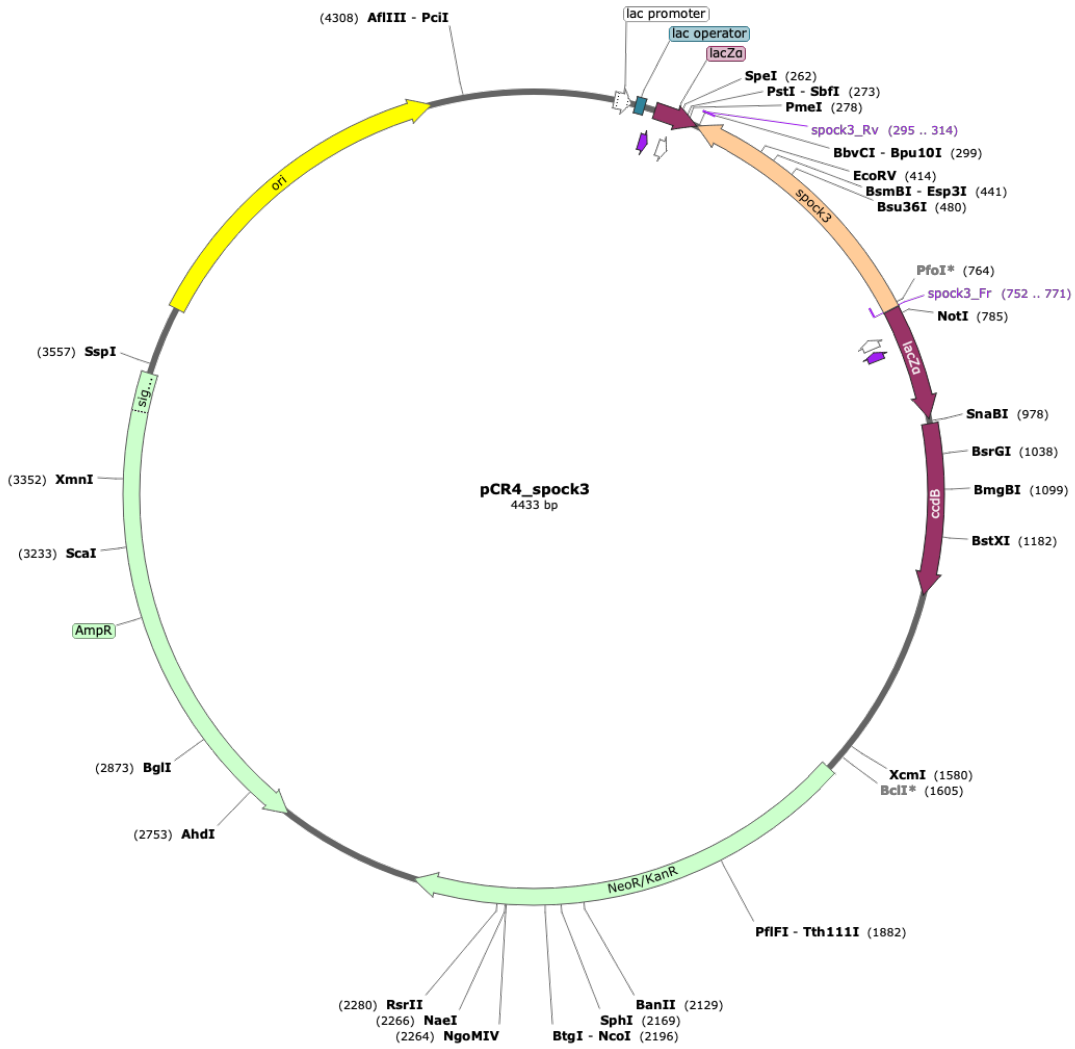

Figure A 5 pCR4_spock3 for the generation of ISH probe

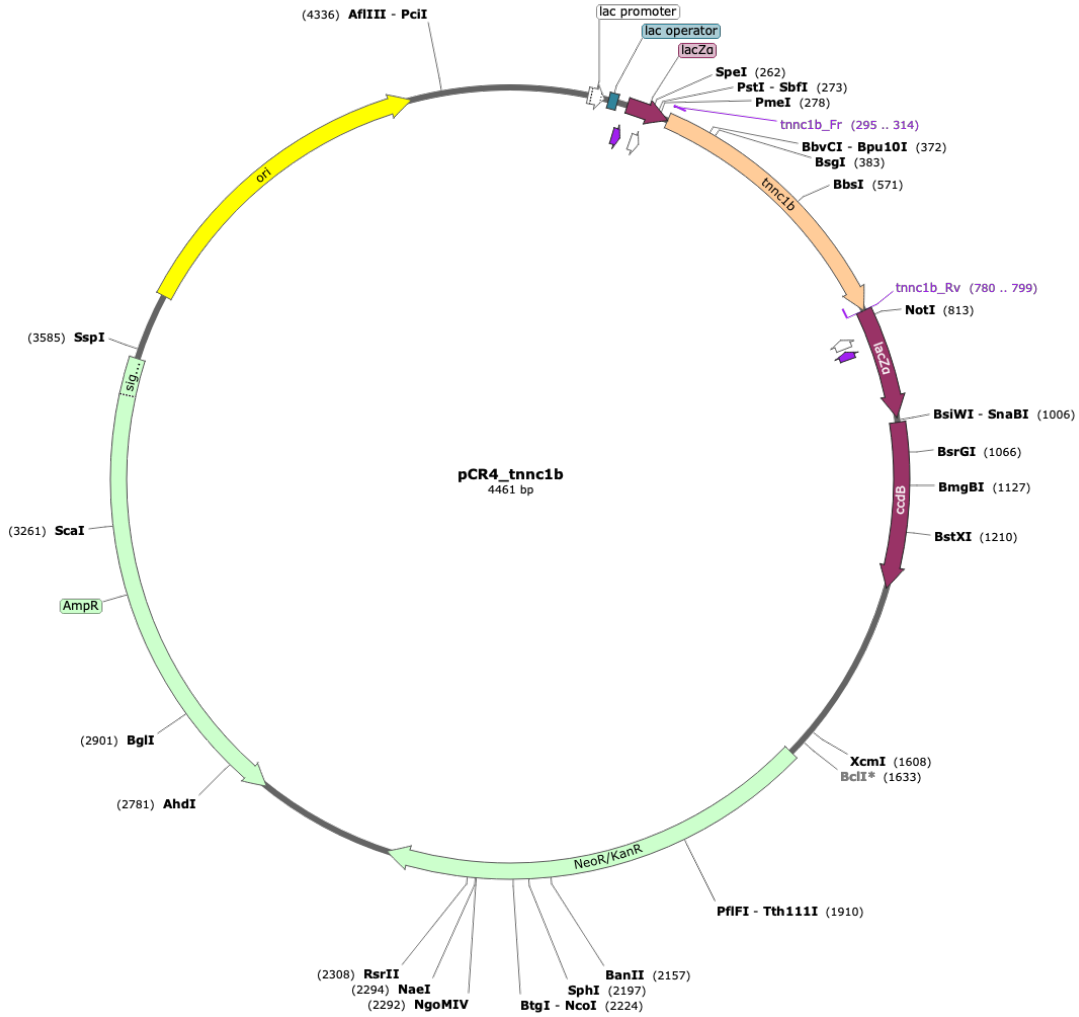

Figure A 6 pCR4_tnnc1b for the generation of ISH probe

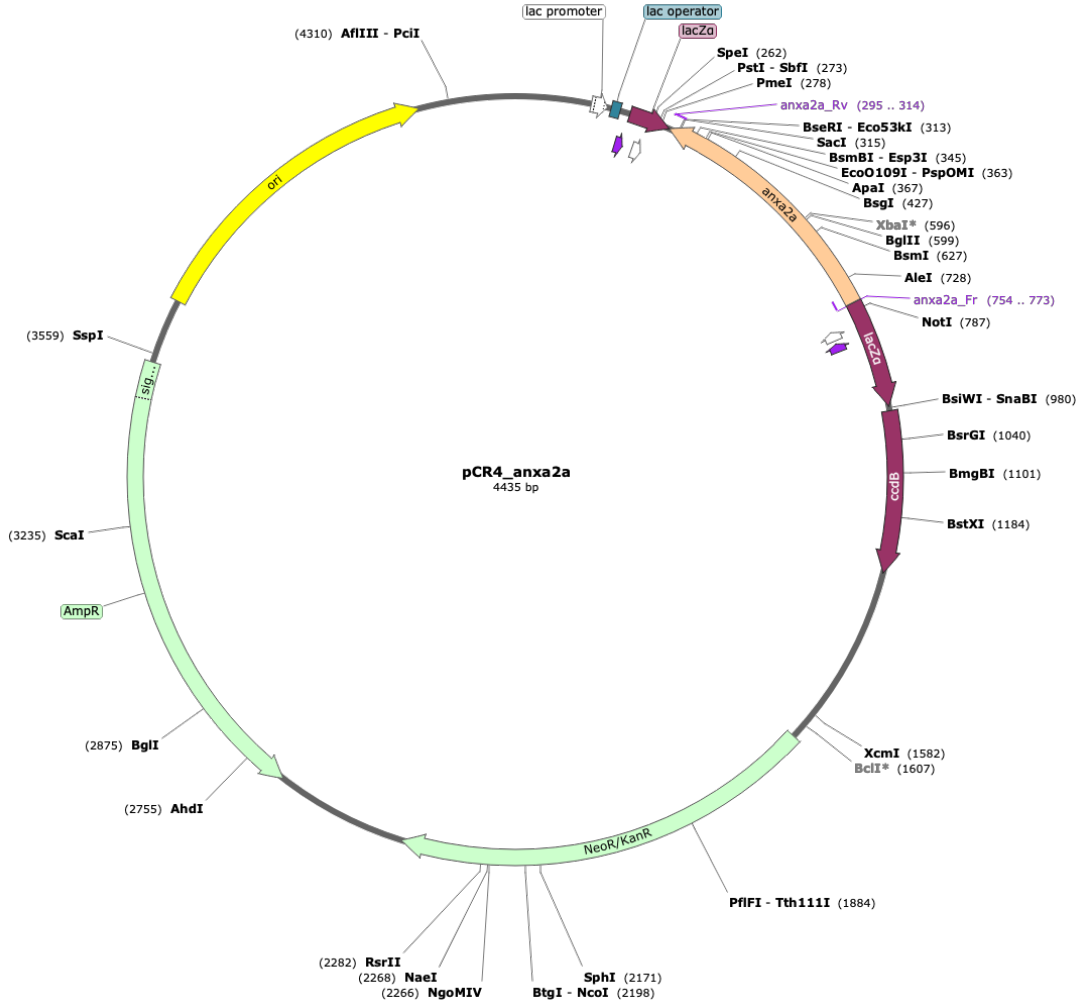

Figure A 7 pCR4_anxa2a for the generation of ISH probe

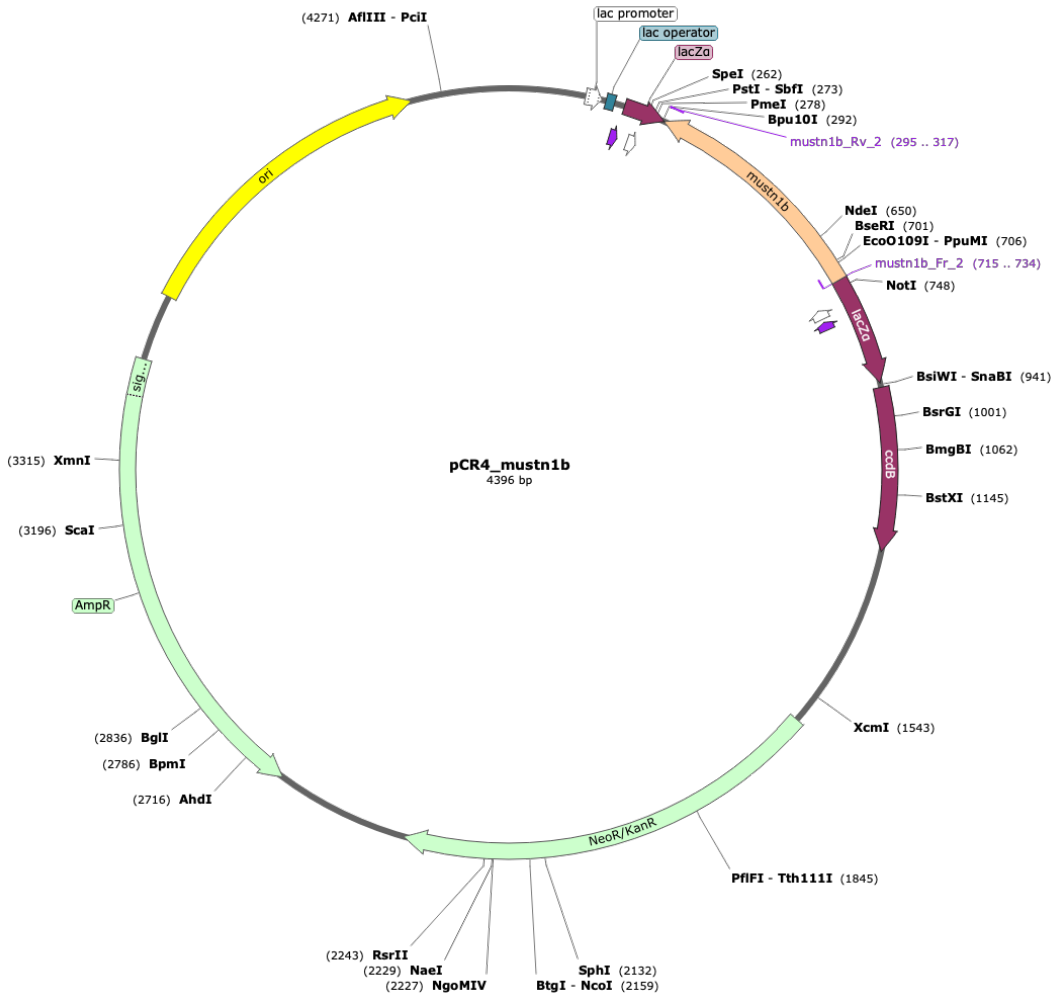

Figure A 8 pCR4_mustn1b for the generation of ISH probes

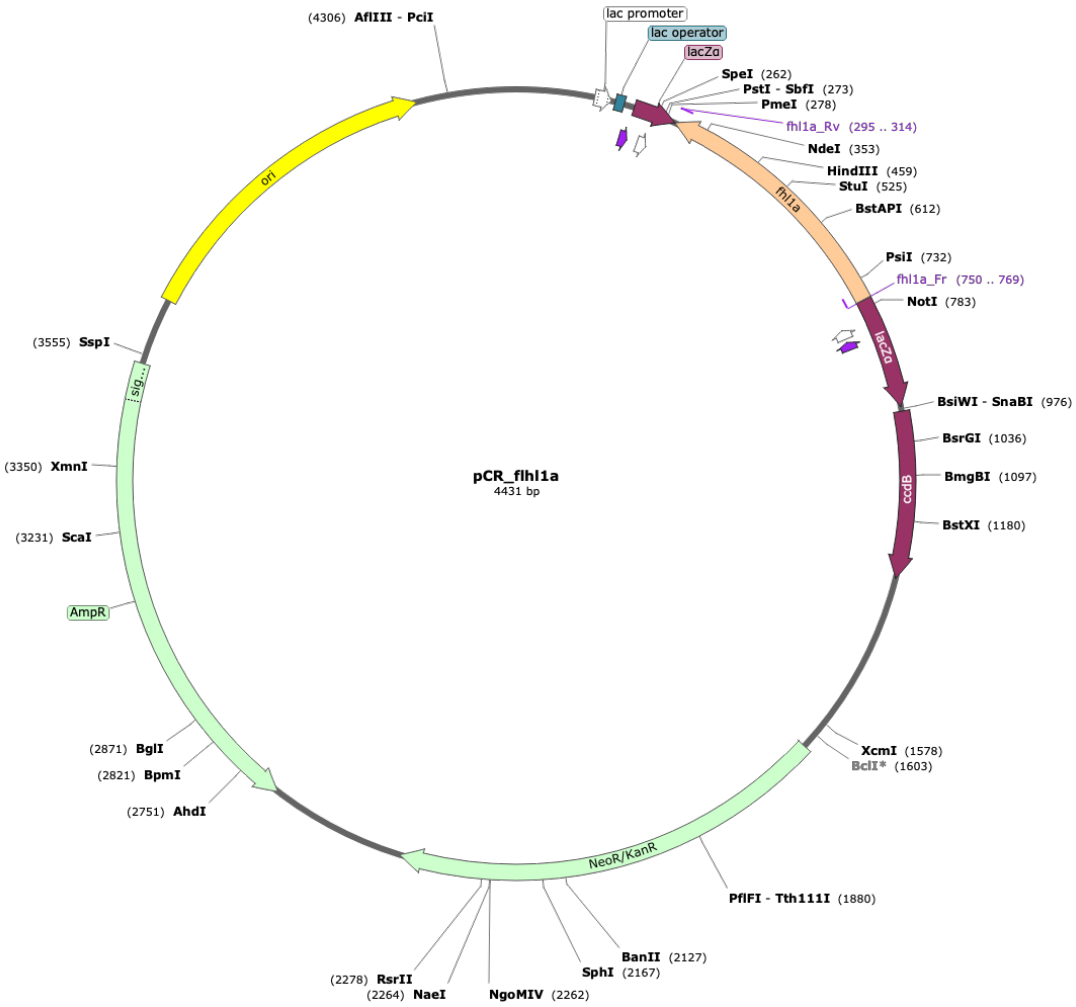

Figure A 9 pCR4_fhl1a for the generation of ISH probe

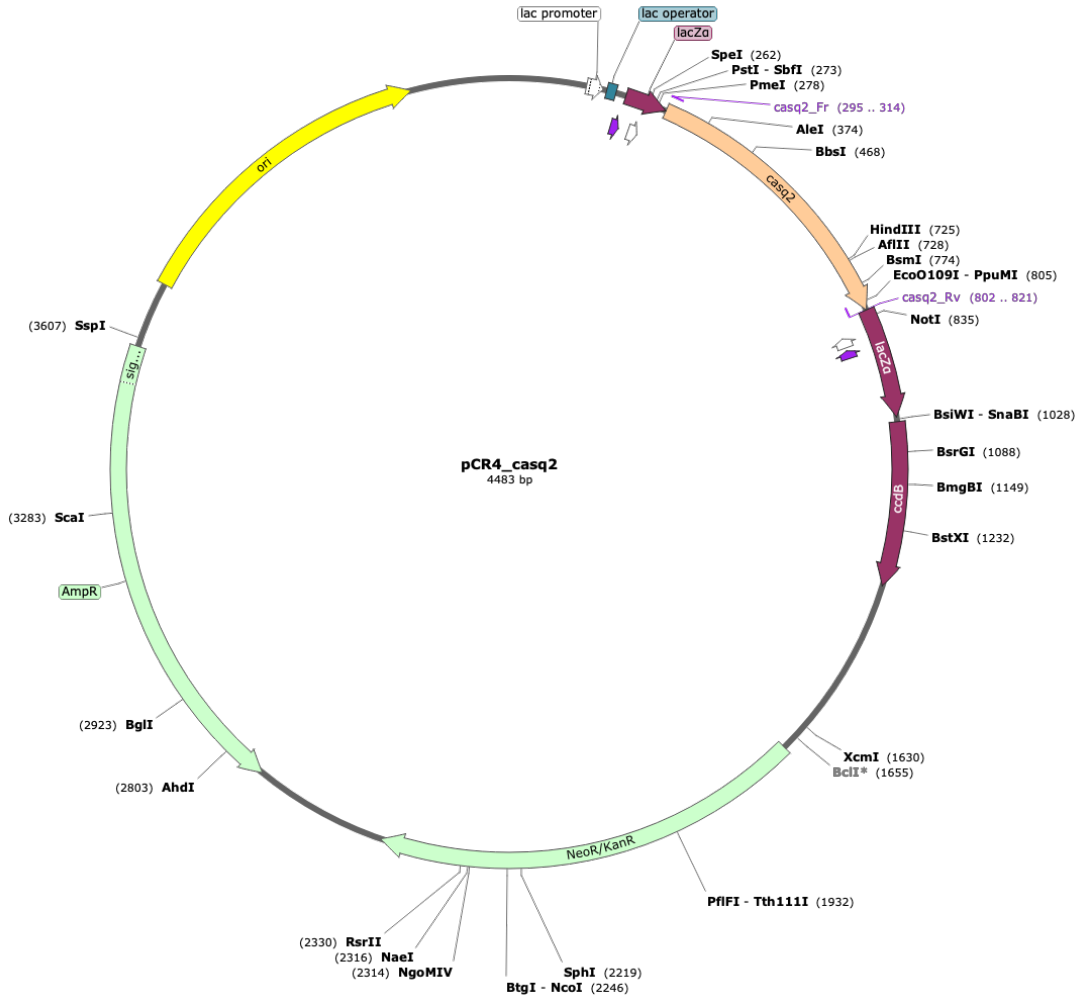

Figure A 10 pCR4_casq2 for the generation of ISH probe

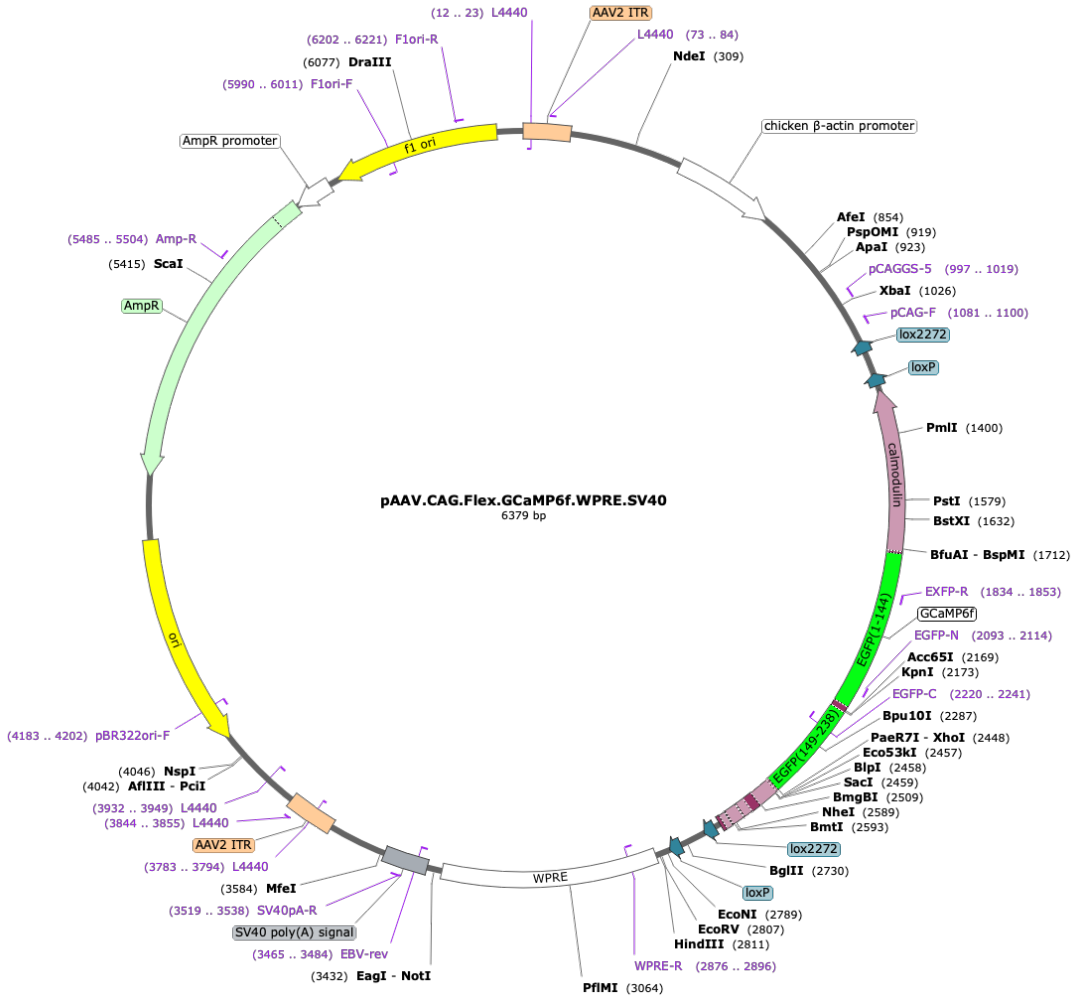

Figure A 11 Donor vector encoding for *GCaMP6f*

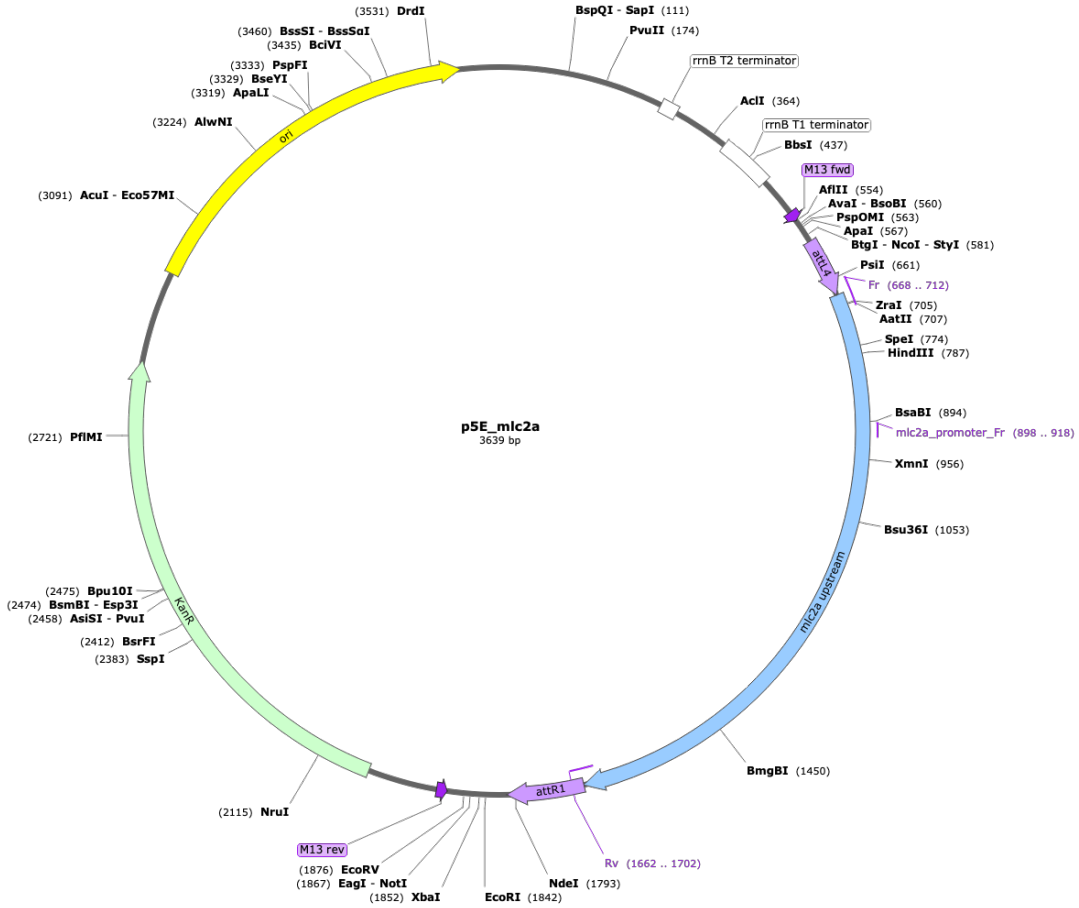

Figure A 12 Tol2kit 5' entry clone with mlc2a promoter

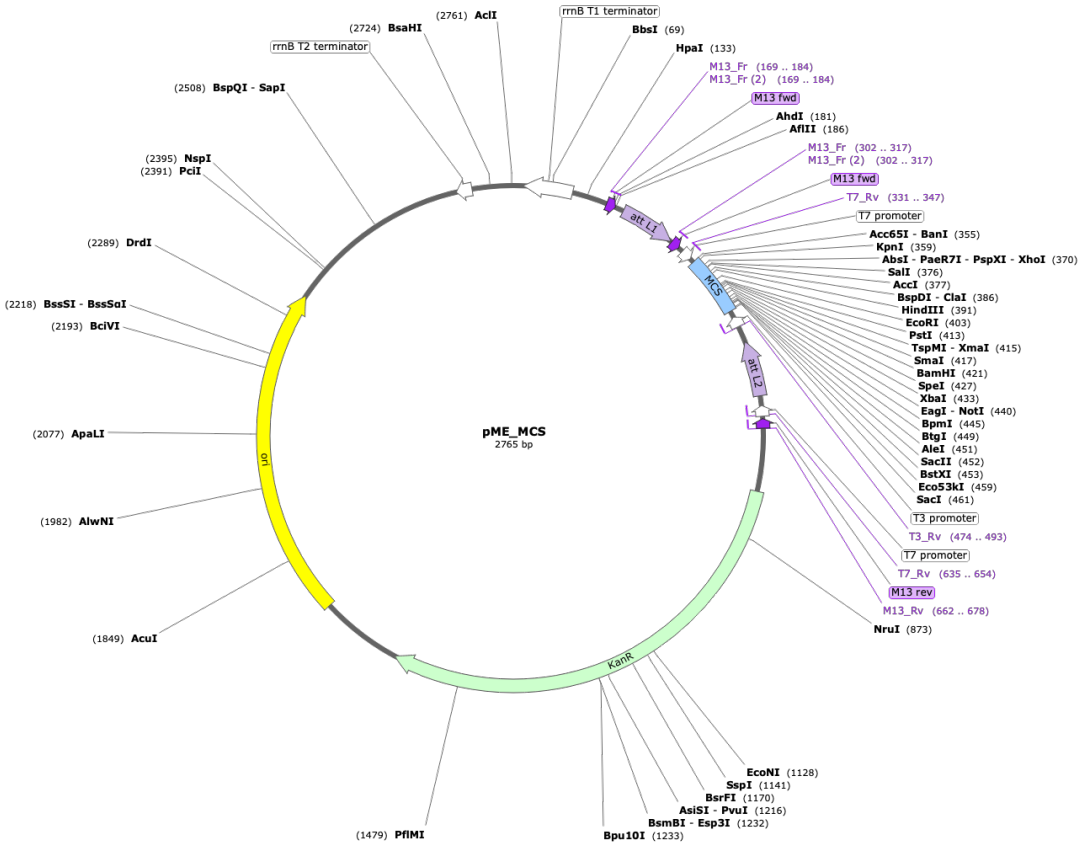

Figure A 13 Tol2kit middle entry clone with multi-cloning site

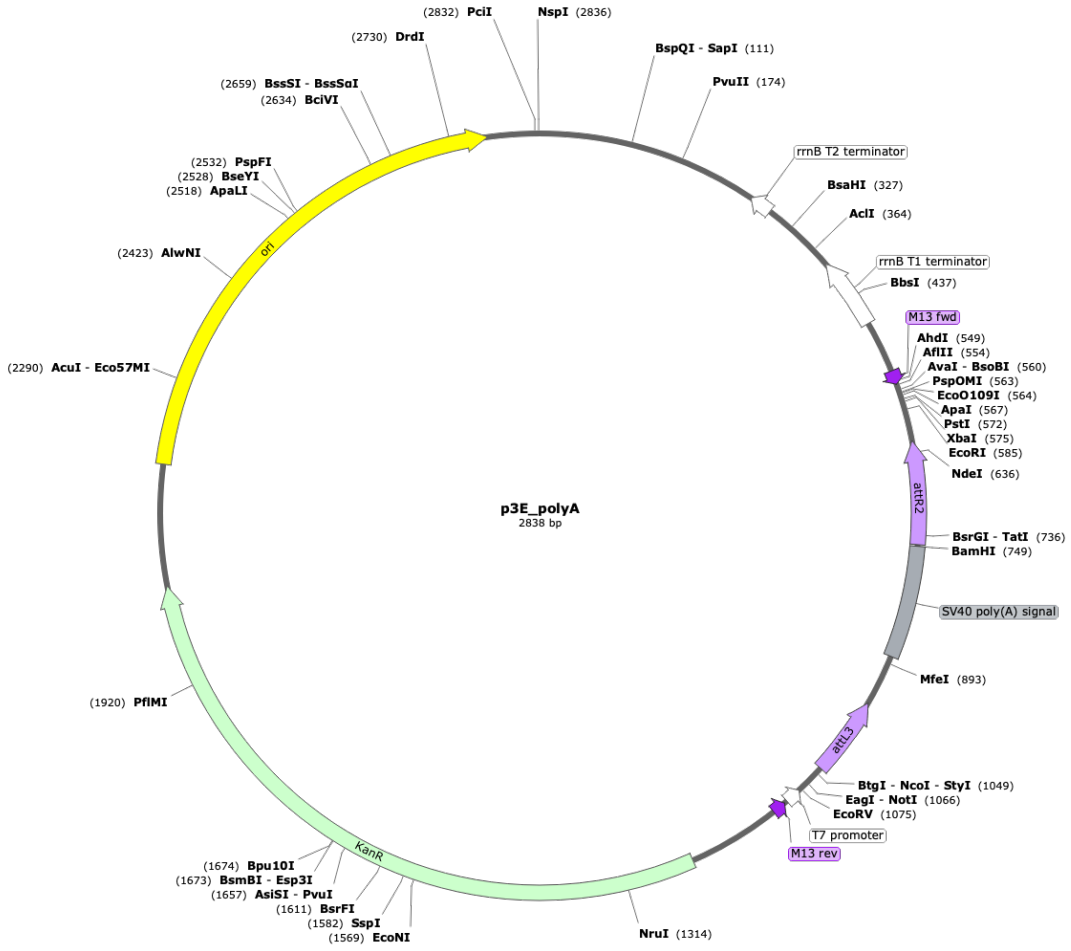

Figure A 14 Tol2kit 3' entry clone with SV40 late polyA signal

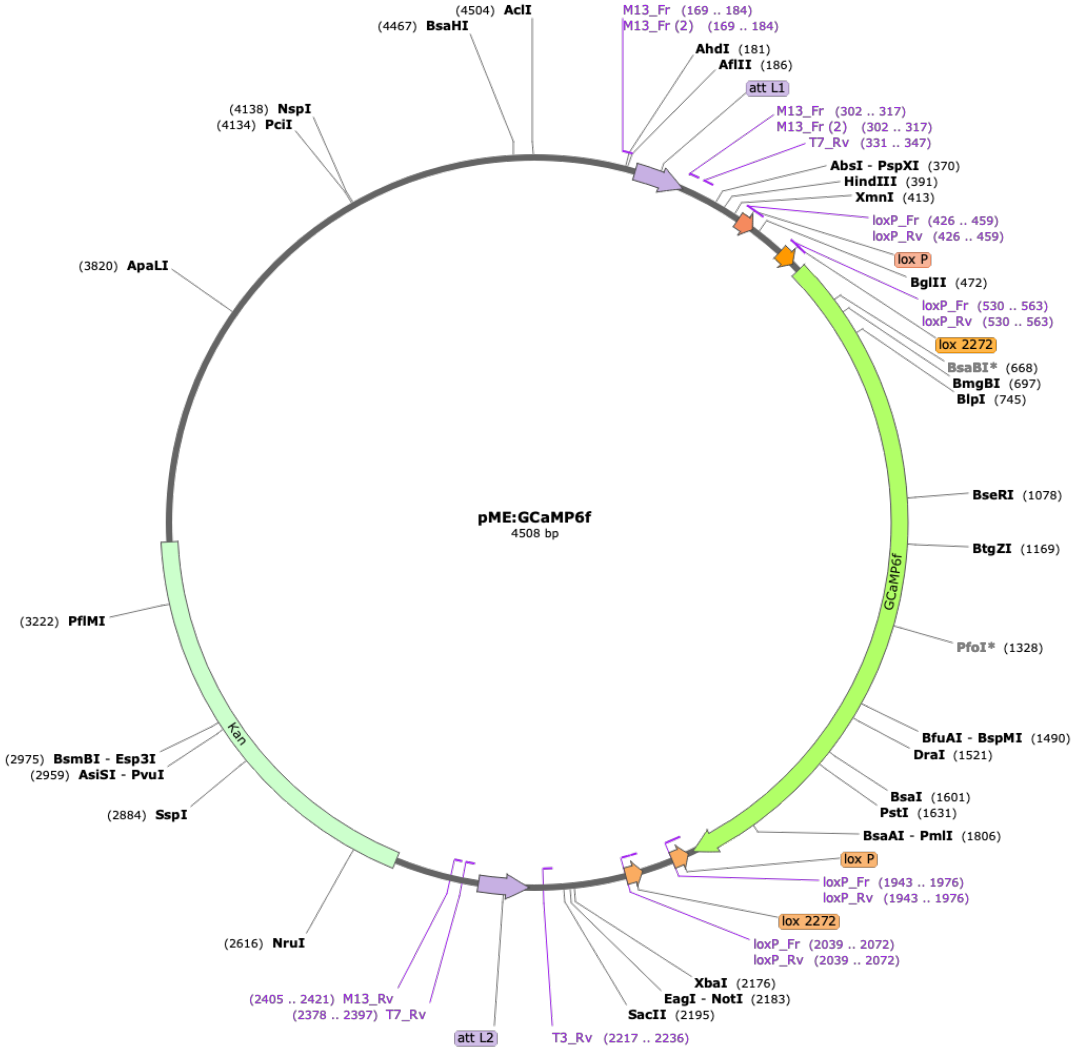

Figure A 15 Tol2kit middle entry clone with GCaMP6f

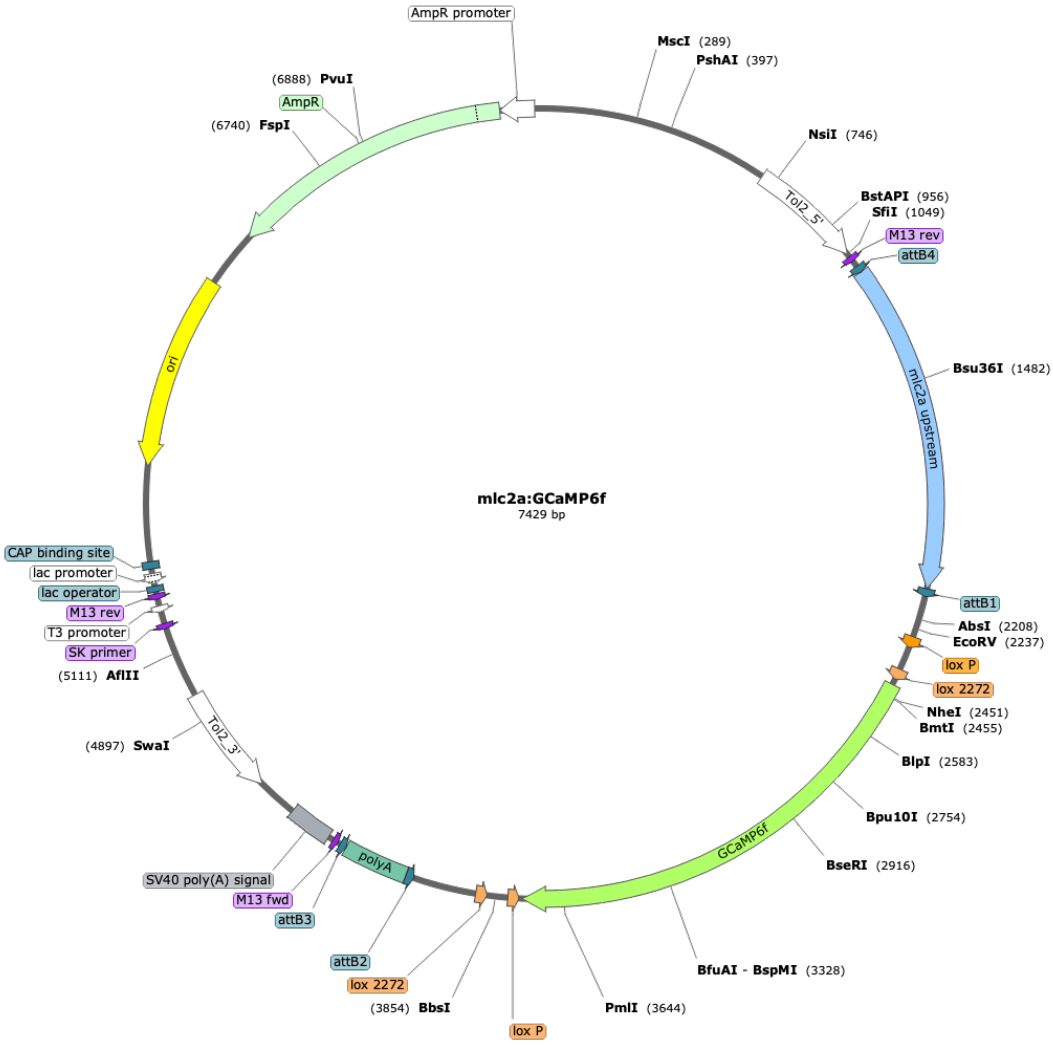

Figure A 16 Tol2 final destination vector for *GCaMP6f* reporter line transgenesis under a cardiomyocyte specific promoter, flanked by minimum Tol2 sequences

Appendix III. Supplementary material from chapter I

All the complementary plots and information for better understanding of chapter I are shown below:

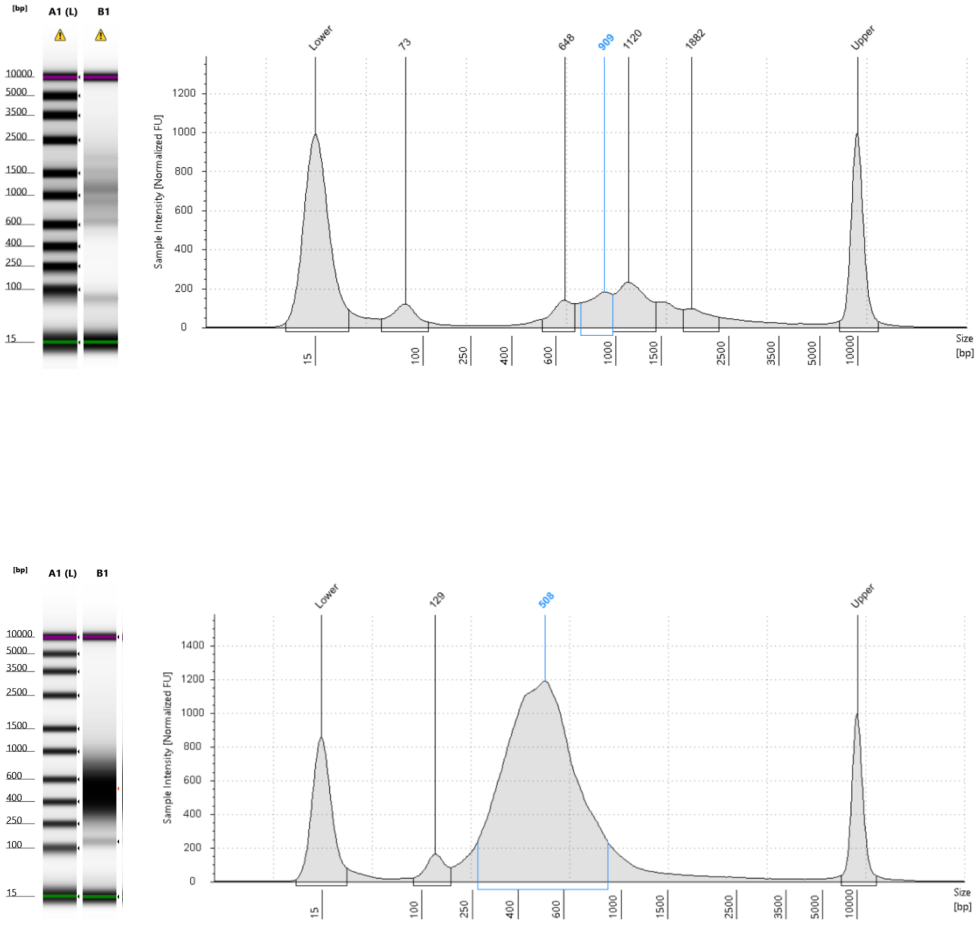

Figure A 17 Tapestation electrophoresis trace of PCR library and Nextera library

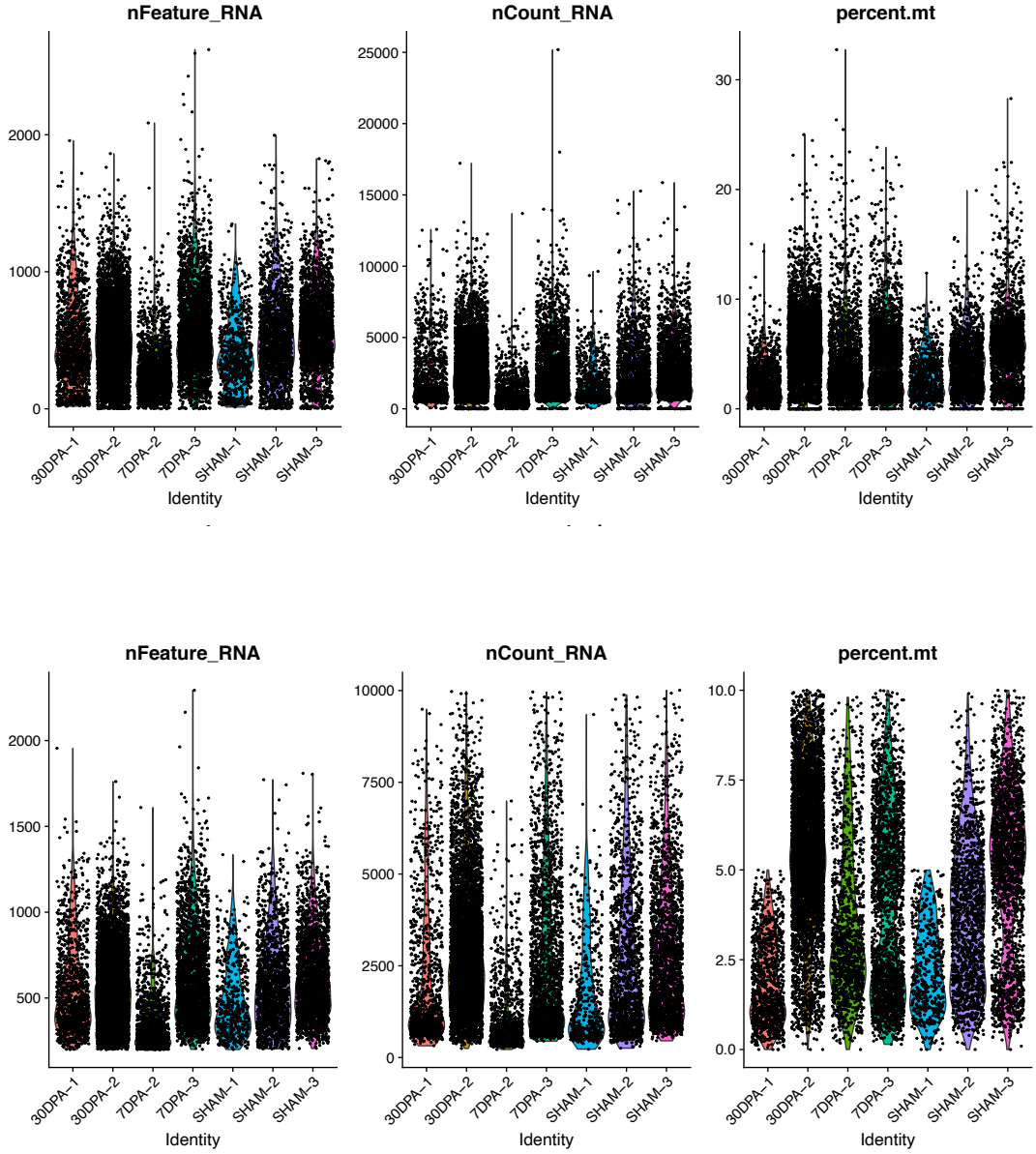

Figure A 18 QC filters of sequenced cells

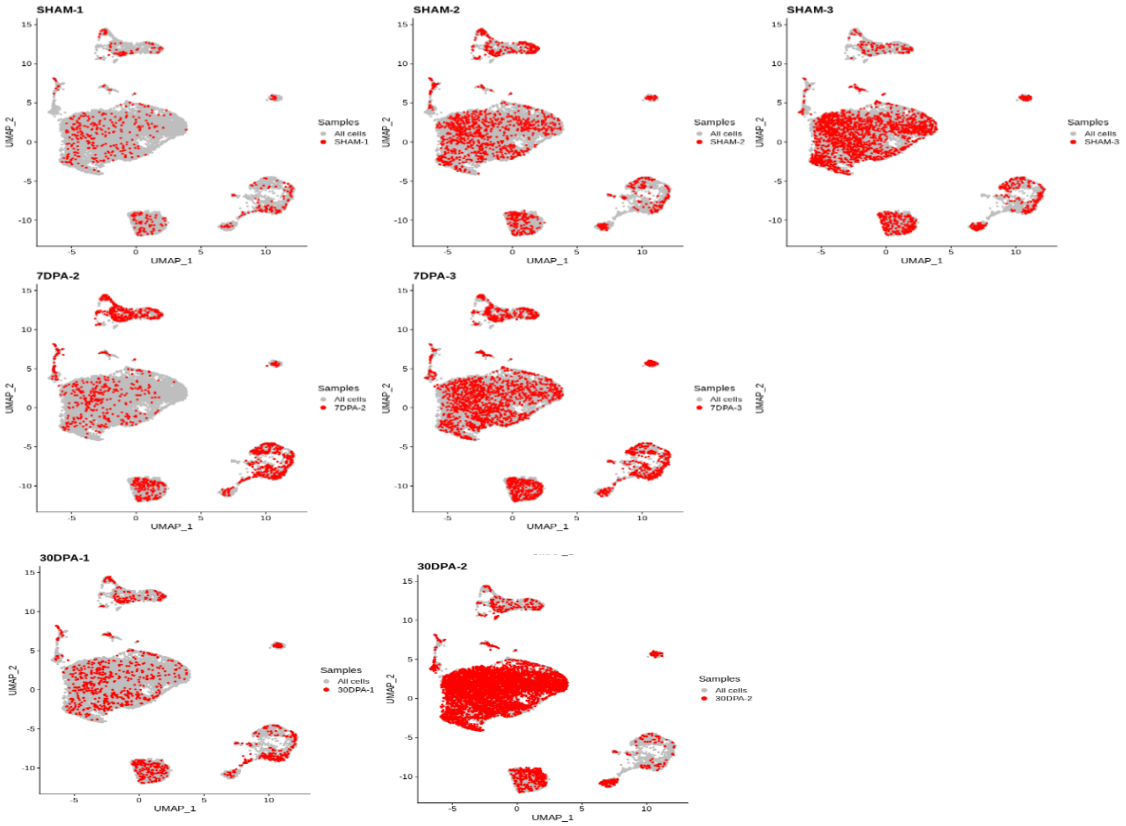

Figure A 19 Combination of datasets and CCA integration

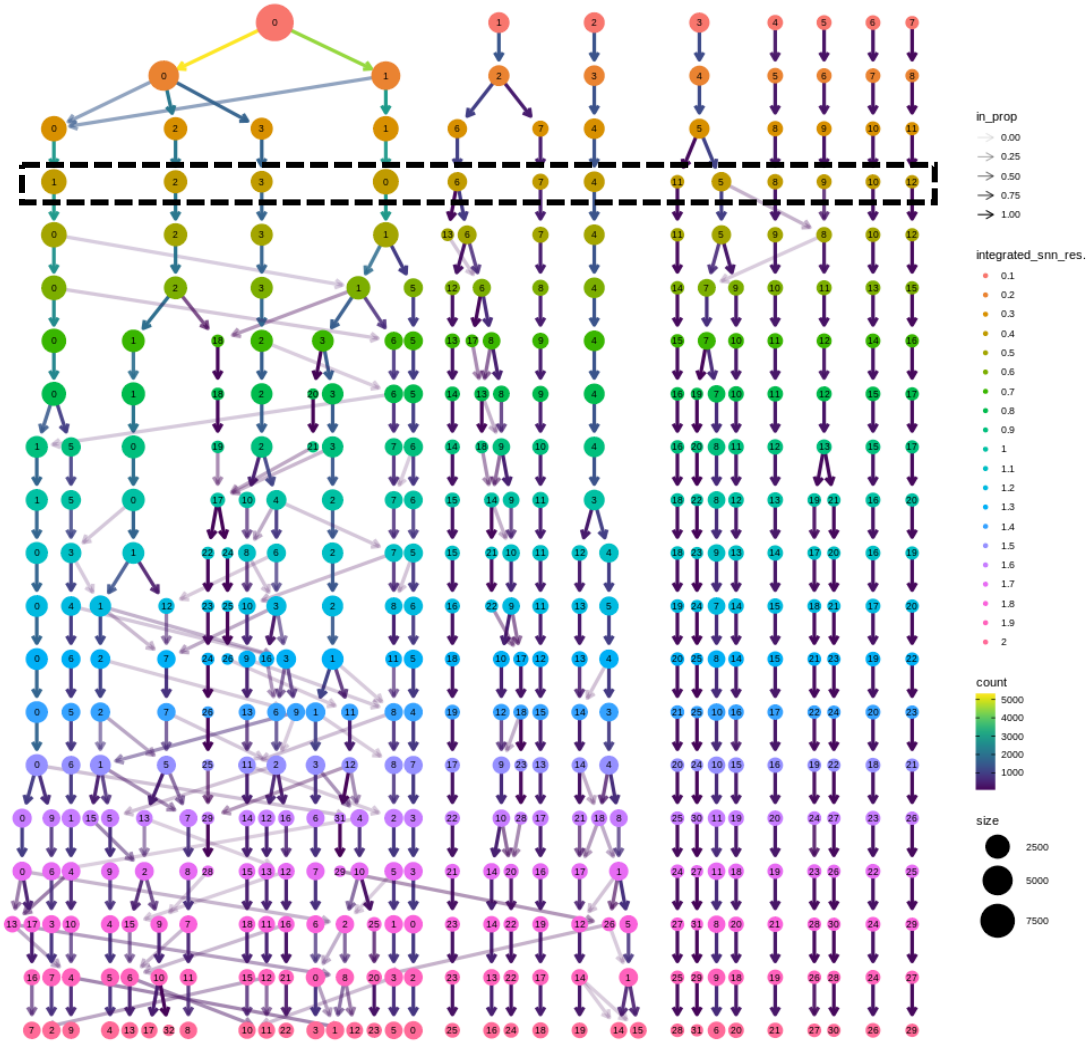

Figure A 20 Cluster tree - Global analysis

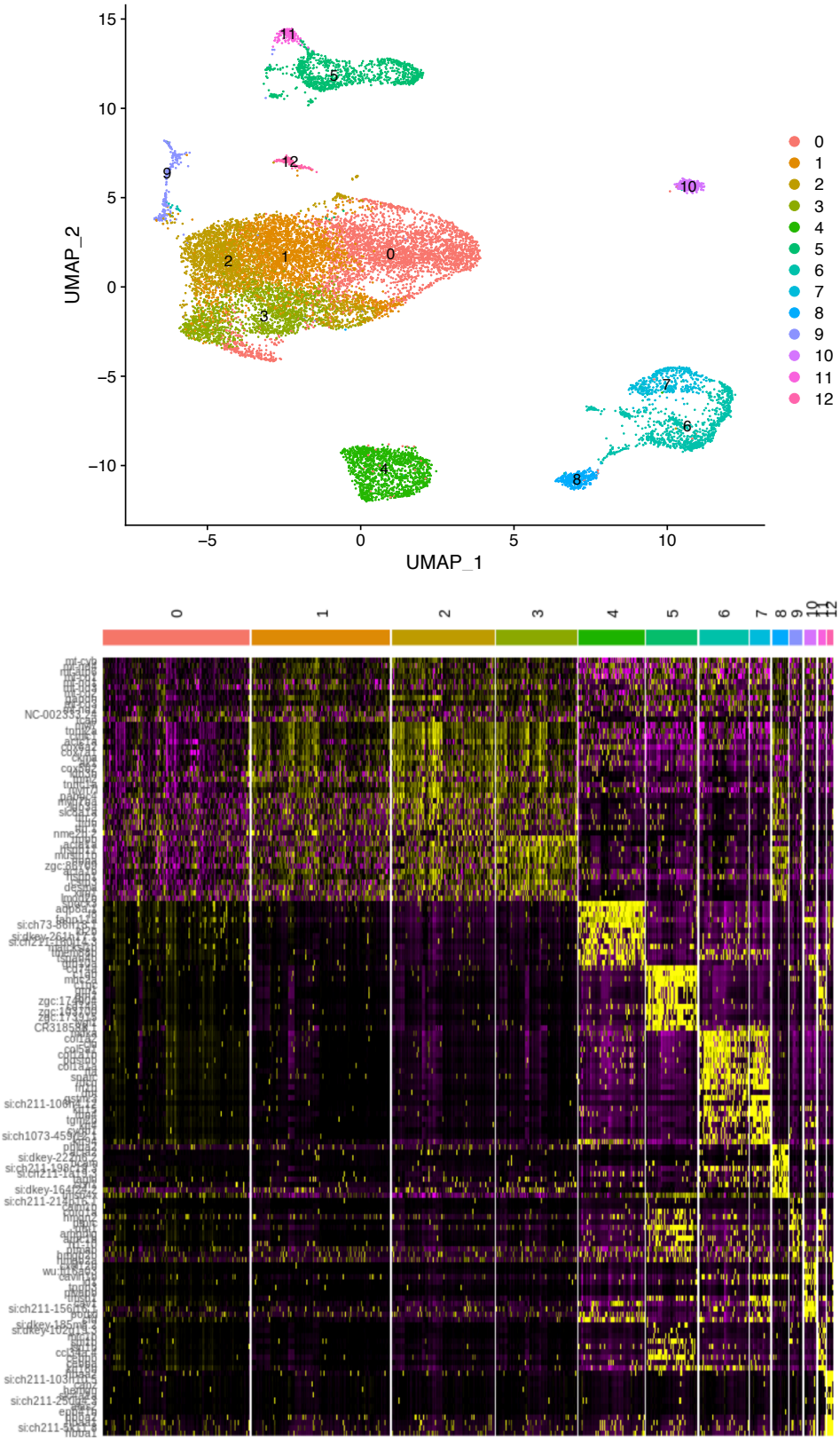

Figure A 21 UMAP and Heatmap - Global analysis

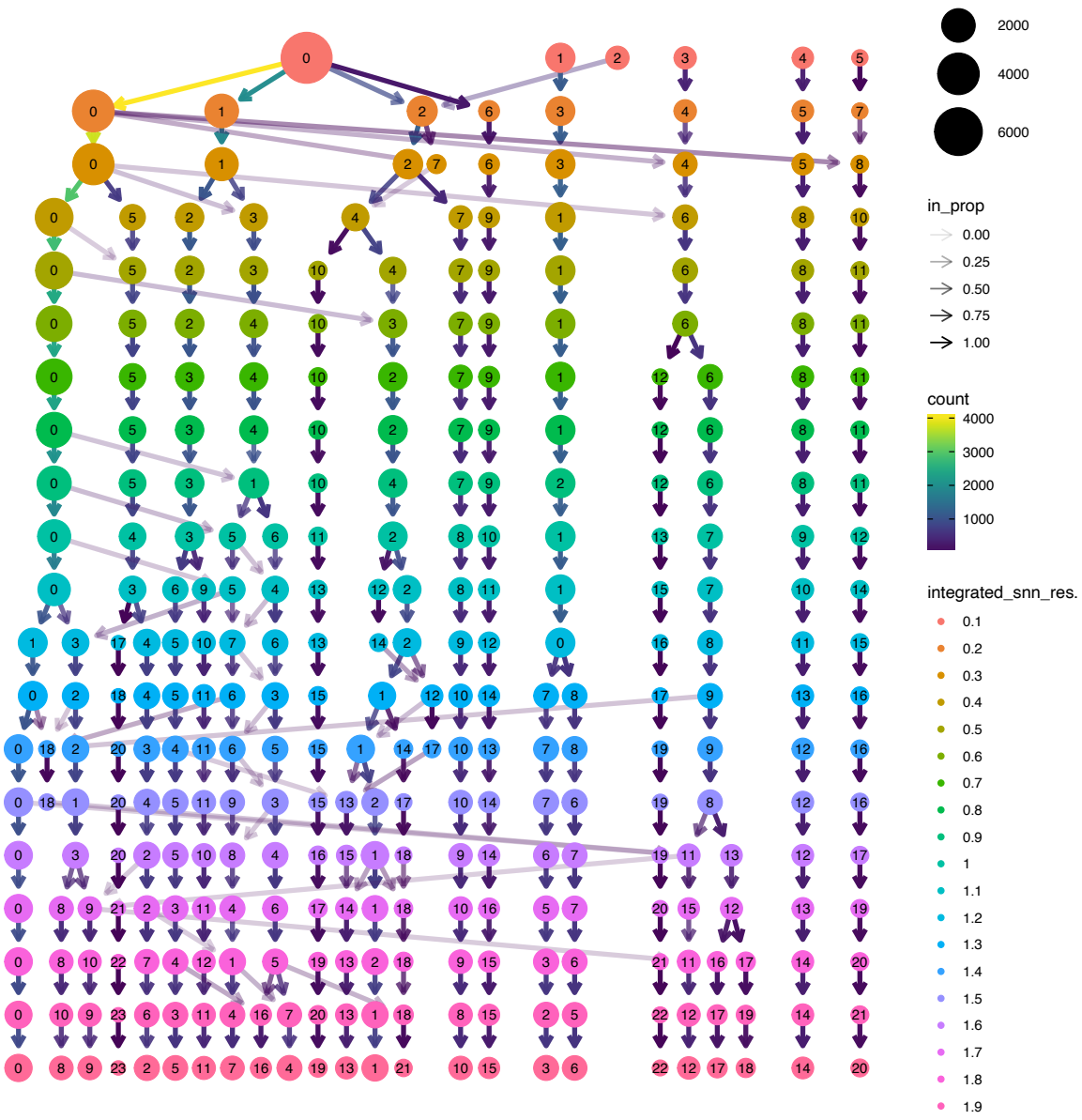

Figure A 22 Cluster tree - Cardiomyocytes analysis

Figure A 23 Heatmap - Cardiomyocytes analysis

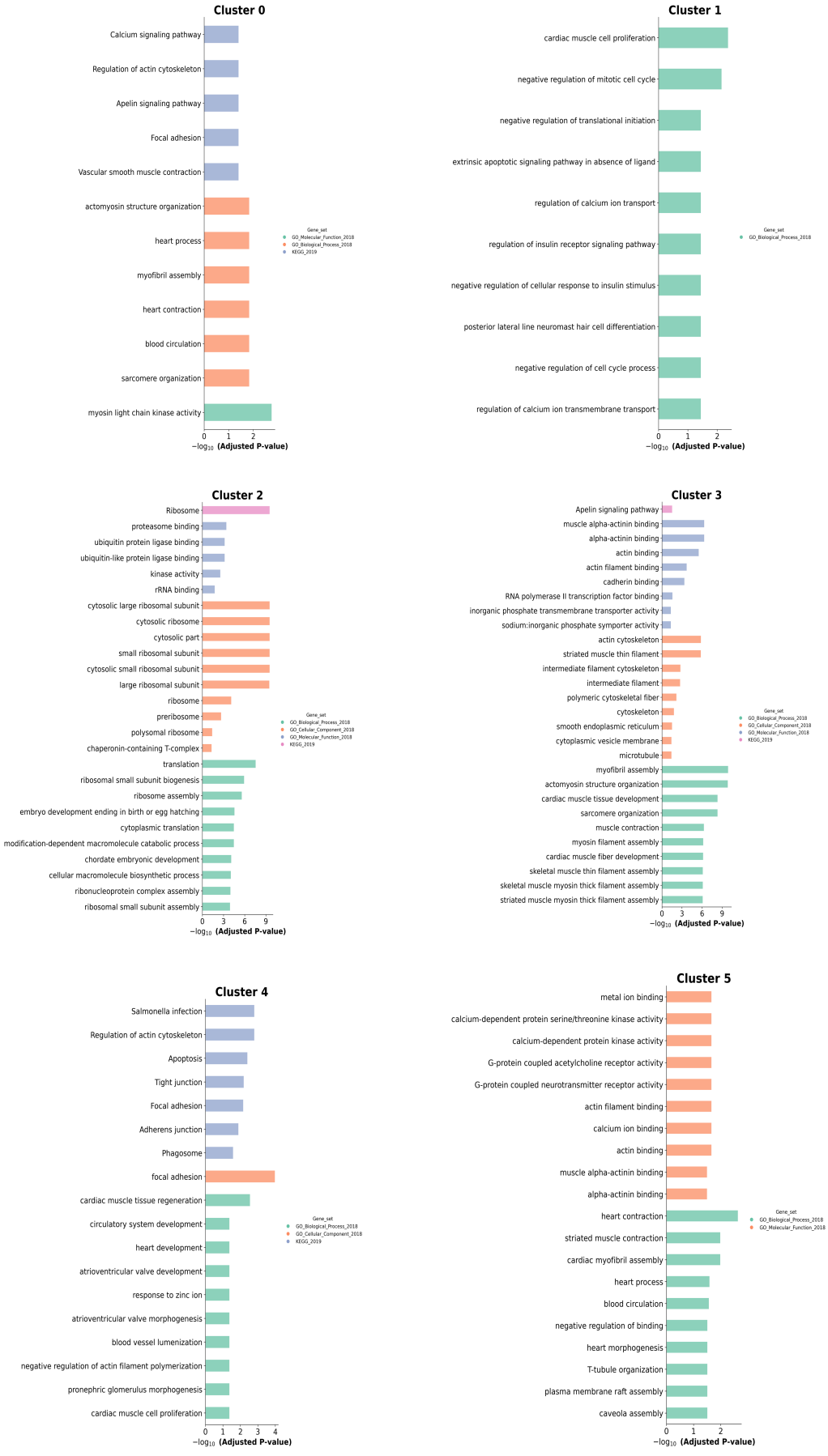

Figure A 24 GO analysis for each cluster

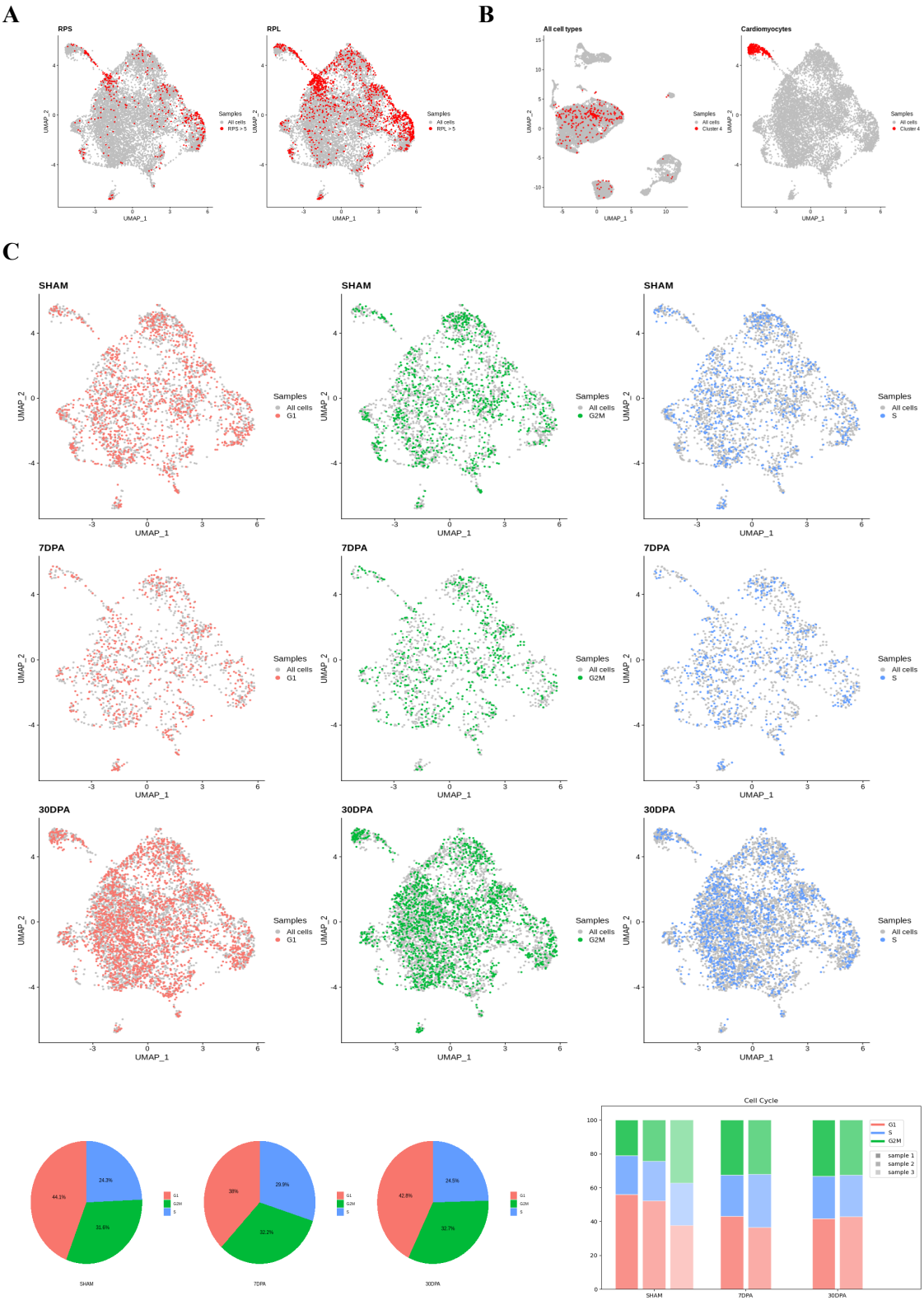

Figure A 25 Excluding bias in clustering of cardiomyocyte cell-state populations

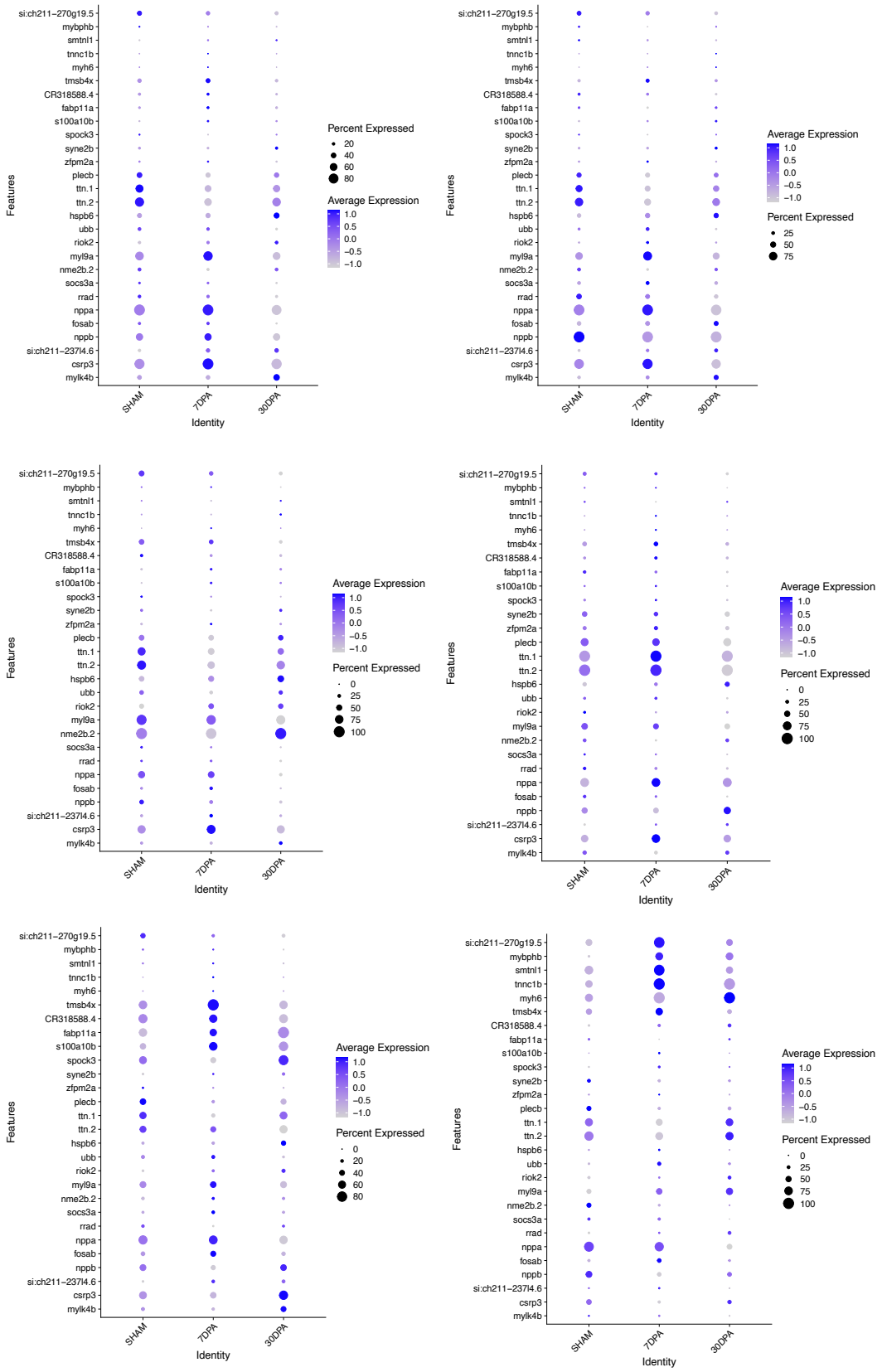

Figure A 26 Average expression of "canonical cluster market", for every cluster, at different timepoints

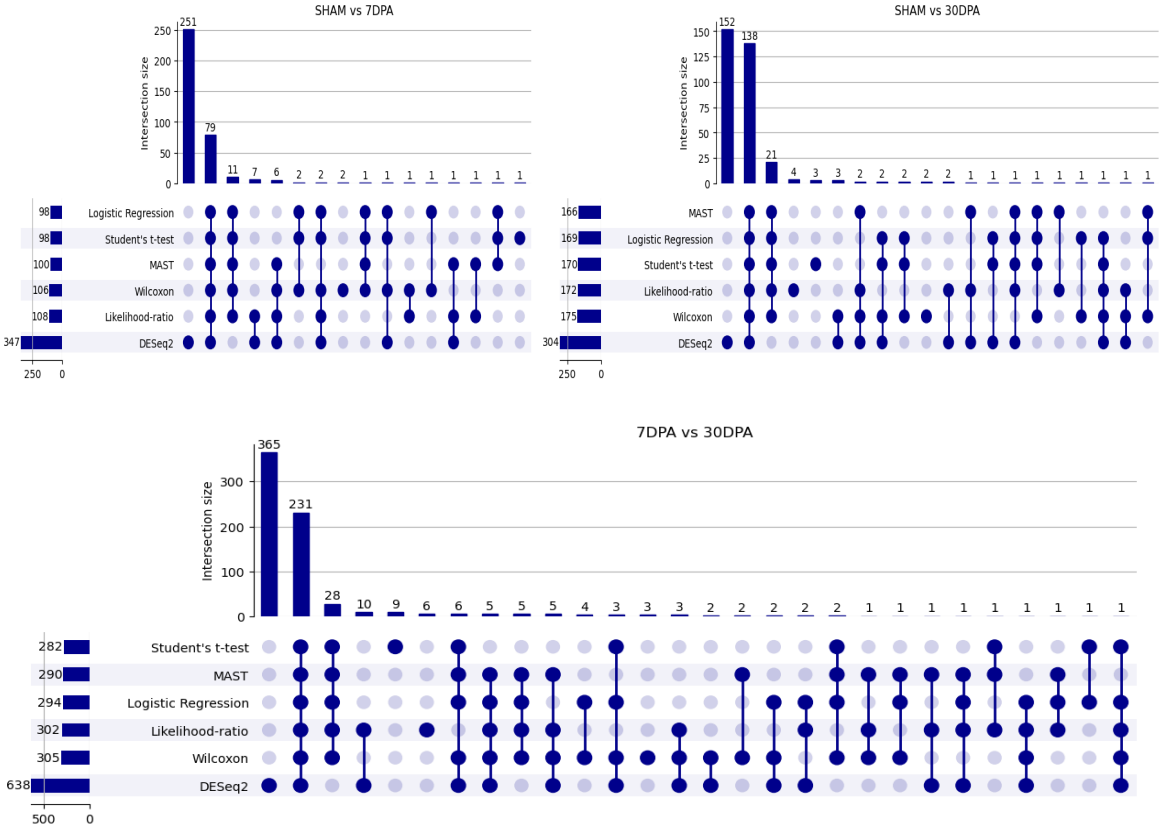

Figure A 27 Intersections and number of common genes in pair-wise differential gene expression analysis with different tools

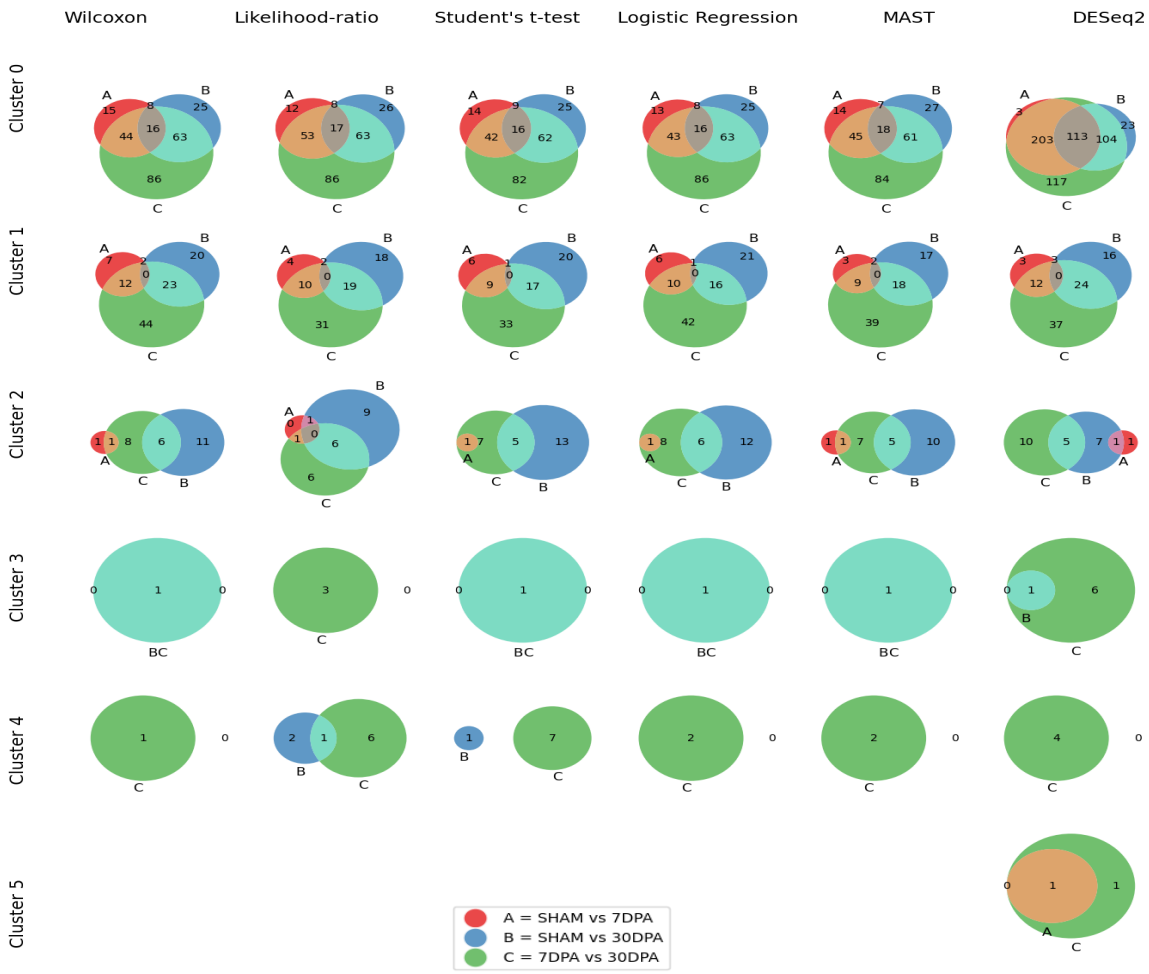

Figure A 28 Venn diagram for common genes in the different methods used for the different clusters

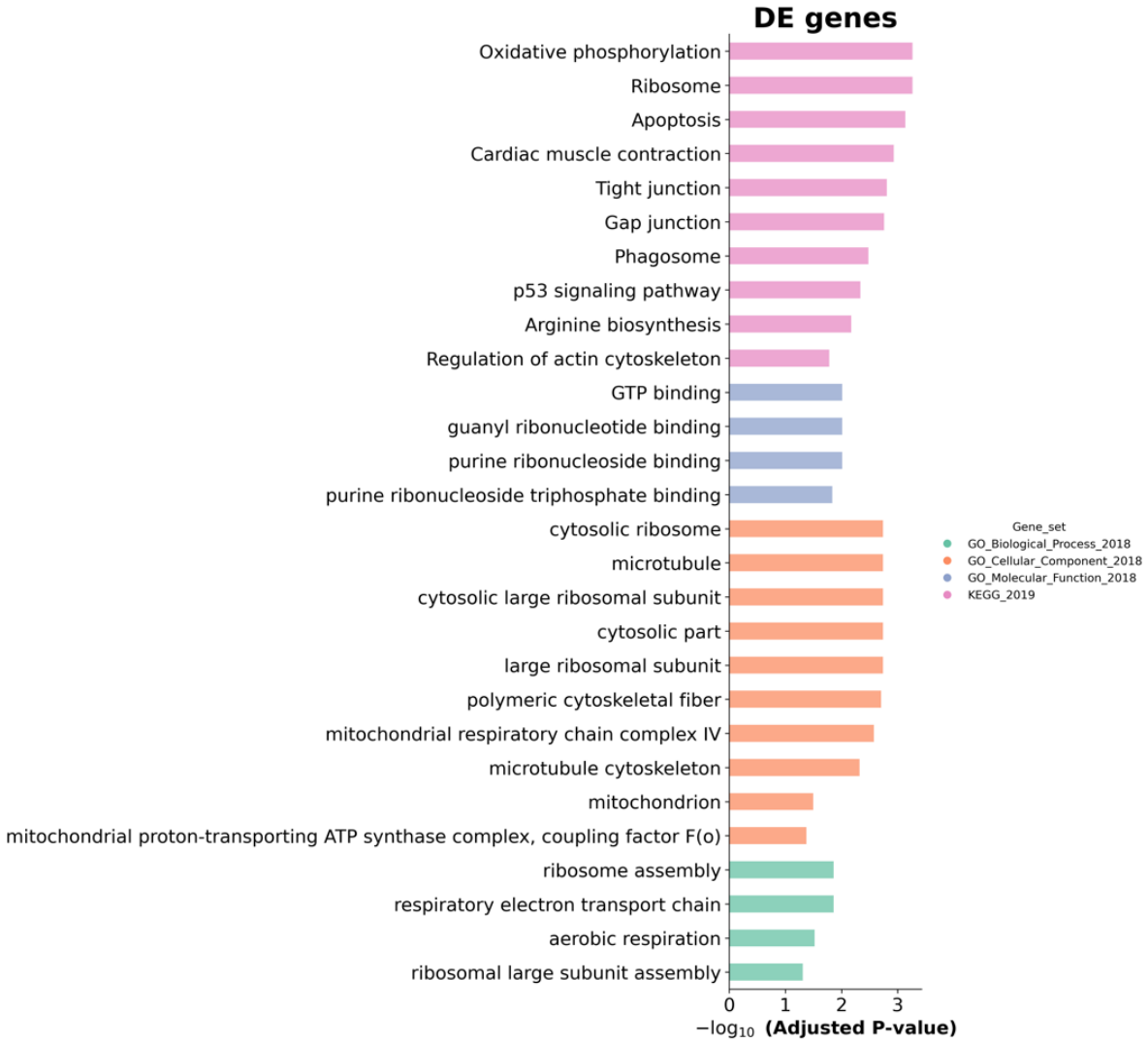

Figure A 29 GO analysis of DE genes

Table A 7: Intersection of significant genes relative to test used

# of gene	Gene and Cluster									
	6 tests		5 tests		4 tests		3 tests		2 tests	
1	mdh1ab	0	ndufs2	0	nppa	0	mylk3	0	COX5B	1
2	myl12.1	0	anxa2a	2	acta1b	1	tmsb4x	0	srl	0
3	hmgb3b	0	lmod2b	0	cox6a1	0			grm8a	0
4	apobec2a	0	acsl1b	0	ppiab	0			alas1	0
5	cycsb	1	gadd45ba	1	uqcrfs1	0			ptmab	0
6	ptmaa	0	cfl1	1	tcap	0			alcama	0
7	tuba8l2	0	mt-cyb	1					gsna	0
8	acta1a	1	anxa2a	1					coq10b	0
9	tdh	0							slc25a33	0
10	higd1a	0							nkx2.5	0
11	COX5B	0								
12	rpl11	0								
13	cycsb	0								
14	crip2l	0								
15	acta1b	0								
16	cox6a2	1								
17	atp5mc3a	0								
18	bsg	0								
19	mustn1b	0								
20	tuba8l	0								
21	si:ch73-138i16.1	0								
22	cebpd	0								
23	si:dkey-20d21.12	0								
24	cfl1	0								
25	pfn2l	0								
26	pdlim5b	0								
27	ndufa4	0								
28	rps20	0								
29	fxyd1	0								
30	tuba1b	0								
31	ccng1	0								
32	gadd45ba	0								
33	cox6b1	0								
34	arg2	0								
35	rpl3	0								
36	slc25a3b	0								
37	uqcrc1	0								
38	rps27l	0								
39	tubb4b	0								
40	anxa2a	0								
41	rpl7	0								
42	acadvl	0								
43	adprhl1	0								
44	cox6a2	0								
45	adprhl1	1								
46	csrp3	0								
47	acta1a	0								
48	actc1a	0								
49	tcaim	0								
50	hbba1	0								
51	got2a	0								
52	FO681286.1	0								
53	slc25a12	0								
54	rps6	0								
55	casq2	0								
56	myl9a	0								
57	mustn1b	1								
58	fhl1a	0								

Appendix IV. Supplementary material from chapter II

CRISPR/Cas9 strategy and technical information for the fabrication of PAA gradient gels are shown below:

Figure A 30 anxa2a$^{-/-}$ gRNAs, primers and Sanger seq

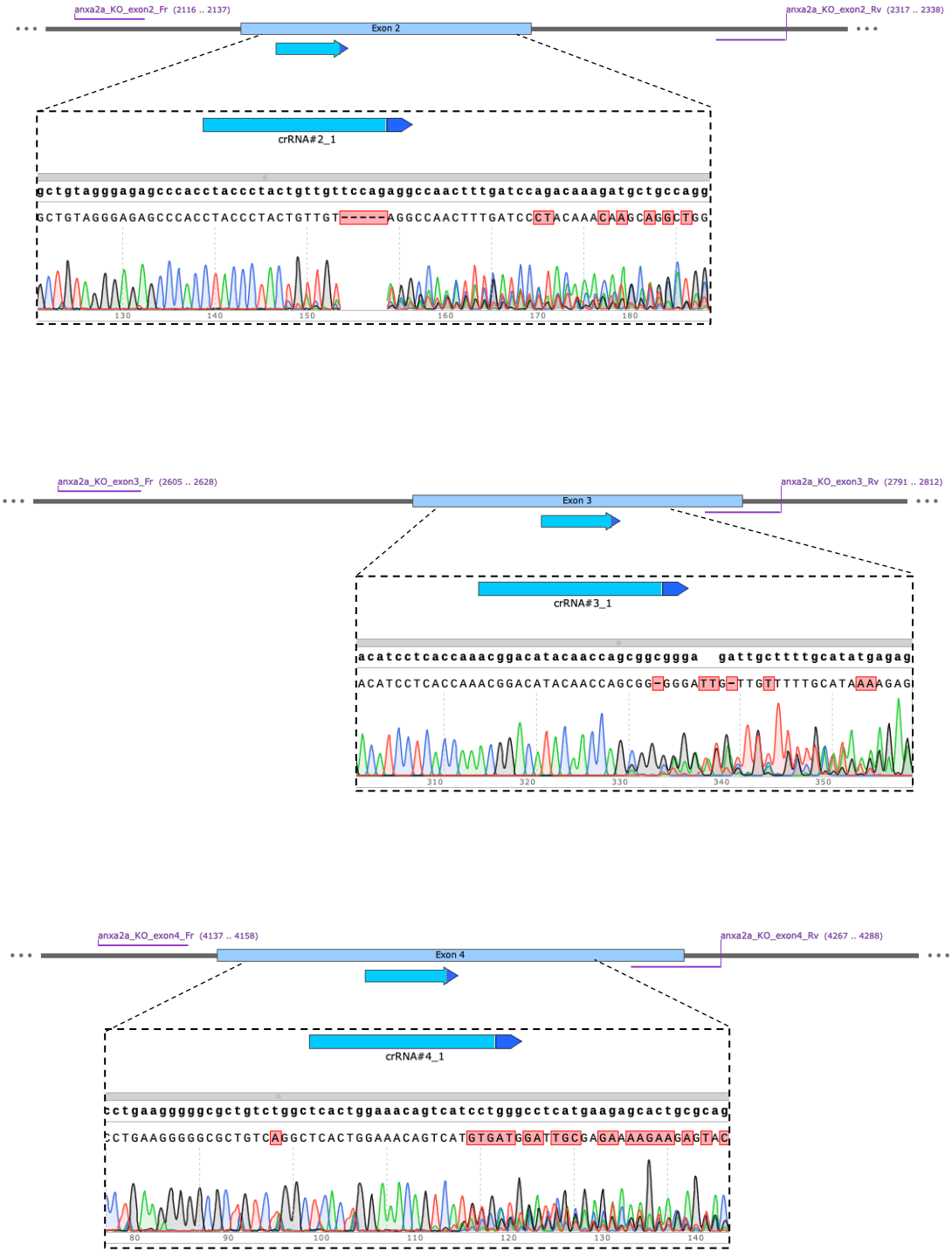

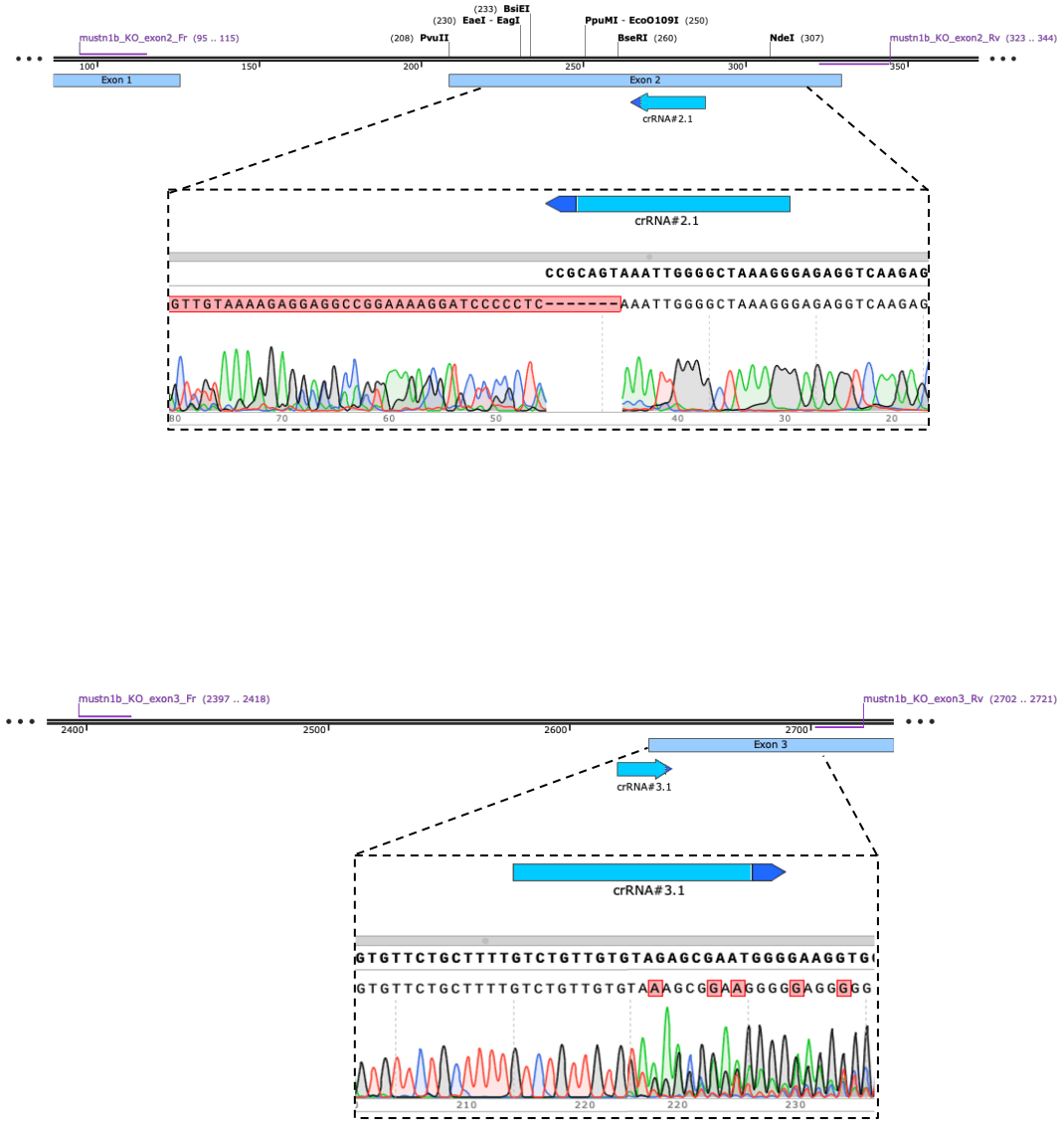

Figure A 31 mustn1b$^{-/-}$ gRNAs, primers and Sanger seq

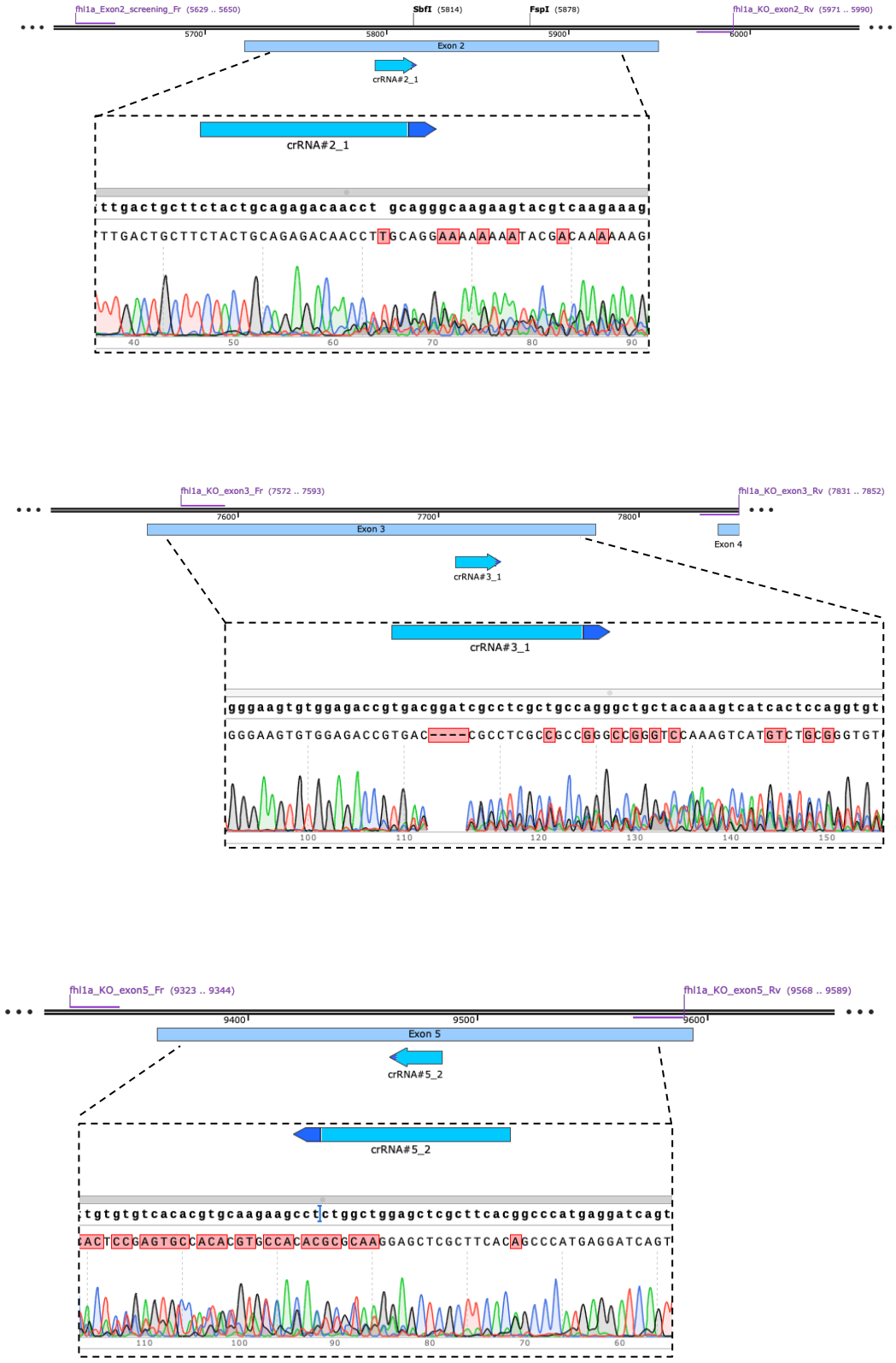

Figure A 32 fhl1a$^{-/-}$ gRNAs, primers and Sanger seq

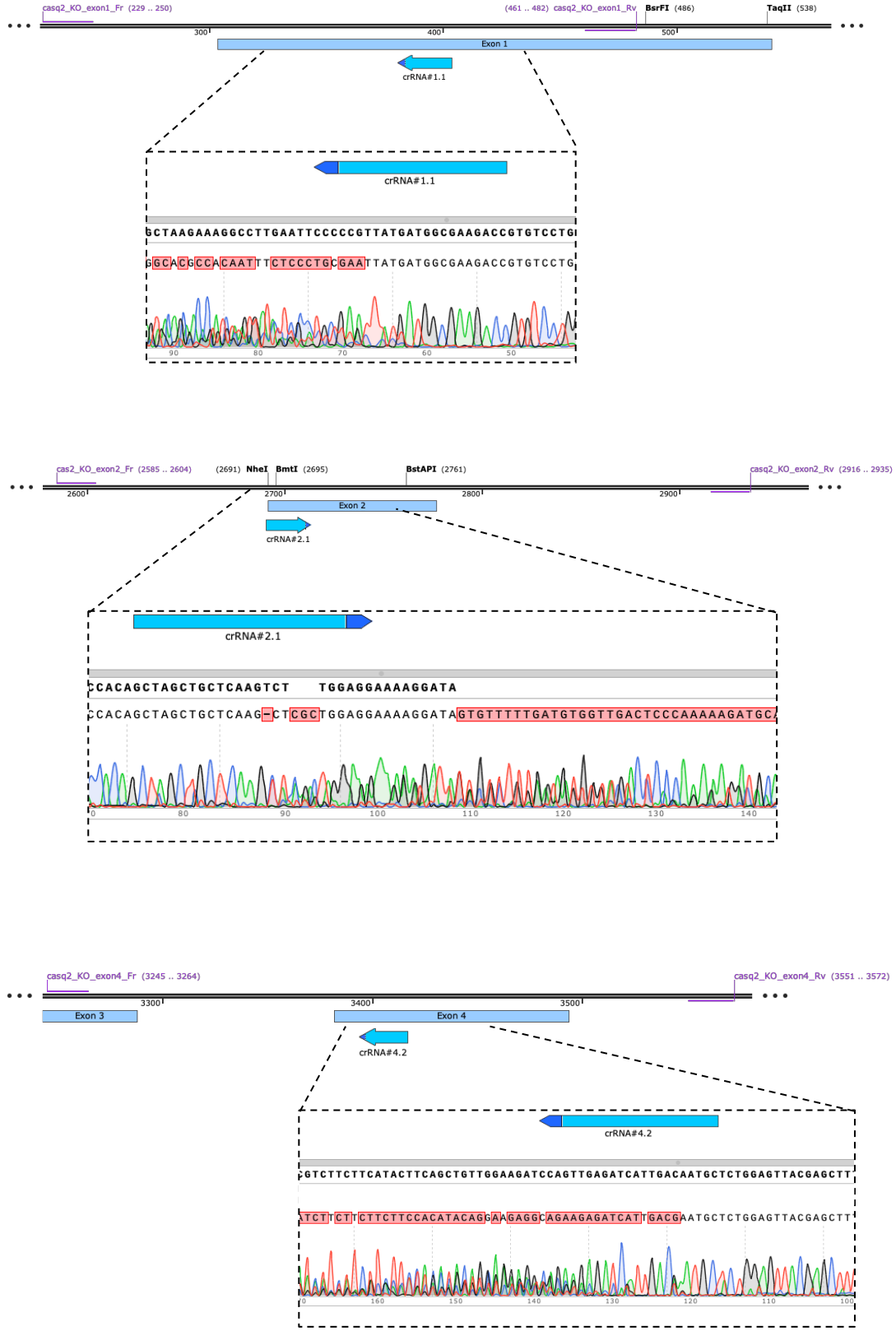

Figure A 33 casq2$^{-/-}$ gRNAs, primers and Sanger seq

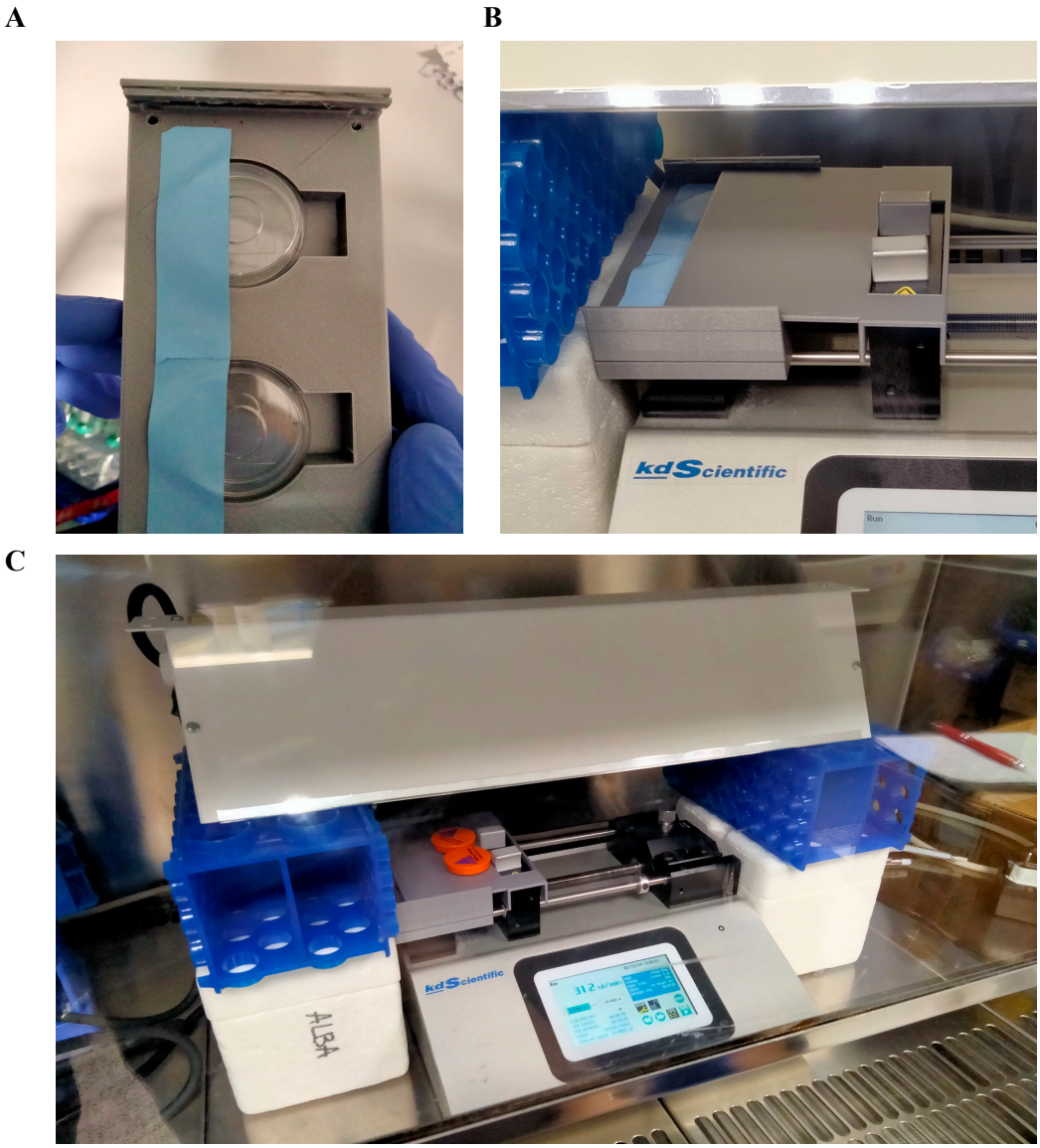

Figure A 34 PAA gel preparation. (A) 3D printed base **(B)** The base with the mask on top of the syringe pump **(C)** UV lamp and syringe pump set-up

Appendix V. Supplementary material from chapter III

All the complementary plots and information for better understanding of chapter III are shown below:

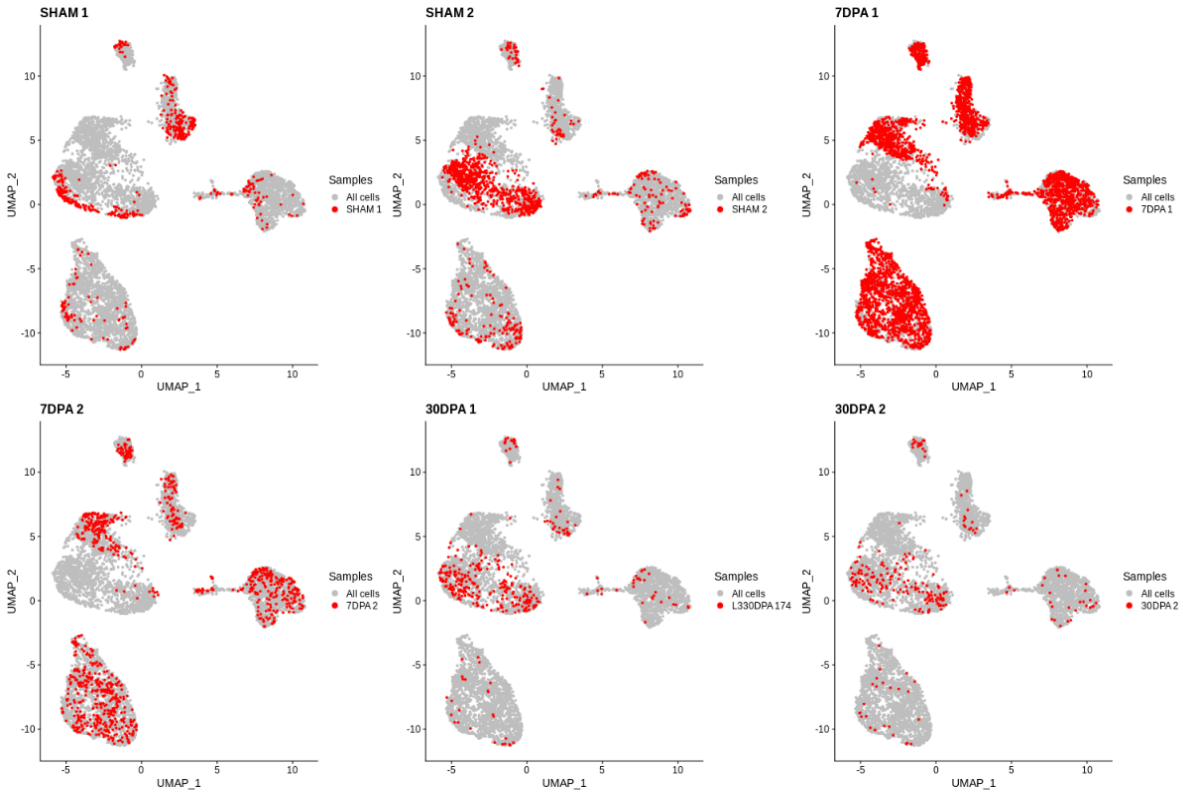

Figure A 35 Combination of scRNA-seq datasets for Sham, 7- and 30- DPA for *postnb*$^{-/-}$

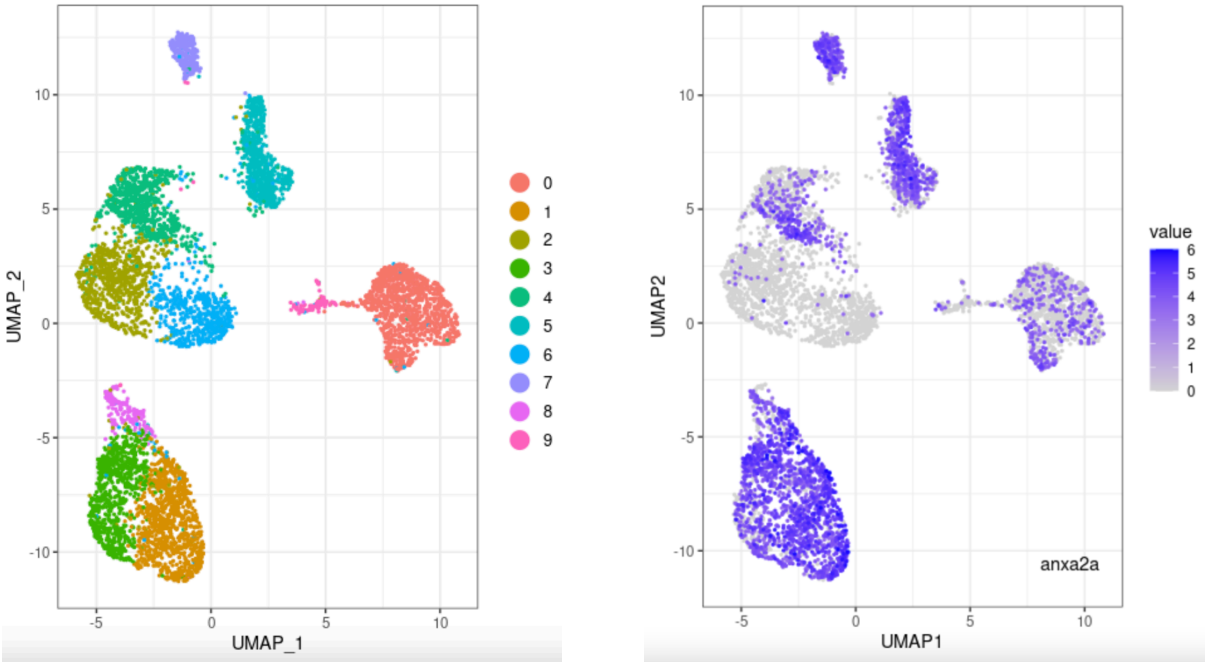

Figure A 36 UMAP representation of *anxa2a* expression in postnb$^{-/-}$ cell types.